uOttawa

Pervaporation separation of butanol using PDMS mixed matrix membranes

Hoda Azimi

Thesis submitted

In partial fulfilment of the requirements

For the Doctorate in Philosophy in Chemical Engineering degree

Department of Chemical and Biological Engineering

Faculty of Engineering

University of Ottawa

Abstract

The increased demand of fossil fuel along with the depletion of economical crude oil resources, environmental challenges such as the accumulation of CO_2 and other greenhouse gases in the atmosphere and the reduction of the dependence on imported oil are some of the motivations for the huge interest in biofuels. Biobutanol produced from ABE fermentation has been considered to be a good partial replacement for fossil fuels. However, challenges such as the need for inexpensive feed-stocks, improved fermentation performance to achieve higher final butanol concentration and higher yield, an efficient method for solvent recovery, and water recycle are the main obstacles to make the production of this alcohol economically viable.

Pervaporation, a membrane-based process, is considered to be an attractive separation method to remove butanol from ABE fermentation broth. Among the membranes used for butanol separation, PDMS membranes showed reasonable performance such as good permeability, and appropriate selectivity for butanol separation by pervaporation. However, PDMS membranes need to be improved in terms of performance to be applicable in large scale butanol production plants.

In this study, activated carbon nanoparticles have been embedded into the matrix of the PDMS membrane to improve its separation performance and, in particular, the permeation flux and butanol selectivity. Result showed that the presence of nanoparticles improves the PDMS membrane performance up to a certain particle loading. Moreover, it was shown that the operating conditions have a major impact on the pervaporation membrane separation process. The best membrane for pervaporation separation of butanol from binary aqueous solutions was obtained for a 6 wt% particle concentration where the total permeation flux and butanol selectivity increased by 42.6% and 51.9%, respectively, compared to neat PDMS membranes. Moreover, the best performance for the separation of butanol from ABE model solutions was achieved for an 8 wt% nanoparticle loading. Both the selectivity for butanol and the total permeation flux more than doubled in comparison to neat PDMS membranes prepared in this study. Moreover, in order to compare the PDMS/AC mixed matrix membrane performance for pervaporation separation of butanol from binary and ABE model solutions with PDMS membranes available on the market, experiments were also performed with a commercial PDMS membrane. Result of butanol separation from ABE model solutions showed that mixed matrix

membranes with 8 wt% nanoparticles loading had a higher permeation flux than that of the commercial membranes. It was clearly shown that the presence of activated carbon nanoparticles in the matrix of the PDMS would be beneficial for the pervaporation separation of butanol from ABE fermentation broths.

To better comprehend how the presence of activated carbon nanoparticles in the polymeric membranes enhance the performance of the membranes, a series of numerical simulations were performed. A finite difference model was developed to simulate the mass transfer of permeating components through mixed matrix membranes by pervaporation for a wide range of relative permeability, nanoparticle loading, particle shape, particle size and different filler adsorption isotherms. Finally, an investigation has been performed to optimize the butanol pervaporation separation process from ABE fermentation broth at an industrial scale.

Résumé

La demande accrue en combustibles fossiles ainsi que l'épuisement des sources économiques de pétrole brut, les défis environnementaux tels que l'accumulation de CO_2 et d'autres gaz à effet de serre dans l'atmosphère et la réduction de notre dépendance à l'égard du pétrole importé sont quelques-unes des raisons de l'intérêt énorme en biocarburants. Le biobutanol produit par la fermentation ABE a été considéré comme un bon remplacement pour les combustibles fossiles. Cependant, des défis tels que la nécessité de matières primaires peu coûteuses, des performances de fermentation améliorées pour atteindre une concentration finale de butanol et un rendement plus élevé, une méthode efficace pour la récupération des solvants et le recyclage de l'eau sont les principaux obstacles pour rendre cet alcool économiquement viable.

La pervaporation, un procédé membranaire, a été suggérée comme un bon procédé pour extraire partiellement le butanol de la fermentation ABE. Parmi les membranes utilisées pour la séparation du butanol, les membranes en PDMS ont montré des performances raisonnables telles qu'une bonne perméabilité et une sélectivité appropriée pour la séparation du butanol par pervaporation. Cependant, les membranes en PDMS devraient être améliorées en termes de performance pour leur utilisation dans les usines de production de butanol à grande échelle.

Dans cette étude, des nanoparticules de carbone activé ont été incorporées dans la matrice de les membranes en PDMS pour améliorer leur performance. Les résultats ont démontré que la présence de nanoparticules améliorait la performance des membranes jusqu'à un certain pourcentage de particules et que les conditions de fonctionnement ont un effet important sur la performance des membranes. La meilleure membrane pour la séparation par pervaporation du butanol à partir d'une solution aqueuse binaire contenait une concentration de 6% sur une base massique de particules et augmentait le flux et la sélectivité de 42,6% et 51,9%, respectivement par rapport à une membrane sans nanoparticules. De plus, une membrane en PDMS contenant 8% sur une base massique de particules a obtenu les meilleures performances pour la séparation du butanol de la solution modèle ABE. La sélectivité pour le butanol et le flux de perméation total a plus que doublé pour cette membrane par rapport aux membranes en PDMS pur préparée dans cette étude.

Pour mieux comprendre la raison de l’amélioration des performances par l’ajout des particules, la deuxième équation de Fick a été solutionnée par différences finies pour calculer le profil de concentration et le flux pour une membrane à matrice mixte. Enfin, une analyse mathématique a été effectuée pour optimiser le procédé de séparation par pervaporation butanol à partir du bouillon de fermentation ABE à l'échelle industrielle.

Statement of contributions of collaborators

Chapter 2, entitled "Effect of embedded nano-activated carbon on the performance of Polydimethylsiloxane (PDMS) membrane for pervaporation separation of butanol", was thoroughly suggested by me. I proposed the use of carbon nanoparticles, designed the experimental setup and performed all experiments. I wrote the first draft of the paper and performed all revisions based on the editorial suggestions and comments of my supervisors and external reviewers.

Chapter 3, entitled "Separation of butanol from ABE model solutions via pervaporation using AC/PDMS/PAN mixed matrix membranes", was thoroughly suggested by me. Arian Ebneyamini helped on with some experiments related to membrane swelling measurements and pervaporation tests. I wrote the first draft of the paper and made numerous revisions based on the comments of my supervisors.

Chapter 4, entitled "The impact of pH on VLE, pervaporation and adsorption of butyric acid solutions", was coordinated and managed by me. Two COOP students assisted in performing some experiments under my supervision: (1) Hervé Guérin Kamwa helped on pervaporation and VLE experiments, and (2) Chinue Joisse De La Merced helped in adsorption experiments. I wrote the first draft of the paper and made numerous revisions based on the comments of my supervisors.

Dr. Jules Thibault provided supervision and guidance throughout this series of experiments.

Chapter 5, entitled "Separation of butanol using pervaporation technique: A review of mass transfer models", is a literature review. I took the initiative to write this review with the objective to learn about the models currently used for butanol pervaporation. I wrote the first draft of the paper and made numerous revisions based on the comments of my supervisors.

Chapter 6, entitled "On the Effective Permeability of Mixed Matrix Membranes", was suggested by Dr. Jules Thibault as a way to better understand the role of nanoparticles in enhancing mixed matrix membrane performance. This work was performed conjunctly with Dr. Jules Thibault. I wrote the first draft of the paper and made numerous revisions based on the comments of my supervisors.

Chapter 7, entitled “Optimization of the in-situ recovery of butanol from ABE fermentation broth via pervaporation”, was performed conjunctly with Dr. Jules Thibault. I provided the equations and required information on pervaporation. Simulation, optimization and coding was performed by Dr. Jules Thibault. I wrote the first draft of the paper and made numerous revisions based on the comments of my supervisors.

Acknowledgments

First and for most I would like to thank my supervisors Dr. Jules Thibault and Dr. Handan Tezel for their patient guidance, encouragement and advice they have provided throughout my time as their student.

I would also like to thank the technical support team at the University of Ottawa: Louis Tremblay, Franco Ziroldo and Gérard Nina who were always the best help to solve the technical issues.

I would like to acknowledge Natural Science and Engineering Research Council (NSERC) for providing the financial support of this work.

I would like to extend my sincerest thanks and appreciation to my family especially my parents for their truly supports, encouragement and patience during my pursuit of the Doctorate in chemical engineering.

Table of Contents

List of Figures

List of Tables

1. Chapter 1

Introduction

The increased concerns about the environmental challenges such as global warming and climate change, along with the volatility of oil supply, increasing crude oil price, and existing legislations restricting the use of non-renewable energy sources resulted in significant interest for renewable fuels like ethanol, butanol and biodiesel during the last decades. This thesis is concerned with some aspects of the butanol production.

Butanol is produced from renewable resources via acetone-butanol-ethanol (ABE) fermentation broth. However, there are significant challenges to overcome to make this alcohol an economically-viable biofuel. Some of these challenges are the need for inexpensive feed-stocks, the need for improved fermentation performance to achieve higher final butanol concentration and higher yield, the need for an efficient method for solvent recovery and water recycle. To improve the low productivity in ABE fermentation process, the in situ removal of the fermentation products, especially butanol as the most toxic product, from fermentation tank is essential [1–3].

As a result, an efficient and economical separation process can be used to perform the in situ separation and the recovery of butanol from the fermentation broth to alleviate product inhibition, in-addition to provide a certain degree of purification for butanol. There are different separation techniques such as adsorption, gas-stripping, liquid-liquid extraction (LLE), perstraction, reverse osmosis (RO) and pervaporation (PV) which have been used for this purpose [1,4]. Among them, pervaporation, a membrane-based process reported to be a promising method for butanol separation, has been mainly used in this study. This technique has the greatest potential due to its high selectivity, low energy requirement and high efficiency. Moreover, it has no harmful effects on the microorganism [5–7]. In pervaporation separation method, a liquid feed solution is in contact with one side of the membrane surface and the permeating product leaves as a low-pressure vapor from the other side that is kept under vacuum. The permeate is then condensed or released depending on the objective of the separation. The driving force for the mass transfer is the chemical potential gradient across the membrane. To achieve a permeate vapor pressure lower than the partial pressure of the feed liquid, the driving force can be maintained using a vacuum pump or an inert purge gas (normally air or steam) on

the permeate side [8]. In recent years, several studies have been undertaken to better understand the pervaporation process and applied this process for numerous separation systems including water and alcohol mixtures using hydrophobic membranes. The separation depends on the chemical nature of the macromolecules that comprise the membrane, the physical structure of the membrane, the physicochemical properties of the mixtures to be separated, and the permeant-permeant and permeant-membrane interactions.

Pervaporation transport can be mainly described in three steps: 1) the penetration of the feed into the membrane surface by sorption, 2) the diffusion within the membrane, and 3) the desorption of the penetrant on the other side of the membrane [9]. There are many studies which tried to improve the butanol pervaporation separation using hydrophobic membranes. Table 1-1 shows the performance of some membranes that have been used for pervaporation separation of butanol from binary and model solutions in the literature. Among these membranes, PDMS-based membranes are favoured for their highly hydrophobic properties, high permeability, good selectivity, ease of preparation, along with good thermal, chemical and mechanical stability. However, PDMS membranes should be improved in terms of performance to be applicable in large scale butanol production plants and achieve economically viable state.

Table 1-1 Summary of butanol pervaporation separation performance from model solutions by using different types of membranes reported in the literature.

Membrane	Feed solution	Feed butanol conc.(g/L)	Flux (g/m^2h)	Membrane thickness (µm)	Separation factor	Feed temp. (°C)	Ref
PDMS	Binary	70	500	80	30	40	[10]
	Binary	20	150	80	30	40	
	Binary	10	100	80	30	40	
T-PDMS	Binary	143	570	145	42	40	[11]
TX-PDMS	Binary	134	530	90	38	40	
PDMS with dual support porous PE sheet and perforated alloy metal	Binary	3	55	90	32	37	[12]
	Binary	10	65	90	30	37	
	ABE model	3	54	90	25	37	
	ABE model	10	61	90	30	37	

Table 1-1 continued							
PDMS/ PE-1 / brass support composite	Binary	20	132	65	32	37	[13]
	Binary	20	41	200	52	37	
	Binary	5	80	65	25	37	
	Binary	20	132	65	32	37	
PDMS/ceramic	Binary	10	993	-	16.56	37	[14]
	ABE model	10	1033	-	21.43	37	
PDMS/ceramic composite membrane	Binary	10	457.7	10	26.1	40	[15]
	Binary	40	730	10	23	40	
	Binary	10	307	10	28	30	
	Binary	10	822	10	25	60	
Silicalite filled PDMS	Binary	10	90	190-210	36.3	40	[16]
	Binary	25	130	190-210	-	40	
	Binary	50	230	190-210	-	40	
	Ternary	10	110	190-210	-	40	
	Ternary	25	160	190-210	-	40	
	Ternary	50	250	190-210	-	40	
Silicalite filled PDMS	Binary	0.4	125	-	18	25	[17]
	Binary	0.4	550	-	10	65	
	Binary	0.35	-	-	-	25	
	Binary	0.35	-	-	-	65	
Silicalite-1/PDMS hybrid	Binary	10	17	-	35	33	
	Binary	10	120	-	75	71	
	Binary	34	27	-	25	33	
	Binary	34	180	-	50	71	
	ABE model	10	65	-	40	33	
	ABE model	10	275	-	70	71	
Commercial Sulzer Co., Perv. 220	Binary	6	250	-	14.2	33	[18]
	Binary	11	420	-	10	33	
	Binary	20	540	-	7.4	33	
	Binary	50	1640	-	2.4	33	
PDMS with 15% w/w	Binary	10	2	-	12	30	[19]
	Binary	100	65	-	40	30	
Styrene butadiene rubber (SBR)	Binary	10	1	-	12	30	
	Binary	100	35	-	20	30	
Celfa b	Binary	2	-	10	24	22	[20]
	Binary	2	-	10	35	40	
P 500-1	Binary	2	-	125	41	22	
	Binary	2	-	125	50	40	

Table 1-1 continued							
PTMSP	Binary	20	2600	16	80	62	
	Binary	20	1100	16	135	37	
PDMS	Binary	20	700	16	84	26	[21]
	Binary	20	250	75	50	62	
	Binary	20	100	40	40	37	
	Binary	20	50	40	30	26	
PTFE	Binary	1.25	170	40	5.6	39	
	Binary	2.5	540	40	2.6	39	
	Binary	3	490	40	2.7	39	
	ABE model	1.25	980	40	9.5	39	
	ABE model	2.5	580	40	12.4	39	
	ABE model	3	530	40	14.8	39	
	Binary	1.25	35	40	5.6	30	[22]
	Binary	1.25	170	40	8.5	40	
	Binary	1.25	805	40	9.9	50	
	Binary	1.25	2100	40	5.2	55	
	ABE model	1.25	19	40	7.2	30	
	ABE model	1.25	980	40	9.5	40	
	ABE model	1.25	1790	40	13.7	50	
PTMSP	Binary	0.3	124	-	51	25	
	Binary	1.5	60	-	55	25	
	Binary	6	436	-	61	25	[23]
	Binary	0.3	762	-	47	70	
	Binary	1.5	1030	-	70	70	
	Binary	6	2097	-	41	70	
PEBA2533	Binary	50	60.2	100	8.2	23	
	Binary	50	179	30	5.9	23	[24]
	Quaternary	19.1	41	100	13.2	23	
PEBA2533	Binary	4	420	30	11	29	
	Binary	4	300	30	19	40	
	Binary	4	200	30	25	50	[17]
	Binary	4	110	30	31	60	
PEBA	ABE model	4	9.975	-	17	37	[25]
PDMS		4	3.911	-		37	

Table 1-1 continued							
Surface modified PVDA	MPAW	75	1710	110	5.47	30	[26]
	MPAW	75	3500	110	4.9	50	
	MPAW	75	5283	110	2.98	70	
	MPAW	75	1000	110	7.2	40	
	MPAW	75	2400	110	5	40	
	MPAW	125	4800	110	3.3	40	
Polyamide-imide (PAI)	n-butanol/t-butanol	200	3.5	80	1.35	-	[27]
		440	10	80	1.35	-	
		825	12	80	0.8	-	
Polyamide-imide (PAI)/ Polyetherimide (PEI) hollow fibre	Binary	~15	846	-	56	75	[22]
HTPB-based Polyurethane urea	Binary	9	14	140	10.5	40	[28]
	Binary	24	17	140	21	40	
	Binary	27.5	19	140	21	40	
	Ternary	20	17	140	-	40	
	Ternary	45	24	140	-	40	
	Ternary	5	-	140	15	40	
	Ternary	8	-	140	24	40	
Oleyl alcohol/ PP	Binary	4	80	25	180	30	[29]
Liquid (Trioctylamine (TOA))	Binary	15	6.4	50	108.4	54	[30]
	Binary	20	8.2	50	126.4	54	
	Binary	25	10	50	141.2	54	
PEBA/CNT	Binary	0.8	153	50	19.4	37	[25]
PEBA/ZIF-71	ABE model	1.2	33.8	10-20	18.8	37	[31]
PEBA/MOF$_s$	ABE model	1.2	630.2	10-20	17.4	40	[32]

Since a pervaporation mass transfer process relies on the solution-diffusion mechanism, to improve the performance of a membrane, the selective sorption and the selective diffusion of butanol within the membrane should be as high as possible [33]. As a result, it has been suggested to incorporate small adsorbent particles, with a high affinity for butanol, within the matrix of the host PDMS [34]. Different inorganic particles such as silicalite [17,33,35–39] and carbon nanotubes [34] have been embedded in this silicone rubber matrix. The improvement on the performance of the host membrane could be due to the capillary driving force that is generated when an adsorbent is used. Furthermore, the presence of these particles increases the permeation flux as well as the mass transfer rate of the components such as butanol through the membranes [34,40–43]. Among the different types of adsorbents used in butanol separation

techniques reported in the literature, activated carbon particles have been suggested as a suitable adsorbent to enhance the adsorption separation of butanol from the other ABE components such as water, acetone and ethanol [44,45].

The main objective of this study was to improve the performance of the PDMS membrane for the pervaporation separation and the recovery of butanol. This was carried out in two parts. The first part was experimental, in which PDMS mixed matrix membranes using activated carbon nanoparticles were fabricated and their performances were measured (Part I). The second part involved modelling, in which a finite difference method was used to gain a better understanding of the impact of the nanoparticles in the matrix of the membrane and the mass transfer of the penetrant through the mixed matrix membranes prepared in our laboratories (Part II).

PDMS/AC nanoparticle mixed matric membranes were fabricated without backing material to be used for pervaporation separation of butanol from binary aqueous solutions. Results revealed that the presence of the particles enhanced the performance of the pervaporation separation process for butanol in comparison to the neat PDMS membrane. These results have been discussed in details in Part I - Chapter 2 of this thesis. In order to improve the performance of the membranes, it was desired to decrease the thickness which has a direct impact on the permeability of the permeating species. In Chapter 3, a Polyacrylonitrile (PAN) membrane was used as a backing material to cast a thin PDMS layer on its surface and the membrane performance was studied using ABE model solutions. Membranes' physical characterizations and the effects of the operating conditions such as the temperature and the ABE initial concentration on the pervaporation separation process were also investigated and the results are presented in this chapter. The membrane thicknesses were 10 times smaller in comparison to the fabricated membranes mentioned in Chapter 2. The membrane performance for 8% particle loading was found to be better than the commercial PDMS membrane also used in this investigation for comparison purposes. In Chapter 4, the results of a comprehensive study on the effect of the pH the solution on different separation methods including distillation, pervaporation and adsorption has been presented. It is believed that the degree of dissociation of butyric acid plays a major role on the separation performance of the majority of the separation processes. In particular, it is essential to study the separation of butyric acid, especially when a membrane pervaporation process is integrated to the fermentation system, since it would highly be desirable to retain the

majority of butyric acid within the fermenter since it is a precursor to the production of butanol. This is especially important for the case where a continuous fermentation is used. The same analysis could be performed for acetic acid and similar conclusion would be obtained.

In order to understand the mass transfer mechanisms taking place during pervaporation, a literature review has been conducted on different models that have been proposed. This literature survey is presented in Chapter 5 of Part II of this thesis. Based on this literature review, the Maxwell-Stefan theory was considered to be an accurate model for describing membrane separation in pervaporation due to its ability to predict the flux and selectivity of multi-component systems. This model was used by Ebneyamini et al. to study the pervaporation separation of butanol from binary aqueous solutions and the model was validated using experimental data that was obtained in this thesis [46]. Moreover, a Resistance-Based (RB) model was used in conjunction with a three-directional Finite Difference (FD) numerical solution to derive a semi-empirical model for calculating the effective permeability of the PDMS/AC mixed matrix membranes [47,48]. In this thesis, the solution-diffusion based FD model was improved to better understand the influence of the permeability and volume fraction of solid fillers within the polymer matrix in the mixed matrix membrane. Numerical simulations were performed for different ratios of permeability coefficients in the dispersed (filler) and continuous (polymer) phases (P_d/P_c), membrane thicknesses, particle sorption isotherms. In addition, the effect of the various structural parameters such as the filler volume fraction, the filler size, shape and orientation were also studied. This model is presented in more details in Chapter 6. The solution-diffusion model was considered in this chapter since it was not possible to study the effect of the filler geometry using the Maxwell-Stefan theory.

In Chapter 7, the integration of a membrane pervaporation separation process with a continuous ABE fermentation system has been simulated and optimized using a multicriteria genetic algorithm to study the effect of the membrane pervaporation in-situ recovery of the butanol from ABE fermentation on the butanol concentration, butanol productivity and sugar conversion.

Finally, a brief summary of the achievements obtained in this thesis and the recommended future studies on this topic were provided in Chapter 8.

Project objectives

The objectives of this project are:

1. To improve the performance of PDMS membranes for the pervaporation separation of butanol from binary and ABE model solutions by developing an efficient membrane to achieve a high selectivity as well as a high butanol permeation flux.
2. To investigate the effect of the feed composition, operating temperature, feed pH level, membrane composition and membrane properties on the pervaporation separation of butanol in terms of butanol permeation flux and selectivity.
3. To develop a mathematical model to gain a deeper understanding of the underlying mass transport mechanisms taking place during pervaporation and to validate the model using experimental data for butanol separation from ABE fermentation by pervaporation.
4. To optimize the butanol production from ABE fermentation for a process comprised of a fermenter and a pervaporation separation module.

Structure of the Thesis

The main body of the thesis is divided into two parts: Part I: Experimental and Part II: Simulation. The thesis is comprised of eight chapters: 1: Introduction, 2: Butanol pervaporation separation from binary aqueous solutions, 3: Butanol pervaporation separation from ABE model solutions, 4: Effect of the pH level on three solvent recovery methods, 5: Literature review on the models that have been used for pervaporation separation of butanol, 6: Pervaporation process modeling, 7: Theoretical optimization of pervaporation separation of butanol combined with ABE fermentation, and 8: Conclusions and recommendations. Chapter 7 are complemented with three Appendices providing some additional details on the models used in the membrane simulation and some membrane and thermodynamic properties. Most of these chapters are scientific articles that have been accepted or are currently being considered for publication in refereed journals. There are six chapters that have been written using the format of specific journals and, for this reason; the method for referencing may vary slightly from chapter to chapter.

Chapter 1: "Introduction" presents a brief summary of the works that have been carried out, the objectives of the project and the structure of the thesis.

Chapter 2: "Effect of embedded nano-activated carbon on the performance of Polydimethylsiloxane (PDMS) membrane for pervaporation separation of butanol" is a comprehensive study on the effect of the activated carbon nanoparticles on the performance of the PDMS membrane for pervaporation separation of the butanol from binary aqueous solutions.

Chapter 3: "Separation of butanol from ABE model solutions via pervaporation using AC/PDMS/PAN mixed matrix membranes" is an investigation on the effect of the activated carbon nanoparticles on the performance of PDMS membranes for the pervaporation separation of butanol from ABE model solutions. In this work, a porous backing material have been used to decrease the thickness of the PDMS membrane and increase the permeation flux.

Chapter 4: "The impact of pH on VLE, pervaporation and adsorption of butyric acid in dilute solutions" is a study on the effect of the pH level of solutions on the VLE of butyric acid and the separation methods such as pervaporation and adsorption.

Chapter 5: "Predictive mass transfer models in pervaporation specifically for butanol separation: A review" is a comprehensive literature review of the mass transfer models that have been used for pervaporation separation processes, especially for butanol separation.

Chapter 6: "On the Effective Permeability of Mixed Matrix Membranes" is about a numerical model developed to predict the mass transport of the components through a mixed matrix pervaporative membrane.

Chapter 7: "Optimization of the in-situ recovery of butanol from ABE fermentation broth via membrane pervaporation" is an optimization on the non-integrated process of butanol production from ABE and the integrated one with the pervaporation separation system. Moreover, a comparison between the performances of these systems has been done.

Chapter 8: "Conclusions and Recommendations" provides the main achievements of this thesis and some works that would need to be performed to further enhance the membrane pervaporation performance.

References

[1] V. Garcia, J. Pakkila, H. Ojamo, E. Muurinen, R.L. Keiski, Challenges in biobutanol production: How to improve the efficiency?, Renew. Sustain. Energy Rev. 15 (2011) 964–980. doi:10.1016/j.rser.2010.11.008.

[2] W.J. Groot, H.S. Soedjak, P.B. Donck, R.G.J.M. van der Lans, K.C.A.M. Luyben, J.M.K. Timmer, Butanol recovery from fermentations by liquid-liquid extraction and membrane solvent extraction, Bioprocess Eng. 5 (n.d.) 203–216. doi:10.1007/BF00376227.

[3] A.P. Mariano, M.J. Keshtkar, D.I.P. Atala, F. Maugeri Filho, M.R. Wolf Maciel, R. Maciel Filho, P. Stuart, Energy Requirements for Butanol Recovery Using the Flash Fermentation Technology, Energy Fuels. 25 (2011) 2347–2355. doi:10.1021/ef200279v.

[4] N. Abdehagh, J. Thibault, F.H. Tezel, Separation techniques in butanol production: Challenges and developments, Biomass Bioenergy. 60 (2014) 222–246. doi:10.1016/j.biombioe.2013.10.003.

[5] W.J. Groot, C.E. Vandenoever, N.W.F. Kossen, Pervaporation for Simultaneous Product Recovery in the Butanol Isopropanol Batch Fermentation, Biotechnol. Lett. 6 (1984) 709–714. doi:10.1007/BF00133061.

[6] E.J. Jeon, A.S. Kim, Y.T. Lee, Pervaporation of butanol/water mixtures using siloxane polymer/ceramic composite membranes, Desalination Water Treat. 48 (2012) 17–26. doi:10.1080/19443994.2012.698723.

[7] N.L. Mai, S.H. Kim, S.H. Ha, H.S. Shin, Y.-M. Koo, Selective recovery of acetone-butanol-ethanol from aqueous mixture by pervaporation using immobilized ionic liquid polydimethylsiloxane membrane, Korean J. Chem. Eng. 30 (2013) 1804–1809. doi:10.1007/s11814-013-0116-6.

[8] S.M. Zhang, E. Drioli, Pervaporation Membranes, Sep. Sci. Technol. 30 (1995) 1–31. doi:10.1080/01496399508012211.

[9] P.D. Chapman, T. Oliveira, A.G. Livingston, K. Li, Membranes for the dehydration of solvents by pervaporation, J. Membr. Sci. 318 (2008) 5–37. doi:10.1016/j.memsci.2008.02.061.

[10] E. Favre, P. Schaetzel, Q.T. Nguygen, R. Clément, J. Néel, Sorption, diffusion and vapor permeation of various penetrants through dense poly(dimethylsiloxane) membranes: a transport analysis, J. Membr. Sci. 92 (1994) 169–184. doi:10.1016/0376-7388(94)00060-3.

[11] S. Schnabel, D. Roizard, T. Nguyen, P. Lochon, P. Aptel, Synthesis of novel block siloxane polymers for the removal of butanols from aqueous feed solutions, Colloids Surf. - Physicochem. Eng. Asp. 138 (1998) 335–343. doi:10.1016/S0927-7757(97)00074-5.

[12] S.-Y. Li, R. Srivastava, R.S. Parnas, Study of in situ 1-butanol pervaporation from A-B-E fermentation using a PDMS composite membrane: validity of solution-diffusion model for pervaporative A-B-E fermentation, Biotechnol. Prog. 27 (2011) 111–120. doi:10.1002/btpr.535.

[13] S.-Y. Li, R. Srivastava, R.S. Parnas, Separation of 1-butanol by pervaporation using a novel tri-layer PDMS composite membrane, J. Membr. Sci. 363 (2010) 287–294. doi:10.1016/j.memsci.2010.07.042.

[14] H. Wu, X.-P. Chen, G.-P. Liu, M. Jiang, T. Guo, W.-Q. Jin, P. Wei, D.-W. Zhu, Acetone-butanol-ethanol (ABE) fermentation using Clostridium acetobutylicum XY16 and in situ recovery by PDMS/ceramic composite membrane, Bioprocess Biosyst. Eng. 35 (2012) 1057–1065. doi:10.1007/s00449-012-0721-5.

[15] Liu Gongping, Hou Dan, Wei Wang, Xiangli Fenjuan, Jin Wanqin, Pervaporation Separation of Butanol-Water Mixtures Using Polydimethylsiloxane/Ceramic Composite Membrane, Chin. J. Chem. Eng. 19 (2011) 40–44. doi:10.1016/S1004-9541(09)60174-9.

[16] A. Jonquières, A. Fane, Filled and unfilled composite GFT PDMS membranes for the recovery of butanols from dilute aqueous solutions: influence of alcohol polarity, J. Membr. Sci. 125 (1997) 245–255. doi:10.1016/S0376-7388(96)00191-3.

[17] E.A. Fouad, X. Feng, Pervaporative separation of n-butanol from dilute aqueous solutions using silicalite-filled poly(dimethyl siloxane) membranes, J. Membr. Sci. 339 (2009) 120–125. doi:10.1016/j.memsci.2009.04.038.

[18] C. Xue, J. Zhao, F. Liu, C. Lu, S.-T. Yang, F.-W. Bai, Two-stage in situ gas stripping for enhanced butanol fermentation and energy-saving product recovery, Bioresour. Technol. 135 (2013) 396–402. doi:10.1016/j.biortech.2012.07.062.

[19] K.D. Jitesh, V.G. Pangarkar, K. Niranjan, Pervaporative stripping of acetone, butanol and ethanol to improve ABE fermentation, Bioseparation. 9 (2000) 145–154. doi:10.1023/A:1008129713552.

[20] V. Garcia, E. Pongracz, E. Muurinen, R.L. Keiski, Recovery of n-butanol from salt containing solutions by pervaporation, Desalination. 241 (2009) 201–211. doi:10.1016/j.desal.2007.12.051.

[21] A.G. Fadeev, M.M. Meagher, S.S. Kelley, V.V. Volkov, Fouling of poly[-1-(trimethylsilyl)-1-propyne] membranes in pervaporative recovery of butanol from aqueous solutions and ABE fermentation broth, J. Membr. Sci. 173 (2000) 133–144. doi:10.1016/S0376-7388(00)00359-8.

[22] D.L. Vrana, M.M. Meagher, R.W. Hutkins, B. Duffield, Pervaporation of Model Acetone-Butanol-Ethanol Fermentation Product Solutions using Polytetrafluoroethylene Membranes, Sep. Sci. Technol. 28 (1993) 2167–2178. doi:10.1080/01496399308016741.

[23] A.G. Fadeev, Y.A. Selinskaya, S.S. Kelley, M.M. Meagher, E.G. Litvinova, V.S. Khotimsky, V.V. Volkov, Extraction of butanol from aqueous solutions by pervaporation through poly(1-trimethylsilyl-1-propyne), J. Membr. Sci. 186 (2001) 205–217. doi:10.1016/S0376-7388(00)00683-9.

[24] F.F. Liu, L. Liu, X.S. Feng, Separation of acetone-butanol-ethanol (ABE) from dilute aqueous solutions by pervaporation, Sep. Purif. Technol. 42 (2005) 273–282. doi:10.1016/j.seppur.2004.08.005.

[25] H.-W. Yen, S.-F. Lin, I.-K. Yang, Use of poly(ether-block-amide) in pervaporation coupling with a fermentor to enhance butanol production in the cultivation of Clostridium acetobutylicum, J. Biosci. Bioeng. 113 (2012) 372–377. doi:10.1016/j.jbiosc.2011.10.025.

[26] K. Srinivasan, K. Palanivelu, A.N. Gopalakrishnan, Recovery of 1-butanol from a model pharmaceutical aqueous waste by pervaporation, Chem. Eng. Sci. 62 (2007) 2905–2914. doi:10.1016/j.ces.2007.02.028.

[27] Y. Wang, T.S. Chung, H. Wang, S.H. Goh, Butanol isomer separation using polyamide-imide/CD mixed matrix membranes via pervaporation, Chem. Eng. Sci. 64 (2009) 5198–5209. doi:10.1016/j.ces.2009.08.034.

[28] Y. Chen, T. Zhou, D. Liu, A. Li, S. Xu, Q. Liu, B. Li, H. Ying, Production of butanol from glucose and xylose with immobilized cells of Clostridium acetobutylicum, Biotechnol. Bioprocess Eng. 18 (2013) 234–241. doi:10.1007/s12257-012-0573-5.

[29] M. Matsumura, H. Kataoka, Separation of Dilute Aqueous Butanol and Acetone Solutions by Pervaporation through Liquid Membranes, Biotechnol. Bioeng. 30 (1987) 887–895. doi:10.1002/bit.260300712.

[30] A. Thongsukmak, K.K. Sirkar, Pervaporation membranes highly selective for solvents present in fermentation broths, J. Membr. Sci. 302 (2007) 45–58. doi:10.1016/j.memsci.2007.06.013.

[31] S. Liu, G. Liu, X. Zhao, W. Jin, Hydrophobic-ZIF-71 filled PEBA mixed matrix membranes for recovery of biobutanol via pervaporation, J. Membr. Sci. 446 (2013) 181–188. doi:10.1016/j.memsci.2013.06.025.

[32] S. Liu, G. Liu, J. Shen, W. Jin, Fabrication of MOFs/PEBA mixed matrix membranes and their application in bio-butanol production, Sep. Purif. Technol. 133 (2014) 40–47. doi:10.1016/j.seppur.2014.06.034.

[33] J. Huang, M.M. Meagher, Pervaporative recovery of n-butanol from aqueous solutions and ABE fermentation broth using thin-film silicalite-filled silicone composite membranes, J. Membr. Sci. 192 (2001) 231–242. doi:10.1016/S0376-7388(01)00507-5.

[34] C. Xue, G.-Q. Du, L.-J. Chen, J.-G. Ren, J.-X. Sun, F.-W. Bai, S.-T. Yang, A carbon nanotube filled polydimethylsiloxane hybrid membrane for enhanced butanol recovery, Sci. Rep. 4 (2014) 5925–5925. doi:10.1038/srep05925.

[35] J.C. Huang, M.M. Meagher, Pervaporative recovery of n-butanol from aqueous solutions and ABE fermentation broth using thin-film silicalite-filled silicone composite membranes, J. Membr. Sci. 192 (2001) 231–242. doi:10.1016/S0376-7388(01)00507-5.

[36] A. Jonquieres, A. Fane, Filled and unfilled composite GFT PDMS membranes for the recovery of butanols from dilute aqueous solutions: Influence of alcohol polarity, J. Membr. Sci. 125 (1997) 245–255. doi:10.1016/S0376-7388(96)00191-3.

[37] P. Garg, R.P. Singh, V. Choudhary, Pervaporation separation of organic azeotrope using poly(dimethyl siloxane)/clay nanocomposite membranes, Sep. Purif. Technol. 80 (2011) 435–444. doi:10.1016/j.seppur.2011.05.020.

[38] H. Zhou, Y. Su, X. Chen, S. Yi, Y. Wan, Modification of silicalite-1 by vinyltrimethoxysilane (VTMS) and preparation of silicalite-1 filled polydimethylsiloxane (PDMS) hybrid pervaporation membranes, Sep. Purif. Technol. 75 (2010) 286–294. doi:10.1016/j.seppur.2010.08.017.

[39] P. Peng, B. Shi, Y. Lan, Preparation of PDMSSilica Nanocomposite Membranes with Silane Coupling for Recovering Ethanol by Pervaporation, Sep. Sci. Technol. 46 (2011) 420–427. doi:10.1080/01496395.2010.527896.

[40] G. Singh, D. Rana, T. Matsuura, S. Ramakrishna, R.M. Narbaitz, S. Tabe, Removal of disinfection byproducts from water by carbonized electrospun nanofibrous membranes, Sep. Purif. Technol. 74 (2010) 202–212. doi:10.1016/j.seppur.2010.06.006.

[41] M. Majumder, K. Keis, X. Zhan, C. Meadows, J. Cole, B.J. Hinds, Enhanced electrostatic modulation of ionic diffusion through carbon nanotube membranes by diazonium grafting chemistry, J. Membr. Sci. 316 (2008) 89–96. doi:10.1016/j.memsci.2007.09.068.

[42] J. Boom, I. Punt, H. Zwijnenberg, R. de Boer, D. Bargeman, C. Smolders, H. Strathmann, Transport through zeolite filled polymeric membranes, J. Membr. Sci. 138 (1998) 237–258. doi:10.1016/S0376-7388(97)00228-7.

[43] M.A. Aroon, A.F. Ismail, T. Matsuura, M.M. Montazer-Rahmati, Performance studies of mixed matrix membranes for gas separation: A review, Sep. Purif. Technol. 75 (2010) 229–242. doi:10.1016/j.seppur.2010.08.023.

[44] N. Abdehagh, F.H. Tezel, J. Thibault, Adsorbent screening for biobutanol separation by adsorption: kinetics, isotherms and competitive effect of other compounds, Adsorption. 19 (2013) 1263–1272. doi:10.1007/s10450-013-9566-8.

[45] N. Qureshi, S. Hughes, I.S. Maddox, M.A. Cotta, Energy-efficient recovery of butanol from model solutions and fermentation broth by adsorption, Bioprocess Biosyst. Eng. 27 (2005) 215–222. doi:10.1007/s00449-005-0402-8.

[46] A. Ebneyamini, H. Azimi, J. Thibault, F.H. Tezel, Description of Butanol Aqueous Solution Transport through Commercial PDMS Membrane via Pervaporation Using Extended Maxwell–Stefan Model, J. Sep. Sci. Technol. (2017) Submitted.

[47] A. Ebneyamini, H. Azimi, F.H. Tezel, J. Thibault, Mixed matrix membranes applications: Development of a resistance-based model, J. Membr. Sci. 543 (2017) 351–360. doi:10.1016/j.memsci.2017.08.065.

[48] A. Ebneyamini, H. Azimi, F.H. Tezel, J. Thibault, Modelling of mixed matrix membranes: Validation of the resistance-based model, J. Membr. Sci. 543 (2017) 361–369. doi:10.1016/j.memsci.2017.08.064.

Part I: Experimental section

2. Chapter 2

Effect of embedded activated carbon nanoparticles on the performance of Polydimethylsiloxane (PDMS) membrane for pervaporation separation of butanol

Short title: Performance of composite membrane (PDMS-AC) for separation of butanol

Hoda Azimi, Handan F. Tezel* and Jules Thibault

Abstract

BACKGROUND: Pervaporation separation method considered to be a promising technique for biobutanol recovery from fermentation broths. In this work, activated carbon nanoparticles were embedded in Polydimethylsiloxane (PDMS) membranes to improve the pervaporation performance.

RESULTS: Adding 6 wt% nano-additives in PDMS membranes increased the flux and separation factor by 42.6% and 51.9%, respectively, compared to neat membranes at 37°C. Enhanced performance is due to: (1) the presence of additional sorption sites within the membrane with a high affinity for butanol, and (2) the porous structure of the nanofillers generate new pathways for facilitated mass transport through the membrane. The effect of the operating temperature and particle concentration on membrane performance was investigated. Membrane performance improved with an increase in the operating temperature. Higher temperature resulted in increased free volume in the PDMS chains leading to higher diffusion of butanol. Mechanical tensile tests showed that nanocomposite membranes have better mechanical stability in comparison with neat PDMS membranes with the best performance observed at 6 wt% of the nano-additives.

CONCLUSION: The presence of activated carbon nanoparticles in the matrix of PDMS membranes leading to higher flux and separation factor can be beneficial for pervaporation separation of butanol from fermentation broths.

Keywords: Biobutanol, Pervaporation, Mixed matrix membrane, PDMS, Activated carbon nanoparticles

Introduction

More recently, biobutanol (aliphatic four-carbon alcohol) has been on the radar of researchers and industry for the production of second generation biofuels[1–3]. Biobutanol is commonly produced via the traditional Acetone-Butanol-Ethanol (ABE) fermentation. However, there are significant challenges to overcome to make biobutanol an economically-viable biofuel using fermentation[4,5] such as the low final butanol concentration in the fermentation broth and the low productivity resulting from relatively low product concentration levels that become toxic for the microorganism[6]. To improve the low butanol productivity in an ABE fermentation process, the in situ removal of the products via integrated recovery technologies, especially for butanol as the most toxic product from the fermentation broth, would lessen product toxicity and allow greater sugar conversion and higher productivity[7–11].

Pervaporation, a membrane-based process, can potentially achieve this objective due to its high selectivity, low energy requirement and high efficiency[12,13]. Moreover, it has no harmful effects on the microorganism[14–16]. The use of hydrophobic membranes such as styrene butadiene rubber (SBR)[17], ethylene propylene diene rubber (EPDM)[18], polytetrafluoroethylene (PTFE)[19], polypropylene (PP)[20], polyurethane (polyether based) (PUR)[21], polyether block-amide (PEBA)[22], poly(vinylidinedifluoride) (PVDF)[23], poly(methoxy siloxane) (PMS)[24], polydimethylsiloxane (PDMS)[25,26], poly(1-(trimethylsilyl)-1-propyne) (PTMSP)[27] and polyamide-imide (PAI)[28] containing cyclodextrin (CD) has been reported in the literature for butanol separation through the process of pervaporation[29,30] .

PDMS membranes are generally selected for butanol separation for their highly hydrophobic properties, high permeability and separation factor, ease of preparation, and their good thermal, chemical and mechanical stability [25]. However, permeability and separation factor of the PDMS membrane is not within the required standards of the industrial scale for butanol production. To improve the performance of PDMS membranes, the selective sorption and diffusion of butanol within the membrane should be enhanced. Different inorganic fillers such as zeolites[11,31], silicalite[32–39] and carbon nanotubes[40] have been embedded in this silicone rubber matrix to improve the solubility and diffusivity of the desired chemical species. It is believed that a capillary driving force is generated when an adsorbent is used. The presence of these particles

enhanced the mass transfer and therefore increased the permeation rate of the components such as butanol through the membranes. Furthermore, the mixed matrix membranes demonstrated a higher separation factor in comparison with the neat membrane[40–44]. However, it is hypothesized that the addition of a particle with higher adsorption capacity of the target component into the membrane matrix would raise the membrane performance even further. In addition, if the diffusivity of butanol in the solid filler is greater than its diffusivity in the continuous polymeric matrix, the flux of butanol should increase. As a result, a solid filler with a higher butanol permeability, i.e. the product of diffusivity and solubility, the effective permeability of the membrane will increase such that the flux of butanol and selectivity will increase.

Considering different types of adsorbents used in butanol separation techniques based on adsorption, activated carbons have been observed to be superior adsorbents for separating butanol from ABE model solutions and fermentation broths. Abdehagh et al. (2013) used two types of activated carbons (AC F600 and F400) and different types of zeolites to determine their potential as adsorbents for butanol separation[45]. Results showed that activated carbons had faster adsorption rate than zeolites and F400 had the highest capacity in comparison to all the other adsorbents that were studied. Moreover, the mechanical stiffness and the large specific surface area of the activated carbon nanoparticles have the potential to improve the mechanical stability and the performance of PDMS membranes. Therefore, the results from other researchers suggest that activated carbon nanoparticles with high adsorption capacity could be an appropriate adsorbent to be embedded in the PDMS matrix.

To the best of our knowledge, this is the first attempt that activated carbon nanoparticles are used as the additive to prepare mixed matrix membranes of PDMS and AC for the purpose of enhancing the properties and performance of the host PDMS membrane.

In this investigation, different concentrations of activated carbon nanoparticles were used in the matrix of the PDMS membranes to study the effects of the nano-additives on the properties and performance of the pervaporation PDMS membranes for butanol separation from aqueous binary solutions.

Experimental Material and Methods

Materials

PDMS and cross-linking agent kit (RTV615 001- KIT) were obtained from Momentive Co. (Hebron, Ohio, USA). Super Activated Porous Carbon Nanopowder (particle size 20-40 nm, pore size of 3.5 nm and specific surface area greater than 1400 m^2/g) US1074 was purchased from US-Nano Company (South Bend, IN, USA). Butanol (99% pure, Acros) was obtained from Fisher Scientific (Fair Lawn, NJ, USA). Deionized distilled water was used to prepare all binary aqueous solutions.

Membrane fabrication

Neat membrane

To fabricate the PDMS membranes, a procedure similar to the one proposed by Li et al. was used[14]. The base solution (PDMS) from the silicone kit was mixed with the cross-linking agent in a ratio of 10:1 by weight. 20 g of toluene was used as a solvent to dilute 10 g of PDMS. The mixture was vigorously stirred on an orbital agitator with a speed of 400 rpm for 30 min. Petri dishes with a diameter of 9.5 cm were used as the casting units to prepare a flat coupon of PDMS membrane. 10 mL of solution was poured into the petri dishes for making the membranes. The petri dishes were then placed in a vacuum oven and carefully leveled to lead to a uniform thickness. A vacuum pressure of 0.8 bar was applied for 30 min at room temperature and then the oven was heated to 90°C for 3 h while maintaining the vacuum. The cured membrane was peeled off from the Pyrex petri dishes by rinsing with water. After drying, the membrane was cut to fit the size of the membrane holder in the membrane module. The effective area of the membrane was $1.35x10^{-3}$ m^2.

Activated Carbon (AC) nanoparticles filled PDMS mixed matrix membranes

A solution of PDMS and toluene was prepared using the procedure described above. Then, a known amount of the Super Activated Porous Carbon Nanopowder was added to the solution.

The solid slurry was thoroughly mixed using a sonicator (Fisher Scientific Model 550 Sonic Dismembrator, Ottawa, ON, Canada) at ambient temperature for 2 h. Sonication ideally produces a homogeneous distribution of the AC nanoparticles in the PDMS polymer solution with negligible particle agglomeration. 10 mL of this homogeneous solid-liquid solution was poured into each 9.5 cm diameter petri dish and cured under vacuum conditions first at room temperature for 30 minutes and then at 90^{o}C for 3 h. Subsequently, the identical procedure as described for the fabrication of neat PDMS membranes was used. A similar procedure was also used successfully by other researchers to manufacture mixed matrix membranes[40,46].

Membrane characterization

Morphology

The SEM images of the membranes were taken using a Scanning Electron Microscope (SEM, Vega-II XMU VPSEM and Anatech Hummer VII, Battle Creek, MI, U.S.). The membrane surfaces were gold sputtered before SEM observation[47]. Each sample was taped on a support using carbon tape to fix the sample and gold sputtered before SEM observations were made.

Thickness

A digital micrometer caliper (0-1", Miutoyo, Illinois, USA) was used to measure the membrane thickness. Measurements were made at five different spots and the average is reported.

Degree of swelling and nanoparticle adsorption capacity

To measure the degree of swelling of the membranes in contact with water and butanol solutions, the same weights of PDMS and AC-PDMS membranes were immersed in a bottle containing pure butanol, pure water and aqueous butanol-water binary solutions (with a concentration range of 5-50 g/L of butanol) separately at a temperature of 25°C. After 24 h, the membrane samples were retrieved from the sealed bottles; the swollen membranes were gently blotted with a paper wiper (Kimwipes, Kimtech) rapidly to remove any surface solution. The swelled membrane samples were then weighed using a precise digital balance and then replaced in the bottle to observe further swelling. The same procedure was repeated until the swollen weight reached a

constant value. The swelling degree of the membrane, SD, expressed as a percentage, was determined by Equation (1).

$$SD = \frac{W_s - W_d}{W_d} \times 100 \quad (1)$$

where W_d and W_s are the weights of the dry and swelled membrane samples, respectively[48].

To measure the maximum adsorption capacity of the activated carbon nanoparticles, batch experiments were used. 2.8 g of nanoparticle was added to 50 mL of 2.5 wt% butanol–water solution. Solution container was then placed in a shaker at room temperature to ensure mixing was adequate. To measure the concentration of butanol in the solution, samples were filtered using a 0.45 μm filter. HPLC was used to measure the concentration of butanol and, by difference, it was possible to measure the equilibrium adsorption capacity of the activated carbon nanoparticles.

Static and dynamic contact angle and surface roughness

The performance of a membrane in the pervaporation separation process for alcohol recovery is related to the hydrophobicity and the organophilicity of the membrane top surface or active layer. The hydrophobicity of a solid surface is usually characterized by its contact angle. To investigate the hydrophobicity and organophilicity of membranes made in our laboratory, the static contact angle (SCA) was measured for each neat and composite membrane using the video optima surface analysis system (Optima AST Product Inc., Billerica, MA, USA) by following the method which has been described elsewhere[49,50]. For each membrane, the static contact angle was measured at five different locations and the values were averaged. The static contact angle was measured for both pure water and a 5 g/L butanol aqueous solution. Moreover, the dynamic contact angle of pure butanol was measured by recording 10 frames for 1 minute considering the rapid change of the butanol droplet contact angle at the surface of the PDMS as a result of butanol moving to expose the fresh surface and wetting the surface of the PDMS.

To measure the surface roughness, SurfCharJ software[51] was used to analyze the SEM pictures by following the procedure that has been used in previous studies. This method was also successfully used by the other researchers[50,52]. This software assigns different pixel values

ranging from 0 to 255 to each element of the 2D image of the surface based upon the darkness and brightness of the picture to convert a 2D image into a 3D image. The pixel values represent the distance z from the membrane surface. A darker surface representing a lower pixel value which implies a deeper valley while a brighter surface with higher pixel value is equivalent to a smoother polymer surface. Moreover, the arithmetic average of the absolute values of the measured peak heights from a one-dimensional plane is reported by Ra (average roughness), while Rq (root mean square) represents the standard deviation. In addition, the maximum profile peak height is shown by Rp.

Tensile strength

The tensile strength and the elongation at the point of rupture were measured using an E3000 Instron Universal Tester and Bluehill 2 Materials Testing Software (TestResources, Inc, Shakopee, USA). Experiments were performed in a temperature and humidity controlled chamber (~27°C and 55% RH). For all tests, membrane samples, 15 cm long and 3 cm wide, were cut from each PDMS and AC-PDMS films without backing support material.

Membrane performance

Pervaporation

Experiments were carried out using the pervaporation experimental setup that is presented in Figure 2-1. The experimental system mainly consists of three membrane modules placed in series where the retentate from the first membrane was directed to the second one and then the retentate of the second membrane was the feed for the third membrane. The feed stream from a binary butanol-water solution was pumped through the retentate side of the first pervaporation cell using peristaltic pump. The three-module membrane system was placed in a temperature-controlled oven. The feed stream flowed through a long stainless steel coil upon entering the oven to ensure the feed stream reaches the desired temperature prior to entering the membrane system. Two thermocouples were used to measure the temperature at the top and at the bottom of the oven and one thermocouple was used to measure the temperature of the feed inside the stainless steel tube just before the feed stream enters the first membrane module.

The vapour phase streams exiting the permeate side of each of the three membrane modules flowed through three individual cold traps. The permeate side of the three membrane modules and the three cold traps were maintained at a very low pressure (3 Torr) using a vacuum pump (Scroll Pump, 78603-11, Cole-Parmer, Montreal, Quebec, Canada). A digital pressure gauge was used to monitor the vacuum pressure. The three cold traps were immersed into a liquid nitrogen Dewar. The level of liquid nitrogen in the Dewar was controlled using an automatic time-fill controller (Gordinier Electronics Inc, model 359 liquid time fill, Roseville, Michigan, USA). At the end of an experiment, the permeate side of the membrane module was returned to atmospheric pressure and the cold traps were removed from the liquid nitrogen Dewar. The permeate samples were thawed, then weighed and analyzed for their composition using High-Performance Liquid Chromatography (HPLC).

To investigate the effect of the operating temperature on the membrane performance, 37°C considered as the reference temperature since it is the temperature of the ABE fermentation broth. Neat and composite PDMS membranes were tested for a fixed concentration of butanol (5 g/L) over a temperature range of 37-57°C.

Moreover, to study the effect of the activated carbon nanoparticle loading on PDMS membrane performance, different concentrations of activated carbon nanoparticles (2-8 wt% of membrane) were incorporated into the polymeric matrix. The performance of PDMS membranes prepared in our laboratory was investigated using an aqueous solution of 5 g/L butanol in the feed.

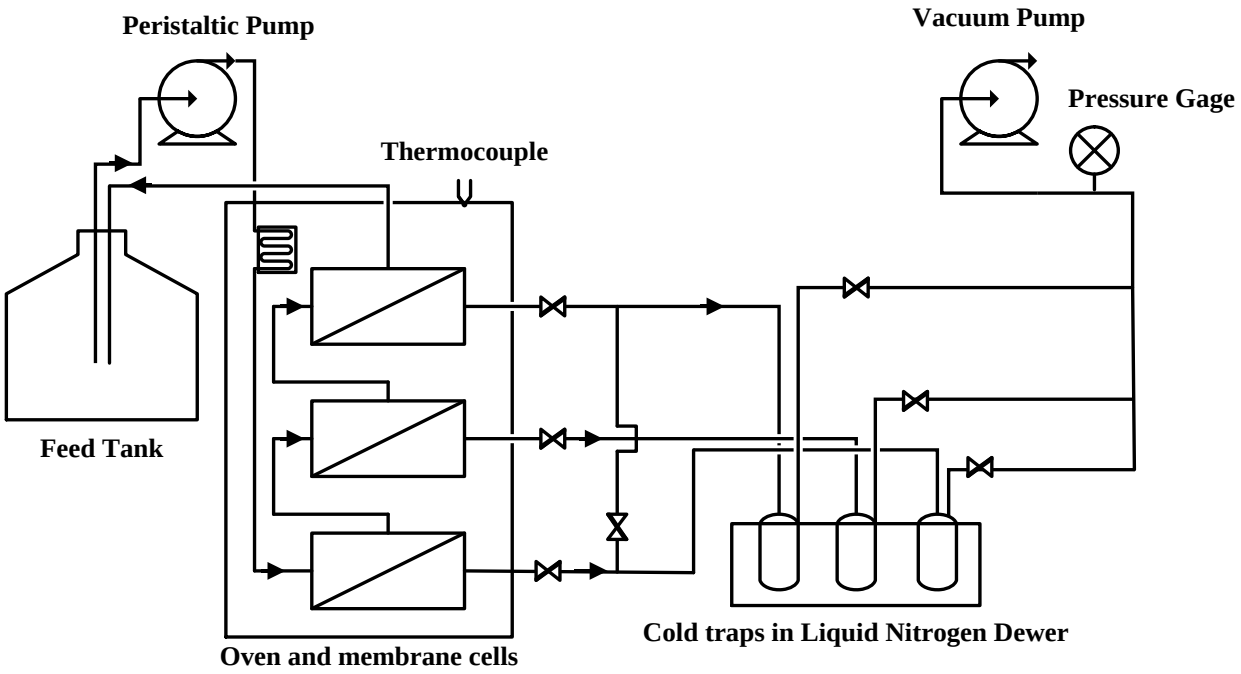

Figure 2-1 Schematic diagram of the three-module pervaporation membrane experimental system used in the present study.

High Performance Liquid Chromatography (HPLC)

The composition of permeate and feed mixtures was measured using High Performance Liquid Chromatography (HPLC - Waters, Mississauga, ON, Canada). The detector, the pump and the auto-sampler were Refractive Index Detector (Waters 2414), Isocratic HPLC pump (Waters 1515) and Autosampler (Waters 717 plus), respectively. To heat the column of the HPLC to the desired temperature, an external column heater was used. The column used in the HPLC to measure the composition of the binary solution was the Vertex column (300x9x8 mm, KNAUER, Berlin, Germany) packed with Eurokat H, 10 µm. Since butanol-water solutions are immiscible over a wide range of concentration, the two-phase mixtures were diluted using known amounts of distilled deionized water to go down to the concentration levels where there is no immiscibility in order to always inject a single phase solution into the HPLC for concentration measurements. At the end of the composition measurements, they were corrected according to the amount of dilution needed with the deionized water.

Performance metrics

To characterise the pervaporation separation performance, the flux (J), the separation factor (α) and the pervaporation separation index (PSI) were used. Ideally, it is desired to have a high permeation flux accompanied by a high separation factor. The separation factor is a metrics which assesses the separation ability of the membrane considering two substances to be separated. The flux is the permeate flow per unit membrane surface area which is normally determined for each species from the individual permeated amounts. It can also be determined for all species for the total permeation flux. The pervaporation separation index is a metrics that enables the comparison of the performance of membranes with different properties. These parameters for individual species *i* are defined in Equations (2)-(4)[53,54]:

$$J_i = \frac{m_i}{At} = \frac{P_i}{L}(\gamma_i x_i P^{sat} - y_i P^p) \quad \textbf{(2)}$$

$$\alpha_i = \frac{{y_i}/{(1-y_i)}}{{x_i}/{(1-x_i)}} \quad \textbf{(3)}$$

$$PSI = J_t(\alpha_i - 1) \quad \textbf{(4)}$$

where m_i is the mass of species *i* in the permeate stream (*g*), *A* is the effective surface area of the membrane (m^2), *t* is the time of permeation (*h*), y_i and x_i are the mass fractions of species *i* in the permeate and feed streams, respectively and P_i is the membrane permeability for component *i*. *L* is the thickness of the membrane, P^{sat} is saturated vapor pressure (*bar*), P^p is permeate side pressure (*bar*) and γ_i is the activity coefficient in feed liquid. These parameters are highly dependent on the membrane material, thickness, vacuum pressure, feed temperature and the feed composition[55].

Results and discussion

Morphology and structure of activated carbon nanoparticle-PDMS

Figure 2-2 shows the SEM images of the neat and nanocomposite PDMS membranes with the latter having an activated carbon nanoparticle loading of 6 wt%. Figure 2-2a clearly shows that a

very uniform, smooth and homogenous surface with no void and defect results from the fabrication of a neat PDMS membrane. With the incorporation of nanoparticles within the matrix of the membrane, as shown in Figure 2-2b, the membrane surface became rougher which leads to a larger surface area. As seen in the SEM images, dispersed activated carbon nanoparticles in the membrane were completely surrounded by the PDMS polymer. It appeared that the AC filler had a good interface compatibility with the hydrophobic PDMS phase. The AC nanoparticles were uniformly dispersed in the PDMS polymer with no apparent defective structure, which resulted in butanol pervaporation separation performance without any leakage problem. This can be attributed to the compatibility of the particle with the silicone elastomeric base, and also to the high volatility of the doping solvent used in membrane preparation[40].

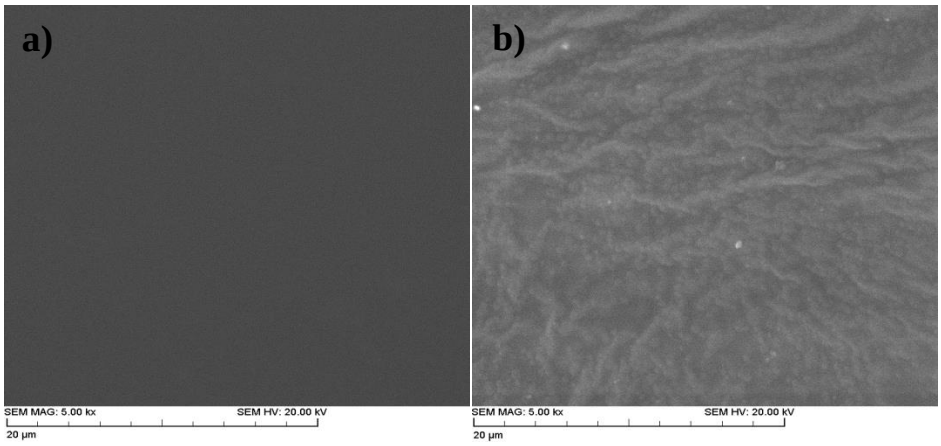

Figure 2-2 SEM images of the surface of the membrane for a) neat PDMS, b) 6 wt% AC-PDMS.

SEM analysis was also done for the other nanocomposite membranes with a filler concentration of 2-8 wt%. Since there were no significant differences between the surface views of the membranes with different nanoparticle concentration, the top view SEM images for those membranes are not included, and only the surface images of the neat and 6 wt% AC-PDMS are shown in Figure 2-2.

It should be noted that the thickness of all membranes has also been measured to be 310-365 µm.

Degree of swelling and nanoparticle adsorption capacity

Table 2-1 shows the degree of swelling for AC-PDMS mixed matrix membranes immersed in pure water, pure butanol and butanol-water binary solutions of different concentrations.

Measurements were made over a period of 48 h and the degree of swelling was calculated using Equation (1). It is important to consider that in the case of mixed matrix membranes, the degree of swelling is confounded with the additional adsorption capacity of the membrane due to the presence of solid adsorbent particles in the PDMS matrix which may not result in actual swelling of the membrane even if there is a mass gain. As can be seen in Table 2-1, the degree of the swelling for water is suddenly increasing by adding the adsorbent due to the water sorption into the particles. However, the degree of swelling by water in general is very small and can be safely neglected.

Results showed that the degree of swelling of the PDMS membranes for butanol obtained in this study were very similar to the results reported in the literature with a degree of swelling of around 15.6% in pure butanol[29]. In addition, the degree of swelling of the AC-PDMS membranes for pure butanol continuously decreased with an increase in the AC nanoparticles loading. This could be due to the strong non-covalent interaction between nanoparticles and PDMS matrix which elevated the cohesive energy of membranes. Also, the chain extension effect increased the modulus of PDMS polymer which is also confirmed by the tensile test[56]. Moreover, the results for the binary butanol aqueous solutions showed that a higher concentration of butanol in the solution increases the degree of swelling of the membrane.

The swelling behavior could be explained by the Hansen's solubility parameters (δ) of each component which consists of three types of interactions: hydrogen bonding interactions (δ_h), polar interactions (δ_p) and dispersion interactions (δ_d)[48]. These parameters are usually used to measure the distance parameter (Δ) defined as the distance between two components based on their respective partial solubility parameter components. A smaller value of Δ implies a greater affinity between two substances.

Table 2-1 Degree of swelling (wt%) of neat and mixed-matrix PDMS membranes for pure water, pure butanol and different butanol concentration in butanol-water binary solutions.

Membrane	*Pure Water*	*Pure Butanol*	*5 g/L*	*20 g/L*	*50 g/L*
Neat PDMS	0.16	14.6	0.38	0.46	0.78
2% AC-PDMS	0.42	16.7	0.27	0.57	1.14
4% AC-PDMS	0.27	16.5	0.38	1.38	0.86
6% AC-PDMS	0.45	15.7	0.59	0.88	1.31
8% AC-PDMS	0.29	15.4	0.45	1.30	1.75

Based on the study of Rozicka et al. on the affinity of butanol and water for PDMS membranes, it was determined that hydrogen bonding and polar interaction parameters control the affinity of the components. Water/PDMS has a greater distance parameter (41.4 $MPa^{1/2}$) than butanol/PDMS (13.0 $MPa^{1/2}$) which indicates that butanol has a higher affinity for PDMS. The component which has a greater affinity with the PDMS membrane will be preferentially absorbed and diffuse through the membrane[48,55].

Moreover, Abdehagh et al.[45] studied the adsorption isotherms of activated carbons (F400 and F600 activated carbon) for the ABE fermentation components and revealed that these adsorbents are excellent candidates for butanol adsorption from ABE solutions. Activated carbons F400 and F600 had a very favorable isotherm with an equilibrium butanol adsorption capacity of 300 and 150 mg/g with solution of 1.4 g/L and 1.75 g/L equilibrium butanol concentration, respectively[45]. It was therefore desired to use particles with similar adsorption properties as the F400 activated carbon, but at a much finer size, to be embedded within the PDMS polymeric matrix. The activated carbon nanoparticles used in this study for the mixed matrix membranes have a size ranging from 20 to 40 nm and their adsorption capacity was measured using batch adsorption experiments at room temperature. Result showed that the equilibrium adsorption capacity of the nanoparticles for equilibrium butanol concentration of 2.97 g/L was 350 (mg/g) which is comparatively very high. It is worth mentioning that the adsorption capacity of the nanoparticles in this study was approximately 130% and 16% higher than activated carbons F600 and F400, respectively. Results of Table 2-1 indicate that the fabricated composite membranes preserved

the high affinity with butanol. Furthermore, based on the results for the different concentrations of butanol, the degree of swelling for the membrane in the range of typical butanol percentage in ABE fermentation broths (in the vicinity of 10 g/L) is relatively small and it could be safely neglected.

Surface hydrophobicity

Figures 2-3 shows the surface static contact angle for pure water and 0.5 wt% butanol. Generally, when the water contact angle is larger than 90º, the membrane surface is considered as hydrophobic. As can be seen in this figure, the surface static contact angle of water on PDMS surfaces increases slightly upon the addition of nanoparticles in the matrix of the membranes. This small increase in the static contact angle leads to slightly higher membrane hydrophobicity. However, the difference in contact angle for water when the nanofiller concentration varies between 2 and 6 wt% is not significant. The contact angle for butanol solution was almost constant within the range of 0-6 wt% of the nanoparticles and a small incremental increase was observed when nanoparticle concentration increased from 6 to 8 wt%. Moreover, the static contact angle of the butanol/water binary solutions is smaller than for pure water as a result of the butanol presence in the solution, resulting in a greater affinity between the liquid and the membrane surface.

Since the mechanism of mass transfer for the pervaporation separation is the solution-diffusion, a more hydrophobic membrane surface contributes to an increase in the butanol sorption selectivity and, as a result, enhance the membrane performance for this separation.

Contact angle measurement images are presented in Figure 2-4 for neat PDMS and 8% AC-PDMS membranes. The small contact angles observed for pure butanol (Figures 2-4c and 2-4d) in comparison to pure water (Figure 2-4a and 2-4b), indicates the higher affinity of butanol with PDMS membranes. The slight change in water static surface contact angle is attributed to the increase in the surface roughness as a result of the incorporation of the AC nanofillers in the PDMS membranes. This behaviour also has been reported by other researchers[57].

Table 2-2 Surface roughness parameters using ImageJ based on the ISO 4287/2000 standard (all units are in pixels).

Membrane	R_q *(root mean square deviation)*	R_a *(arithmetical mean deviation)*	R_v *(lowest valley)*	R_p *(highest peak)*
Neat PDMS	3.54	2.83	-14.88	15.14
2% AC-PDMS	3.70	2.95	-14.93	17.78
4% AC-PDMS	3.91	3.11	-15.47	17.55
6% AC-PDMS	5.05	4.02	-20.33	22.94
8% AC-PDMS	5.24	4.18	-21.62	23.65

Roughness index parameters are given in Table 2-2. Measurements showed that the roughness of the membrane increased slightly by adding AC nanofillers from 0 wt% to 4 wt% of activated carbon nanoparticle. Furthermore, by adding 6 wt% AC nanoparticles in the matrix of the membrane, the roughness increased by 29% compared to the one at 4 wt % AC nanoparticles in the PDMS membrane. This increase might be attributed to the small aggregation of the AC nanoparticles when the concentration of the particle increases.

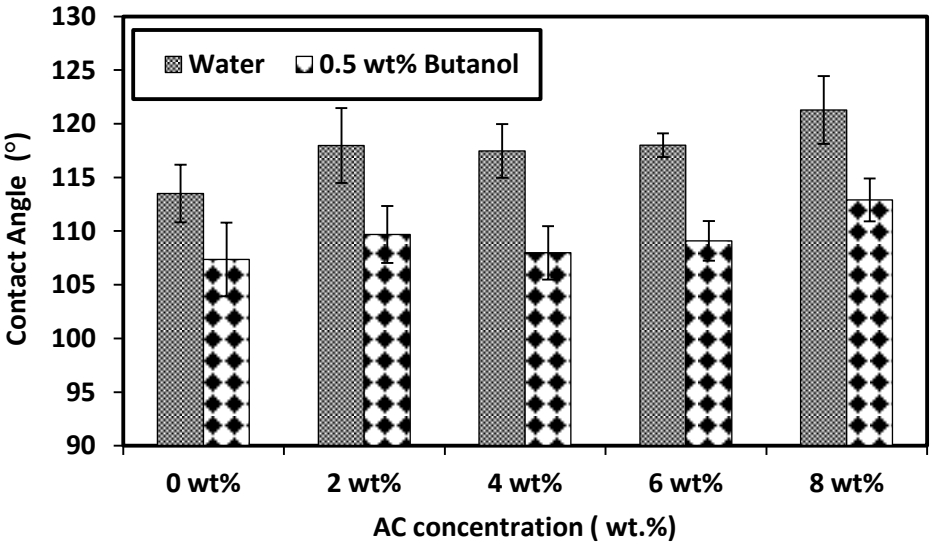

Figure 2-3 Surface static contact angle of PDMS composite membranes for pure water and 0.5 wt% butanol solution.

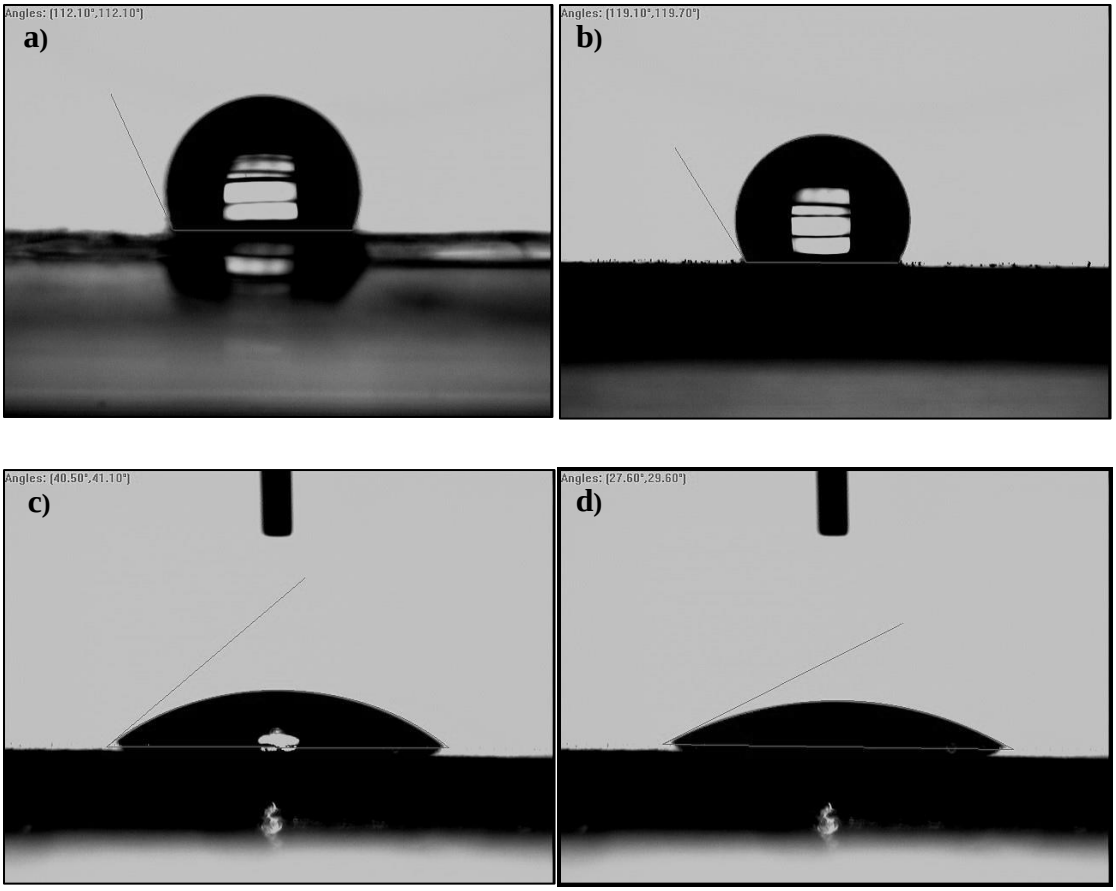

Figure 2-4 Contact angle images of a) Neat PDMS/water after 6 s, b) 8 % AC-PDMS/water after 6 s, c) 8 % AC-PDMS/pure butanol after 6 s, and d) 8% AC-PDMS/pure butanol after 1 min.

Mechanical stability

Tensile tests were performed on the neat PDMS and AC-PDMS nanocomposite membranes where the elongation of the membrane samples was recorded against the applied force. Results in terms of stress-strain curves are presented in Figure 2-5. Significant improvement in the mechanical properties of the mixed matrix membranes is observed with an increase in the AC nanofiller content. As a higher stress was required in the case of the nanocomposite PDMS membranes to produce the same strain, the addition of AC nanoparticles within the polymer matrix has stiffened the mixed matrix PDMS membranes.

Results show that, by increasing the amount of activated carbon nanoparticles, the initial

Young's modulus of elasticity increased as indicated by the slope of the stress-strain curves. This phenomenon was also observed for different nanoparticles such as carbon nanotubes[58]. The increase in the modulus of elasticity is attributed to the cross-linking effect of nanoparticles at the low concentrations with PDMS which results in an improved rigidity of the membrane matrix[59]. Moreover, the 6% AC-PDMS composite membrane has the best mechanical stability among all membranes. The engineering stress decreased after increasing the amount of activated carbon nanoparticles from 6 to 8 wt%. This could be as a result of the agglomeration of the nanoparticles in the matrix of the membrane at higher concentrations which would lead to a weaker structure. However, it should be noted that the mechanical strength of the nanocomposite membrane at 8 wt% is still significantly higher than the one for neat PDMS membrane. The same trend in the result was also reported for the carbon-nanotube PDMS composite membranes[40].

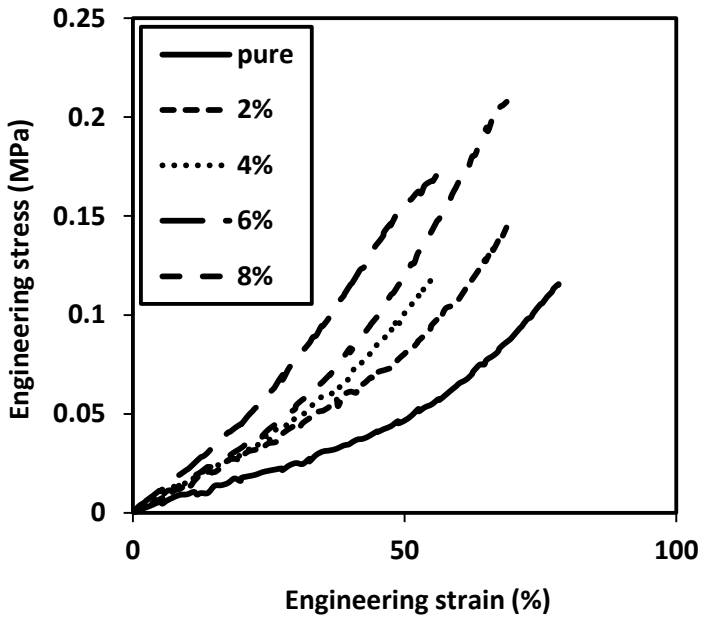

Figure 2-5 Relation between tensile stress and strain for neat PDMS and AC-PDMS membranes with different loading of the AC in PDMS.

Effect of the concentration of activated carbon nanoparticles on the membrane performance

The effect of the addition of activated carbon nanoparticles in the matrix of PDMS membranes on the butanol pervaporation separation from binary aqueous solutions at a feed temperature of 57°C was studied for different percentages of AC nanoparticles ranging from 2 to 8 wt% in the PDMS matrix. Table 2-3 shows that by increasing the percentage of activated carbon nanoparticles in the matrix of PDMS membranes, the separation factor increased continuously where a 39% increase was observed at a nanoparticle concentration of 8 wt% compared to the neat PDMS membrane. The effective permeability of butanol and water reached their maximum values at a concentration of the nanofillers of 6 wt% where increases of 99% and 47% in their values were observed, respectively, compared to the neat PDMS membrane. Moreover, the highest value of the *PSI* was 1076 ($g/m^2.h$) which was obtained with the 6% AC-PDMS membrane at 57°C. Based on the results of Table 2-3, the membrane effective permeability for both water and butanol decreased when the nanoparticle concentration increased from 6 to 8 wt%. According to the results of the mechanical stability, the polymer chain rigidification and the hindrance in chain movements at higher AC filler concentrations could be the reasons which resulted in the lower flux and effective permeability.

Table 2-3 Pervaporation performance of neat PDMS and AC-PDMS composite membranes in contact with a 0.5 wt% butanol feed aqueous solution at 57°C.

Membrane	α_b	P_b *(g.cm/s.cm^2.bar)*	P_w *(g.cm/s.cm^2.bar)*	*PSI (g /m^2.h)*
Neat PDMS	18.6	4.55×10^{-7}	1.46×10^{-7}	570.6
2% AC-PDMS	20.9	7.17×10^{-7}	2.09×10^{-7}	806.0
4% AC-PDMS	21.3	7.75×10^{-7}	2.22×10^{-7}	862.8
6% AC-PDMS	25.2	9.49×10^{-7}	2.3×10^{-7}	1076.2
8% AC-PDMS	25.9	7.76×10^{-7}	1.83×10^{-7}	879.0

Results show that the activated carbon nanoparticles could have an important contribution on the improvement of the pervaporation performance. The presence of nanoparticle adsorbents in the matrix of the membrane would potentially result in a faster adsorption rate of butanol which would further bring about a larger flux and a higher separation factor. Moreover, the AC nanoparticles act as active sorption sites which, because of their relatively high porosity, provide an alternative pathway for mass transport through the inner pores of the adsorbent or along the smooth and hydrophobic surface area between the AC particles and the polymer matrix. Figure 2-6 shows a schematic diagram of the AC nanoparticles assisting the butanol permeation through the membrane. The permeability of butanol and water increased as a result of the lower resistance for mass transfer across the membrane when the concentration of nanoparticles increases with a maximum being reached at 6 wt%. This means that the presence of the nanoparticles has a beneficial effect on both butanol and water permeation fluxes. Since the permeability of butanol increased much more than the permeability of water with the same amount of the activated carbon particles, the total flux and butanol separation factor were enhanced by the incorporation of nanoparticles.

The separation factor enhancement obtained by adding nanoparticles could also be attributed to the dual sorption mode when activated carbon nanoparticles are present in the PDMS matrix: one in the polymer matrix and the other in the activated carbon particles. The high adsorptive capacity of activated carbon for butanol could potentially enhance the pervaporation separation performance of the resulting mixed-matrix membrane.

The enhanced adsorption rate at the liquid/membrane interface, as a result of the contribution of the adsorptive effect of the nanoparticles, also leads to an increase in the butanol flux of the PDMS composite membranes.

A comparison between membranes fabricated in this study and some membranes reported in the literature is presented in Table 2-4. It should be mentioned that the operating conditions and membrane thicknesses presented in Table 2-4 were the closest data in the literature to those used in this study such that an exact comparison was not possible. The common method of studying the membrane pervaporation performance is with reporting data in terms of fluxes and separation factors. However, these values are not only a function of the exact properties of the membranes

which were studied, but also depend on the operating conditions such as the feed concentration, permeate pressure and feed temperature as well as the PDMS molecular weight.

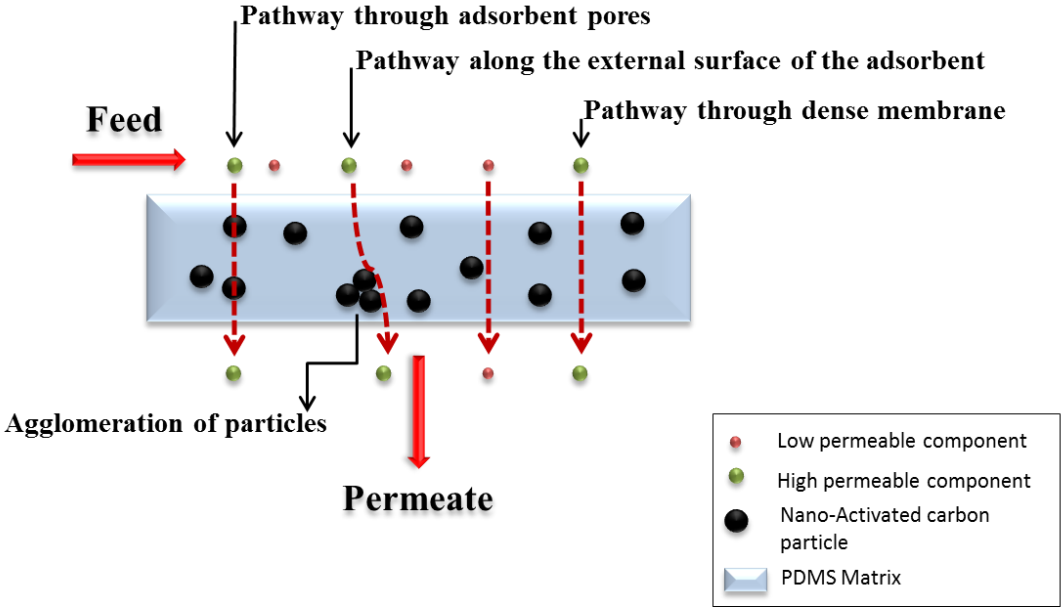

Figure 2-6 Schematic diagram of a membrane with AC nanoparticle assisting butanol permeation

Therefore, it appears that the flux and separation factor are not appropriate metrics to compare the pervaporation data sets obtained under different operating conditions. A better method of reporting the pervaporation data is the membrane permeability and permeance. Comparing the membrane developed in this study with PDMS-PS[60] and PDMS-POSS[61] membranes, the nanocomposite membranes tested in this investigation had a 460% and 236% higher separation factor, respectively, as well as higher permeability. As can be noted in Table 2-4, PDMS-CNTs membrane has a higher flux and separation factor than the 6% AC-PDMS membrane. However, it is important to emphasize that the thickness of the membrane is 33% less than the membrane used in this work which obviously results in higher flux for CNTs-PDMS. In addition, the operating temperature was 23^{o}C higher than the temperature used this study which contributed to the higher separation factor and flux for the CNTs-PDMS membrane[62,63]. It should be mentioned that the CNT filler concentration in the work of Xue et al. was 10 wt%[40] which is approximately 66% higher than the loading used in this work. Furthermore, carbon nanotubes are generally much more expensive than activated carbon particles which would impact the economic viability of the membrane at an industrial scale. Nevertheless, this is an avenue to explore especially if

carbon nanotubes can be preferentially aligned perpendicularly to the membrane surface. In addition, considering the effect of the membrane thickness on the membrane performance, a decrease in the thickness of the membrane is desirable and should be an objective[63].

Table 2-4 Comparison between the performances of PDMS mixed matrix membranes of this study and other studies.

Membrane	*T (°C)*	*L (μm)*	*(α_b)*	*J_T (g/m^2h)*	*P_b ($g.cm/s.cm^2.bar$)*	*Ref*
PS-PDMS	50	100-150	4.5	-	2.00×10^{-7}	[60]
CNTs-PDMS[*]	80	200	32.9	244	-	[40]
POSS-PDMS	40	9	7.5	-	3.00×10^{-7}	[61]
6% AC-PDMS	57	310-365	25.2	44.5	9.49×10^{-7}	This work

[*] CNT concentration at 10 wt%

Effect of the operating temperature

The effect of the operating temperature on the pervaporation separation performance of PDMS-activated carbon nanoparticles is illustrated in Figure 2-7. Results show that both the permeate flux and the separation factor increased as the operating temperature increased from 37 to 57°C. With an increase in temperature, the movement of the segments of the polymer through its matrix increases thereby resulting in the presence of a larger free volume and an increase in permeate flux. Furthermore, as the temperature increases, the driving force which is the partial pressure difference across the membrane increases significantly which also leads to an enhancement in the permeate flux.

a)

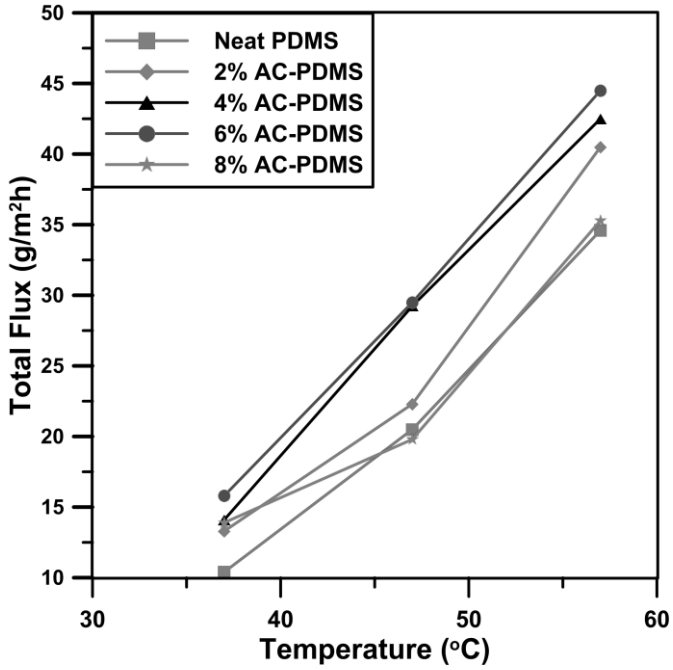

b)

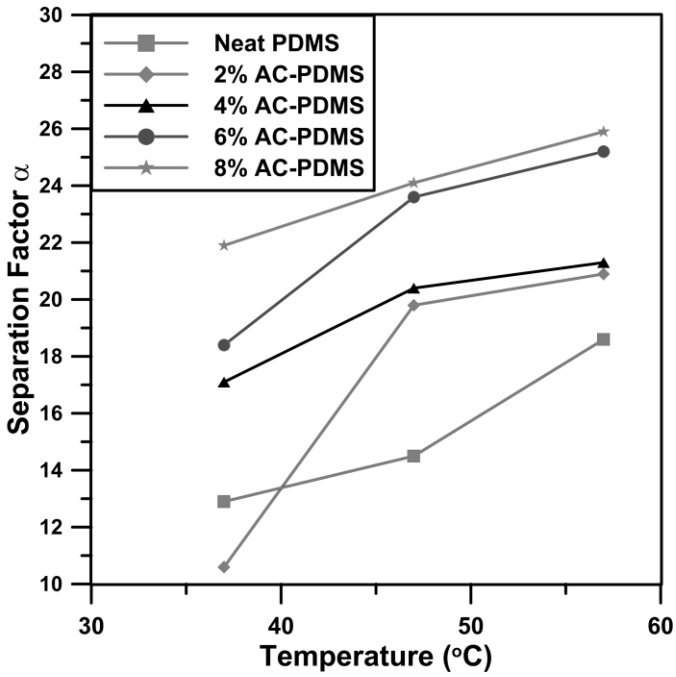

Figure 2-7 Effect of the operating temperature on the performance of AC-PDMS membranes: a) total permeation flux and b) separation factor.

The temperature dependence of the flux usually follows the Arrhenius expression given by Equation (5):

$$J = J_0 \exp\left(\frac{-E_a}{RT}\right) \quad (5)$$

In Figure 2-8, the natural logarithm of the flux is plotted as a function of the inverse absolute temperature for the 6%AC-PDMS membrane for a feed concentration of 0.5 wt% butanol. The slope of the line for each component is related to the activation energy of the permeation of each component. For the data of Figure 2-8, the activation energy of permeation for butanol was estimated to be 66.4 (*kJ/mol*) which is higher than the one for water at 43.9 (*kJ/mol*). As a result, the permeation of butanol through the membrane is more sensitive to temperature than the one of water. With an increase in temperature, the permeation flux of butanol would increase more than the permeation flux of water. This is equivalent to an improvement in the separation factor with an increase in temperature[64].

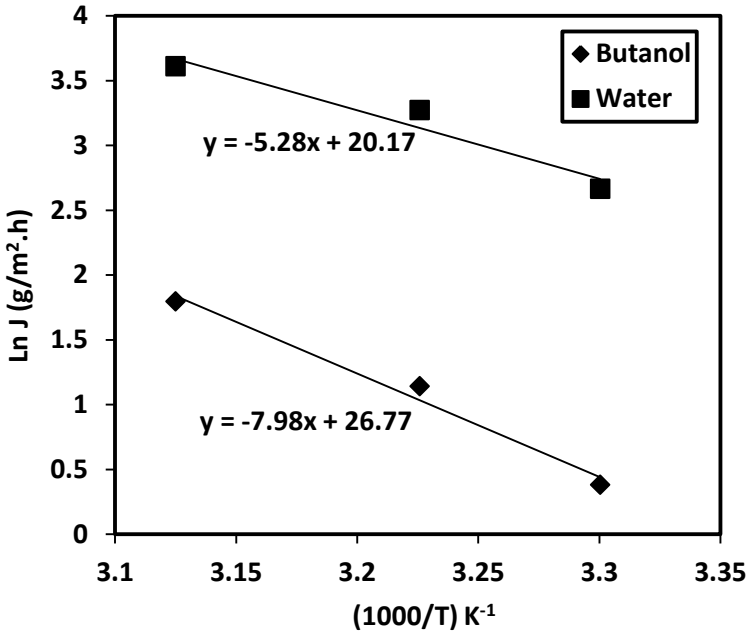

Figure 2-8 Arrhenius plots of the flux of water and butanol for 6% AC-PDMS membrane for a feed mass concentration of 0.5% butanol in water.

Conclusions

Composite membranes made of PDMS and activated carbon nanoparticles were developed for the pervaporation separation of butanol from binary aqueous solutions. The addition of the AC

nanofillers enhanced remarkably the mechanical stability of the mixed matrix membranes and the level of enhancement increased with the concentration of nanoparticles.

Results of the membrane performance showed that a maximum permeate flux was achieved for a PDMS nanocomposite membrane at 37°C with a nanoparticle concentration of 6 wt% with a 42.6% increase compared to the neat PDMS whereas the separation factor increased continuously with the incorporation of the activated carbon nanoparticles with a 58.1% increase compared to neat PDMS at a concentration of 8 wt% of the nano-fillers. Additional sorption sites resulted from the incorporation of the activated carbon nanoparticles along with the new pathways for permeation of the butanol through the membrane due to the porous structure of the nanofillers resulted in an enhanced performance of the membrane. Results also demonstrated that the increase in the operating temperature from 37 to 57°C resulted in an improvement of the PDMS composite membrane performance. This study indicates that the presence of a nanoparticle adsorbent in the matrix of a membrane would be useful for pervaporation separation of biobutanol from ABE fermentation broth.

Acknowledgements

The authors would like to acknowledge the financial support of the Natural Science and Engineering Research Council of Canada.

Nomenclature

A	Effective surface area of the membrane (m^2)
J	Permeation flux ($g/m^2.h$)
L	Membrane thickness (m)
m_i	Mass of species i in the permeate stream (g)
P_i	Permeability of component i ($g.cm/s.cm^2.bar$)
P^{sat}	Saturation pressure (bar)
P^p	Permeate side pressure (bar)

PSI	Pervaporation separation index ($g/m^2.h$)
SD	Degree of swelling
t	Time of permeation (h)
W_d	Weight of the dry membrane (g)
W_d	Weight of the swelled membrane (g)
x_i	Mass fraction of species i in the feed streams
y_i	Mass fraction of species i in the permeate
α_i	Separation factor of species i
γ_i	Activity coefficient

Abbreviations

ABE	Acetone, Butanol, Ethanol
AC	Activated carbon
CNTs	Carbon nanotubes
EPDM	Ethylene propylene diene rubber
HPLC	High Performance Liquid Chromatography
LLE	Liquid-liquid extraction
MMM	Mixed matrix membrane
PAI	Polyamide-imide
PAN	Polyacrylonitrile
PDMS	Polydimethylsiloxane
PE	Polyethylene
PEBA	Polyether block-amide

PMS	Poly (methoxy siloxane)
PP	Polypropylene
PTFE	Polytetrafluoroethylene
SCA	Static contact angle
SEM	Scanning Electron Microscope

References

1 Abdehagh N, Thibault J, Tezel, F.H. Separation techniques in butanol production: Challenges and developments. *Biomass Bioenergy* 2014; **60**: 222–246.

2 Zhu Y, Xin F, Chang Y, Zhao Y, Weichong W. Feasibility of reed for biobutanol production hydrolyzed by crude cellulase. *Biomass Bioenergy* 2015; **76**: 24–30.

3 Harvey BG, Meylemans HA. The role of butanol in the development of sustainable fuel technologies. *J Chem Technol Biotechnol* 2011; **86**: 2–9.

4 Jadhav SB, Harde S, Bankar SB, Granstrom T, Ojamo H, Singhal RS, Survase SA. A green process for the production of butanol from butyraldehyde using alcohol dehydrogenase: process details. *Rsc Adv* 2014; **4**: 14597–14602.

5 Xue C, Wang Z, Wang S, Zhang X, Chen L, Mu Y, Bai F-W. The vital role of citrate buffer in acetone–butanol–ethanol (ABE) fermentation using corn stover and high-efficient product recovery by vapor stripping–vapor permeation (VSVP) process. *Biotechnol Biofuels* 2016; **9**: 146.

6 Liu X, Gu Q, Liao C, Yu X. Enhancing butanol tolerance and preventing degeneration in Clostridium acetobutylicum by 1-butanol–glycerol storage during long-term preservation. *Biomass Bioenergy* 2014; **69**: 192–197.

7 Dong H, Tao W, Dai Z, Yang L, Gong F, Zhang Y, Li Y. Biobutanol. *Adv Biochem Eng-Biotechnol* 2012; **128**: 85–100.

8 Groot WJ, Vandenoever CE, Kossen NWF. Pervaporation for Simultaneous Product Recovery in the Butanol Isopropanol Batch Fermentation. *Biotechnol Lett* 1984; **6**: 709–714.

9 Mariano AP, Keshtkar MJ, Atala DIP, Maugeri Filho F, Wolf Maciel MR, Maciel Filho R, Stuart P. Energy Requirements for Butanol Recovery Using the Flash Fermentation Technology. *Energy Fuels* 2011; **25**: 2347–2355.

10 Mariano AP, Qureshi N, Maciel Filho R, Ezeji TC. Assessment of in situ butanol recovery by vacuum during acetone butanol ethanol (ABE) fermentation. *J Chem Technol Biotechnol* 2012; **87**: 334–340.

11 Xue C, Yang D, Du G, Chen L, Ren J, Bai FW. Evaluation of hydrophobic micro-zeolite-mixed matrix membrane and integrated with acetone–butanol–ethanol fermentation for enhanced butanol production. *Biotechnol Biofuels* 2015; **8**: 105.

12 Qureshi N, Blaschek HP. Butanol recovery from model solution/fermentation broth by pervaporation: evaluation of membrane performance. *Biomass Bioenergy* 1999; **17**: 175–184.

13 Xue C, Liu F, Xu M, Zhao J, Chen L, Ren J, Bai FW, Yang ST. A novel in situ gas stripping-pervaporation process integrated with acetone-butanol-ethanol fermentation for hyper n-butanol production. *Biotechnol Bioeng* 2016; **113**: 120–129.

14 Li S-Y, Srivastava R, Parnas RS. Study of in situ 1-Butanol Pervaporation from A-B-E Fermentation Using a PDMS Composite Membrane: Validity of Solution-Diffusion Model for Pervaporative A-B-E Fermentation. *Biotechnol Prog* 2011; **27**: 111–120.

15 Lipnizki F, Hausmanns S, Laufenberg G, Field R, Kunz B. Use of pervaporation/bioreactor hybrid processes in biotechnology. *Chem Ing Tech* 1998; **70**: 1587–1595.

16 Liu G, Wei W, Wu H, Dong X, Jiang M, Jin W. Pervaporation performance of PDMS/ceramic composite membrane in acetone butanol ethanol (ABE) fermentation-PV coupled process. *J Membr Sci* 2011; **373**: 121–129.

17 Essawy H, Tawfik M, El-Sabbagh S, El-Gendi A, El-Zanati E, Abdallah H. Novel amphiphilic conetworks based on compatibilized NBR/SBR–montmorillonite nanovulcanizates as membranes for dehydrative pervaporation of water–butanol mixtures. *Polym Eng Sci* 2014; **54**: 1560–1570.

18 Jitesh KD, Pangarkar VG, Niranjan K. Pervaporative stripping of acetone, butanol and ethanol to improve ABE fermentation. *Bioseparation* 2000; **9**: 145–154.

19 Vrana DL, Meagher MM, Hutkins RW, Duffield B. Pervaporation of Model Acetone-Butanol-Ethanol Fermentation Product Solutions Using Polytetrafluoroethylene Membranes. *Sep Sci Technol* 1993; **28**: 2167–2178.

20 Müller M, Pons M-N. Coupling of gas membrane smooth pervaporation and alcoholic fermentation. *J Chem Technol Biotechnol* 1991; **52**: 343–358.

21 Hu M, Gao L, Fu W, Liu X, Huang F, Luo Y, Huang C. High-performance interpenetrating polymer network polyurethane pervaporation membranes for butanol recovery. *J Chem Technol Biotechnol* 2015; **90**: 2195–2207.

22 Liu F, Liu L, Feng X. Separation of acetone–butanol–ethanol (ABE) from dilute aqueous solutions by pervaporation. *Sep Purif Technol* 2005; **42**: 273–282.

23 Jalal TA, Bettahalli NMS, Le NL, Nunes SP. Hydrophobic Hyflon AD/Poly(vinylidene fluoride) Membranes for Butanol Dehydration via Pervaporation. *Ind Eng Chem Res* 2015; **54**: 11180–11187.

24 Hickey PJ, Juricic FP, Slater CS. The Effect of Process Parameters on the Pervaporation of Alcohols through Organophilic Membranes. *Sep Sci Technol* 1992; **27**: 843–861.

25 Li S-Y, Srivastava R, Parnas RS. Separation of 1-butanol by pervaporation using a novel tri-layer PDMS composite membrane. *J Membr Sci* 2010; **363**: 287–294.

26 Xue C, Du G-Q, Chen L-J, Ren J-G, Bai FW. Evaluation of asymmetric polydimethylsiloxane-polyvinylidene fluoride composite membrane and incorporated with acetone-butanol-ethanol fermentation for butanol recovery. *J Biotechnol* 2014; **188**: 158–165.

27 Borisov IL, Malakhov AO, Khotimsky VS, Litvinova EG, Finkelshtein ES, Ushakov NV, Volkov VV. Novel PTMSP-based membranes containing elastomeric fillers: Enhanced 1-butanol/water pervaporation selectivity and permeability. *J Membr Sci* 2014; **466**: 322–330.

28 Wang Y, Chung TS, Wang H. Polyamide–imide membranes with surface immobilized cyclodextrin for butanol isomer separation via pervaporation. *AIChE J* 2011; **57**: 1470–1484.

29 Mai NL, Kim SH, Ha SH, Shin HS, Koo Y-M. Selective recovery of acetone-butanol-ethanol from aqueous mixture by pervaporation using immobilized ionic liquid polydimethylsiloxane membrane. *Korean J Chem Eng* 2013; **30**: 1804–1809.

30 Jeon EJ, Kim AS, Lee YT. Pervaporation of butanol/water mixtures using siloxane polymer/ceramic composite membranes. *Desalination Water Treat* 2012; **48**: 17–26.

31 Vane LM, Namboodiri VV, Meier RG. Factors affecting alcohol–water pervaporation performance of hydrophobic zeolite–silicone rubber mixed matrix membranes. *J Membr Sci* 2010; **364**: 102–110.

32 Huang J, Meagher MM. Pervaporative recovery of n-butanol from aqueous solutions and ABE fermentation broth using thin-film silicalite-filled silicone composite membranes. *J Membr Sci* 2001; **192**: 231–242.

33 Fouad EA, Feng X. Pervaporative separation of n-butanol from dilute aqueous solutions using silicalite-filled poly(dimethyl siloxane) membranes. *J Membr Sci* 2009; **339**: 120–125.

34 Huang JC, Meagher MM. Pervaporative recovery of n-butanol from aqueous solutions and ABE fermentation broth using thin-film silicalite-filled silicone composite membranes. *J Membr Sci* 2001; **192**: 231–242.

35 Jonquieres A, Fane A. Filled and unfilled composite GFT PDMS membranes for the recovery of butanols from dilute aqueous solutions: Influence of alcohol polarity. *J Membr Sci* 1997; **125**: 245–255.

36 Garg P, Singh RP, Choudhary V. Pervaporation separation of organic azeotrope using poly(dimethyl siloxane)/clay nanocomposite membranes. *Sep Purif Technol* 2011; **80**: 435–444.

37 Zhou H, Su Y, Chen X, Yi S, Wan Y. Modification of silicalite-1 by vinyltrimethoxysilane (VTMS) and preparation of silicalite-1 filled polydimethylsiloxane (PDMS) hybrid pervaporation membranes. *Sep Purif Technol* 2010; **75**: 286–294.

38 Peng P, Shi B, Lan Y. Preparation of PDMSSilica Nanocomposite Membranes with Silane Coupling for Recovering Ethanol by Pervaporation. *Sep Sci Technol* 2011; **46**: 420–427.

39 Liu X, Li Y, Liu Y, Zhu G, Liu J, Yang W. Capillary supported ultrathin homogeneous silicalite-poly(dimethylsiloxane) nanocomposite membrane for bio-butanol recovery. *J Membr Sci* 2011; **369**: 228–232.

40 Xue C, Du G-Q, Chen L-J, Ren J-G, Sun J-X, Bai FW, Yang ST. A carbon nanotube filled polydimethylsiloxane hybrid membrane for enhanced butanol recovery. *Sci Rep* 2014; **4**: 5925–5925.

41 Singh G, Rana D, Matsuura T, Ramakrishna S, Narbaitz RM, Tabe S. Removal of disinfection byproducts from water by carbonized electrospun nanofibrous membranes. *Sep Purif Technol* 2010; **74**: 202–212.

42 Majumder M, Keis K, Zhan X, Meadows C, Cole J, Hinds BJ. Enhanced electrostatic modulation of ionic diffusion through carbon nanotube membranes by diazonium grafting chemistry. *J Membr Sci* 2008; **316**: 89–96.

43 Boom J, Punt I, Zwijnenberg H, de Boer R, Bargeman D, Smolders C, Strathmann H. Transport through zeolite filled polymeric membranes. *J Membr Sci* 1998; **138**: 237–258.

44 Aroon MA, Ismail AF, Matsuura T, Montazer-Rahmati MM. Performance studies of mixed matrix membranes for gas separation: A review. *Sep Purif Technol* 2010; **75**: 229–242.

45 Abdehagh N, Tezel FH, Thibault J. Adsorbent screening for biobutanol separation by adsorption: kinetics, isotherms and competitive effect of other compounds. *Adsorption* 2013; **19**: 1263–1272.

46 Anson M, Marchese J, Garis E, Ochoa N, Pagliero C. ABS copolymer-activated carbon mixed matrix membranes for CO2/CH4 separation. *J Membr Sci* 2004; **243**: 19–28.

47 Chen D, Chen F, Hu X, Zhang H, Yin X, Zhou Y. Thermal stability, mechanical and optical properties of novel addition cured PDMS composites with nano-silica sol and MQ silicone resin. *Compos Sci Technol* 2015; **117**: 307–314.

48 Zhou H, Su Y, Chen X, Wan Y. Separation of acetone, butanol and ethanol (ABE) from dilute aqueous solutions by silicalite-1/PDMS hybrid pervaporation membranes. *Sep Purif Technol* 2011; **79**: 375–384.

49 Baghbanzadeh M, Rana D, Matsuura T, Lan CQ. Effects of hydrophilic CuO nanoparticles on properties and performance of PVDF VMD membranes. *Desalination* 2015; **369**: 75–84.

50 Kwok DY, Neumann AW. Contact angle measurement and contact angle interpretation. *Adv Colloid Interface Sci* 1999; **81**: 167–249.

51 ImageJ. http://rsb.info.nih.gov/ij/, accessed November 2015. .

52 Agboola O, Maree J, Mbaya R. Characterization and performance of nanofiltration membranes. *Environ Chem Lett* 2014; **12**: 241–255.

53 Niemisto J, Kujawski W, Keiski RL. Pervaporation performance of composite poly(dimethyl siloxane) membrane for butanol recovery from model solutions. *J Membr Sci* 2013; **434**: 55–64.

54 Karlsson H, Tragardh G. Pervaporation of Dilute Organic-Waters Mixtures - a Literature-Review on Modeling Studies and Applications to Aroma Compound Recovery. *J Membr Sci* 1993; **76**: 121–146.

55 Hasanoglu A, Salt Y, Keleser S, Ozkan S, Dincer S. Pervaporation separation of organics from multicomponent aqueous mixtures. *Chem Eng Process* 2007; **46**: 300–306.

56 Liu G, Zhou T, Liu W, Hu S, Pan F, Wu H ,Jiang Z, Wang B, Yang J, Cao X. Enhanced desulfurization performance of PDMS membranes by incorporating silver decorated dopamine nanoparticles. *J Mater Chem A* 2014; **2**: 12907–12917.

57 Lan Y, Yan N, Wang W. Application of PDMS pervaporation membranes filled with tree bark biochar for ethanol/water separation. *RSC Adv* 2016; **6**: 47637–47645.

58 Frogley MD, Ravich D, Wagner HD. Mechanical properties of carbon nanoparticle-reinforced elastomers. *Compos Sci Technol* 2003; **63**: 1647–1654.

59 Baghbanzadeh M, Rana D, Lan CQ, Matsuura T. Effects of Inorganic Nano-Additives on Properties and Performance of Polymeric Membranes in Water Treatment. *Sep Purif Rev* 2016; **45**: 141–167.

60 Shin C, Chelsea Chen X, Prausnitz JM, Balsara NP. Effect of block copolymer morphology controlled by casting-solvent quality on pervaporation of butanol/water mixtures. *J Membr Sci* 2017; **523**: 588–595.

61 Liu G, Hung W-S, Shen J, Li Q, Huang Y-H, Jin W, Lee KR, Lai JY. Mixed matrix membranes with molecular-interaction-driven tunable free volumes for efficient bio-fuel recovery. *J Mater Chem A* 2015; **3**: 4510–4521.

62 Baker RW, Wijmans JG, Huang Y. Permeability, permeance and selectivity: A preferred way of reporting pervaporation performance data. *J Membr Sci* 2010; **348**: 346–352.

63 Wijmans JG. Process performance = membrane properties + operating conditions. *J Membr Sci* 2003; **220**: 1–3.

64 Zhou H, Su Y, Chen X, Wan Y. Separation of acetone, butanol and ethanol (ABE) from dilute aqueous solutions by silicalite-1/PDMS hybrid pervaporation membranes. *Sep Purif Technol* 2011; **79**: 375–384.

3. Chapter 3

Separation of organic compounds from ABE model solutions via pervaporation using AC-PDMS-PAN mixed matrix membranes

Hoda Azimi, Arian Ebneyamini, F. Handan Tezel and Jules Thibault*

Abstract

The pervaporation separation of organic compounds from acetone-butanol-ethanol (ABE) fermentation model solutions was studied using activated carbon (AC) nanoparticle-PDMS mixed matrix membranes (MMM). The effects of the operating conditions and nanoparticle loading content on the membrane performance have been investigated. While the separation factor increased continuously with an increase in the concentration of nanoparticles, the total flux reached a maximum in the MMM with 8 wt% nanoparticle loading in PDMS. Both the separation factor for butanol and the total permeation flux more than doubled for the MMM in comparison to those of neat PDMS membranes prepared in this study. In addition, the flux and separation factor of the AC-PDMS mixed matrix membranes were superior to the performance reported for commercial PDMS membranes also tested in this study. Moreover, increasing the feed temperature led to a decrease in the separation factor of all ABE components whereas the total flux increased for the mixed matrix membranes. Higher initial concentration of the organic components in the feed solution resulted in a higher total flux whereas the separation factor decreased with an increase in the nanoparticle loading up to 8 wt%. The trend in the total flux with respect to butanol concentration increased with AC loading up to 8 wt% and then decreased for 10 wt% AC loading.

Keywords: Pervaporation; Activated carbon nanoparticle; PDMS; ABE; Mixed matrix membrane

Introduction

In comparison to distillation which is the most common separation method used in industry, pervaporation is considered as a highly promising technique for recovering volatile components from alcoholic fermentation broths. Pervaporation, which combines permeation and vaporisation, has advantages such as: (1) it is not harmful to microorganisms and (2) it requires less energy

since only the permeates are converted to the vapour phase [1]. In alcoholic fermentations, in situ recovery can alleviate product inhibition and improve productivity [2]. Butanol is the main alcohol produced in the acetone-butanol-ethanol (ABE) fermentation and can be used as a gasoline replacement fuel or for numerous other applications [3]. Butanol becomes toxic to the microorganisms when its concentration reaches approximately 1 wt%. It would be advantageous to partly removing butanol in situ during fermentation to reduce product inhibition and increase butanol productivity. Pervaporation can be used to selectively remove butanol from the fermentation broth [4–8]. To make the pervaporation process economically viable for the selective removal of butanol from ABE fermentation broths, factors such as membrane stability, butanol separation factor and permeation flux need to be as high as possible [9]. Different polymers have been used to manufacture membranes that were evaluated for butanol pervaporation separation: styrene butadiene rubber (SBR) [10], ethylene propylene diene rubber (EPDM) [11], polytetrafluoroethylene (PTFE) [12], polypropylene (PP) [13], polyurethane (polyether based) (PUR) [14], polyether block-amide (PEBA) [15], poly (vinylidinedifluoride) (PVDF) [16], poly (methoxy siloxane) (PMS) [17], poly (dimethylsiloxane) (PDMS) [18], poly (1-(trimethylsilyl)-1-propyne) (PTMSP) [19] and polyamide-imide (PAI) containing cyclodextrin (CD) [20]. Amongst all these membranes, silicone membranes like PDMS have been reported to be a good choice for butanol pervaporation separation [21–24].

However, despite the relatively good performance of PDMS membranes, there is a clear need to further enhance their performance. Indeed, pervaporation PDMS membranes suffer from low permeability and low separation factor in addition to possessing weak mechanical strength. Moreover, making PDMS membranes is very challenging in terms of controlling the thickness of the membrane and selecting an appropriate backing material.

The pervaporation mass transfer process relies on the solution-diffusion mechanism. As a result, to improve the performance of a membrane for ABE fermentation broth, the selective sorption and the selective diffusion of butanol within the membrane should be as high as possible [25]. To improve the solubility and diffusivity of the desired chemical species, it has been suggested to incorporate small adsorbent particles, with a high affinity for butanol, within the matrix of the PDMS [18, 26]. Activated carbon particles have been reported as a suitable adsorbent to enhance the separation of butanol from the other ABE components such as water, acetone and ethanol [4,

27]. In this study, mixed matrix PDMS membranes have been fabricated by adding different concentrations of activated carbon nanoparticles in the matrix of the PDMS to improve their performance for the separation of butanol from ABE model solutions. To better control the membrane fabrication process, spray-coating using an airbrush pen has been adopted.

To the best of our knowledge, this is the first time that activated carbon nanoparticles have been embedded within the matrix of PDMS membranes for the pervaporation separation of organic compounds from ABE model solutions. A previous study reported the performance of AC-PDMS membranes for binary butanol aqueous solutions [18]. In order to decrease the thickness of the membranes and thereby increase the permeation flux, an airbrush was used in this investigation to uniformly spray the PDMS-AC solution on top of a backing material. Furthermore, this is the first time that the use of an airbrush pen is used for coating PDMS as a thin and uniform layer on top of the backing material to manufacture pervaporation membranes.

Materials and Methods

Materials

Polyacrylonitrile (PAN) membranes, used as a support for PDMS in this study, were purchased from Synder Filtration (Vacaville, CA, USA) with a molecular weight cut-off of 30 000 Da and a thickness (Polyester + PAN) of 0.15 mm. PDMS and cross-linking agent kit (RTV615 001- KIT) were obtained from Momentive Co. (Hebron, Ohio, USA). Super activated porous carbon nanopowder (US1074: particle size 20-40 nm, with a pore size of 3.5 nm and specific surface area greater than 1400 m^2/g) was purchased from US-Nano Company (South Bend, IN, USA). Commercial PDMS membranes with a total thickness of 200-235 μm (130, 100, 3-5 μm for Polyethylene terephthalate (PET), Polyimide (PI) and PDMS, respectively) were obtained from Pervatech B.V. Company (Rijssen, Netherlands). Butanol (99% pure, Acros), acetone (95% pure, Acros) and ethanol (99% pure, Acros) were obtained from Fisher Scientific (Fair Lawn, NJ, USA). Deionized distilled water was used to prepare all solutions.

Membrane fabrication

Neat PDMS membrane active layer

Polyacrylonitrile (PAN) membrane was used as a backing material to deposit a thin PDMS layer. The PAN membrane was first immersed in water and then taped on a glass plate. A 1 wt% PDMS-toluene solution without adding crosslinking agent was prepared as the pre-layer solution and sprayed on the surface of the PAN in order to have a better attachment between the active layer and the support. The PDMS solution for the active layer was prepared by mixing 5 g of the base PDMS solution from the silicone kit in 20 g of toluene. The solution was thoroughly mixed using a stirrer (RZR 2102, Heidolph Electronic, Illinois, USA) for one hour and then 0.5 g of the crosslinking agent was added to this mixture and stirred for an additional 30 min. The PDMS solution was then sprayed onto the PAN membrane using an air pen brush (Paasche VL-SET Double Action Siphon Feed Airbrush) in two successive layers. The main solution was first sprayed as uniformly as possible in one direction onto the PAN support and, after one hour under ambient conditions, the membrane was turned 90^{o} and the second layer was sprayed as for the first layer. The glass plate with the membrane was then placed in a vacuum oven. The vacuum oven was maintained at an absolute pressure of 0.2 bar for 30 min at room temperature and then the oven was heated up to 90°C for 3 h (including the pre heating) while maintaining the same vacuum pressure. Following this curing procedure, the membrane was taken out of the oven and cooled to room temperature. Coupons of 5.0 cm in diameter of the cured membrane were cut to fit the size of the membrane holder in the membrane test module. The active area of the membrane was 13.5 cm^2.

Activated Carbon (AC) nanoparticles-PDMS mixed matrix membranes

To fabricate the mixed matrix membranes, a procedure similar to the one mentioned above for the neat PDMS membrane was followed. However, different weight percentages of activated carbon nanoparticles in the range of 4 to 10 wt% were added to the main solution for the preparation of the active layer. The different nanoparticle percentages were evaluated using Equation (1). The nanoparticles were first thoroughly mixed within 20 g of toluene using a sonicator (QSONICA, Part No.Q700, Fullerton, USA) at ambient temperature for 2 h. Then, 5 g

of PDMS was added to the mixture and mixed. After 1 hour, 0.5 g of the crosslinking agent was added and mixed for 30 min. The spray nozzle was large enough to spray the solution without any clogging and to ensure that the AC-PDMS solution was sprayed uniformly. The same procedure described in the previous section was then used to apply the two successive layers of the AC-PDMS solution, including the subsequent curing of the membrane.

$$wt_{AC}\% = \frac{W_{AC}}{W_{PDMS} + W_{AC}} \times 100 \quad (1)$$

where, W_{AC} and W_{PDMS} are the weights of the nanoparticle and the polymer in the membrane casting solution.

Membrane characterization

Morphology

The top surface and the cross section of all membranes were examined using a Scanning Electron Microscope (SEM, Vega-II XMU VPSEM and Anatech Hummer VII, Battle Creek, MI, U.S.). To prepare the samples for SEM analysis, membranes were immersed in liquid nitrogen and then cut sharply. The samples were broken perpendicular to the membrane surface in order to take SEM images of the cross-sectional area. Each sample was fixed on a support using carbon tape and was gold sputtered before SEM observations were made [28, 29].

Degree of swelling (DS)

To measure the degree of swelling of the active layer of the membranes in contact with the feed solutions, PDMS and AC-PDMS films were prepared without backing material (PAN membrane). Membrane films of the same weight were immersed into bottles containing pure components of water, butanol, ethanol, acetone as well as ABE model solutions at room temperature. The concentrations of the three swelling tests performed with ABE model solutions were (A: 0.25, B: 0.5, E: 0.08) wt%, (0.5, 1.0, 0.17) wt% and (1.0, 2.0, 0.33) wt%, respectively, with the rest of the solution being water. These latter concentrations are based on the ABE ratio of a typical fermentation: 3:6:1. Following an immersion of 24 h, the membrane samples were retrieved from the sealed bottles; the swollen membranes were gently blotted with a paper wiper

(Kimwipes, Kimtech) to rapidly remove any surface solution. The swelled membrane samples were then weighed using a precise digital balance and returned to the bottle to observe if further swelling would occur. The same procedure was repeated until saturation was reached and no further weight change was observed. The degree of swelling (DS) of the membranes, expressed as a weight percentage, was determined via Equation (2).

$$DS = \frac{W_s - W_d}{W_d} \times 100 \quad (2)$$

where W_s and W_d are the weights of the swelled and dry membrane samples, respectively [21].

Gas chromatography (GC)

The gas chromatograph (GC) used in this study was purchased from chromatographic specialties (SRI Instrument, Brockville, Canada). The GC was equipped with a flame ionization detector (FID). A Stabilwax column (10655-126), 30 m long and 0.53 mm internal diameter and a 5 m long guard column (Restek, Chromatography Specialties, Brockville, Canada) was used to determine the concentrations of acetone, ethanol and butanol in the feed model solutions and in the permeate samples. Helium was used as the carrier gas and the column temperature was initially set at 80˚C when a sample was injected and this temperature was kept constant for 2 min and then increased to 200˚C at a rate of 20˚C/min. The column needed around 2 min for cooling down prior to the injection of the next sample. Effectively, the GC was capable of analyzing one injection every 11 min. The injector and FID detector temperatures were 250˚C and 110˚C, respectively.

Pervaporation

Pervaporation experiments were performed using the experimental setup that is schematically presented in Figure 3-2. Three membrane modules were connected in series to ensure identical flow rate in the retentate side of each membrane module. The feed flow rate was high enough to consider a nearly constant retentate concentration in each module and to ensure nearly zero-stage cut condition. Moreover, the decrease in temperature of the feed solution while flowing through

each membrane module was negligible since the permeate flow rate was on average 30000 times smaller than the feed flow rate. The feed stream from the ABE model solution was pumped through the first pervaporation cell using a peristaltic pump. The three-module membrane system was placed in a temperature-controlled oven. The feed stream flowed through a long stainless steel coil upon entering the oven to ensure the feed stream reaches the temperature set point prior to entering the first membrane module. A thermocouple was used to measure the temperature of the feed inside the stainless steel tube just before the feed stream enters the first membrane module. The temperature was monitored using LabVIEW. At the exit of the oven, the retentate flow passed through a cooling coil which was immersed into a cold water bath prior to be returned to the feed tank.

The vapour permeate stream of each of the three membrane modules passed through a cold trap immersed in liquid nitrogen Dewar where permeates were condensed. The permeate side of the membrane modules and the cold traps were maintained at a very low pressure (less than 6 torr) using a vacuum pump (vacuum pressure air pump 115V, Cole-Parmer, Montreal, Quebec, Canada). A digital pressure gauge was used to monitor the vacuum pressure. The level of liquid nitrogen in the Dewar was controlled using an automatic time-fill controller (Gordinier Electronics Inc, model 359 liquid time fill, Roseville, Michigan, USA) to ensure the Dewar flask contained sufficient liquid nitrogen to immerse the cold traps. The average time of each pervaporation experiment was about 18 h. Furthermore, numerical simulations were performed to estimate the time necessary to reach steady state and it was found to be negligible compared to the time of the experiment. At the end of each experiment, permeates were thawed, then weighed and analyzed for their composition using gas chromatography (GC).

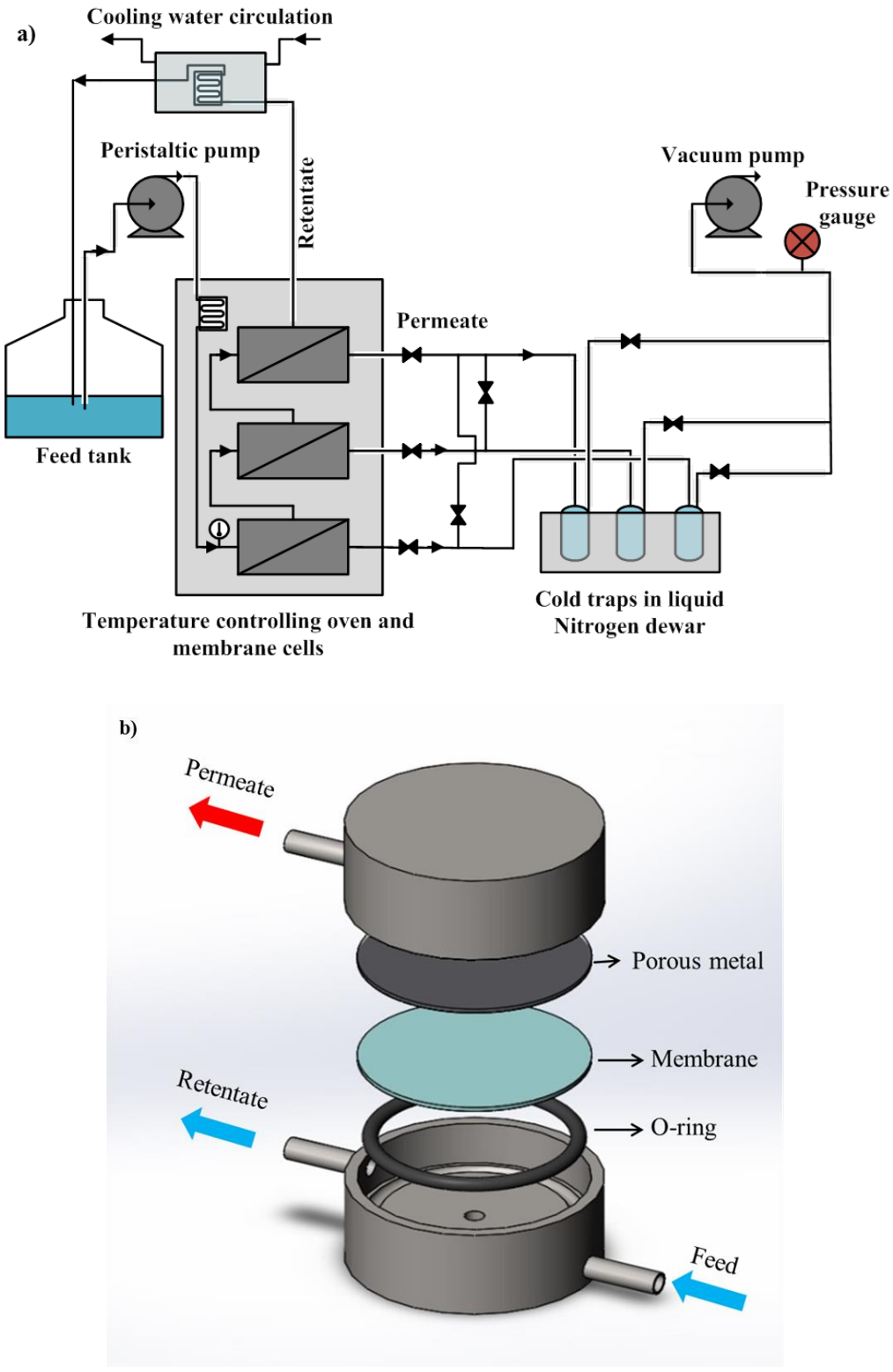

Figure 3-1 Schematic diagram of a) the three-module membrane pervaporation experimental system, b) an exploded view of a membrane testing module.

Three different feed butanol concentrations between 0.5-2 wt% have been used to study the effect of the initial feed concentration on the performance of the membranes. The concentrations of acetone and ethanol have been also changed accordingly to maintain a 3:6:1 ABE solvent ratio of a typical ABE fermentation broth.

To investigate the effect of the operating temperature on the membrane performance, membranes were tested for a fixed concentration of butanol over a temperature range of 40-80°C.

Moreover, to study the effect of the activated carbon nanoparticle loading in the matrix of PDMS membranes, different concentrations of activated carbon nanoparticles (4-10 wt% embedded in the membrane) have been considered.

Performance metrics

To characterise the pervaporation separation performance, the flux (J) and the separation factor (α) were used. The flux (J) is the permeate flow rate per unit membrane surface area which is normally determined for each species from the total permeation flux and permeate mass fraction of each species. The separation factor is a metrics that assesses the separation ability of the membrane considering two substances to be separated. These parameters for individual species i are defined in Equations (3) and (4):

$$J_i = \frac{m_i}{At} \quad \textbf{(3)}$$

$$\alpha_i = \frac{\frac{y_i}{1-y_i}}{\frac{x_i}{1-x_i}} \quad \textbf{(4)}$$

where m_i is the mass of species i in the permeate stream (g), A is the effective surface area of the membrane (m^2), t is the time of permeation (h), y_i and x_i are the mass fractions of species i in the permeate and feed streams, respectively.

Results and discussion

Morphology and structure of AC-PDMS

SEM images in Figure 3-2 show the cross section and the surface morphology of the 8 wt% AC-PDMS layer deposited on a PAN membrane. The active layer average thickness of the membrane was about 30 μm which is the dense AC-PDMS layer and the average total thickness of the backing material or the PAN membrane was around 130 □m. Furthermore, Figure 3-2a shows clearly that a uniform PDMS active layer has been deposited on the PAN porous layer where an intimate contact clearly seems to exist between the two layers. Moreover, it can be seen that there is no defect or void which could have been caused by the agglomeration of the nanoparticles in the membrane.

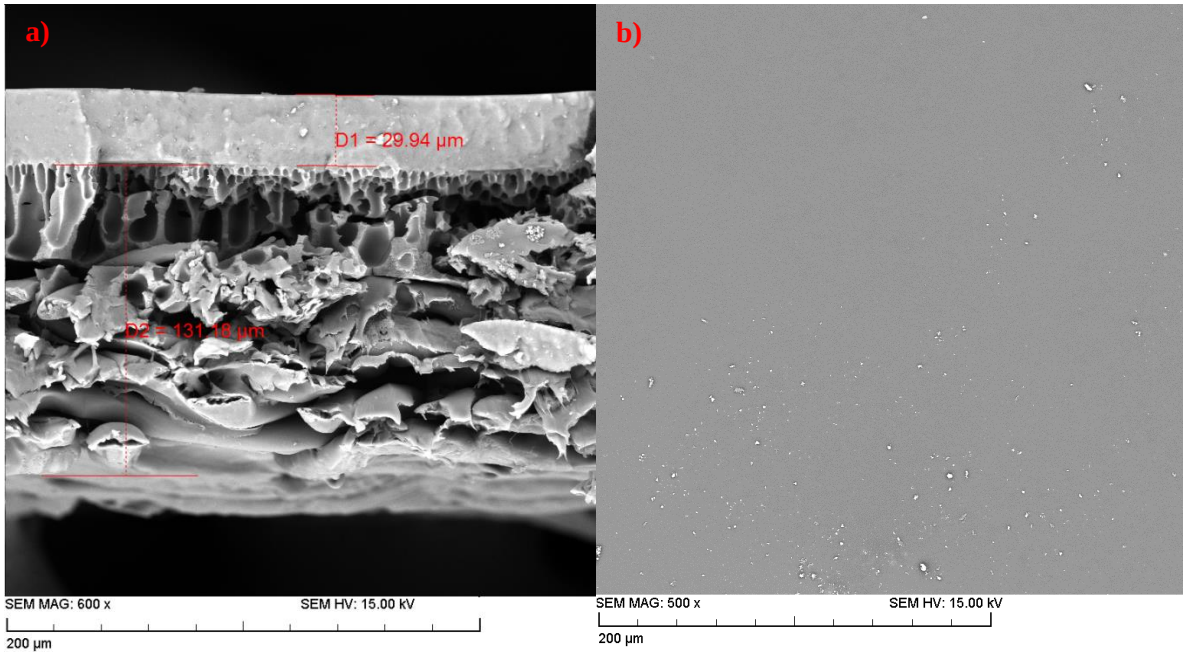

Figure 3-2 SEM pictures of a) cross section of the 8 wt% AC-PDMS layer deposited on a PAN membrane, b) top surface of the 8 wt% AC-PDMS membrane.

The top surface SEM image in Figure 3-2b shows the dense structure of the PDMS membrane. In addition, the top layer of the membrane is very smooth, further suggesting a uniform distribution of the nanofillers throughout the membrane. Since there were no significant differences between the surface views and the cross-section images of the membranes with

different nanoparticle concentrations, the SEM images for other membranes are not presented, and only the surface image and the cross-section image of 8 wt% AC-PDMS are shown in Figure 3-2.

Degree of swelling (DS)

The pervaporation separation process is assumed to follow the solution-diffusion model. The sorption of species into the membrane is a selective step based on the different solubility properties of the components, depending mainly on their polarity and the cohesive energy density. For a greater sorption, the target component and the membrane should have approximately similar polarities. The rate of transportation of a species through the membrane is determined by diffusion, which is influenced by the shape and the molar volume of the permeant. Smaller molecules such as water and ethanol in the case of ABE fermentation broth have higher mobility. The interaction of the membrane and the species can be defined by the swelling degree of the membrane for each component. Swelling of PDMS-based membranes is a common phenomenon, and it has a critical impact on the structure and performance of the membranes. The degree of swelling is a direct parameter that is used to evaluate the swelling-resistance of membranes [30].

The swelling behaviour of the PDMS and AC-PDMS films are shown in Figure 3-3a for pure acetone, butanol, ethanol and water components as a function of the nanoparticle loading. Based on the experimental data, acetone led to the highest level of swelling which indicates that the affinity between acetone and the membrane is the highest with roughly 21% degree of swelling for neat PDMS membranes. Butanol also led to a relatively high degree of swelling with approximately 15% followed by ethanol and water for neat PDMS membranes with approximately 4% and 0.4%, respectively. These results follow the same trend as reported by Mai et al. [31]. Furthermore, increasing the amount of particle loading had a negligible effect on the swelling degree of the PDMS mixed matrix membranes for pure organic components.

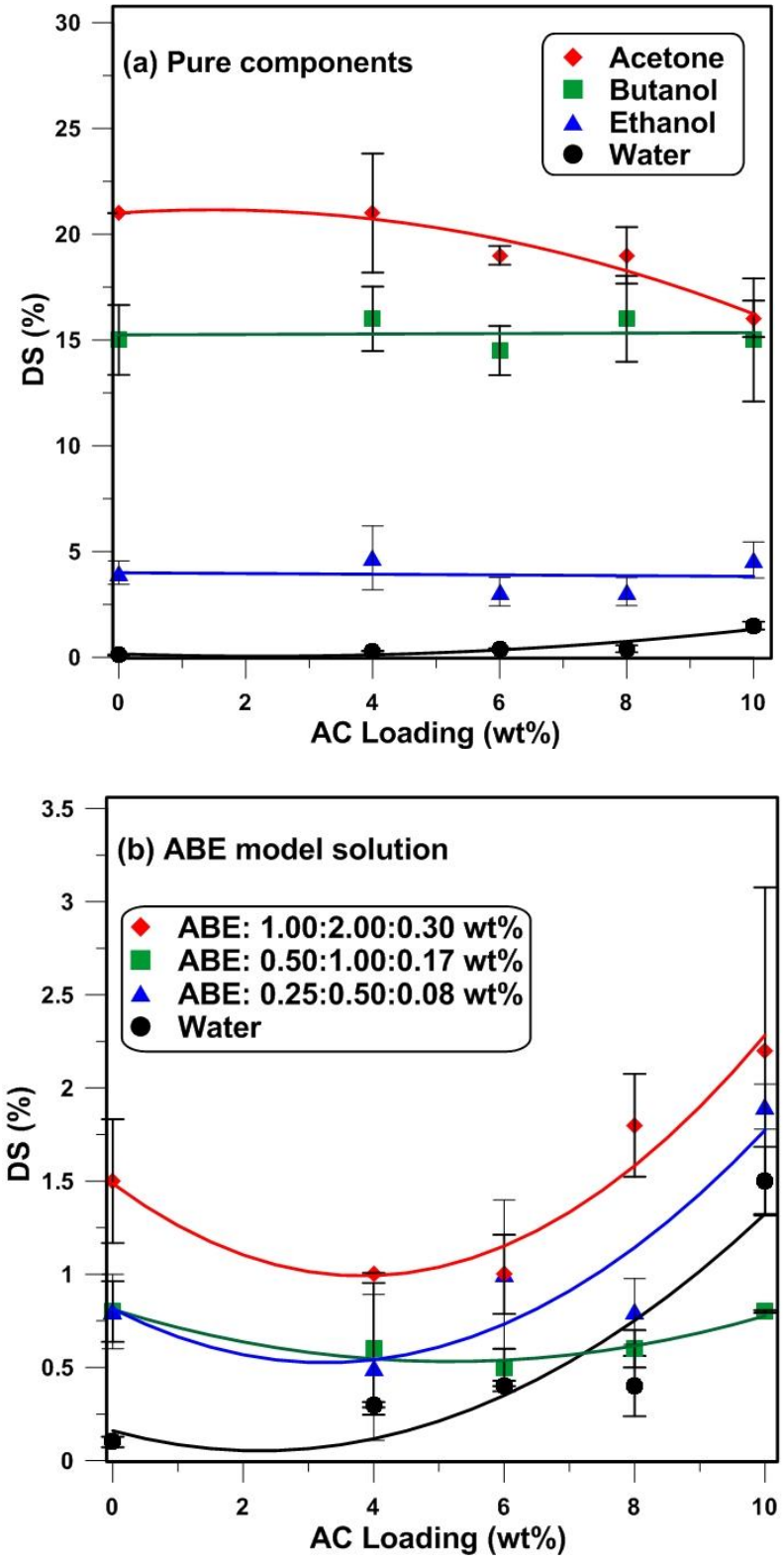

Figure 3-3 Degree of swelling of the mixed matrix membranes as a function of the nanoparticle loading in a) pure components and b) ABE model solutions at the room temperature.

The degree of swelling of mixed matrix membranes for pure water and for different concentrations of ABE model dilute solutions are presented in Figure 3-3b. Results show that, generally, an increase in the ABE solvent concentration leads to an increase in the degree of swelling. This is due to the high solubility of the ABE components [32, 33]. Figure 3-3b also reveals that by increasing the nanoparticle loading in the matrix of the PDMS, the sorption of the ABE components and especially water increased. This results in an increase on the weight of the sample and, as a result, higher degree of swelling is calculated.

Niemisto et al. [34] examined the solvent-PDMS membrane interaction of each of the ABE components in terms of the distance ($\Delta_{PDMS,i}$) calculated from the three Hansen solubility parameters (HSPs). These three parameters are: hydrogen bonding interactions (δ_h), polar interactions (δ_p) and dispersion interactions (δ_d) which are cohesive forces keeping liquid molecules together and resulting in the interactions between the membrane and the feed solution molecules. These parameters were developed as a way of predicting if one material will dissolve in another and form a solution. The Hansen solubility parameters are usually used to calculate the distance parameter (Δ) defined as the distance between two components based on their respective partial solubility parameter components. Two components having a distance value (Δ) closer to zero are more likely to have a higher affinity to each other. Therefore, a smaller value of (Δ) implies a greater affinity between two substances. Table 3-1 presents the distance parameter reported by Niemisto et al. for PDMS for the main components of the ABE fermentation solution. As can be seen from this table, PDMS has the highest affinity towards acetone, followed by butanol, ethanol and water. The same order is also observed in the degree of swelling for pure components as shown in Figure 3-3a. In addition, the adsorption capacity of the activated carbon nanoparticles was measured in a previous study [18]. It was shown that these particles have high adsorption capacity for some ABE compounds. For binary butanol aqueous solutions, the adsorption capacity was 350 (*mg/g*) in equilibrium with a solution of 3 g/L. For ABE model solutions, the competitive adsorption capacities of activated carbon F400 were 193.3, 25, 7 (*mg/g*) for butanol, acetone and ethanol respectively with the solution of 5 g/L butanol [35].

Table 3-1 Solubility parameters of the ABE components [34].

Solvent-membrane interaction	***Acetone***	***Butanol***	***Ethanol***	***Water***
$\Delta_{PDMS,i}$ ($J^{1/2}.m^{-3/2}$)	10.6	12.4	17.1	40.9

Effect of the activated carbon nanoparticle loading on the membrane performance

The effect of the nanoparticle concentration on the performance of the MMM has been studied by performing a series of pervaporation experiments with a typical ABE model solution to measure the separation factor and the permeation flux with the AC nanoparticle concentration varying from 0 to 10 wt% in the PDMS membrane. Results are presented in Figure 3-4. As can be seen in Figure 3-4a, the addition of the activated carbon nanoparticles to the PDMS matrix strongly affects the pervaporation performance of the membrane. The mixed matrix membrane total permeation flux reached a maximum at 8 wt% nanoparticle loading, which is more than twice the value observed for the neat PDMS membrane. It is important to note that the permeation flux for the mixed matrix membrane with 8 wt% of nanoadditives is higher than that of the commercial PDMS membrane despite that the PDMS layer of the commercial membrane is approximately seven times thinner. The increase in permeation flux with the higher concentration of nanoparticles is due to the creation of additional sorption sites and the cave-like porous structure resulting from the partial incompatibility of the polymer chain and the activated carbon nanoparticles. The cave-like pores and the porous structure of the particles are providing new pathways of higher permeability for the components in the feed to pass through the membrane. The decrease of the flux from a concentration of 8 to 10 wt% AC nanoparticles could be due to restriction in the polymer chains mobility because of its rigidification at higher concentrations of nanoparticles. This reduction in mobility results in a slower diffusion of the components across the membrane.

In addition, while the membrane separation factor of butanol was lower than the one for the neat membrane for a 4 wt% activated carbon nanoparticle concentration, it increased continuously by increasing the loading of the adsorbent from 6 wt% (Figure 3-4b). The decrease in the butanol

separation factor from 0 to 4 wt% could be due to the change in the structure of the membrane; however, a significant increase, i.e. 3.4 times, was observed for the mixed matrix membranes when the nanoparticle loading increased from 4 to 10 wt%. It is worth mentioning that the mixed matrix membrane with a nanoparticle concentration of 10 wt% is roughly 65% more selective for butanol compared to the commercial PDMS membrane. The selectivity of PDMS membranes for acetone and ethanol were at their lowest values at 4 wt% whereas their highest separation factor was observed at 8 wt% of particle loading. While the separation factor for acetone and ethanol decreased for an AC nanoparticle concentration higher than 8 wt%, their values are still superior to those for the neat PDMS membrane. Results reveal that there is a high chemical affinity between the components and the MMMs. Moreover, an increase in adsorption capacity or dual sorption mode improves the selectivity of the membranes. As can be seen from Figure 3-4, the flux and separation factor of the components increased with a higher nanoparticle concentration. It can therefore be concluded that the presence of activated carbon nanoparticles improves the performance of the PDMS membrane for pervaporation separation of butanol from ABE model solutions.

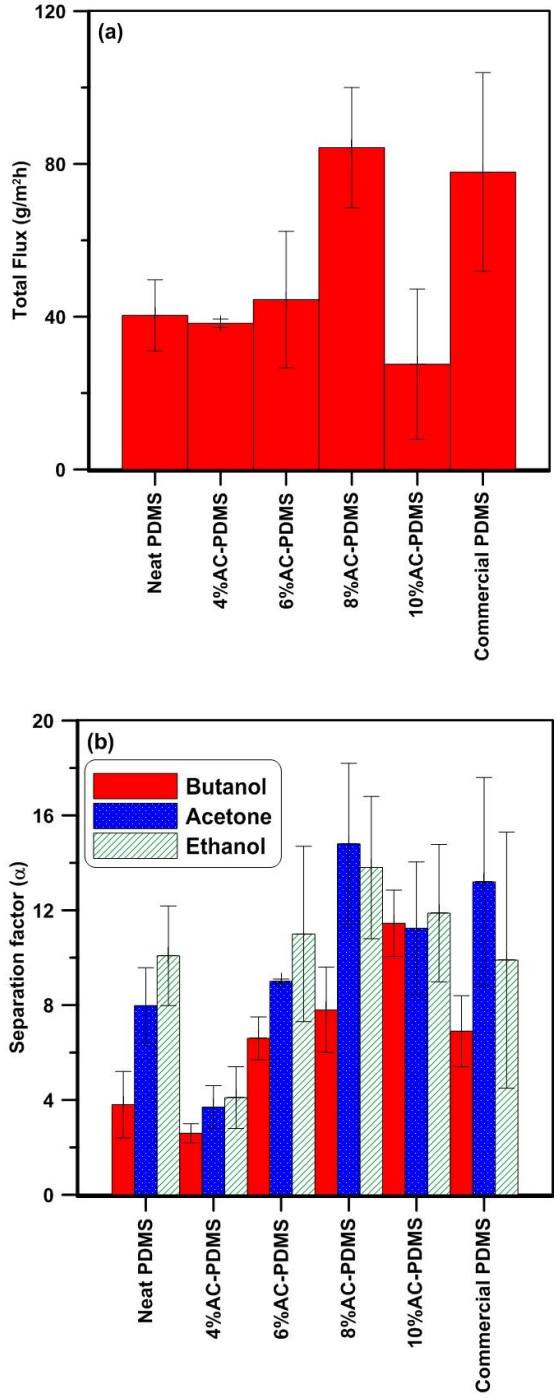

Figure 3-4 Pervaporation separation performance of ABE model solutions (A:B:E: 0.1,0.25,0.08 wt%) for the pure PDMS (laboratory-made and commercial) membranes and AC-PDMS (4-10 wt% AC in PDMS) membranes at 40°C: a) Total Flux, b) Separation factor.

Effect of the operating temperature

To investigate the effect of the operating temperature on the separation factor of acetone, butanol and ethanol and on the total permeation flux, permeation experiments were performed at three different temperatures. Results for pervaporation experiments performed at different temperatures are presented in Figure 3-5 for different concentrations of the AC nanoparticles. As shown in Figures 3-5a, 5b and 5c, the separation factor generally decreased with an increase in temperature, with the exception of butanol for the neat PDMS membrane. On the other hand, the total permeation flux (Figure 3-5d) increased steadily with an increase in temperature. This increase in total flux could be due to the higher activation energy of permeation for water and, as a result, an increase in the water flux when the temperature is increased. At higher temperatures, plasticizing or an increase in the chain mobility of the polymer facilitated the transport of the components and more so for water being the smallest molecule. This increase in chain mobility results in a weaker interaction of the components with the membrane and, more importantly, to a larger amount of water in the permeate stream. Therefore, both the concentration of the organic components in the permeate solution and the separation factor decreased.

It has been reported in previous studies that the separation factor of butanol increases with temperature [36–38]. This increase in the butanol separation factor was also observed in this investigation for the neat PDMS membranes. This could be due to the diffusion selectivity domination when there is no particle present in the matrix of the membrane. However, this behavior was not observed for the AC-PDMS membranes in this work. Results also showed that the membrane selectivity for acetone and ethanol decreased with an increase in temperature. The high increase of the water permeation by increasing the operating temperature for the mixed matrix membrane could be one of the main reasons that results in a diluted permeate with lower concentration of acetone, butanol and ethanol. In addition, the coupling effect between the components of the ABE model solutions, i.e. acetone, ethanol and water, could affect the separation factor of butanol with the operating temperature as well as their mutual separation factor.

Results of Figure 3-5 also show that the decrease in the separation factor with an increase in temperature becomes more pronounced, i.e. higher slope, when the concentration of the nanoparticles in the membrane increased. This behavior could be due to the less-entangled

PDMS chains at higher concentration of nanoparticles and, as a result, a further increase in polymer free volume occurs at a higher operating temperature. It should be mentioned that the increase in the free volume contributed to a lower resistance pathway for the permeating components and more so for smaller molecules like water. Given the high concentration of water, a higher permeation rate of water results in an increase in the total flux and a decrease in the membrane selectivity for organic components.

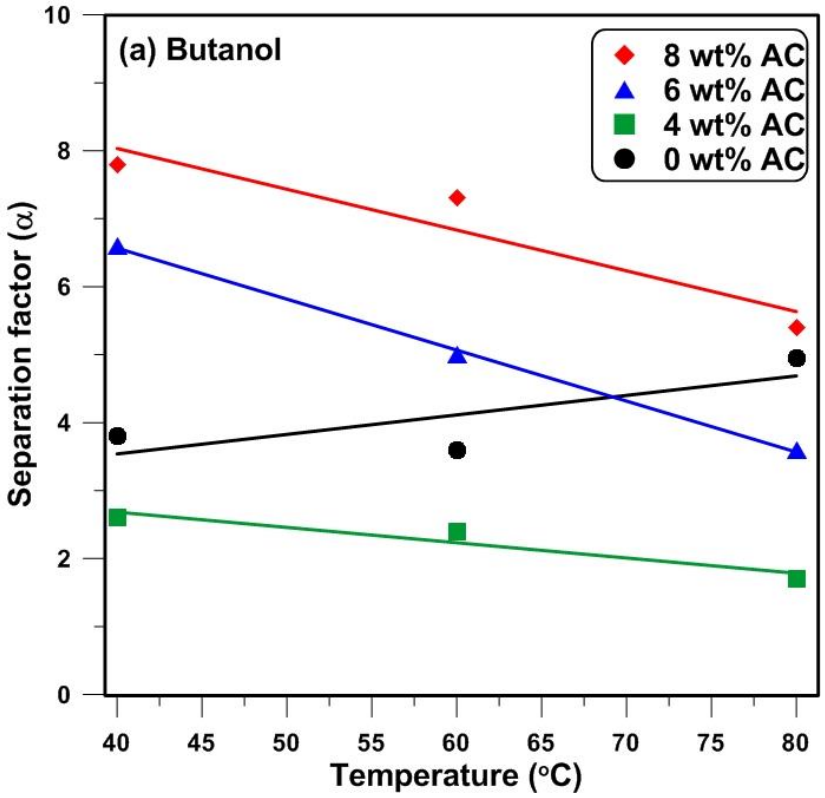

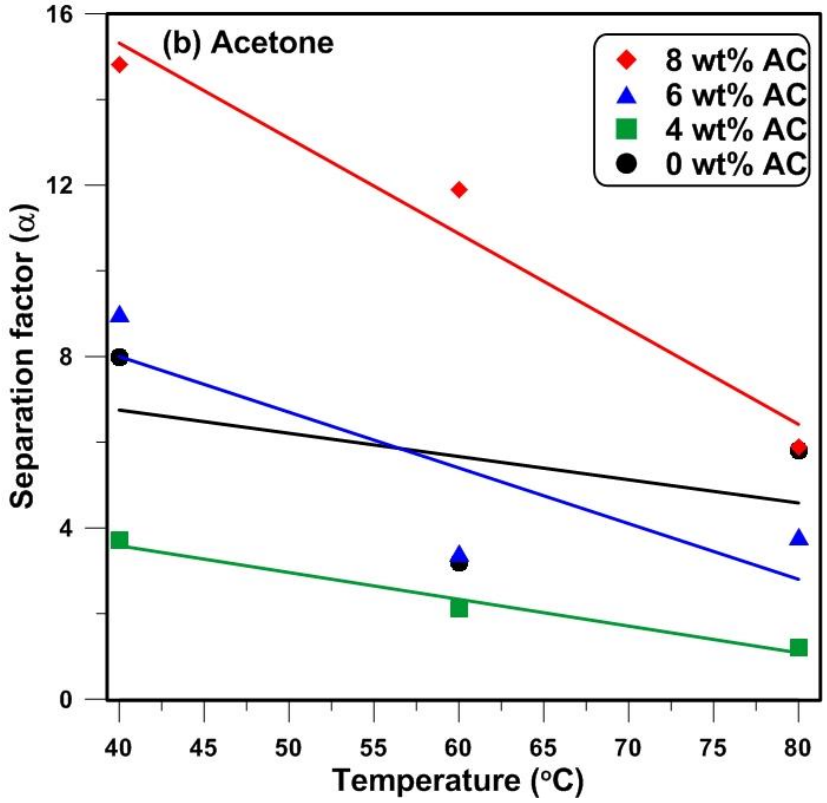
(b) Acetone
8 wt% AC
6 wt% AC
4 wt% AC
0 wt% AC
Separation factor (α)
Temperature (°C)
0
4
8
12
16
40
45
50
55
60
65
70
75
80

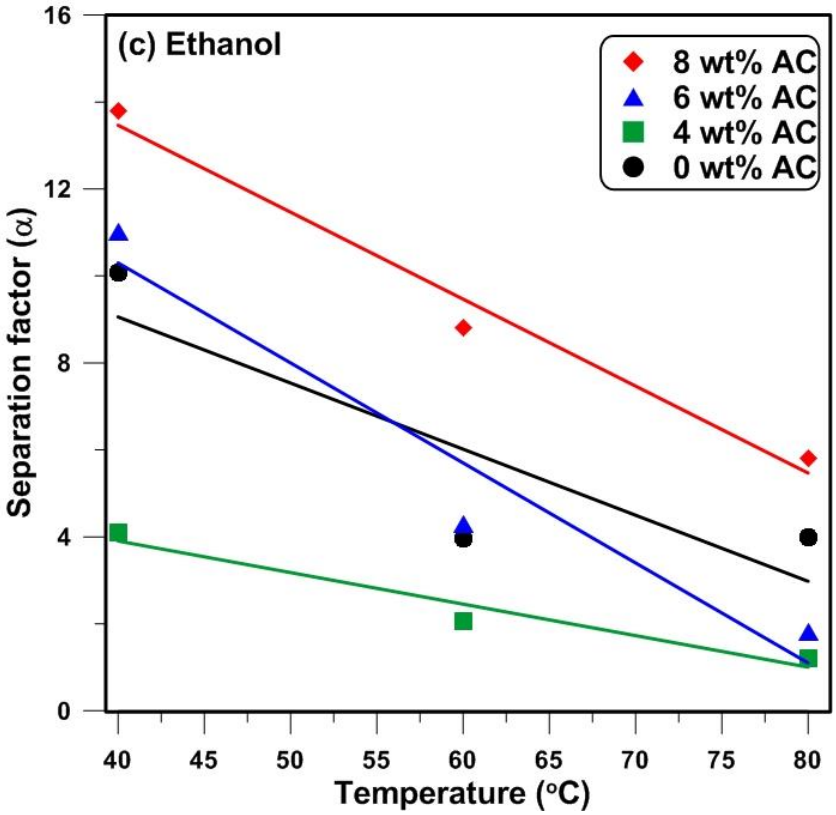
(c) Ethanol
8 wt% AC
6 wt% AC
4 wt% AC
0 wt% AC
Separation factor (α)
Temperature (°C)
0
4
8
12
16
40
45
50
55
60
65
70
75
80

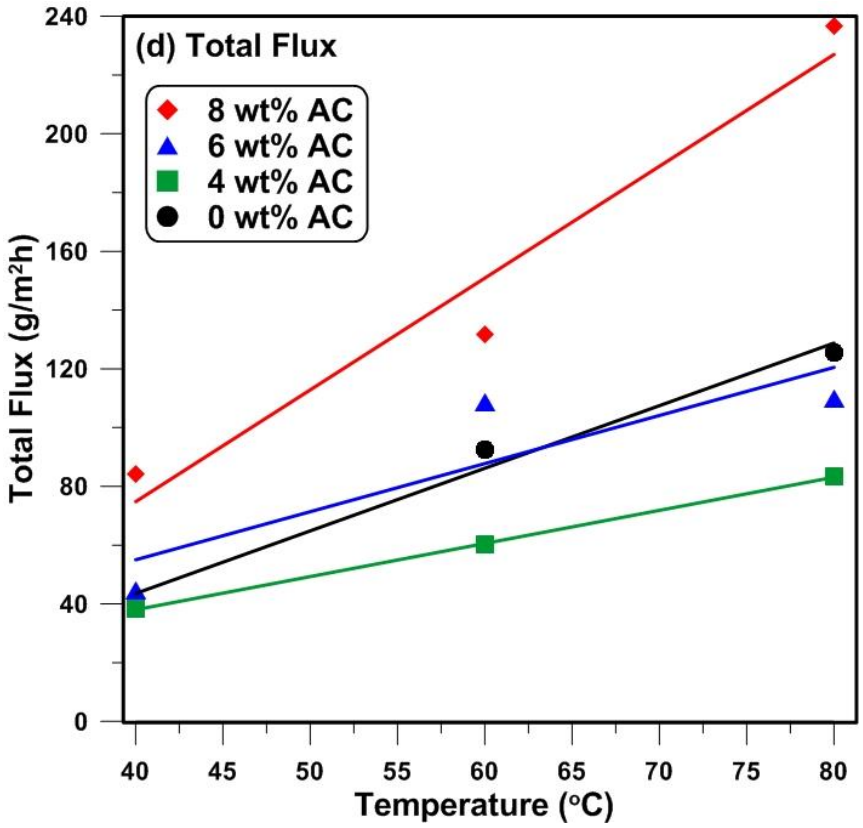

Figure 3-5 Effect of the operating temperature on the performance (separation factor of butanol, acetone and ethanol as well as the total permeation flux) of PDMS mixed matrix membranes.

The temperature dependence of the flux usually follows the Arrhenius expression given by Equations (5) and (6) [39]:

$$J = J_0 \exp\left(\frac{-E_a}{RT}\right) \tag{5}$$

$$\ln(J) = \ln(J_0) - \frac{E_a}{R}\left(\frac{1}{T}\right) \tag{6}$$

In Figure 3-6, the natural logarithm of the flux is plotted as a function of the inverse temperature. The slope of the plot for each component is related to the activation energy of permeation. Based on the data of Figure 3-6, the activation energy of permeation for water, with a value of 24.7 (*kJ/mol*), is higher than the estimated permeation activation energies for butanol, ethanol and acetone with values of 11.9, 4.7, and 4.2 (*kJ/mol*), respectively. As a result, for the AC-PDMS membranes used in this study, the permeation of water through the membrane is more sensitive

to temperature than for the other three components of the ABE model solution, and the permeation flux of water increases more rapidly with temperature than for the other three components. This increase in water flux leads to a decrease in the separation factor and an increase in the total flux. It should be mentioned that, since, the Arrhenius plots of the flux for other concentrations of the nanoparticles had a similar trend, those plots were not included.

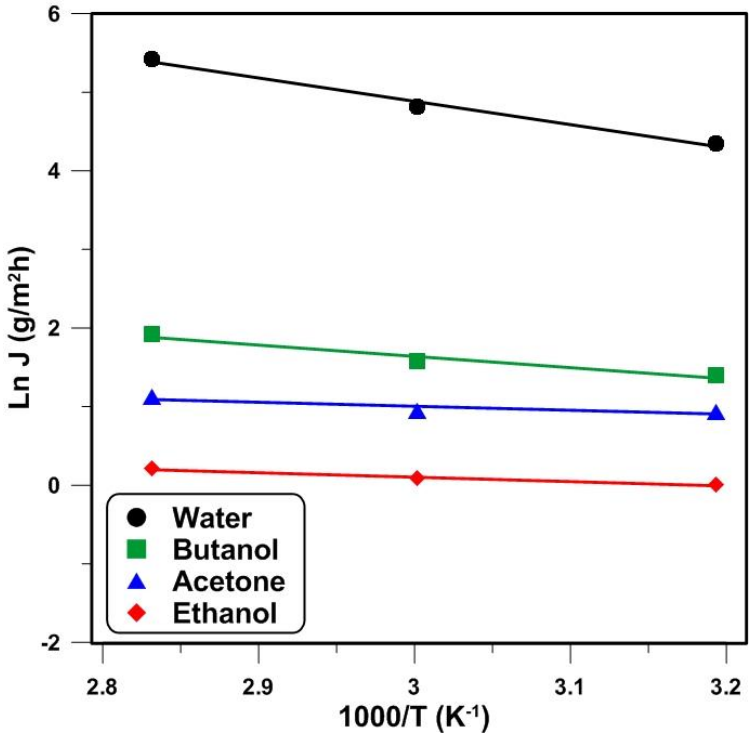

Figure 3-6 Arrhenius plots of the flux of ABE components for 8 wt% AC-PDMS membrane for a feed mass concentration of (A: B: E: 0.25, 0.5, 0.08) wt%.

Effect of the initial feed concentration

The impact of the feed concentration on the performance of the membrane was examined by varying the feed concentration from 0.5 to 2 wt% for butanol while keeping the acetone and ethanol concentrations in the same proportion as a typical ABE fermentation broth (A:B:E = 3:6:1). Results of this series of experiments are presented in Figure 3-7 for the neat PDMS membrane and the AC-PDMS membranes with different nanoparticle concentrations. Results show that an increase in the feed concentration leads to a decrease in the separation factor (Figure 3-7a, 3-7b, 3-7c). Moreover, as depicted in Figure 3-7, the slope of the separation factor with the feed concentration for the three mixed-matrix membranes is identical whereas the slope

for the neat PDMS membrane is more pronounced. As a result, the neat PDMS membrane is more sensitive to the feed concentration. This could be due to the lower ratio of the polymer in the matrix of the AC-PDMS membrane by increasing the particle loading in comparison to the pure PDMS structure.

Figure 3-8 shows that the total permeation flux increases with an increase in the feed ABE concentration with the exception of the 8 wt% AC-PDMS membrane. As the feed concentration increases, the amount of each component sorbed in the polymer and in the activated carbon will increase. Moreover, based on the swelling results in Figure 3-3, an increase in the concentration of the feed components leads to an increase in the degree of swelling which results in an increase in the free volume within the polymeric membrane. As a result, the energy barrier for permeation will be lowered which contributes to an increase in the total flux [36]. With a higher level of swelling, a larger amount of the components of the lower affinity such as water (see Table 3-1) could go through the swelled membrane. It is worth mentioning that, flux decreased by increasing the initial feed concentration for the higher (8 wt %) loading of the AC nanoparticles (Figure 3-8) and also the major increase of the flux was for the neat PDMS membrane at higher feed concentration.

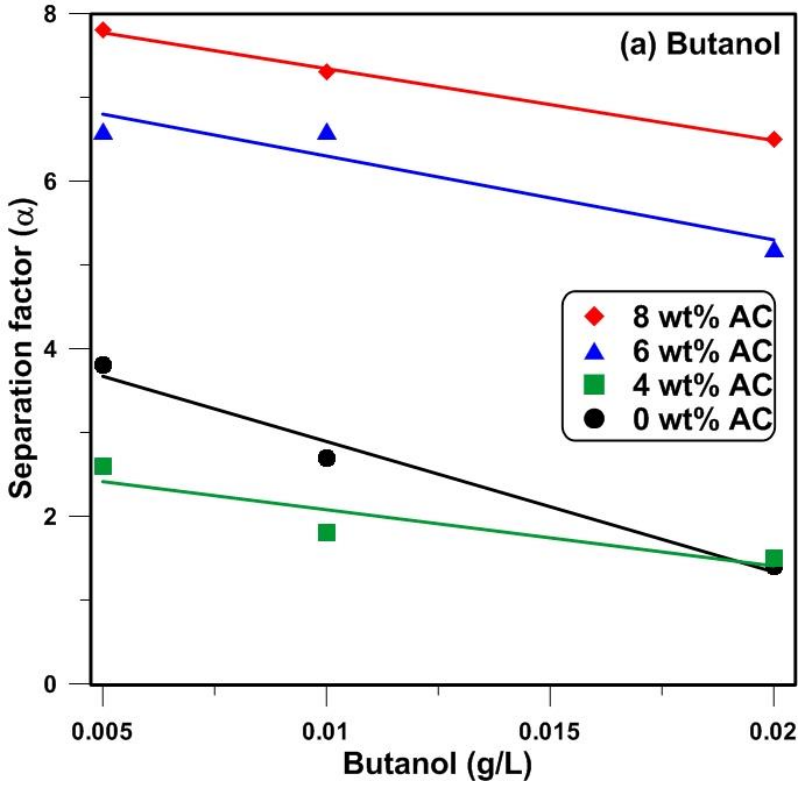
(a) Butanol
Separation factor (α)
Butanol (g/L)
8 wt% AC
6 wt% AC
4 wt% AC
0 wt% AC
0
2
4
6
8
0.005
0.01
0.015
0.02

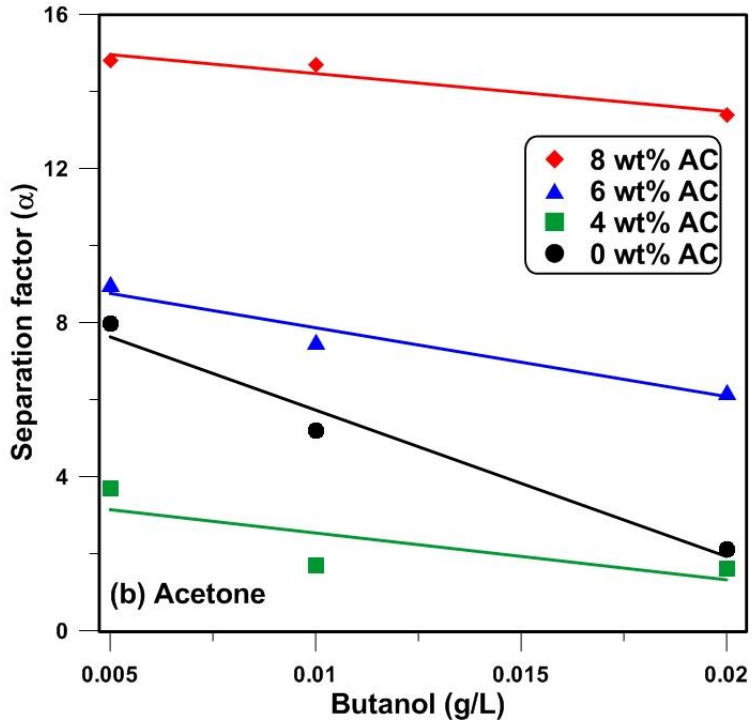
(b) Acetone
Separation factor (α)
Butanol (g/L)
8 wt% AC
6 wt% AC
4 wt% AC
0 wt% AC
0
4
8
12
16
0.005
0.01
0.015
0.02

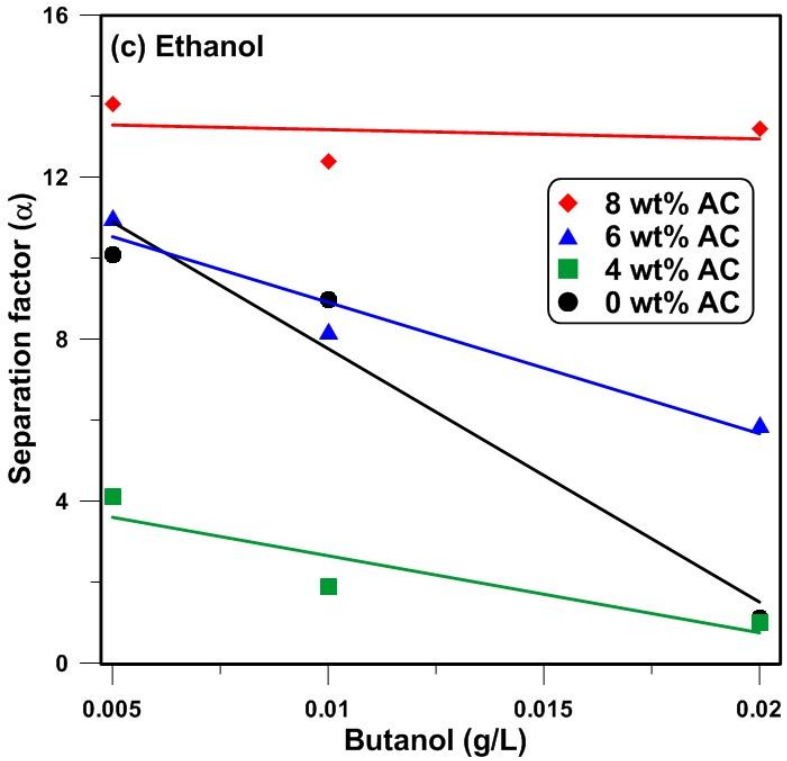

Figure 3-7 Effect of the feed concentration on the separation factor of the membranes at 40°C.

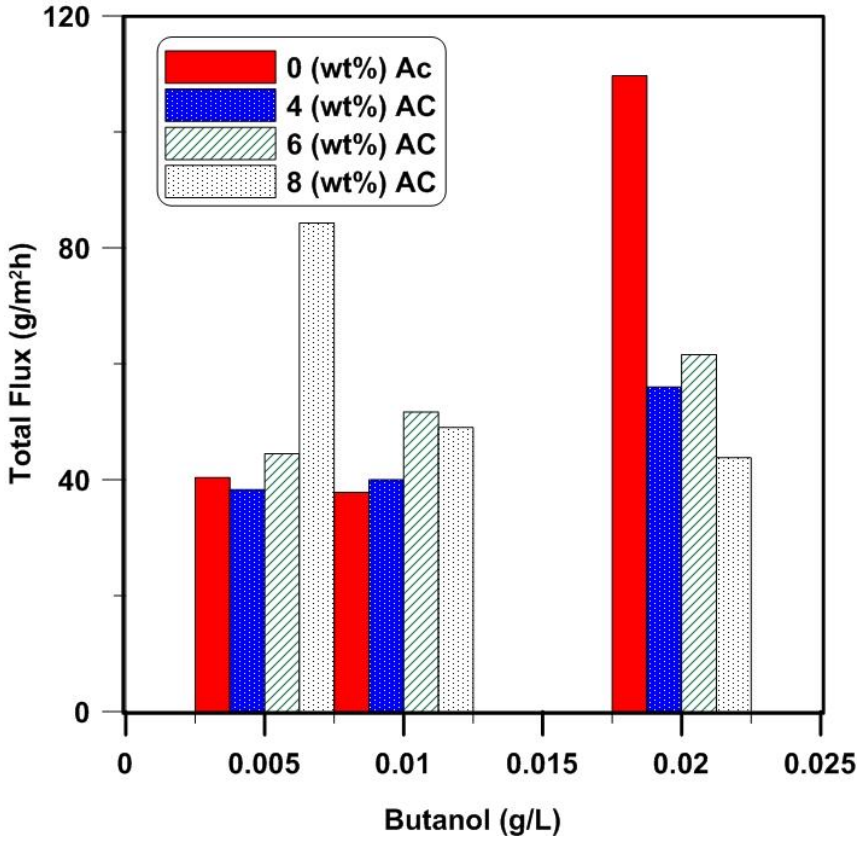

Figure 3-8 Effect of ABE feed concentration on the total permeation flux of the PDMS mixed matrix membranes at 40°C.

Conclusions

Activated carbon nanoparticles were embedded in the matrix of the PDMS membrane to improve the pervaporation separation of butanol from ABE model solutions. Butanol selectivity of the PDMS mixed matrix membranes increased with an increase in the concentration of the AC nanoparticles up to 10 wt% of AC nanoparticles in the PDMS. Furthermore, the total flux increased with the concentration of nanoparticles up to 8 wt% where a maximum was observed. In addition, the separation factor of butanol has more than doubled when the concentration of the nanoparticles increased from 0 to 10 wt%. The total flux also increased to more than twice in comparison to the neat PDMS membrane for a nanoparticle concentration of 8 wt%.

The impact of the operating conditions on the pervaporation separation of butanol from ABE model solutions has been studied. With increasing temperature, the total permeation flux

increased and the separation factor decreased. Moreover, by increasing the feed concentration of all ABE components, the total permeation flux of the MMM increased but the separation factor decreased.

In general, the presence of the activated carbon nanoparticles in the matrix of the PDMS membrane enhanced the performance of the membrane for pervaporation separation of butanol from ABE model solutions. Membranes developed in this work showed higher flux (at 8 wt%) and higher separation factor for butanol (at 10 wt%) compared to the commercial PDMS membrane.

Acknowledgements

The authors would like to acknowledge the financial support of the Natural Science and Engineering Research Council of Canada.

Nomenclature

A	Surface area of the membrane (m^2)
DS	Degree of swelling (%)
E_a	Activation energy of permeation (kJ/mol)
J	Flux ($g/m^2.h$)
J_0	Pre-exponential factor in the Arrhenius-type equation of the flux ($g/m^2.h$)
m_i	Mass of species i in the permeate stream (g)
R	Gas constant ($kJ/kmol\ K$)
t	Time of permeation (h)
T	Temperature (K)
$wt_{AC\%}$	Weight percent of the activated carbon nanoparticle in the membrane
W_{AC}	Weight of the activated carbon nanoparticles (g)
W_d	Weight of the dry membrane (g)

W_{PDMS}	Weight of the PDMS polymer (*g*)
W_s	Weight of the swelled membrane (*g*)
x_i	Mass fraction of species *i* in the feed streams (*g i/g solution*)
y_i	Mass fraction of species *i* in the permeate (*g i/g solution*)
α_i	Separation factor of species *i*
$\Delta_{PDMS,i}$	Solvent-PDMS membrane interaction ($J^{1/2}.m^{-3/2}$)

Abbreviations

ABE	Acetone, Butanol, Ethanol
AC	Activated carbon
EPDM	Ethylene propylene diene rubber
GC	Gas Chromatography
MMM	Mixed matrix membrane
PAI	Polyamide-imide
PAN	Polyacrylonitrile
PDMS	Polydimethylsiloxane
PE	Polyethylene
PET	Polyethylene terephthalate
PEBA	Polyether block-amide
PI	Polyimide
PMS	Poly (methoxy siloxane)
PP	Polypropylene
PTFE	Polytetrafluoroethylene
SEM	Scanning Electron Microscope

References

1. Qureshi, N., & Blaschek, H. P. (1999). Butanol recovery from model solution/fermentation broth by pervaporation: evaluation of membrane performance. *Biomass and Bioenergy*, *17*(2), 175–184. doi:10.1016/S0961-9534(99)00030-6
2. Bankar, S. B., Survase, S. A., Ojamo, H., & Granstrom, T. (2013). Biobutanol: the outlook of an academic and industrialist. *Rsc Advances*, *3*(47), 24734–24757. doi:10.1039/c3ra43011a
3. Rom, A., & Friedl, A. (2016). Investigation of pervaporation performance of POMS membrane during separation of butanol from water and the effect of added acetone and ethanol. *Separation and Purification Technology*, *170*, 40–48. doi:10.1016/j.seppur.2016.06.030
4. Abdehagh, N., Tezel, F. H., & Thibault, J. (2013). Adsorbent screening for biobutanol separation by adsorption: kinetics, isotherms and competitive effect of other compounds. *Adsorption*, *19*(6), 1263–1272. doi:10.1007/s10450-013-9566-8
5. Abdehagh, N., Thibault, J., & Tezel, F. H. (2014). Separation techniques in butanol production: Challenges and developments. *Biomass & Bioenergy*, *60*(Journal Article), 222–246. doi:10.1016/j.biombioe.2013.10.003
6. Qureshi, N., & Blaschek, H. P. (2001). Recovery of butanol from fermentation broth by gas stripping. *Renewable Energy*, *22*(4), 557–564. doi:10.1016/S0960-1481(00)00108-7
7. Vahdani, S., & Bayat, Z. (2011). Computational approaches to the predication of the octanol-water partition coefficient (LogPo/w). *J. Chem. Pharm. Res*, *3*(Journal Article), 565–575.
8. Mariano, A. P., Keshtkar, M. J., Atala, D. I. P., Maugeri Filho, F., Wolf Maciel, M. R., Maciel Filho, R., & Stuart, P. (2011). Energy Requirements for Butanol Recovery Using the Flash Fermentation Technology. *Energy & Fuels*, *25*(5), 2347–2355. doi:10.1021/ef200279v
9. Liu, G., Wei, W., & Jin, W. (2014). Pervaporation Membranes for Biobutanol Production. *Acs Sustainable Chemistry & Engineering*, *2*(4), 546–560. doi:10.1021/sc400372d
10. Essawy, H., Tawfik, M., El-Sabbagh, S., El-Gendi, A., El-Zanati, E., & Abdallah, H. (2014). Novel amphiphilic conetworks based on compatibilized NBR/SBR–

montmorillonite nanovulcanizates as membranes for dehydrative pervaporation of water–butanol mixtures. *Polymer Engineering & Science*, *54*(7), 1560–1570. doi:10.1002/pen.23699

11. Jitesh, K. D., Pangarkar, V. G., & Niranjan, K. (2000). Pervaporative stripping of acetone, butanol and ethanol to improve ABE fermentation. *Bioseparation*, *9*(3), 145–154. doi:10.1023/A:1008129713552
12. Vrana, D. L., Meagher, M. M., Hutkins, R. W., & Duffield, B. (1993). Pervaporation of Model Acetone-Butanol-Ethanol Fermentation Product Solutions using Polytetrafluoroethylene Membranes. *Separation Science and Technology*, *28*(13–14), 2167–2178. doi:10.1080/01496399308016741
13. Müller, M., & Pons, M.-N. (1991). Coupling of gas membrane smooth pervaporation and alcoholic fermentation. *Journal of Chemical Technology & Biotechnology*, *52*(3), 343–358. doi:10.1002/jctb.280520307
14. Hu, M., Gao, L., Fu, W., Liu, X., Huang, F., Luo, Y., & Huang, C. (2015). High-performance interpenetrating polymer network polyurethane pervaporation membranes for butanol recovery. *Journal of Chemical Technology & Biotechnology*, *90*(12), 2195–2207. doi:10.1002/jctb.4533
15. Liu, F., Liu, L., & Feng, X. (2005). Separation of acetone–butanol–ethanol (ABE) from dilute aqueous solutions by pervaporation. *Separation and Purification Technology*, *42*(3), 273–282. doi:10.1016/j.seppur.2004.08.005
16. Jalal, T. A., Bettahalli, N. M. S., Le, N. L., & Nunes, S. P. (2015). Hydrophobic Hyflon AD/Poly(vinylidene fluoride) Membranes for Butanol Dehydration via Pervaporation. *Industrial & Engineering Chemistry Research*, *54*(44), 11180–11187. doi:10.1021/acs.iecr.5b02754
17. Hickey, P. J., Juricic, F. P., & Slater, C. S. (1992). The Effect of Process Parameters on the Pervaporation of Alcohols through Organophilic Membranes. *Separation Science and Technology*, *27*(7), 843–861. doi:10.1080/01496399208019729
18. Azimi, H., Tezel, F. H., & Thibault, J. (2017). Effect of embedded activated carbon nanoparticles on the performance of polydimethylsiloxane (PDMS) membrane for pervaporation separation of butanol. *Journal of Chemical Technology & Biotechnology*. doi:10.1002/jctb.5306

19. Borisov, I. L., Malakhov, A. O., Khotimsky, V. S., Litvinova, E. G., Finkelshtein, E. S., Ushakov, N. V., & Volkov, V. V. (2014). Novel PTMSP-based membranes containing elastomeric fillers: Enhanced 1-butanol/water pervaporation selectivity and permeability. *Journal of Membrane Science*, *466*, 322–330. doi:10.1016/j.memsci.2014.04.037
20. Wang, Y., Chung, T. S., & Wang, H. (2011). Polyamide–imide membranes with surface immobilized cyclodextrin for butanol isomer separation via pervaporation. *AIChE Journal*, *57*(6), 1470–1484. doi:10.1002/aic.12360
21. Zhou, H., Su, Y., Chen, X., & Wan, Y. (2011). Separation of acetone, butanol and ethanol (ABE) from dilute aqueous solutions by silicalite-1/PDMS hybrid pervaporation membranes. *Separation and Purification Technology*, *79*(3), 375–384. doi:10.1016/j.seppur.2011.03.026
22. Li, S., Qin, F., Qin, P., Karim, M. N., & Tan, T. (2013). Preparation of PDMS membrane using water as solvent for pervaporation separation of butanol-water mixture. *Green Chemistry*, *15*(8), 2180–2190. doi:10.1039/c3gc40291f
23. Li, S.-Y., Srivastava, R., & Parnas, R. S. (2010). Separation of 1-butanol by pervaporation using a novel tri-layer PDMS composite membrane. *Journal of Membrane Science*, *363*(1–2), 287–294. doi:10.1016/j.memsci.2010.07.042
24. Mai, N. L., Kim, S. H., Ha, S. H., Shin, H. S., & Koo, Y.-M. (2013). Selective recovery of acetone-butanol-ethanol from aqueous mixture by pervaporation using immobilized ionic liquid polydimethylsiloxane membrane. *Korean Journal of Chemical Engineering*, *30*(9), 1804–1809. doi:10.1007/s11814-013-0116-6
25. Huang, J., & Meagher, M. M. (2001). Pervaporative recovery of n-butanol from aqueous solutions and ABE fermentation broth using thin-film silicalite-filled silicone composite membranes. *Journal of Membrane Science*, *192*(1–2), 231–242. doi:10.1016/S0376-7388(01)00507-5
26. Xue, C., Du, G.-Q., Chen, L.-J., Ren, J.-G., Sun, J.-X., Bai, F.-W., & Yang, S.-T. (2014). A carbon nanotube filled polydimethylsiloxane hybrid membrane for enhanced butanol recovery. *Scientific Reports*, *4*(Journal Article), 5925–5925. doi:10.1038/srep05925
27. Qureshi, N., Hughes, S., Maddox, I. S., & Cotta, M. A. (2005). Energy-efficient recovery of butanol from model solutions and fermentation broth by adsorption. *Bioprocess and Biosystems Engineering*, *27*(4), 215–222. doi:10.1007/s00449-005-0402-8

28. Chen, D., Chen, F., Hu, X., Zhang, H., Yin, X., & Zhou, Y. (2015). Thermal stability, mechanical and optical properties of novel addition cured PDMS composites with nano-silica sol and MQ silicone resin. *Composites Science and Technology*, *117*(Journal Article), 307–314. doi:10.1016/j.compscitech.2015.07.003
29. Patterson, D. A., Havill, A., Costello, S., See-Toh, Y. H., Livingston, A. G., & Turner, A. (2009). Membrane characterisation by SEM, TEM and ESEM: The implications of dry and wetted microstructure on mass transfer through integrally skinned polyimide nanofiltration membranes. *Separation and Purification Technology*, *66*(1), 90–97. doi:10.1016/j.seppur.2008.11.022
30. Liu, G., Zhou, T., Liu, W., Hu, S., Pan, F., Wu, H., … Cao, X. (2014). Enhanced desulfurization performance of PDMS membranes by incorporating silver decorated dopamine nanoparticles, *2*(32), 12907–12917. doi:10.1039/C4TA01778A
31. Mai, N. L., Kim, S. H., Ha, S. H., Shin, H. S., & Koo, Y.-M. (2013). Selective recovery of acetone-butanol-ethanol from aqueous mixture by pervaporation using immobilized ionic liquid polydimethylsiloxane membrane. *Korean Journal of Chemical Engineering*, *30*(9), 1804–1809. doi:10.1007/s11814-013-0116-6
32. Tan, H., Wu, Y., & Li, T. (2013). Pervaporation of n-butanol aqueous solution through ZSM-5-PEBA composite membranes. *Journal of Applied Polymer Science*, *129*(1), 105–112. doi:10.1002/app.38704
33. Lan, Y., Yan, N., & Wang, W. (2016). Application of PDMS pervaporation membranes filled with tree bark biochar for ethanol/water separation, *6*(53), 47637–47645. doi:10.1039/C6RA06794H
34. Niemisto, J., Kujawski, W., & Keiski, R. L. (2013). Pervaporation performance of composite poly(dimethyl siloxane) membrane for butanol recovery from model solutions. *Journal of Membrane Science*, *434*(Journal Article), 55–64. doi:10.1016/j.memsci.2013.01.047
35. Abdehagh, N., Gurnani, P., Tezel, F. H., & Thibault, J. (2015). Adsorptive separation and recovery of biobutanol from ABE model solutions. *Adsorption*, *21*(3), 185–194. doi:10.1007/s10450-015-9661-0
36. Liu, G., Hou, D., Wei, W., Xiangli, F., & Jin, W. (2011). Pervaporation Separation of Butanol-Water Mixtures Using Polydimethylsiloxane/Ceramic Composite Membrane.

Chinese Journal of Chemical Engineering, *19*(1), 40–44. doi:10.1016/S1004-9541(09)60174-9

37. Fouad, E. A., & Feng, X. (2009). Pervaporative separation of n-butanol from dilute aqueous solutions using silicalite-filled poly(dimethyl siloxane) membranes. *Journal of Membrane Science*, *339*(1–2), 120–125. doi:10.1016/j.memsci.2009.04.038
38. Qureshi, N., Meagher, M. M., & Hutkins, R. W. (1999). Recovery of butanol from model solutions and fermentation broth using a silicalite silicone membrane. *Journal of Membrane Science*, *158*(1–2), 115–125. doi:10.1016/S0376-7388(99)00010-1
39. Zhou, H., Su, Y., Chen, X., & Wan, Y. (2011). Separation of acetone, butanol and ethanol (ABE) from dilute aqueous solutions by silicalite-1/PDMS hybrid pervaporation membranes. *Separation and Purification Technology*, *79*(3), 375–384. doi:10.1016/j.seppur.2011.03.026

4. Chapter 4

The impact of pH on VLE, pervaporation and adsorption of butyric acid in dilute solutions

Hoda Azimi, F. Handan Tezel and Jules Thibault*

Abstract

Butyric acid (BA) is an intermediate product and a precursor to the production of butanol in ABE fermentation. Ideally, it would be beneficial to retain as much BA in the fermenter to increase butanol productivity. In this study, experiments were performed to assess the impact of the pH of the feed solution on the separation of BA from dilute aqueous solutions using three separation methods: distillation, pervaporation and adsorption. Results confirm that the pH of the solution, which dictates the level of BA dissociation, controls the degree of separation of BA from dilute aqueous solutions. Indeed, results show that the vapour-liquid equilibrium (VLE) curve, the membrane selectivity and the adsorption capacity for BA in dilute aqueous solutions decreased steadily as the pH is increased from below to above its pKa value of 4.82. The separation performance is strongly correlated with the pH of the feed solution, and, as anticipated, a pH increase reduces the level of separation for these three processes. This is advantageous for the ABE fermentation incorporating a solvent recovery process since the BA would remain in fermenter and improve the production of butanol. However, the pH cannot increase excessively as there exists an optimum pH for conducting the fermentation process such that a judicious level of pH must be sought to optimize a fermentation-separation integrated process.

Keywords: Biobutanol; Butyric acid; VLE; Pervaporation; Adsorption; pH

Introduction

Biobutanol produced from Acetone-Butanol-Ethanol (ABE) fermentation is considered a potential biofuel candidate to partially replace fossil fuels [1–4]. This alcohol is produced via fermentation using anaerobic bacteria such as *Clostridium acetobutylicum (CA)* and *Clostridium beijerinkii (CB)*. The ABE fermentation is producing acetone, butanol and ethanol in a typical proportion of 3:6:1, respectively. In addition to the three solvents, other fermentation products are mainly butyric acid (BA), acetic acid (AC), hydrogen, and carbon dioxide [5]. The

microorganisms responsible for ABE fermentation have the advantage over many other microorganisms to be able to use both 5- and 6-carbon sugars directly so that they can use fermentable sugars from lignocellulosic biomass in addition to more common substrates such as starch (corn, potato, wheat, and manioc) and sucrose (sugarcane, beet, and molasses) [5]. The ABE fermentation process is a two-stage fermentation: acidogenic and solventogenic stages. During the acidogenic stage, the bacteria synthesize butyric and acetic acids which is accompanied by a decrease in pH. Subsequently, in the solventogenic stage, butanol, acetone and ethanol are produced [6] where butyric acid and acetic acid are re-assimilated by the microorganisms to produce butanol and acetone, respectively. This fermentation can proceed in batch, fed batch and continuous modes. In batch, the fermentation process lasts two to six days, which depends on the choice of the substrate and culture conditions. The butanol concentration in the product could sometimes approach 2 wt% but it is usually in the vicinity of 1 wt%. The low butanol final concentration has serious consequences on the energy and cost required for separation and recovery. In addition to the low concentration, butanol must also be separated from numerous other fermentation products which significantly adds to the cost of separation.

To render butanol as an economically-viable biofuel, a more efficient overall bioconversion process that transforms cellulose and hemicellulose to butanol is required. Various ways have been proposed to partly remedy this challenge. Some researchers have investigated the modification of microorganisms such as the genetic manipulation of *Clostridia* to increase the yield of butanol and the tolerance of strains to butanol inhibition in addition to reducing or eliminating the formation of other co-products such as acetone and ethanol [7–9]. Jiang et al. investigated the weakening of the acetone pathway in order to increase the butanol-to-acetone ratio. They showed that butanol-to-acetone ratio increased by 70% to 80%, and the production of acetone decreased to approximately 0.21g/L in the acetoacetate decarboxylase gene (adc)-disrupted mutant [10]. In another work, to increase the solvent production and aero-tolerance of *C. acetobutylicum*, the gshAB genes from *E. coli* were incorporated into *C. acetobutylicum DSM1731*, which resulted in more robust *C. acetobutylicum* bacteria and higher solvent production [7]. Although some progress has been accomplished, the mechanism of butanol production by fermentation still remains complex and the search for an ideal microorganism is still continuing.

Other studies have been conducted to understand the underlying mechanisms of the acid crash which results of the accumulation of non-dissociated fatty acids at lower pH. As a result, the bacterial culture stops growing and enters into the sporulation stage [11,12]. This situation occurs in uncontrolled pH fermentation and contributes to the interruption of glucose uptake, acids and butanol production and the initiation of solventogenesis where butyric acid and acetic acid are re-assimilated to produce butanol and acetone [11–14]. The initiation of the solventogenesis stage is related to the concentration of the non-dissociated butyric acid [15–17]. Monot et al. studied the effect of pH and non-dissociated butyric acid on the production of acetone and butanol in batch cultures of *Clostridium acetobutylicum* at pH between 4.5 and 6.0. Results showed that the effect of pH was related to the concentration of the non-dissociated butyric acid and the solvent production stage was initiated when the non-dissociated butyric acid reached a minimum of 1.5 g/L [17].

On the process point of view, to partly alleviate the inhibiting effect of ABE organic solvents on microorganisms, which has for consequence to limit the concentration of butanol, it is possible to incorporate a separation unit to the fermentation system to remove a portion of the solvent and thereby prolong the fermentation. Different types of solvent recovery methods have been proposed to remove ABE solvent, especially butanol, to enhance butanol productivity. Some of these separation methods are vacuum fermentation [18], gas stripping [19,20], liquid/liquid extraction [21], adsorption [22], perstraction [23] and pervaporation [24,25]. However, information on the effect of pH on the performance of these separation processes for the in situ recovery of butanol is scarce.

It is believed that the degree of dissociation of butyric acid plays a major role on the separation performance of the majority of the separation processes. The objective of this investigation is to examine the effect of pH on the performance of three separation processes, namely vacuum fermentation, pervaporation and adsorption, which could be coupled to a fermentation system for the in situ removal of ABE solvents. In particular, it is desired to investigate the separation of butyric acid since it would highly be desirable to retain the majority of it within the fermenter because it is a precursor to the production of butanol. This is especially important for the case where a continuous fermentation is used. In this investigation, the effect of the feed solution pH on (1) the vapour-liquid equilibrium (VLE) of butyric acid, (2) the permeability of butyric acid

through a flat PDMS pervaporation membrane, and (3) the adsorption of butyric acid on activated carbon were studied experimentally.

Materials and Methods

Materials

N-butyric Acid (99% pure, Acros) and butanol (99% pure, Acros) were obtained from Fisher Scientific (Fair Lawn, NJ, USA). sodium hydroxide (NaOH) was purchased from Sigma Aldrich (Ottawa, Canada). Deionized distilled water was used to prepare all aqueous solutions. A flat sheet commercial PDMS three-layer membrane with a total thickness of 200-235 μm (130, 100, 3-5 μm for polyethylene terephthalate (PET), polyimide (PI) and PDMS, respectively) was obtained from Pervatech B.V. Company (Rijssen, Netherlands) for pervaporation separation experiments. Activated carbon (F400) adsorbent was purchased from Calgon Carbon Corporation (Markham, Ontario, Canada) to conduct adsorption experiments.

Vapour-liquid equilibrium (VLE) experiments

VLE experiments at different pH were conducted for dilute butyric acid aqueous solutions having concentrations in the range of 4.5-15 g/L butyric acid. Binary solutions of butyric acid and distilled deionized water were prepared and different quantities of NaOH were added to each solution to increase the pH to the desired value. The amount of NaOH required for a specific pH value was calculated using computer code developed in Visual Basic for Applications (VBA) and validated prior to each experiment by recording the pH of the feed solution. Eqs. (1) and (2) were solved simultaneously to determine the amount of NaOH required to achieve the desired H^+ equilibrium concentration in solution. Knowing the initial concentration of butyric acid in solution, these two equations allow to determine the degree of dissociation of butyric acid and the H^+ equilibrium concentration which satisfy these two equations and from which the pH is calculated.

$$k_a = \frac{[H^+][CH_3CH_2CH_3COO^-]}{[CH_3CH_2CH_3COOH]} \quad \textbf{(1)}$$

$$k_w = \frac{[H^+][OH^-]}{[H_2O]} \quad \textbf{(2)}$$

where K_a and K_w are the butyric acid and water dissociation constants, respectively, and concentrations are expressed in mol/L. pK_a and pK_w are 4.82 and 14, respectively

Figure 4-2 presents the schematic diagram of the VLE experimental setup which essentially consists of a round-bottom flask containing the solution to be evaporated, an electrical round bottom flask heater (Thermo Fisher Scientific Limited, Ottawa, Canada) and a water-cooled glass condenser. The flask was initially loaded with an aqueous solution of butyric acid with the pH adjusted to the desired level using the pellets of NaOH and brought to its boiling point temperature under atmospheric conditions. A thermocouple was immersed in the liquid to record the temperature. The electrical power of the heater was set to maintain the liquid solution under light boiling conditions. The rising vapour condensed in the water-cooled condenser and was returned to the boiling flask. For each VLE experiment, the closed circuit system was operated for at least one hour which was more than sufficient to establish steady-state conditions. Samples from the flask solution and the condenser trap were collected and analyzed for their content in butyric acid using high performance liquid chromatography (HPLC - Waters, Mississauga, ON, Canada) equipped with a Vertex column (300×9×8 mm, KNAUER, Berlin, Germany) packed with Eurokat H, 10 µm. The detector, the pump and the auto-sampler of the HPLC were Refractive Index Detector (Waters 2414), Isocratic HPLC pump (Waters 1515) and Autosampler (Waters 717 plus), respectively. In addition, the pH of both samples was recorded using a pH meter (Thermo Scientific Orion 3-star benchtop pH meter, Cole-Parmer, Ottawa, Ontario, Canada).

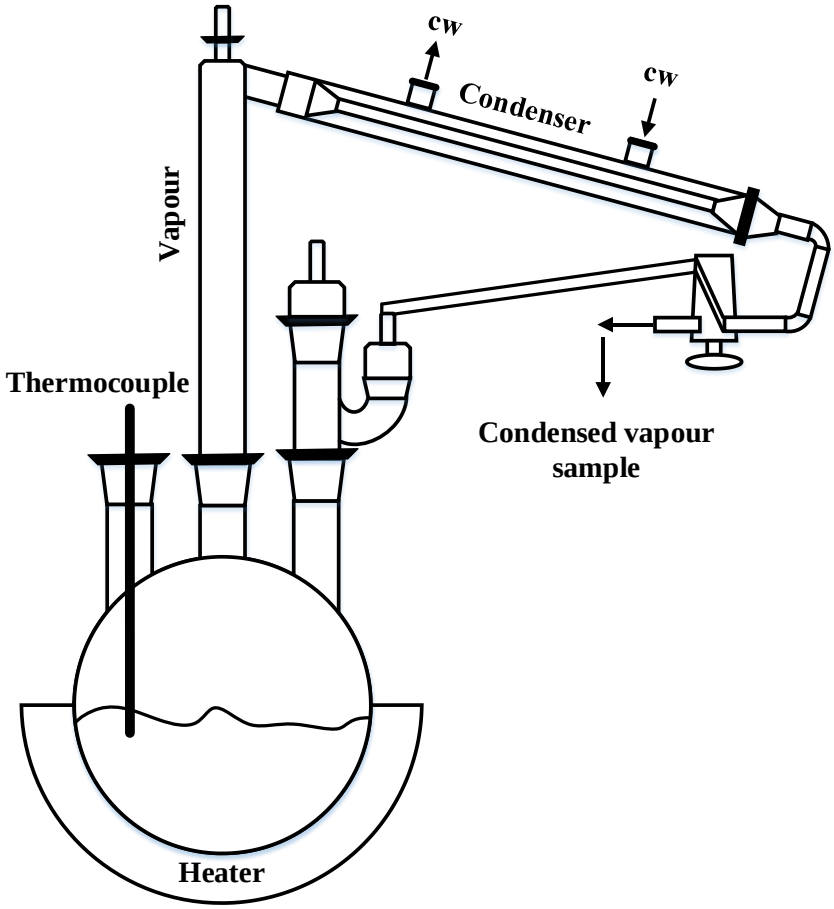

Figure 4-1 The schematic diagram of the apparatus used to obtain VLE data.

Pervaporation experiments

To investigate the effect of pH on the membrane performance for the separation of butyric acid, commercial PDMS membranes were tested for an aqueous butyric acid solution at a temperature of 37°C. This temperature corresponds to the temperature at which ABE fermentation is normally conducted. Since the permeation rate of butyric acid was very small, it was decided to also add butanol to the feed solutions. Butanol has a high affinity with PDMS membranes and the addition of butanol could be helpful for studying the effect of the deprotonated butyric acid and NaOH on the membrane performance. Adding a high permeable component could also show the pH effects more significantly. In addition, it was possible to study the effect of the pH of the feed solution on the permeation of butanol at the same time. An aqueous feed solution consisting

of 10 g/L butanol and 5 g/L butyric acid was used. The appropriate amount of NaOH has been added to bring the feed solution to the desired pH.

Permeation experiments were conducted in the pervaporation experimental system illustrated schematically in Figure 4-2. The experimental system essentially consists of three membrane modules placed in series. The retentate from the first membrane was used as the feed for the second module and the retentate of the second membrane was fed to the third membrane module. The feed flow rate was high enough to consider a nearly constant retentate concentration in each module and to ensure nearly zero-stage cut condition. Moreover, the decrease in temperature of the feed solution while flowing through each membrane module was negligible since the permeate flow rate was on average 30 000 times smaller than the feed flow rate. A peristaltic pump has been used to pump the feed stream from the solution through the retentate side of the first pervaporation module. The three-module membrane system was placed in an oven maintained at a constant temperature. To ensure the feed stream reaches the desired temperature prior to entering the membrane module, the feed stream flowed through a long stainless steel coil also located in the oven. A thermocouple measured the temperature of the feed stream just before entering the first membrane module. The active area of the membrane coupon for each test module was 13.5 cm^2.

The permeate of each membrane module was collected in individual cold traps. The permeate side of the three membrane testing units and the three cold traps were maintained at a very low pressure (3 Torr) using a vacuum pump (Scroll Pump, 78603-11, Cole-Parmer, Montreal, Quebec, Canada). To monitor the vacuum pressure, a digital pressure gauge was used. Cold traps were immersed into a liquid nitrogen Dewar to condense the permeate streams. The level of liquid nitrogen in the Dewar was controlled using an automatic time-fill controller. The average time of each pervaporation experiment was about 18 h. Furthermore, numerical simulations were performed to estimate the time necessary to reach steady state and it was found to be negligible compared to the duration of the experiment. At the end of the experiments, samples were collected from the cold traps, weighed and concentrations were analyzed by the HPLC.

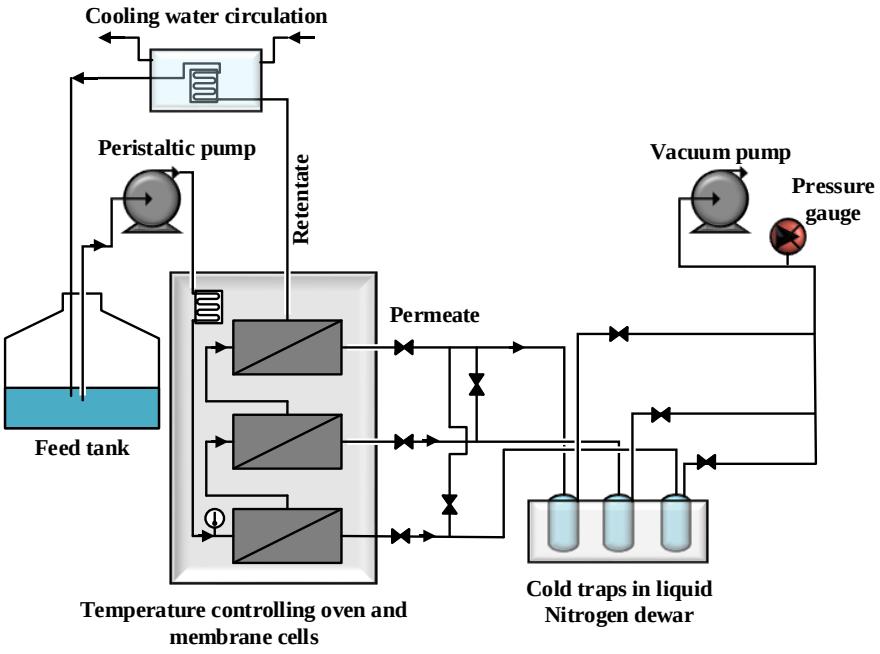

Figure 4-2 Schematic diagram of the three-module pervaporation system used in the present study.

To characterise the pervaporation separation performance, the flux (J) and the separation factor (α) have been calculated using Eqs. (3) and (4), respectively. The separation factor is a metric which assesses the separation ability of the membrane considering two substances to be separated. The flux is the permeate flow per unit membrane surface area and per unit time, which is normally determined for each species from the individual permeation flow rates [26–28].

$$J_i = \frac{m_i}{At} \tag{3}$$

$$\alpha_i = \frac{y_i/(1-y_i)}{x_i/(1-x_i)} \tag{4}$$

where m_i is the mass of species i in the permeate stream (g), A is the effective surface area of the membrane (m^2), t is the time of permeation (h), y_i and x_i are the mass fractions of species i in the permeate and feed streams, respectively [1].

Adsorption experiments

Adsorption can be used to selectively remove butanol from ABE fermentation broths to partly mitigate its inhibition. It was determined in previous experiments that butyric acid was also adsorbed significantly on activated carbon [22]. Ideally, in a fermentation system integrated with an adsorption system for in situ recovery of ABE solvents, it would be desirable to adsorb the least amount of butyric acid such that the unadsorbed portion of butyric acid will be returned to the fermenter and re-assimilated by the microorganism to produce butanol. The pH of the solution would be a function of the amount of butyric acid in the solution and thereby the dissociation of this weak acid. Adsorption experiments were therefore conducted at room temperature with butyric acid aqueous feed solutions at different pH, similarly to the solutions that were prepared for the VLE experiments.

Figure 4-3 shows the schematic diagram of the adsorption setup. The adsorption column was packed with F400 activated carbon adsorbents purchased from Calgon Corporation (Mississauga, ON, Canada). This adsorbent has excellent adsorption capacity and favorable kinetics for adsorption of butanol but also to a lesser extend for butyric acid. The length and diameter of the packed column were 17.5 and 1.5 cm, respectively. The feed solution was continuously pumped, using a peristaltic pump, to flow through the packed column and then returned to the feed tank. The experiment was conducted until equilibrium between the feed solution and the adsorbent was reached. The concentrations of the initial and final feed samples were measured by HPLC. For each experiment conducted with an initial concentration at a constant temperature, one point on the isotherm curve could be obtained at equilibrium.

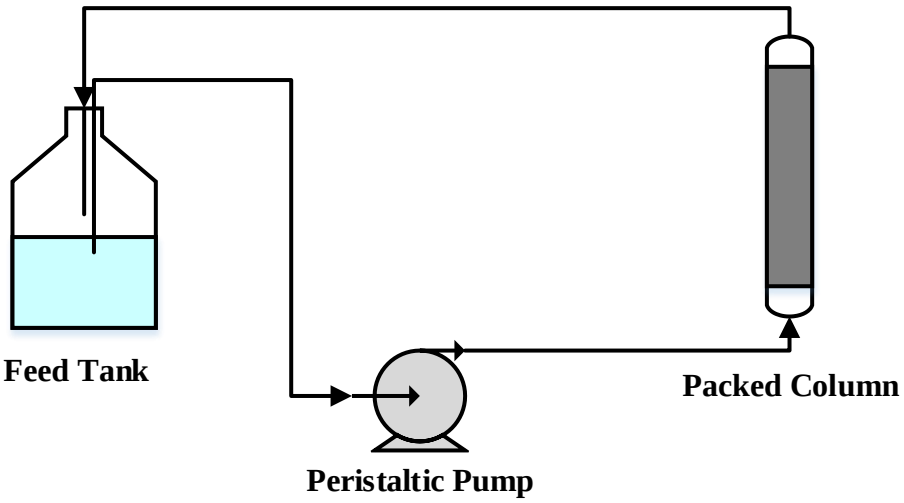

Figure 4-3 Schematic diagram of the adsorption system.

To analyze the experimental results, the Langmuir isotherm model was used (Eq. 5) to represent the experimental data. This isotherm model was used to characterize the butyric acid equilibrium adsorption capacity of the adsorbent as a function of equilibrium concentration obtained for various pH of the feed solutions.

$$q_e = \frac{q_s b C_e}{1 + b C_e} \tag{5}$$

where q_e is the component adsorption capacity at equilibrium (g/g), q_s is maximum (saturation) component adsorption capacity (g/g), b is Langmuir constant (L/g) and C_e is the equilibrium component concentration in solution (g/L).

Results and discussion

Effect of pH on the vapour-liquid equilibrium measurement for butyric acid

NaOH was used to increase the pH of the feed butyric acid aqueous solution. Figure 4-4 shows the titration curve for butyric acid by adding NaOH. This figure was very useful to determine the amount of NaOH to be added to a butyric acid feed solution of different concentrations to

achieve the desired pH. Since butyric acid is a weak acid with a pK_a value of 4.82, it acts as a buffer.

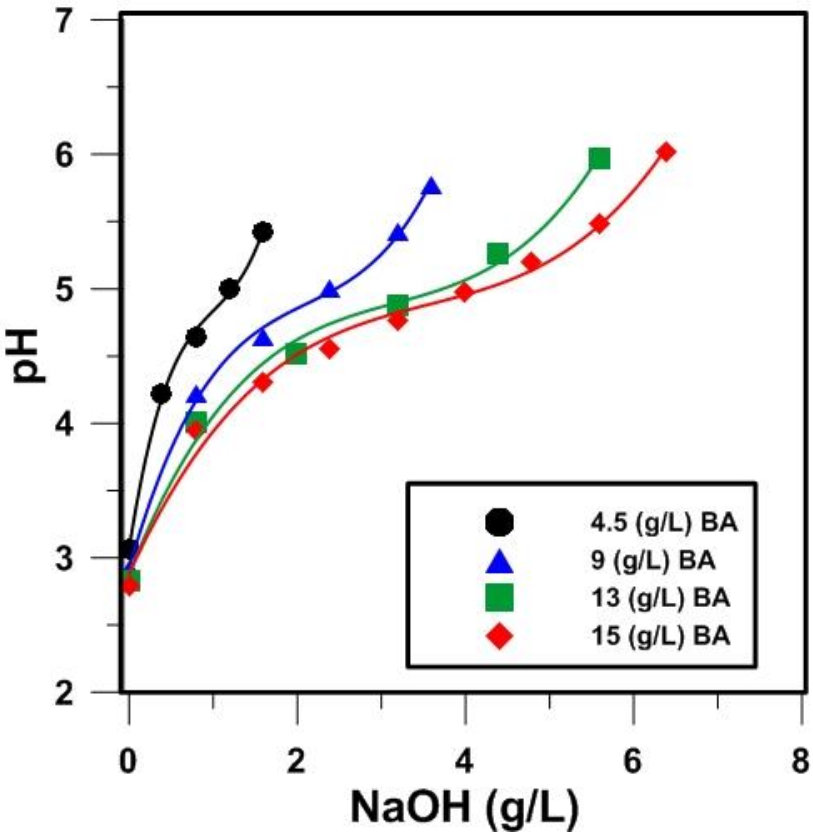

Figure 4-4 Titration curves of the butyric acid aqueous solutions by adding NaOH (lines only show the trend and they are not experimental data).

Figure 4-5 depicts the equilibrium vapour concentration of butyric acid as a function of pH for four different butyric acid feed concentrations. Results clearly show the effect of pH on the vapour liquid equilibrium and its strong correlation with the level of acid dissociation. At pH in the vicinity of 3 where butyric acid would be essentially all associated, a much higher volatility based on the total concentration of butyric acid is obtained compared to the volatility of butyric acid at higher pH. At a pH above of 5.5, where nearly all butyric acid is dissociated, the volatility reached a minimum value. In the case of vacuum fermentation, this data will be very useful to determine the amount of butyric acid that would end up in the vapour phase and how much will remain in the fermentation broth for a given pH.

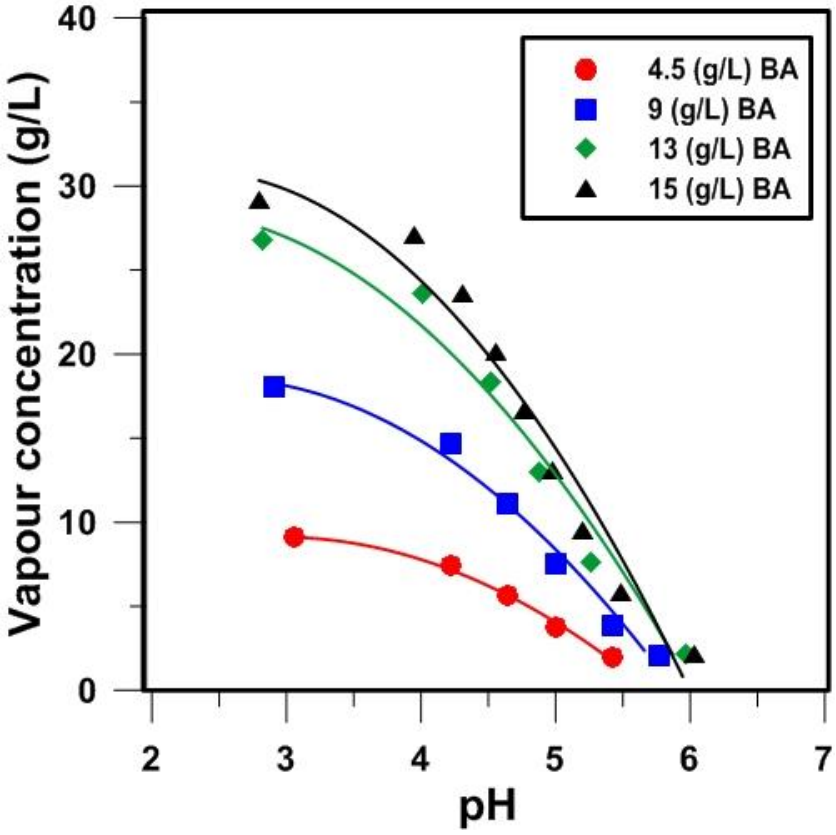

Figure 4-5 Vapour concentration of butyric acid solution at different pH and for four different initial feed concentrations of butyric acid (lines only show the trend and they are not experimental data).

It was desired to compare VLE data for butyric acid for a constant pH with the prediction obtained using two commercial process engineering softwares, namely Honeywell Unisim and Aspen Plus. The VLE curves predicted by the two commercial softwares and for two thermodynamic packages (NRTL and UNIQUAC) are plotted in Figure 4-6 along with the experimental VLE data obtained for 4 different pH levels. The VLE curves of Figure 4-6a are plotted as a function of the total mole fraction of butyric acid, i.e. the non-dissociated and dissociated butyric acid, in the liquid phase whereas the VLE curves of Figure 4-6b are plotted as a function of the estimated non-dissociated butyric acid molar fraction. The non-dissociated BA mole fraction was calculated based on the pH value of the solution and the initial concentration of the butyric acid. Results show that, at lower pH values, the experimental data are in between

the two VLE curves estimated by Unisim and Aspen Plus. It is important to note that the commercial software like Honeywell UniSim and Aspen Plus do not take into account the solution pH such that the predictions are performed for non-dissociated butyric acid. However, increasing the pH of the solution and favouring a higher concentration of dissociated butyric acid resulted in the VLE curves deviation from the curves for lower pH and, obviously, NRTL and UNIQUAC were unable to offer good predictions. For a given liquid mole fraction, the equilibrium vapour mole fraction decreases as the solution pH is increased.

These results clearly show that, when considering only the estimated concentration of the non-dissociated butyric acid, all the points fall approximately on the same VLE curve. Therefore, in a vacuum fermentation, a higher retention rate of butyric acid in the fermenter would be achieved. In addition, it seems that the experimental VLE data for non-dissociated butyric acid is better predicted with Honeywell Unisim.

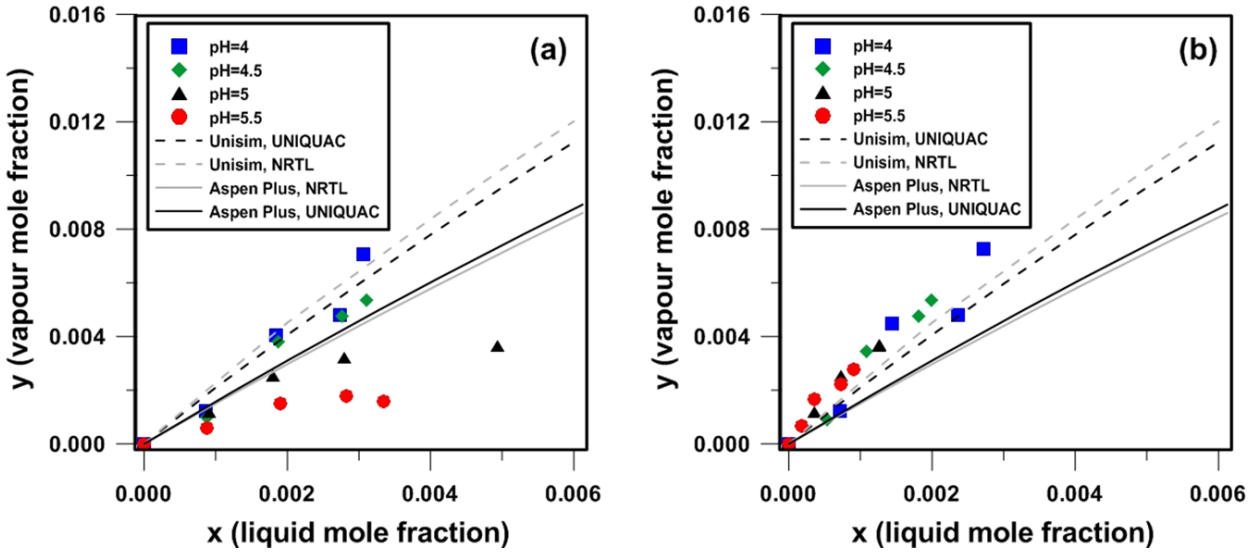

Figure 4-6 Vapour-liquid equilibrium of butyric acid solution at different pH (a: based on the initial concentration of BA in the liquid, b: based on the estimated non-dissociated concentration of BA in the liquid).

Effect of pH on butyric acid pervaporation

The effect of the pH of the feed solution on the pervaporation separation of butanol and butyric acid using a PDMS commercial membrane was investigated in terms of the separation factor, the

permeate concentration, and the permeate flux are shown in Figure 4-7 and 4-8. Results of Figure 4-7a clearly show that an increase of pH of the feed solution leads to a decrease in the separation factor of both butyric acid and butanol. As a result, the butyric acid would have a lower solubility in the membrane and consequently the separation factor for butyric acid decreases, as pH increases. Moreover, the concentration of butanol and BA in permeate decreased with an increase in pH of the feed solution (Figure 4-7b) which resulted in a lower value for separation factor in Figure 4-7a.

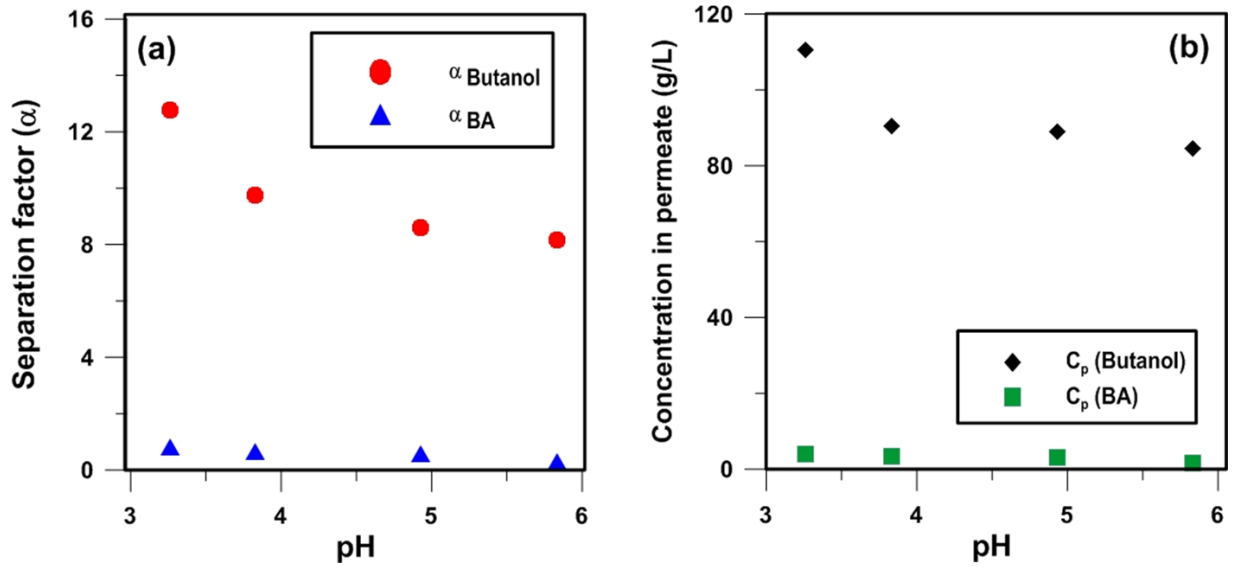

Figure 4-7 Effect of pH on (a) the separation factor of PDMS membrane, and (b) permeate concentration, (at 37°C, with a butanol and BA feed concentration of 10 g/L and 5 g/L, respectively).

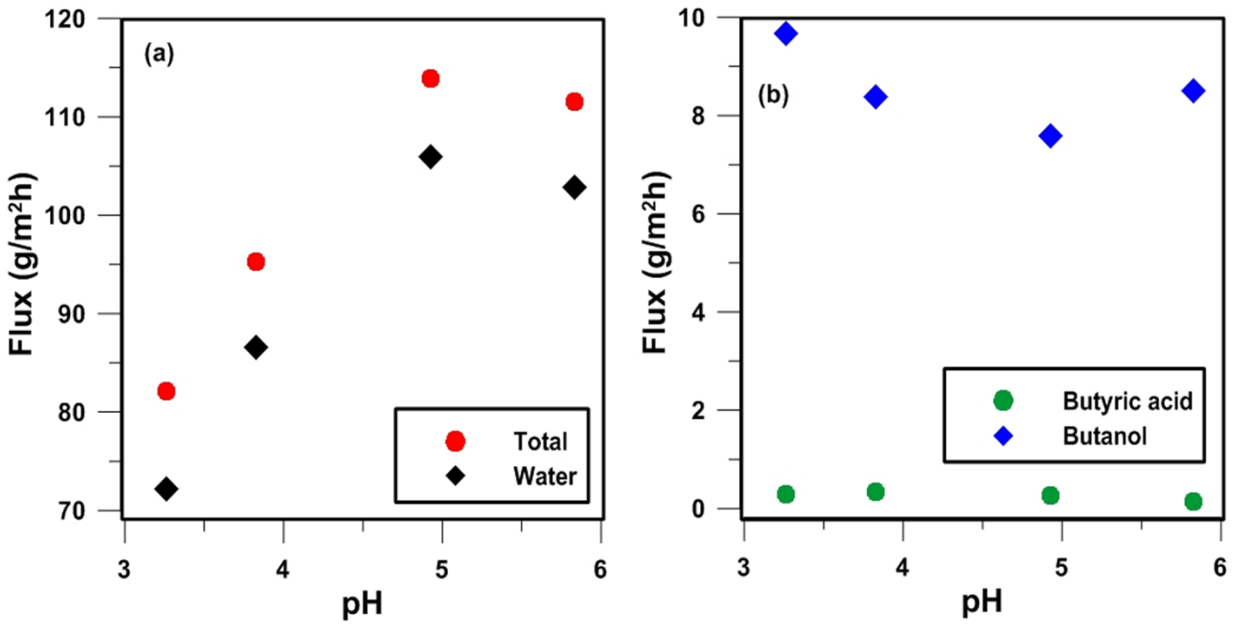

Figure 4-8 Effect of pH on the PDMS membrane permeation flux, (a) total and water flux, (b) butyric acid and butanol (at 37°C, with a butanol and BA feed concentration of 10 g/L and 5 g/L, respectively).

Results of Figure 4-8 show that by increasing the amount of sodium hydroxide in order to increase the pH of the feed solution, the total flux increased due to the increase in the permeation flux of water (Figure 4-8a). In addition, the flux of butanol decreased slightly with an increase in pH whereas the permeation flux of butyric acid was very small and did remained essentially unchanged (Figure 4-8b). The higher flux of water and the lower flux of butanol could be as a result of the decrease in surface hydrophobicity of the PDMS membrane due to the presence of sodium ions and deprotonated BA at the membrane surface and higher pH. It has been reported that sodium hydroxide has been used to make the surface of the PDMS more hydrophilic [29,30]. Furthermore, the higher concentrations of water in the permeate side of the membrane could be another reason for the decrease in the separation factor of the PDMS membrane. Results show that an increase in the pH of the feed solution has a negative effect on the pervaporation separation performances of PDMS membranes.

In the case where pervaporation is integrated to a continuous ABE fermentation system for the in situ removal to decrease the concentration of butanol in the fermenter to favour higher butanol productivity, the effect of pH has a very minor impact on the removal of butyric acid such that it

is not necessary to consider the solution pH for the retention of butyric acid within the fermenter. On the other hand, the addition of NaOH appeared to have a detrimental effect on the separation of butanol.

Effect of pH on adsorption separation performance

A series of adsorption experiments were performed at different initial pH levels (3.5-7) to investigate the influence of the pH on the adsorption capacity of butyric acid using F400 activated carbon as adsorbents. Results, presented in Figure 4-9, revealed that by increasing the initial pH level of the feed solutions, the maximum adsorption capacity (q_s) of the activated carbon decreased. The highest value for the maximum adsorption capacity was obtained at a pH of 3.5. Moreover, the Langmuir isotherm model was able to model the experimental data very accurately. In addition to level of dissociation; it is hypothesized that the decrease in the adsorption capacity of butyric acid may be due to the higher adsorption capacity of water. The presence of the sodium ions at the surface of the activated carbon adsorbents increases the hydrophilicity of the adsorbent particles and, as a result, a higher adsorption capacity for water [31–33]. It was reported that water molecules are strongly adsorbed on hydrophilic groups via H-bonding. The adsorption of butyric acid, assumed here its non-dissociated state, on activated carbon leads to a lower concentration of the butyric acid in solution and a higher pH since the same amount of NaOH is present in the solution. As a result, it is desired to measure the pH of the solution during the adsorption process. The final pH of the solutions was measured when equilibrium between the feed solution and the adsorbent was reached. Results confirm that the pH of the solution increases due to the adsorption of butyric acid onto the activated carbon adsorbent. Figure 4-10 shows the plot of the maximum adsorption capacity (q_s in Eq. 5) as a function of both the initial and final pH of the solution. The final pH of the solution was measured when equilibrium was reached. Based on the results, increases in pH and the concentration of dissociated butyric acid result in a decrease of the maximum adsorption capacity of activated carbon. This figure also revealed that there is an exponential relation between the maximum adsorption capacity and the pH of the solution which has been presented in Eq. 6.

The exponential expression for q_s was substituted in the Langmuir isotherm model (Eq. 7). Then the modified Langmuir model was fitted with the experimental data.

$$q_s = \beta e^{-\theta \times pH} \tag{6}$$

$$q_e = \left(\beta e^{-\theta \times pH}\right)\left(\frac{bC_e}{1+bC_e}\right) \tag{7}$$

where β and θ are the constants for the exponential fitted curve of the maximum adsorption capacity versus the final pH. A similar fit was obtained for the equilibrium adsorbed amount based on the initial pH. To determine the adsorbed amount for a given operating condition, it is more convenient using the initial pH because it more easily known. Table 4-1 presents the values for the constants of Eq. 7. The Sips model was also fitted to the experimental data but the exponent on the equilibrium concentration was nearly unity such that the Langmuir model was used.

Table 4-1 Constants values for the modified Langmuir model.

pH	β	θ	b (*L/g*)
Initial pH	1795.8	0.61	0.61
Final pH	1301.3	0.37	1.39

The proposed model was used to estimate the adsorption isotherm of the F400 activated carbon for different values of the final pH. The Langmuir constant values in Table 4-1 are obviously different for the initial and final pH; however, for an equilibrium butyric acid concentration, an equal estimated value of the adsorbed amount can be estimated. Figure 4-11 shows the modified Langmuir isotherm as a function of the final pH value. Based on these results, the protonated form of butyric acid has a higher affinity for the F400 activated carbon in comparison to deprotonated form prevailing at higher pH. The low affinity of the deprotonated butyric acid could be also explained in terms of the hydrophobicity. The deprotonated butyric acid is more polar than the protonated molecules and as a result it has less affinity with the F400 activated carbon. This lower adsorption at higher pH could be beneficial for the ABE fermentation process since it is desired to keep the intermediate components in the fermenter such as butyric acid and acetic acid that are re-assimilated to produce butanol and acetone, respectively. Moreover,

butanol and butyric acid have a high affinity for F400 activated carbon and they are in competition with each other in adsorption separation process. An increase in the pH of the solution, even slightly higher than the pKa of butyric acid could contribute to decrease the affinity of the butyric acid and increase butanol separation in a fermentation-adsorption integrated process.

Throughout the literature, few studies have been performed to investigate the effect of pH on separation processes involving weak organic acids but without specifically referring to their degree of dissociation [34–36]. For instance, Faisal et al. studied the effect of the pH on the adsorption separation process of butanol from ABE fermentation broths using MFI (Mobil Five) zeolite adsorbents. Based on the reported results, the adsorption capacity of the butyric acid decreased by 80% when the pH of the solution increased from 4 to 6 [36]. Similar decrease in butyric acid adsorption was observed by Petrick who used activated carbon as the adsorbent [34]. Furthermore, Reinsel et al. [37] investigated the effect of pH on the partition coefficients for short-chain organic acids, including butyric acid, for crude oil/water systems. They found that the partition coefficients decreased steadily as the pH was increased and the amount of organic acids moving from the water solution to the oil phase decreased to almost negligible values when the pH increased above 6. All these results, akin to the results found in this investigation, point to the fact that only the non-dissociated form of butyric acid participated in the butyric acid separation processes.

Altogether, the adsorption capacity of butyric acid is strongly pH dependent and an appropriate pH not only could retain a greater proportion of the intermediate organic acids in the fermenter to produce more butanol and acetone, and increase the sugar conversion. In addition, it can also enhance the adsorption separation of butanol in competition with the acetic and butyric acids.

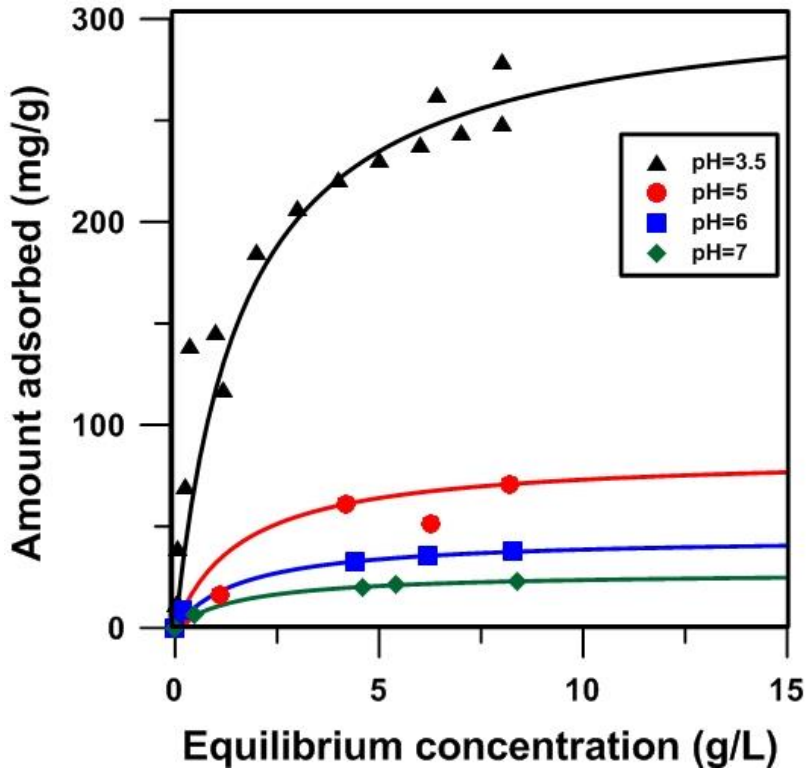

Figure 4-9 Effect of pH level on the adsorption capacity of the F400 for butyric acid separation from aqueous solution (lines represent the fitted Langmuir model).

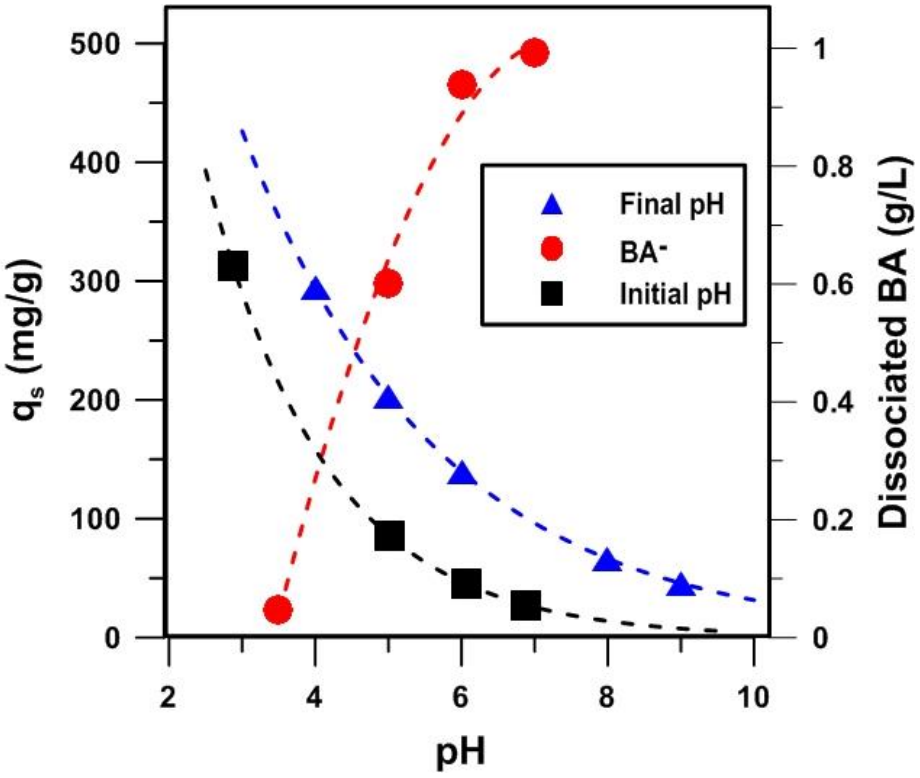

Figure 4-10 Effect of pH on the maximum adsorption capacity of butyric acid (BA0=1 g/L) on F400 activated carbon and on the level of dissociated amount of the butyric acid.

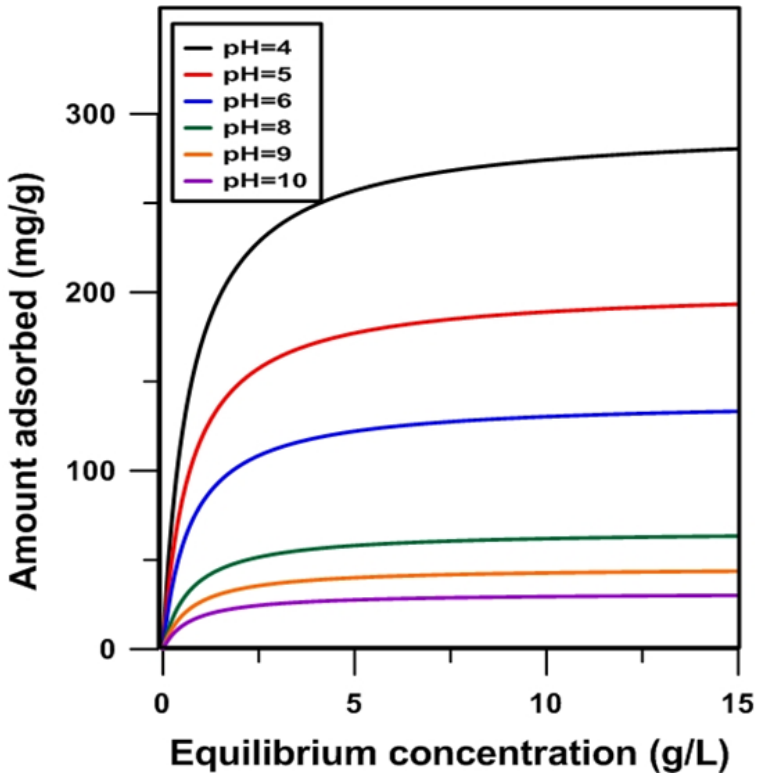

Figure 4-11 Effect of the final pH on the adsorption capacity of the F400 for butyric acid separation from aqueous solution (data presented are based on simulations using Eq. 7).

Conclusion

The effect of pH on the separation of butyric acid has been investigated for dilute aqueous solutions. Experiments were performed to determine the effect of the pH of the feed solution on VLE curves for the butyric acid/water system, the performance of pervaporation membranes in terms of separation factor and permeation flux of butyric acid and, finally, the adsorption capacity of activated carbon adsorbent for dilute solutions of butyric acid. Furthermore, a model was proposed to estimate the adsorption capacity of the adsorbents based on the initial and final pH of the solution. In all cases, increasing the pH of the feed solution decreased the amount of butyric acid that could be separated as the level of separation is strongly related to the level of dissociation of butyric acid. Indeed, it is the non-dissociated fraction of butyric acid that contributes to the driving force for the separation of butyric acid by distillation, membrane pervaporation and adsorption.

The higher concentration of the butyric acid in the fermenter could be beneficial for increasing the butanol production since this acid is a precursor to the production of butanol. However, there would be a limitation on the increase of pH for ABE fermentation and it should be monitored and controlled in both the growing phase and the production phase using batch fermentation. At the production stage, the organic acid will be re-assimilated to produce acetone, butanol and ethanol, which will be accompanied by an increase in pH. Keeping the pH at a high value at this stage of fermentation would be useful for butanol recovery and keeping the butyric acid within the fermentation.

Acknowledgment

The authors would like to acknowledge the financial support of the Natural Science and Engineering Research Council (NSERC) of Canada.

The Assistance of Hervé Guérin Kamwa and Chinue Joisse De La Merced, two COOP students of the University of Ottawa in performing some of the experiments is greatly appreciated.

Abbreviation

ABE	Acetone-Butanol-Ethanol
BA	Butyric acid
CA	*Clostridium acetobutylicum*
CB	*Clostridium beijerinkii*
HPLC	High-performance liquid chromatography
NRTL	Non-random two-liquid model
PDMS	Polydimethylsiloxane
UNIQUAC	Universal quasichemical
VLE	Vapor–liquid equilibrium

Nomenclature

A	effective surface area of the membrane (m^2)
b	Langmuir constant (L/g)
BA_0	initial concentration of butyric acid in solution (g/L)
C_e	equilibrium concentration of the component in solution (g/L)
C_p	concentration of the component in permeate (g/L)
J	flux ($g/m^2.h$)
m_i	mass of species i in the permeate stream (g)
q_e	adsorption capacity of the component at equilibrium state (g/g)
q_s	maximum adsorption capacity of the component (g/g)
t	time of permeation (h)
x_i	mass fraction of species i in the permeate streams
y_i	mass fraction of species i in the feed streams
α_i	separation factor of species i
β	constant in Eq.6, (dimensionless)

References

[1] N. Qureshi, H. Blaschek, Biotechnol. Prog. **1999**, 15, 594.

[2] H. Dong, W. Tao, Z. Dai, L. Yang, F. Gong, Y. Zhang, Y. Li, Adv. Biochem. Eng.-Biotechnol. **2012**, 128, 85.

[3] S.B. Bankar, S.A. Survase, H. Ojamo, T. Granstrom, Rsc Adv. **2013**, 24734.

[4] C.L. Gabriel, Ind. Eng. Chem. **1928**, 20, 1063.

[5] G. Festel, BUTALCO "Competence for Second Generation Biofuels Based on Lignocellulose," BUTALCO GmbH company, **2014**.

[6] T. Ezeji, N. Qureshi, H. Blaschek, Chem. Rec. **2004**, 4, 305.

[7] L. Zhu, H. Dong, Y. Zhang, Y. Li, Metab. Eng. **2011**, 13, 426.

[8] J. Wang, X. Yang, C.-C. Chen, S.-T. Yang, Curr. Opin. Chem. Eng. **2014**, 6, 43.

[9] X. Liu, Q. Gu, C. Liao, X. Yu, Biomass Bioenergy. **2014**, 69, 192.

[10] Y. Jiang, C. Xu, F. Dong, Y. Yang, W. Jiang, S. Yang, Metab. Eng. **2009**, 11, 284.

[11] I. Maddox, E. Steiner, S. Hirsch, S. Wessner, N. Gutierrez, J. Gapes, K. Schuster, J. Mol. Microbiol. Biotechnol. **2000** 2, 95.

[12] S. Wang, Y. Zhang, H. Dong, S. Mao, Y. Zhu, R. Wang, G. Luan, Y. Li, Appl. Environ. Microbiol. **2011**, 77, 1674.

[13] J. Martin, H. Petitdemange, J. Ballongue, R. GAY, Biotechnol. Lett. **1983**, 5, 89.

[14] V.V. Zverlov, O. Berezina, G.A. Velikodvorskaya, W.H. Schwarz, Appl. Microbiol. Biotechnol. **2006**, 71, 587.

[15] L. Huang, C. Forsberg, L. Gibbins, Appl. Environ. Microbiol. **1986**, 51, 1230.

[16] M. Husemann, E. Papoutsakis, Biotechnol. Bioeng. **1988**, 32, 843.

[17] F. Monot, J. Eengasser, H. Petitdemange, Appl. Microbiol. Biotechnol. **1984**, 19, 422.

[18] A.P. Mariano, N. Qureshi, R. Maciel Filho, T.C. Ezeji, J. Chem. Technol. Biotechnol. **2012**, 87, 334.

[19] K.-M. Lu, S.-Y. Li, J. Taiwan Inst. Chem. Eng. **2014**, 45, 2106.

[20] T.C. Ezeji, N. Qureshi, H.P. Blaschek, World J. Microbiol. Biotechnol. **2003**, 19, 595.

[21] W.J. Groot, H.S. Soedjak, P.B. Donck, R.G.J.M. van der Lans, K.C.A.M. Luyben, J.M.K. Timmer, Bioprocess Eng. **1990**, 5, 203..

[22] N. Abdehagh, P. Gurnani, F.H. Tezel, J. Thibault, Adsorption. **2015**, 21, 185.

[23] N. Qureshi, I.S. Maddox, Food Bioprod. Process. **2005**, 83, 43.

[24] W.J. Groot, C.E. Vandenoever, N.W.F. Kossen, Biotechnol. Lett. **1984**, 6, 709.

[25] A. Hasanoglu, Y. Salt, S. Keleser, S. Ozkan, S. Dincer, Chem. Eng. Process. **2007**, 46, 300.

[26] M. Baghbanzadeh, D. Rana, C.Q. Lan, T. Matsuura, Sep. Purif. Rev. **2016**, 45, 141.

[27] N.L. Mai, S.H. Kim, S.H. Ha, H.S. Shin, Y.-M. Koo, Korean J. Chem. Eng. **2013**, 30, 1804.

[28] H. Azimi, F.H. Tezel, J. Thibault, J. Chem. Technol. Biotechnol. **2017**.

[29] I. Hoek, F. Tho, W.M. Arnold, Lab. Chip. **2010**, 10, 2283.

[30] J. Zhang, Y. Chen, M.A. Brook, Langmuir. **2013**, 29, 12432.

[31] X. Yao, L. Li, H. Li, S. He, J. Mater. Sci. **2014**, 49, 4807.

[32] F.-C. Wu, R.-L. Tseng, J. Hazard. Mater. **2008**, 152, 1256.

[33] A.L. Cazetta, A.M.M. Vargas, E.M. Nogami, M.H. Kunita, M.R. Guilherme, A.C. Martins, T.L. Silva, J.C.G. Moraes, V.C. Almeida, Chem. Eng. J. **2011**, 174, 117.

[34] T Tim Petrik, combined acetone, butanol, ethanol and organic acid fermentation by a degenerated strain of clostridium acetobutylicum and subsequent esterification, doctor of philosophy, Michigan, Michigan State University, **2011**.

[35] L. Nielsen, M. Larsson, O. Holst, B. Mattiasson, Appl. Microbiol. Biotechnol. **1988**, 28, 335.

[36] A. Faisal, A. Zarebska, P. Saremi, D. Korelskiy, L. Ohlin, U. Rova, J. Hedlund, M. Grahn, Adsorption. **2014**, 20, 465.

[37] M.A. Reinsel, J.J. Borkowski, J.T. Sears, J. Chem. Eng. Data. **1994**, 39, 513.

Appendix I

pH program equations

A computer program has been written to calculate the equilibrium concentration of the dissociated butyric acid based on initial concentrations of butyric acid (BA) and NaOH. In the program, the amount of BA dissociation is first calculated given the concentration $[H^+]$, $[BA^-]$ and [BA] such that the pKa is equal to 4.82. In the second part, ions $[H^+]$ and $[OH^-]$ are reacted such that their product becomes equal to 10^{-14}. This procedure is followed until the two equilibrium relations are satisfied within a given tolerance.

First part of the code: Calculations related to BA dissociation

Introduction

$$A = NaOH \quad or\left[OH^-\right]$$

$$B = \frac{1\times10^{-14}}{NaOH} \quad or\left[H^+\right]$$

$$C = 0 \quad (Conjugated\ BA)$$

$$DO$$

$$\frac{\left[H^+ + Y\right]\left[BA^- + Y\right]}{\left[BA_0 - BA^- - Y\right]} = 10^{-4.82} = E$$

$$\left[H^+\right]\left[BA^-\right] + Y\left(\left[BA^-\right] + \left[H^+\right]\right) + Y^2 = E\left[BA_0 - BA^- - Y\right]$$

$$Y^2 + \left(E + \left[H^+\right] + \left[BA^-\right]\right)Y + \left[H^+\right]\left[BA^-\right] + E\left[-BA_0 + BA^-\right] = 0$$

$$A_2 = 1$$

$$B_2 = E + \left[H^+\right] + \left[BA^-\right]$$

$$C_2 = \left[H^+\right]\left[BA^-\right] + E\left[-BA_0 + BA^-\right]$$

$$Y = \frac{\left(-B_2 + \sqrt{B_2^2 - 4A_2C_2}\right)}{2A_2}$$

$$B = B + Y$$

$$C = C + Y$$

Second part of the code: Calculations related to $[H^+]$ and $[OH^-]$ equilibrium

$$\left[H^+ - X\right]\left[OH^- - X\right] = 10^{-14}$$

$$X^2 + -\left(\left[H^+\right] + \left[OH^-\right]\right)X + \left[H^+\right]\left[OH^-\right] = 10^{-14}$$

$$A_1 = 1$$

$$B_1 = -\left(\left[H^+\right] + \left[OH^-\right]\right)$$

$$C_1 = \left[H^+\right]\left[OH^-\right] - 10^{-14}$$

$$X = \frac{\left(-B_1 + \sqrt{B_1^2 - 4A_1C_1}\right)}{2A_1}$$

$$A = A - X$$

$$B = B - X$$

LOOP UNTIL $\left(X \le 10^{-18} \text{ and } Y \le 10^{-18}\right)$

Part II: Simulation section

5. Chapter 5

Separation of butanol using pervaporation: A review of mass transfer models

Hoda Azimi, Jules Thibault and F. Handan Tezel*

Abstract

Pervaporation is deemed to be a suitable separation technique for butanol recovery from different aqueous solutions especially ABE fermentation broths. The performance of the membrane, in terms of permeate flux and selectivity, depends on the mass transfer of the migrating species across the membrane. As a result, modeling of mass transfer through membranes provides a deeper understanding on species permeation across membranes, which assist to orient the research and the development of the pervaporation process. Modeling of the mass transport through the membrane was mainly focused on sorption and diffusion of the components into and across the membrane. For each step, different models have been suggested and the overall mass transfer has been modeled by considering resistance-in-series models. In this study, an overview of the different models used for the pervaporation separation of butanol from aqueous solutions is presented considering the sorption and diffusion steps as well as the overall mass transfer in a single model. Up to now, the solution-diffusion based models were the main methods used to account for the mass transfer of butanol in the pervaporation process. The application of Maxwell-Stefan theory is very limited and the pore-flow model, to our knowledge was not used for the modeling of butanol separation by pervaporation.

Keywords: pervaporation; butanol; modeling; mass transfer

Introduction

The depletion of fossil fuels and world concerns about climate change have motivated researchers to find replacement fuels that would be renewable and near carbon neutral such as biodiesel, bioethanol and biobutanol. Many studies have been performed to propose ways to make the production of biofuels, and specially biobutanol, economically viable [1–7]. Biobutanol, a four-carbon alcohol, has enviable properties in comparison to the other biofuels. Some advantages of using biobutanol as a biofuel are its low volatility, low hydroscopicity and

lower corrosiveness. The biological production of n-butanol is achieved via Acetone-Butanol-Ethanol (ABE) fermentation. ABE fermentation using *Clostridium acetobutylicum* yields acetone, butanol and ethanol in a typical ratio of 3:6:1, respectively. However, to make butanol economically viable as a biofuel, the bioconversion efficiency and product purity via the ABE fermentation process should be improved to compensate for the currently very low product yield, product toxicity to microorganisms and multiple end-products [5,8–18].

Many studies have been undertaken in an attempt to increase the efficiency of butanol produced from ABE fermentation [3,4,19–24]. One method to improve the productivity of the ABE fermentation, the in-situ recovery of the solvents, has attracted considerable attention. The main separation methods used for butanol separation from the ABE fermentation process are vacuum fermentation [25] adsorption [26], gas-stripping [27], liquid-liquid extraction [28], perstraction [29], reverse osmosis [30] and pervaporation [1]. Among these methods, pervaporation is a highly regarded separation technique because of its low energy consumption, high selectivity and absence of harmful effect on microorganisms [1,31,32]. To mitigate the higher cost associated with the incorporation of a pervaporation membrane for the in situ recovery of ABE solvents from fermentation broths, it is necessary to resort to highly efficient membranes.

The performance of a pervaporation membrane is assessed by the permeation flux and selectivity. To improve membrane performance, a judicious synergistic combination of theory and laboratory work is necessary. To explain the migration of species across pervaporation membranes, a few models have been proposed: solution-diffusion model [33], Maxwell-Stefan theory [34], and pore-flow model [35,36]. With these models, it is possible to infer the performance of pervaporation membranes, but pervaporation remains a complex process to be modeled.

Until now, many reviews have considered the pervaporation fundamentals and membranes; however, there are only few studies published in the literature to review the mathematical models for pervaporation processes [37–45]. In this review paper, a brief summary of the mass transfer models used in pervaporation separation is presented followed by the discussion on the models applied for butanol recovery via this process.

Introduction to pervaporation

Pervaporation is a partial pressure or more generally concentration driven process, which is the combination of two mass transfer mechanisms: permeation and evaporation [46–48]. During pervaporation, a phase change from liquid to vapour occurs. A liquid feed solution to be separated is in contact with one side of the membrane surface and the permeating product leaves at a low vapor pressure from the other side that is kept under vacuum [49] or swept with a purge gas [50]. The permeate is then condensed or released depending on the objective of the separation [51]. Because of the presence of vacuum or the sweeping of an inert purge gas on the permeate side, a driving force across the membrane prevails. The required heat of vaporization comes from the liquid feed such that the temperature of the feed must be set accordingly. In recent years, several studies have been undertaken to better understand the pervaporation process and use it for numerous separation processes including the separation of water and alcohol mixtures using hydrophobic membranes [41,46,51–54]. Generally, pervaporation applications fall under three categories: (i) removal of water from organic solvents, (ii) removal of organic compounds from aqueous solutions, such as the recovery of the aromatic components and biofuels from fermentation broths, and (iii) separation of anhydrous organic mixtures. In this process, the separation depends on the chemical nature of the macromolecules that comprise the membrane, the physical structure of the membrane, the physicochemical properties of the mixtures to be separated, and the permeant-permeant and permeant-membrane interactions. Figure 5-1 shows the simplified schematic diagram of a typical pervaporation separation experimental system used to test pervaporation membranes.

Pervaporation membranes

Membranes, which have been used for pervaporation separation of butanol, are either zeolite membranes such as silicalite zeolite membranes and ultrathin zeolite X films [55–58] or polymeric membranes. Different kinds of polymers have been reported in the literature for butanol separation such as styrene butadiene rubber (SBR) [59], ethylene propylene diene rubber (EPDM) [60], polytetrafluoroethylene (PTFE) [61], polypropylene (PP) [62], polyurethane (polyether based) (PUR) [63], polyether block-amide (PEBA) [64], poly (vinylidinedifluoride) (PVDF) [65], poly (methoxy siloxane) (PMS) [66], poly (dimethylsiloxane) (PDMS) [20], poly

(1-(trimethylsilyl)-1-propyne) (PTMSP) [67] and polyamide-imide (PAI) containing cyclodextrin (CD) [68]. Polymeric membranes are less expensive and more flexible in comparison to zeolite membranes [46,69]. However, a composite membrane incorporating these two materials have also been used by some researchers [70–73] to benefit from the outstanding characteristics of each medium to enhance membrane performance.

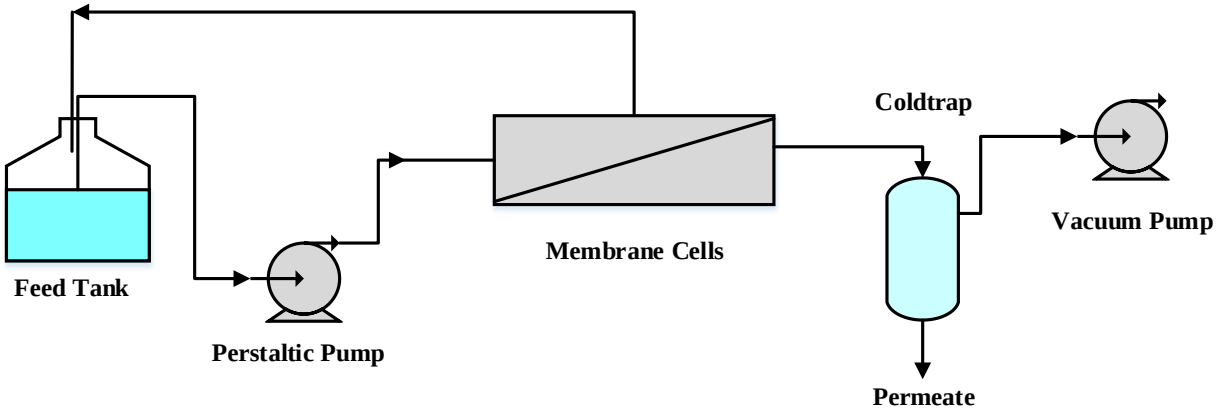

Figure 5-1 Simplified schematic diagram for a typical pervaporation separation setup.

Models used for mass transfer in pervaporation

Description of mass transport through membranes is essential to enhance the design efficiency and consequently obtaining better separation performance. Up to now, different models have been introduced to study the pervaporation separation process by considering the species behaviour, membrane properties and operating conditions. Similar to the proposed models for membrane-based gas separation applications, a resistance-in-series theory can be used to describe the mass transfer of components through membranes in pervaporation separation system. According to this theory, the sorption of species in the liquid feed takes place at the membrane surface and species then diffuse through the membrane prior to desorbing on the other side of the membrane. However, the mass transfer at the permeate side has been reported to be negligible in the overall mass transfer due to considerably lower pressure in the permeate side [45]. Therefore, desorption step can be modeled in a similar way to the sorption step such that it

will not be discussed individually in this study. Figure 5-2 provides an overview of the different mass transfer models, which have been used in pervaporation separation processes.

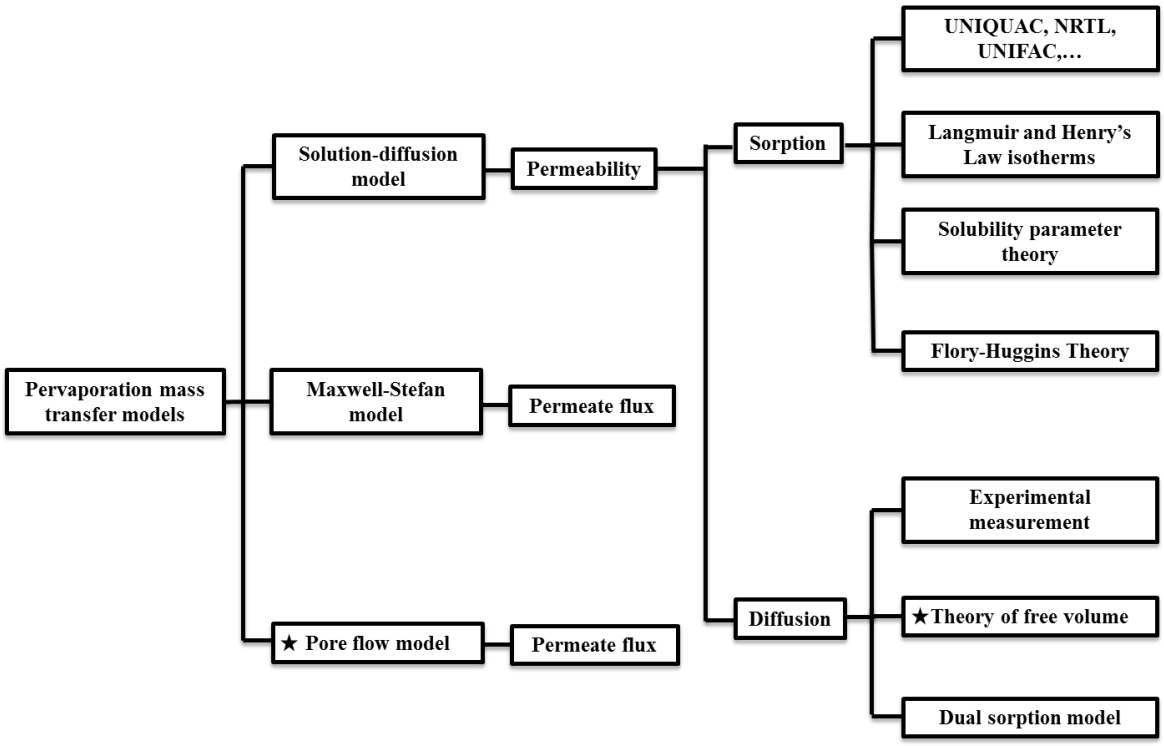

Figure 5-2 Summary of different mass transfer models used for pervaporation separation processes (star refers to models not yet used for butanol mixtures).

In addition, Figure 5-3 shows the chemical potential (μ), total pressure (p) and concentration (C) profiles of a migrating species across the membrane thickness in the pervaporation separation process assuming a high vacuum on the permeate side and linear concentration profile within the membrane.

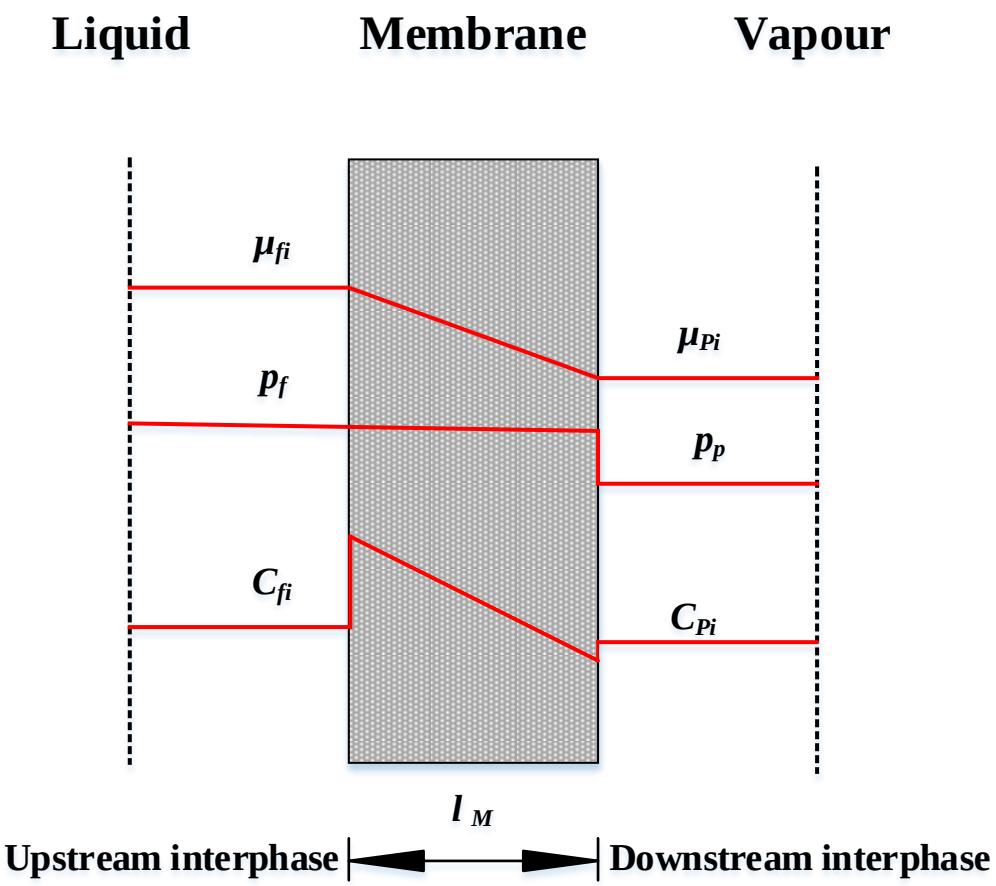

Figure 5-3 Gradient profiles across the membrane and the two boundary layers prevailing for the pervaporation system.

Solution-diffusion model

The solution-diffusion model is used for membranes under the assumption that the mass transport across the membrane proceeds in three steps: (1) the sorption of the penetrants into the membrane, (2) the diffusion of the sorbed components through the membrane as a result of concentration gradient, and (3) the desorption of the diffused components on the permeate side. Moreover, it is assumed that the total pressure is constant within the membrane and the thermodynamic equilibrium has been reached at the two interfaces.

Considering the Fick's first law of diffusion, the permeation flux of component *i* can be obtained using Eq. (1) [45].

$$J_i = -D_{M,i}\frac{dC_{M,i}}{dz} \quad (1)$$

where J_i is the permeation flux of component i, $D_{M,i}$ is the diffusion coefficient of component i through the membrane ($m^2.s^{-1}$) and $C_{M,i}$ is the concentration of component i within the membrane ($kmol.m^{-3}$). This equation can be expressed in terms of the bulk concentration or activity of component on both sides of the membrane [43,45] as the mass transfer driving force (Eq. (2)).

$$J_i = \frac{P_{M,i}}{l_M}\left(a_{f,i} - a_{p,i}\right) \quad (2a)$$

$$P_{M,i} = D_{M,i}S_{M,i} \quad (2b)$$

In Eq.(2), $P_{M,i}$ is the permeability ($kmol.m^{-1}.s^{-1}$) of component i, which is the product of solubility coefficient ($S_{M,i}$) and diffusion coefficient ($D_{M,i}$) [45]. The solution-diffusion model has been widely used for the development and optimization of membranes. However, for a more accurate prediction of membrane performances, it is necessary to determine the diffusion coefficient and the solubility coefficent or their combined product (permeability). The experimental determination of these parameters comes with a significant level of uncertainties, which makes it difficult to use the solution-diffusion model with confidence. Moreover, the permeability by itself does not provide any information that could used for membrane development. In addition, the original solution-diffusion theory cannot consider the coupling effect between the migrating species and, consequently, this model is only applicable when the coupling flux is negligible in comparison with individual fluxes of penetrants. However, the influence of the coupling flux may be a significant factor which should be taken into account in modeling the mass transfer in pervaporation separation [74]. The interactions between the dissolved components that have high affinity with each other result in the coupling of the species through the membrane penetration. In other words, the presence of one species in a mixture affects the Gibbs free energy of the other components and consequently results in changing the penetration behavior through the membrane [75–77]. However, the coupling effect consideration in a model would increase the level of complexity of the model and needs additional experimental parameters.

A semi-empirical approach was proposed [45] for the solution-diffusion model where the driving force in the original solution-diffusion model was replaced by a pressure-based fugacity and the equation was derived from Fick's first law of diffusion for a one-directional mass transfer through the membrane as given in Eq.(3).

$$J_i = -\dot{C}_i \frac{D_i^T}{f_i^0} \frac{1}{\gamma_i} \frac{df_i}{dz} \tag{3}$$

where, D^T is the thermodynamic diffusion coefficient ($m^2.s^{-1}$), f_i is the fugacity (*bar*) and γ_i is the activity coefficient of component i. The coupling effect of the species was considered in this model by introducing coupling coefficients B_{ij} and B_{ji} to establish a relationship between the local activity coefficients and the local fugacity parameters as given in Eq. (4).

$$\gamma_i = \exp\left(B_{ii}\left[1 - \left[\frac{f_i}{f_i^0} + B_{ij} \frac{f_i}{f_j^0} \right] \right] \right) \tag{4a}$$

$$\gamma_j = \exp\left(B_{jj}\left[1 - \left[\frac{f_j}{f_j^0} + B_{ji} \frac{f_i}{f_i^0} \right] \right] \right) \tag{4b}$$

Eq.(4) can be further extended to consider ternary feed solutions as discussed by Lipnizki and Tragardh [45].

The integration of Eq. (3) and taking a geometric average ($\gamma_{M,i}$) between the activity coefficient of the components result in Eq. (5) for the calculation of the permeation flux.

$$J_i = \frac{\bar{D}_i^T}{\gamma_{M,i}} \left[\frac{f_{f,i} - f_{P,i}}{f_i^0} \right] = \frac{\bar{D}_i^T}{\gamma_{M,i}} \left(a_{f,i} - a_{P,i} \right) \tag{5a}$$

$$\bar{D}_i^T = \frac{C_{M,i} D_i^T}{l_M} \tag{5b}$$

where $\bar{D}_i^T$ is the modified thermodynamic diffusion coefficient. According to Franke [78], this model showed a fairly good agreement with the experimental data for a ternary feed mixture of water, ethanol, and butanol using a PAN/PAV pervaporation membrane.

The modified solution-diffusion model would be very useful when coupling impacts the mass transfer through the membrane. However, if coupling effects are negligible, this equation would only add unnecessary complexity to the model. Akin to the main solution-diffusion model, semi-empirical models based on the solution-diffusion model can also be used for process and module design.

In the following section the models which have been used to estimate the sorption peoperties and the diffusivity of the components through membranes are dicussed.

Predictive models for the sorption properties

One of the major mass transfer steps in the pervaporation process is the transfer of a penetrant from the boundary layer to the membrane surface where it can be sorbed. The boundary layer is the thin layer in the vicinity of the membrane interface in which the diffusive mass transfer is the dominating transport mechanism as a result of the decrease of the flow velocity in comparison to the velocity of the bulk liquid [44]. The diffusive flux at the boundary layer of the membrane is a function of the bulk phase velocity, the membrane module geometry, the viscosity of the feed solution and the properties of the penetrants [79]. The diffusion rate of a species in the boundary layer is dictated by the difference of concentration between the bulk liquid and the liquid-membrane interface. The concentration at the interface depends on the solubility of a species in the membrane and the rate of diffusion within the membrane. However, for pervaporation, the rate of diffusion through the membrane in relatively small and the concentration at the surface of the membrane is usually in equilibrium with the liquid bulk concentration. At the interface, there exists a competition for sorption between the different components. The more soluble components with the highest affinity with the membrane material will sorb preferentially into the membrane whereas the other components will sorb less into the polymer and mostly remain in the bulk of the fluid.

Sorption isotherms are used to represent the sorption capacity of a membrane for each species, which is related to the activity or volume fraction of the penetrant in the membrane. Modelling of sorption behavior is relatively well established and will be briefly reviewed in the following sections.

Langmuir and Henry's law isotherms

The most common way to represent sorption capacity is through isotherms, which are most often determined experimentally. Henry's law isotherm (Eq. (6)) is typically used for rubbery membrane, while Langmuir isotherm (Eq. (7)) is more accurate in the case of glassy polymers [80].

$$C_{H,i} = k_{D,i} p_i \tag{6}$$

$$C_{H,i} = \frac{C'_{H,i} b_i p_i}{1 + b_i p_i} \tag{7}$$

where, $k_{D,i}$ is the Henry's law constant referring to component i (bar^{-1}) , p_i is the partial pressure (bar), $C'_{H,i}$ is the Langmuir maximum sorption capacity in the polymeric membrane ($kmol.m^{-3}$) and b_i is the adsorption or hole affinity constant (bar^{-1}). Langmuir's and Henry's law isotherms are theoretical models to predict the equilibrium sorption of component i inside the membrane. Even though the parameters of these isotherms must usually be obtained experimentally, some attempts have been made with molecular dynamic simulations to predict species solubility [81,82]. However, these isotherms are representative for the prediction of sorption capacity of pure feed in the membrane; therefore, these models are only applicable for dilute solutions where the competition among species sorption is negligible. In addition, more complex models such as the extended Langmuir and dual-mode sorption models might be more appropriate to predict the sorption behaviour of multicomponent mixtures which will be discussed in more details in a subsequent section [45,83,84].

Solubility parameter theory

Solubility parameter theory is a semi-empirical model that has generally been used for the selection of membrane material to separate a specific component from mixtures. This parameter represents the affinity between the migrating species and the membrane by taking into account the interactions between the solute and the polymer [85]. A high affinity between the penetrating component and the membrane prevails when the solubility parameter for them are similar. However, excessive similarity between them would result in the immobilization of the components in the membrane.

The solubility parameter is defined by Eq. (8) where δ_i is the solubility parameter ($J^{1/2}.m^{-3/2}$), $\Delta E_{vap,i}$ ($J.mol^{-1}$) is the total energy required to remove a molecule from its adjacent molecules, and V_i is the molar volume of component i ($m^3.mol^{-1}$) [86].

$$\delta_i = \sqrt{\frac{\Delta E_{vap,i}}{V_i}} \tag{8}$$

To improve the estimation accuracy of the solubility parameter, Hansen [87] proposed a three-dimensional solubility parameter by considering the total energy ($\Delta E_{vap,i}$) as a summation of energies required to overcome dispersion forces ($\Delta E_{df,i}$), dispersion polar interactions ($\Delta E_{di,i}$) and breaking hydrogen bonds ($\Delta E_{hb,i}$), i.e. $\Delta E_{vap,i} = \Delta E_{df,i} + \Delta E_{di,i} + \Delta E_{hb,i}$. Therefore, the three-dimensional solubility parameter is defined as follows (Eq. (9)):

$$\delta_i = \sqrt{\delta_{df,i}^2 + \delta_{di,i}^2 + \delta_{hb,i}^2} \tag{9}$$

These parameters are normally used to measure the distance parameter ($\Delta_{p,i}$) defined as the distance between two components, polymer and penetrant. A smaller value of Δ implies a greater affinity between the polymer and the penetrant, which would also increase the membrane swelling during pervaporation.

$$\Delta_{p,i} = \left[\left(\delta_{df,P} - \delta_{df,i}\right)^2 + \left(\delta_{di,P} - \delta_{di,i}\right)^2 + \left(\delta_{hb,P} - \delta_{hb,i}\right)^2\right]^{1/2} \tag{10}$$

Zhou et al. studied the affinity of butanol and water for PDMS membranes. Their result revealed that hydrogen bonding and polar interaction parameters are the dominating parameters, which control the affinity of the components. Moreover, Water/PDMS has a greater distance parameter (41.4 $MPa^{1/2}$) compared to butanol/PDMS (13.0 $MPa^{1/2}$). The smaller distance for butanol indicates that it has a higher affinity for PDMS compared to water and will be preferentially sorbed into the membrane [88,89].

In another work, the distance parameter for acetone-butanol-ethanol (ABE) solution was reported by Niemisto et al. [90]. A pair of components having a distance value ($\Delta_{PDMS,i}$) closer to zero are more likely to have a higher affinity to each other. According to their study, PDMS has the highest affinity towards acetone ($\Delta_{PDMS,A}$=10.6), followed by butanol ($\Delta_{PDMS,B}$=12.4), ethanol ($\Delta_{PDMS,E}$=17.1) and water ($\Delta_{PDMS,w}$=40.9).

To increase the estimation accuracy of the three-dimensional solubility parameter model presented by Hansen, weight factors could be added to Eq. (10) as shown in Eq. (11). The weight factors (*W*) correspond to the chemical nature of the components [91] and need to be obtained experimentally [92].

$$\Delta_{p,i} = \left[W_1\left(\delta_{df,P} - \delta_{df,i}\right)^2 + W_2\left(\delta_{di,P} - \delta_{di,i}\right)^2 + W_3\left(\delta_{hb,P} - \delta_{hb,i}\right)^2\right]^{1/2} \quad (11)$$

Froehling et al. [93] proposed a modified model to estimate the solubility parameters for a ternary system composed of a binary mixture and the membrane (Eq. (12)). In this equation, ϕ_i accounts for the volume fraction of component *i* in the binary mixture.

$$\delta_{df,ij}^{mix} = \phi_i \delta_{df,i} + \phi_j \delta_{df,j} \quad (12a)$$

$$\delta_{di,ij}^{mix} = \phi_i \delta_{di,i} + \phi_j \delta_{di,j} \quad (12b)$$

$$\delta_{hb,ij}^{mix} = \phi_i \delta_{hb,i} + \phi_j \delta_{hb,j} \quad (12c)$$

As mentioned before, the solubility parameter theory has been mostly used for qualitative and not quantitative purposes. In other words, this theory contributes more to material selection

whereas it cannot be employed for process and module design or for the simulation of the mass transfer through polymeric membranes.

Flory-Huggins Theory

The Flory-Huggins theory, as a semi-empirical model, has been widely used to estimate the sorption properties of pure species and binary solutions in polymeric materials. Regarding the butanol sorption properties on polymeric membranes, the Flory-Huggins model has been successfully applied for the prediction of the sorption capacity of this component in blended poly (dimethylsiloxane)–benzyl-3-butylimidazolium tetrafluoroborate membranes [90].

According to this theory, the solubility of components in membranes will be a function of Gibbs free energy of interacting substances and could be represented by a set of dimensionless parameters, which are called Flory-Huggins interaction parameters (χ_{ij}). For a ternary system including a binary mixture of components *i* and *j* and the polymeric membrane (non-crosslinked high molecular weight), the Flory-Huggins model is expressed using Eq. (13).

$$\ln a_i = \ln \phi_i + (1-\phi_i) - (\frac{V_i}{V_j})\phi_j - (\frac{V_i}{V_p})\phi_p + \left[\left(\chi_{i,j}\phi_j + \chi_{i,p}\phi_p\right)\left(\phi_j + \phi_p\right)\right] - \chi_{j,p}(\frac{V_i}{V_j})\phi_j\phi_p \qquad (13)$$

In Eq. (13), $\chi_{i,j}$ is the interaction parameter between components *i* and *j*, while $\chi_{i,p}$ and $\chi_{j,p}$ represent the interaction between the components and the polymer. For a binary system consisting of a pure component and a polymeric membrane, Eq. (13) reduces to Eq. (14) by considering that ϕ_j is equal to zero.

$$\ln a_i = \ln \phi_i + (1-\phi_i) - (\frac{V_i}{V_p})\phi_p + \chi_{i,p}\phi_p^2 \qquad (14)$$

Moreover, for a binary system (a_i = 1 and $V_i << V_p$), Eq. (15) could be substituted into Eq. (14) to obtain the Flory-Huggins binary interaction parameter between component *i* and the polymer (Eq. (16)). Furthermore, the activity coefficient (a_i) in the Flory-Huggins equation can be determined using different thermodynamic fluid packages such as NRTL, UNIQUAC, or UNIFAC models.

$$\phi_i + \phi_p = 1 \tag{15}$$

$$\chi_{i,p} = -\left(\frac{\ln(1-\phi_P) + \phi_P}{\phi_P^2} \right) \tag{16}$$

In Eq. (16), $\chi_{i,p}$ is assumed constant at fixed temperature and could be obtained experimentally by performing swelling measurement of the polymer in contact with pure components, by sorption measurement of species in polymer or by inverse gas chromatography. However, since the latter method depends on temperature and concentration, it would be difficult to have an accurate estimation of the Flory-Huggins interaction parameter. Therefore, swelling and sorption experiments are the preferred approaches to estimate the Flory-Huggins interaction parameter.

As far as it was mentioned before, selecting the proper thermodynamic fluid package is required to estimate the activity of species and consequently predicting the sorption properties of the components in polymeric membranes via Flory-Huggins theory. Extended Raoult's law could be used to predict the activity of components in equilibrium with the liquid feed composition at different operating conditions (Eq. (17)). In this equation, γ_i and x_i are the activity coefficient and molar fraction in the feed, respectively.

$$a_i = \frac{p_i}{p^{sat}} = \gamma_i x_i \tag{17}$$

The experimental activity coefficient of butanol has been summarised in Table 5-1 along with the predicted values by different models such as NRTL [94], MOSCED [95], UNIQUAC models [94] for certain specific temperatures. Although the variation between reported experimental activity coefficients is considerable, in general the reported values seem to be different from the ones predicted by theoretical models especially for estimated amounts by the MOSCED method.

Table 5-1 Summary of the updated data in the literature for infinite dilution activity coefficients of butanol in water.

T (K)	γ	Method	Ref	T (K)	γ	Method	Ref
273.15	40.21	HSA	[96]	313.15	54.60	COSMO-RS	[97]
273.15	32.59	HSA	[98]	318.15	60.22	TENS	[98]
283.15	40.41	HSA	[98]	320	15.55	MOSCED	[95]
288.15	49.01	IGS	[99]	323.15	73.11	PRV	[100]
290	20.72	MOSCED	[95]	323.15	61.37	RDIST	[101]
293.15	46.48	IGS	[99]	323.15	62.30	RDIST	[101]
293.15	41.39	HSA	[102]	323.15	61.50	TENS	[98]
293.15	48.38	HSA	[98]	323.15	58.67	HSA	[98]
298.15	46.48	IGS	[103]	323.15	59.38	HSA	[98]
298.15	52.88	DDST	[104]	323.2	58.67	GLC	[105]
298.15	48.18	TENS	[106]	323.23	78.73	TENS	[107]
298.15	44.48	IGS	[108]	328.15	61.62	NSGLC	[109]
298.15	54.98	HSA	[110]	328.15	62.80	TENS	[98]
298.15	52.83	HSA	[111]	330	14.09	MOSCED	[95]
298.15	47.09	IGS	[99]	333.15	47.80	TENS	[106]
298.15	49.45	HSA	[96]	333.15	59.32	GLC	[112]
298.15	53.68	NSGLC	[113]	333.15	79.28	VPC	[114]
298.15	53.30	HSA	[115]	333.15	73.70	PRV	[100]
298.15	58.85	HSA	[116]	333.15	66.69	RDIST	[101]
298.15	48.18	HSA	[117]	333.15	64.39	RDIST	[101]
298.15	53.62	WWC	[118]	333.15	65.10	RDIST	[101]
298.15	57.40	IGS	[119]	333.15	63.37	TENS	[98]
298.15	56.90	UNIQUAC	[94]	333.2	61.13	GLC	[105]
298.15	58.10	LSG	[94]	340	12.76	MOSCED	[95]
298.15	56.20	GEM-RS	[94]	343.15	59.32	EBUL	[120]
298.15	55.80	NRTL	[94]	343.15	67.83	EBUL	[121]
298.15	51.37	GLC	[94]	343.15	79.68	VPC	[114]
298.2	55.20	GLC	[105]	343.15	75.04	PRV	[100]
298.45	51.11	HSA	[122]	343.15	63.82	RDIST	[101]
300	18.89	MOSCED	[95]	353.15	57.23	EBUL	[120]
303.15	81.61	HSA	[123]	353.15	46.48	EBUL	[121]
303.15	51.68	HSA	[117]	353.15	73.19	VPC	[114]
303.15	53.41	TENS	[98]	353.15	76.55	PRV	[100]
308.15	39.49	HSA	[117]	353.15	62.80	RDIST	[101]
308.15	57.23	TENS	[98]	363.15	55.48	EBUL	[120]
310	17.16	MOSCED	[95]	363.15	79.52	PRV	[100]
313.15	49.50	GLC	[112]	372.15	27.11	EBUL	[121]

Table 5-1 continued							
T (K)	**γ**	**Method**	**Ref**	**T (K)**	**γ**	**Method**	**Ref**
313.15	89.57	VPC	[114]	372.15	56.09	CIRC	[98]
313.15	73.19	PRV	[100]	373.15	54.00	EBUL	[120]
313.15	58.91	TENS	[98]	373.15	88.23	EBUL	[124]

Predictive models for diffusivity

Diffusion is the second step in pervaporation mass transfer, which is the movement of the molecules based on the chemical potential difference across the membrane. It is also stated that in a highly swollen polymer, the diffusion coefficient of the permeant is related to the degree of swelling, the structure of the polymer, and the permeant size. An increase in the degree of swelling is accompanied by an increase in the free volume inside the polymer which leads to a more permeable pathway for mass transfer of the penetrants and an increase in diffusivity [125–127].

All of the above reports demonstrate that the estimation of the diffusion coefficient is paramount importance for studying the behavior of components and the mass transfer through membranes in pervaporation separation processes. Therefore, different models used to calculate the diffusion coefficient are reviewed in the following sections.

Empirical models

Typically, in empirical models, the diffusion coefficient is represented by an exponential function of the solute concentration as shown in Eq. (18).

$$D_i = D_i^0 \exp\left(\varepsilon_i \phi_i\right) \tag{18}$$

where D_i^0, ε_i, and ϕ_i are, respectively, the diffusion coefficient at infinite dilution of the solute (reference value), the softener [128] (empirical constant), and the volume fraction of the solute, for a single component diffusion in a rubbery polymer [45,129].

In a multicomponent separation, the model would be extended since the interactions of the polymer-component and component-component need to be taken into consideration. For instance, in a ternary system, including the membrane, Eq. (19) is applicable [129,130].

$$D_i = D_i^0 \exp(\varepsilon_i \phi_i + \varepsilon_j \phi_j) \quad (19a)$$

$$D_j = D_j^0 \exp(\varepsilon_i \phi_i + \varepsilon_j \phi_j) \quad (19b)$$

In some studies, a linear relationship between the diffusion coefficient and the solute concentration has been suggested [131,132] for glassy polymers [45].

As it is the case with all the empirical models, the complexity of the suggested model would depend highly on the studied system. In other words, as the number of components increases, the empirical parameters that need to be found experimentally increases, which implies time-consuming laboratory work and calculations. Therefore, these types of models can only be used to design the process and membrane module, while it cannot be used for membrane development.

Theory of free volume

According to the free volume theory, the molecular movement, a physical phenomenon within the polymer matrix, is the basis of diffusion. The model was fundamentally developed from Fick's first law of diffusion, which is applicable for ideal binary solutions. According to this theory, a penetrant molecule can only be transferred through the polymer if adequate free spaces exist. The free volumes are generated due to the random movement of the polymer segments. In other words, the free volume can be considered as a series of temporary micro-voids that are created in the polymer structure. In addition, in a pervaporation process, the sorption and desorption rates are much higher than that of the diffusion and could be assumed to happen instantly in comparison to the diffusion of species through membrane.

The diffusion coefficient D_i^T for a binary system (component *i* and polymer) can be estimated by Eq. (20) [133,134].

$$D_i^T\left(\phi_i,\phi_{C,p},T\right)=RTA_{di}\exp\left(-\frac{B_{di}}{f_p^{FV}\left(\phi_i,\phi_{C,p},T\right)}\right) \quad (20)$$

where T, A_{di} and B_{di} are the temperature (should be higher than glass transition temperature of the polymer), a measure of shape and size of the penetrant, and a measure of the size of the sorption area in the polymer, respectively. f_p^{FV} is called the free volume and it depends on the volume fraction of the permeant in the polymer(ϕ_i), the volume fraction of crystalline parts of the polymer (i.e. $\phi_{C,p}$) and temperature. In several studies, different equations have been proposed for the determination of f_p^{FV} in glassy and semi-crystalline polymers [135,136].

For a ternary system, Eq. (20) can be extended to Eq. (21) [137].

$$D_i^T\left(\phi_i,\phi_{C,p},T\right)=RTA_{di}\exp\left(\frac{-f_p^{FV}\left(0,0,T\right)}{B_i^{FV}}+\frac{\beta_i\left(T\right)}{B_i^{FV}}\phi_i+\frac{\beta_i\left(T\right)B_j^{FV}}{B_i^{FV}}\phi_j\right)^{-1} \quad (21)$$

In eq. (21), B_i^{FV} is a generalised type of B_{di} to make the equation applicable for both semi-crystalline and glassy polymers, and is evaluated using Eq. (22).

$$B_i^{FV}=\frac{B_{di}}{\left(1-\phi_{C,P}\right)} \quad (22)$$

The free volume theory has been reported to give a fairly good approximation of the diffusion coefficient and is applicable for membrane development in different pervaporation systems. It can be used to analize the diffusion through different types of membranes [138].

Dual-mode sorption model

The dual-mode sorption model, similar to the free volume theory, considers the presence of microvoids within the polymer structure as a transportation and accumulation medium. This model is mainly used for glassy polymers even though it could also be applied for rubbery polymers. It is assumed that the microvoids are uniformly distributed throughout the membrane.

The solute molecules may be captured by a neighbouring microvoid if the size of the molecule matches the size of the free space. The solute molecule is able to move through the microvoids if it has a sufficient amount of energy. If another solute molecule occupies the place of the transported molecule, diffusion will take place. Two mechanisms which have been considered for mass transfer in this model: (1) the diffusion of molecules through the microvoids (Henry's sorption sites-$C_{D,i}$) and the immobilised molecules in the free space ($C_{H,i}$). The total concentration of species *i* in the membrane is given by the summation of the two populations as expressed in Eq. (23) [45,83].

$$C_i = C_{D,i} + C_{H,i} = k_{D,i} p_i + \frac{C'_{H,i} b_i p_i}{1 + b_i p_i} \tag{23}$$

The first term of Eq. (23) corresponds to the normal dissolution of the permeant and is represented by the Henry's law linear isotherm. The second term, corresponding to the immobilised molecules in the microvoids, is nonlinear and expressed by the Langmuir isotherm. In Eq. (23), b_i is the microvoid affinity constant and represents the ratio of sorption and desorption rate constants of the penetrant through the free space and $C'_{H,i}$ is the Langmuir maximum sorption capacity of component *i* in the polymeric membrane.

The permeability of component *i*, according to the dual-mode sorption model can be calculated using Eq. (24).

$$P_i = k_{D,i} D_{D,i} + \frac{C'_{H,i} b_i D_{H,i}}{1 + b_i p_i} = k_{D,i} D_{D,i} \left(1 + \frac{F_i K_i}{1 + b_i p_i} \right) \tag{24a}$$

$$F_i = \frac{D_{H,i}}{D_{D,i}} \tag{24b}$$

$$K_i = \frac{C'_{H,i} b_i}{k_{D,i}} \tag{24c}$$

where F_i is the ratio of the mobile phase to the immobilized phase diffusion coefficients, i.e. partial immobilization and K_i is the ratio of the nonlinear to the linear sorption parameters.The extended version of the dual-mode sorption model is applicable for multicomponent systems. For a binary mixture, Eq. (25) can be used [84].

$$C_i = k_{D,i} p_i + \frac{C'_{H,i} b_i p_i}{1 + b_i p_i + b_j p_j} \tag{25a}$$

$$C_j = k_{D,j} p_j + \frac{C'_{H,j} b_j p_j}{1 + b_i p_i + b_j p_j} \tag{25b}$$

Considering Eq. (24) and Eq. (25), the permeability of component *i* in a binary mixture can be obtained using Eq. (26) [139].

$$P_i = k_{D,i} D_{D,i} \left(1 + \frac{F_i K_i}{1 + b_i p_i + b_j p_j} \right) \tag{26}$$

The dual-mode sorption model has been typically used for gas separation. However, this model could be a suitable model to predict the permeability in a pervaporation process [140]. Morover, this model could be applied for the purpose of membrane development.

In addition to the models which were discussed in this section, dynamic molecular simulation was also performed for the prediction of the diffusion parameters for the mass transfer through a membrane [141,142]. Although there is no study on butanol diffusion through organic membranes using molecular simulation, it has been mentioned that the molecular simulation would be the model that could be used in the future for analizing the diffusion behaviour [45].

Solution-diffusion model for butanol pervaporation separation

Instead of considering the sorption, diffusion and desorption steps separately, the overall mass transfer models take all three steps globally to calculate the permeation flux. The models do not offer a comprehensive understanding of the underlying phenomena but are nevertheless very useful for pervaporation process design and cost estimation. Different empirical models were

proposed in the literature and consider the entire mass transfer mechanisms as a whole without considering directly the physico-chemical interactions. These models relies on experimental results to estimate the model parameters and the resulting models are then used for predicting the permeation flux and selectivity. The predictions are obviously valid to specific cases that are similar to the experimental system that was used to generate the data for fitting the model. Therefore, they have very limted use for membrane development.

El-Zanati et al. used the resistance-in-series model based on the solution-diffusion concept to validate the pervaporation process of a binary solution of butanol and water via Pervap 2200 (PVA crosslinked/PAN support) membranes [143]. In this work, to predict the permeation flux, the overall mass transfer resistance was considered including three resistance steps: bulk feed convection, diffusion through the membrane, and the convective removal of permeating species on the permeate side. The flux associated with these three steps can be calculated using Eq. (27).

$$J_{f,i} = k_L C_{tot,L}\left(x_{f,i} - x_i^*\right) \tag{27a}$$

$$J_{f,i} = \frac{P_i}{l_M}\left(p_i^{sat}\gamma_i x_i^* - p_i^*\right) \tag{27b}$$

$$J_{P,i} = k_V\left(p_i^* - p_{P,i}\right) \tag{27c}$$

where k_L is the mass transfer coefficient at the liquid side, l_M is the thickness of the membrane (m) and k_v is the mass transfer coefficient at the vapour side. Under steady state conditions, the molar flux is constant at all positions within the membrane, which can be represented with a simple equation in terms of an overall mass transfer coefficient or overall mass transfer resistance ($1/K_{ov}$) as presented in Eq. (28).

$$J_i = K_{ov}\left(p_i^{sat}\gamma_i x_{i,b} - p_{i,P}\right) \tag{28a}$$

$$\frac{1}{K_{ov}} = \left(\frac{p_i^{sat}\gamma_i}{k_L C_{tot,L}}\right) + \left(\frac{l}{P_i}\right) + \left(\frac{1}{k_V}\right) \tag{28b}$$

In the case that the partial pressure on the permeate side approaches zero, the flux in Eq. (28) can be further simplified to Eq. (29).

$$J_i = K_{ov}\left(p_i^{sat}\gamma_i x_{i,b}\right) \tag{29}$$

El-Zanati et al. used Eq. (29) to determine the change of butanol concentration as a function of time during the pervaporation process [143]. Performing a mass balance on the feed tank and using Eq. (29), Eq. (30) was obtained to estimate the butanol concentration in the feed tank as a function of time.

$$C_b = \left(\frac{C_{tot,L}\left(\frac{J_b}{J_{tot}}\right) - C_{b0}}{\left(\frac{J_{tot}A_m}{V_0^T C_{tot,L}}\right)t - 1}\right) + C_{tot,L}\left(\frac{J_b}{J_{tot}}\right) \tag{30}$$

Based on the results presented by El-Zanati et al., the prediction model provided a good approximation of the flux and butanol concentration as a function of pervaporation time and represented the experimental results very well.

In a different work, Plaza et al. [33] used experimental sweep gas pervaporation data for the separation of butanol from ABE mixtures using a supported PTFE-gelled ionic liquid membrane and a resistance-in-series model to predict the mass transfer and diffusion coefficients. A semi-empirical procedure was used to estimate the diffusion coefficient, where the theoretical flux was assumed equal to the experimental flux and the diffusion coefficient was obtained by minimizing the mean-squared differences between the calculated and experimental values. Results showed a good fit with experimental data. However, as it was mentioned in their paper, a large difference between the calculated diffusion coefficients and values reported in similar works was observed. The values of the diffusion coefficient for butanol in ionic liquid (IL) membranes calculated in their work were approximately twice the values reported by Vopicka et al. [33,144,145].

Li et al. [19] used the solution-diffusion model based on the first Fick's law of diffusion for butanol pervaporation separation from a binary solution of water/butanol, ABE model solutions

containing different concentrations of glucose and other main metabolites, and ABE fermentation broths. The authors used a PDMS membrane and were able to quantify the coupling effect through the calculation of the overall mass transfer coefficient for each case. The overall mass transfer coefficient was estimated via the slope of the flux versus the concentration plot. Results showed that the estimated overall mass transfer coefficient for the binary solutions was larger than the estimated coefficient of the ABE model and real fermentation broths by approximately 16 and 28%, respectively. In addition, the coupling effects in ABE model solutions and fermentation broths, the complex interactions among the metabolites, media broth, and bio-macromolecules (such as blocking sorption sites and free volume) could also partly explain the difference between the calculated mass transfer coefficients. As the estimation of the overall mass transfer coefficients was strictly based on experimental data, it is not possible to generalize this information to other pervaporation separation systems. However, the insight regarding the effect of coupling and other complex interactions is useful.

Non-equilibrium solution-diffusion was applied by Yang et al. [146] for the pervaporation separation of organic compounds (acetone-butanol-ethanol) from binary aqueous solutions using PDMS membranes. In order to estimate the permeation flux, Eq. (31) has been applied under steady state conditions and concentration polarization and coupling effects have been considered negligible.

$$J = k_s C_f - k_d C_{f,M} = \frac{D_{M,i}}{l_M}\left(C_{f,M} - C_{P,M}\right) = k_d C_{P,M} - k_s C_P \tag{31}$$

where k_s and k_d are the sorption and desorption constants, respectively. In a pervaporation process, the rate of sorption at the permeate side is negligible. Therefore, after some rearrangements of Eq. (31), the flux can be calculated via Eq. (32).

$$J = \frac{C_f}{\frac{l_M}{\theta D_{M,i}} + \frac{2}{k_s - \frac{\theta D_{M,i}}{l_M}}} \tag{32a}$$

$$\theta = \frac{C_{f,M}}{C_f} = \frac{C_{P,M}}{C_P} = \frac{k_s}{k_d} \tag{32b}$$

The diffusion coefficient of the components and the sorption rate in Eq. (32) were estimated semi-empirically based on the data from the reciprocal of the flux versus the change in membrane thickness. The model demonstrated a good agreement with the experimental data at low feed concentrations. However, some deviations were observed at high concentrations of the organic compounds in the feed due to the intensified swelling of organics with PDMS polymer chain.

Li et al. [147] used a resistance-in-series model to study the effects of concentration polarization on the pervaporation separation of butanol from an aqueous binary solution by a tri-layer PDMS membrane, where a layer of hydrophobic PE was placed in between a PDMS layer and the metal support. In their work, the overall mass transfer coefficient was estimated using solution-diffusion model. However, the mass transfer coefficient of butanol in the feed channel was calculated semi-empirically using a Sherwood number correlation for rectangular membrane module (Eq. (33)).

$$Sh = \frac{k_b d_H}{D_b} = 1.85\left(\mathrm{Re}\, Sc \frac{d_H}{l_m}\right)^{0.33} \tag{33}$$

where d_H and l_m are the characteristic length of the rectangular membrane channel (hydrulic diameter) and the membrane module length, respectively. For this semi-empirical model, the mass transfer coefficient of butanol in the bulk layer is more than three times higher than that of the overall mass transfer coefficient. This clearly indicates that mass transfer is controlled by membrane diffusion, and the concentration polarization has a negligible effect on the transport process even when the system is operating in the laminar flow regime at a Reynolds number of 140.

In another work, Valentínyi et al. [148] improved the basic solution-diffusion model of Rautenbach et al. by considering that the transport coefficient as an exponential function of the permeating compound. In the basic solution-diffusion model, it is assumed that the transport

coefficient has negligible concentration dependency and can be considered constant [149]. However, a large deviation between the experimental data and the model predictions was found at higher concentrations. The transport coefficient or permeance of component *i* ($\dot{D}_i$), defined in Eq. (34), was used by Rautenbach et al. because the concentration dependence of the diffusion coefficient was considered to be negligible.

$$\dot{D}_i = \frac{CD_i}{l_M} \tag{34}$$

In the work of Valentínyi et al., the authors assumed that the transport coefficient varies exponentially with concentration as shown in Eq. (35) since the model suggested by Rautenbach et al. could not be used at high concentrations of the permeating component.

$$\dot{D}_i = \dot{D}_i \exp\left(B^* x_{f,i}\right) \tag{35}$$

where B^* is a constant. Results obtained by Valentínyi et al. for the dehydration of butanol aqueous solutions by pervaporation using commercial hydrophilic membranes (Poly (vinyl acetate) (PVA)/PAN) showed that the estimation of the transport coefficient using Eq. (35) provides a better predictions of butanol and water fluxes than the estimations using Eq. (34). The improved solution-diffusion model suggested by Valentínyi et al. could be used for azeotropic solutions with high water content as well as for modeling, design, and optimization of pervaporation processes.

Ashraf et al. used the model proposed by Valentínyi et al. to calculate the size and arrangement of the pervaporation modules [150]. The experimental results for the dehydration of an aqueous solution of butanol using a commercial pervaporation membrane were in good agreement with the proposed model. However, the model is limited to the type of membrane, components and operating conditions used in their experiments [150].

Petrychkovych et al. used the solution-diffusion model for calculating the pervaporation of butanol flux for a binary butanol/water mixture using a PE membrane. The calculated permeation

flux was obtained assuming a constant diffusion coefficient, with a good agreement with the experimental permeation flux [151].

To gain a better understanding of the permeation of ABE species through polymeric membranes, it is paramount to investigate the solubility coefficient and diffusion coefficient of these components in various membranes. However, there are not many values reported in the literature for the solubility of ABE components in membranes. Table 5-2 presents the diffusion coefficients of ABE components reported in several investigations. It is shown that the diffusion coefficients for butanol in PDMS membranes are of the same order of magnitude in the different studies except for the values reported by Yang et al. [146] which are significantly smaller. The same trend was observed for the diffusion coefficients of acetone. For ethanol, the variation of the diffusion coefficients in PDMS membranes was more pronounced.

Table 5-2 Diffusion coefficients of ABE components reported in the literature for different pervaporation membranes.

Polymer/Solution	Component	Temperature (K)	Diffusivity (m^2/s)	Ref
PDMS/Pure component	Acetone	308	$0.85x10^{-10}$	[152]
	n-Butanol	308	$0.3x10^{-10}$	
	Ethanol	308	$0.60x10^{-10}$	
	Water	308	$0.55x10^{-10}$	
PDMS/Ethanol-Water mixture	Ethanol	298.15	$0.6x10^{-9}$	[153]
	Water	298.15	$4.4x10^{-9}$	
	Ethanol-water	298.15	$0.37x10^{-9}$	
PDMS/Pure component	n-Butanol	303.15	$3.11x10^{-10}$*	[154]
	t-Butanol	303.15	$2.66x10^{-10}$*	
	s-Butanol	303.15	$2.25x10^{-10}$*	
	Water	303.15	$129.05x10^{-10}$*	
PDMS (GE615)/Pure water	Water	298.15	$1.7x10^{-9}$ (a)	[155]
PDMS (PS342.5)/Pure water	Water	298.15	$2x10^{-9}$ (a)	
PDMS/Pure water	Water	298.15	$7.8x10^{-10}$ (a)	
PDMS/Alcohols aqueous binary solutions	n-Butanol	303.15	$0.65x10^{-10}$	[156]
	Ethanol	353.15	$7.1x10^{-10}$*	
	n-Butanol	353.15	$5.5x10^{-10}$	
	Ethanol	353.15	$12x10^{-10}$	
	Water	353.15	$12x10^{-10}$	
	Water	298.15	$3x10^{-10}$	

Table 5-2 continued				
Polymer/Solution	**Component**	**Temperature (K)**	**Diffusivity (m^2/s)**	**Ref**
PDMS/Aqueous solutions	n-Butanol	299.15	$1.6x10^{-10}$ (b)	[157]
Crosslinked PVA/Dilute solutions	n-Butanol	398.15	$0.563x10^{-10}$*	[158]
	Ethanol	398.15	$0.793x10^{-10}$*	
	Ethanol	393.15	$0.787x10^{-10}$*	
	Ethanol	383.15	$0.92x10^{-10}$ *	
	Water	393.15	$39.08x10^{-10}$ *	
	Water	383.15	$8.89x10^{-10}$*	
PDMS/Pure component	Ethanol	300	$0.45x10^{-9}$	[141]
	Water	300	$1.45x10^{-9}$	
PE/Pure	Ethanol	300	$0.07x10^{-9}$	
	Water	300	$0.78x10^{-9}$	
PDMS/Aqueous binary solutions	Acetone	313.2	$6.106x10^{-12}$	[146]
	n-Butanol	313.2	$2.589x10^{-12}$	
	Ethanol	313.2	$2.05x10^{-12}$	
	Water	313.2	$1.867x10^{-12}$	
PERVAP®4060/Aqueous binary solutions	Ethanol	303.15	$9.55x10^{-9}$	[159]
	Water	303.15	$6.52x10^{-10}$	
Silicalite-1 zeolite/Pure component	n-Butanol	293	$4.5x10^{-15}$	[160]
	Ethanol	293	$13.2x10^{-16}$	
Silicalite-1 zeolite/Pure component	Water	298	$1.7x10^{-9}$	[161]
IL gel layer/ABE solutions	Acetone	303.15	$4.6x10^{-10}$-$4.9x10^{-10}$	[162]
	n-Butanol	303.15	$4.2x10^{-11}$-$3.9x10^{-10}$	
	Ethanol	303.15	$5.6x10^{-12}$-$5.2x10^{-10}$	
Methylated silica/ Aqueous binary solutions	n-Butanol	333.15	$4.7x10^{-14}$ (c)	[34]
	Ethanol	333.15	$1.1x10^{-13}$ (c)	
	Water	333.15	$3.7x10^{-12}$–$7.1x10^{-12}$ (c)	

* infinite dilute diffusion coefficient
(a) determined on the transient slope
(b) determined at half saturation of transient
(c) Maxwell–Stefan single-file diffusivities

Maxwell-Stefan theory

The generalized Maxwell-Stefan equation is based on the assumption that the migration of species is the result of a driving force that is counteracted by the friction of the migrating species from the other species and the immediate environment. It was formalized by Mason and

Viehland for multicomponent systems and later implemented for membrane separation processes such as gas separation and pervaporation [163–166]. According to this theory, for multicomponent systems, the sum of the friction forces for a component balances the driving force as expressed in Eq. (36) [45]. In this equation, $\hat{D}_{ij}$ represents the inverse draging force between species *i* and *j*.

$$\frac{1}{RT}\frac{d\mu_i}{dz} = \sum_{j=1}^{n} \phi_j \frac{v_j - v_i}{\hat{D}_{ji}} \tag{36}$$

The chemical potential in Eq. (36) is related to the activity of components within the membrane assuming to have an ideal gas mixture. Eq. (37) represents a simplified form of Maxwell-Stefan equation for a ternary system including binary solution and the membrane material [45,167].

$$\frac{d\,ln\phi_i}{dz} = \phi_j \frac{v_j - v_i}{\tilde{D}_{ij}} - \phi_M \frac{v_i}{\tilde{D}_{Mi}} \tag{37a}$$

$$\frac{d\,ln\phi_j}{dz} = \phi_j \frac{v_i - v_j}{\tilde{D}_{ji}} - \phi_M \frac{v_{ji}}{\tilde{D}_{Mj}} \tag{37b}$$

$$\tilde{D}_{ij} = \hat{D}_{ij} \frac{d\,ln\,a_i}{d\,ln\,\phi_i} \tag{37c}$$

The diffusion coefficients in Eq. (37), i.e. $\tilde{D}_{ij}$ and $\tilde{D}_{ji}$ are the effective diffusion coefficients for component *i* and *j*.

Eq. (37) was rearranged to calculate the permeation flux of each component through the membrane (this model needs to be solved numerically) and it was assumed that the effective diffusion coefficients are equal ($\tilde{D}_{ij} = \tilde{D}_{ji}$) due to symmetrical conditions, which led to Eq. (38) [45].

$$J_i = -\frac{\tilde{D}_{Mi}}{\phi_M}\left(\frac{\phi_i\tilde{D}_{Mj}+\phi_M\tilde{D}_{ij}}{\phi_M\tilde{D}_{ij}+\phi_i\tilde{D}_{Mj}+\phi_j\tilde{D}_{Mi}}\right)\frac{dC_i}{dz}+\frac{\tilde{D}_{Mi}}{\phi_M}\left(\frac{\phi_i\tilde{D}_{Mj}}{\phi_M\tilde{D}_{ij}+\phi_i\tilde{D}_{Mj}+\phi_j\tilde{D}_{Mi}}\right)\frac{dC_j}{dz} \quad (38a)$$

$$J_j = -\frac{\tilde{D}_{Mj}}{\phi_M}\left(\frac{\phi_j\tilde{D}_{Mi}+\phi_M\tilde{D}_{ij}}{\phi_M\tilde{D}_{ij}+\phi_j\tilde{D}_{Mi}+\phi_i\tilde{D}_{Mj}}\right)\frac{dC_j}{dz}+\frac{\tilde{D}_{Mj}}{\phi_M}\left(\frac{\phi_j\tilde{D}_{Mi}}{\phi_M\tilde{D}_{ij}+\phi_j\tilde{D}_{Mi}+\phi_i\tilde{D}_{Mj}}\right)\frac{dC_i}{dz} \quad (38b)$$

When coupling effects are negligible, $\hat{D}_{ij}$ (and consequently $\tilde{D}_{ij}$) approaches to infinity and Eq. (38) would be simplified to the Fick's first law of diffusion, where $\tilde{D}_{Mi}/\phi_M$ and $\tilde{D}_{Mj}/\phi_M$ are the Fick's difussion coefficients as shown in Eq. (39) [45,167].

$$J_i = -\frac{\tilde{D}_{Mi}}{\phi_M}\frac{dC_i}{dz} \quad (39a)$$

$$J_j = -\frac{\tilde{D}_{Mj}}{\phi_M}\frac{dC_j}{dz} \quad (39b)$$

Other researchers have used the same type of equations where the volume fraction was simply replaced by the weight or mole fraction in Eq. (38) [168,169]. Moreover, some modifications has been applied in different studies to obtain analytical solutions from the differential equations (Eq. (38)) using a few assumptions to simplify the integration procedure. The main advantage of Maxwell-Stefan theory could be its ability to predict the flux and selectivity for non-ideal multicomponent systems based on the results of single components, which significantly decreases the number of pervaporation experiments to be performed. Moreover, it has the potential to be used for module and process design together with membrane development.

Bettens et al. [34] investigated the deviations observed between the experimental results and a theoretical model that combined the extended Langmuir model for sorption and the Maxwell-Stefan diffusion for pervaporation of butanol/water and butanol/methanol. However, in their study, the desired components to be separated were water and methanol. Different types of methylated microporous silica membranes were used for this purpose. In addition, to predict the Maxwell–Stefan diffusion coefficients, three Maxwell–Stefan diffusivities were determined: $\tilde{D}_{ij}$,

$\tilde{D}_{iM}$ and $\tilde{D}_{jM}$. Moreover, for the counter-exchange Maxwell–Stefan diffusivity, the Vignes equation was used $\left(\tilde{D}_{ij}=\left(\tilde{D}_{iM}\right)^{\frac{C_{H,i}}{C_{H,i}+C_{H,j}}}\left(\tilde{D}_{jM}\right)^{\frac{C_{H,i}}{C_{H,i}+C_{H,j}}}\right)$. The single-species Maxwell–Stefan diffusivities were assumed for the conditions where there were no interactions between species and the corresponding counter-exchange coefficient was infinite ($\tilde{D}_{ij}\to\infty$). In this case, species were not able to pass each other in the narrow pores. The single-species Maxwell–Stefan diffusivities could either be independent of the amount adsorbed $\left(\tilde{D}_{iM}=\tilde{D}_{iM}\left(0\right),\tilde{D}_{jM}=\tilde{D}_{jM}\left(0\right)\right)$ or dependent on the amount adsorbed $\left(\tilde{D}_{iM}=\tilde{D}_{iM}\left(0\right)\left(1-C_{H,i}-C_{H,j}\right),\tilde{D}_{jM}=\tilde{D}_{jM}\left(0\right)\left(1-C_{H,i}-C_{H,j}\right)\right)$. The comparison was made by assuming different case scenarios where the diffusion coefficients between the components and the membrane in the Maxwell-Stefan model were estimated. The pure alcohol Maxwell–Stefan diffusivity at zero coverage $\left(\tilde{D}_{jM}\left(0\right)\right)$was derived from the experimental pure alcohol flux and the pure water Maxwell–Stefan micropore diffusivity at zero coverage$\left(\tilde{D}_{iM}\left(0\right)\right)$ was achieved by fitting the experimental water flux data. The four scenarios that were proposed are as follows.

1) There are no interactions between feed species ($\tilde{D}_{ij}\to\infty$). Moreover, $\tilde{D}_{iM}$ and $\tilde{D}_{jM}$ are independent from the amount adsorbed $\left(\tilde{D}_{iM}=\tilde{D}_{iM}\left(0\right),\tilde{D}_{jM}=\tilde{D}_{jM}\left(0\right)\right)$;
2) There are no interactions between feed species ($\tilde{D}_{ij}\to\infty$). Moreover $\tilde{D}_{iM}$ and $\tilde{D}_{jM}$ are dependent on the amount adsorbed
   $\left(\tilde{D}_{iM}=\tilde{D}_{iM}\left(0\right)\left(1-C_{H,i}-C_{H,j}\right),\tilde{D}_{jM}=\tilde{D}_{jM}\left(0\right)\left(1-C_{H,i}-C_{H,j}\right)\right)$;
3) There are interactions between feed species and $\tilde{D}_{ij}$ can be obtained by Vignes equation $\left(\tilde{D}_{ij}=\left(\tilde{D}_{iM}\right)^{\frac{C_{H,i}}{C_{H,i}+C_{H,j}}}\left(\tilde{D}_{jM}\right)^{\frac{C_{H,i}}{C_{H,i}+C_{H,j}}}\right)$. Moreover, $\tilde{D}_{iM}$ and $\tilde{D}_{jM}$ are independent from the amount adsorbed $\left(\tilde{D}_{iM}=\tilde{D}_{iM}\left(0\right),\tilde{D}_{jM}=\tilde{D}_{jM}\left(0\right)\right)$;

4) There are interactions between feed species and $\tilde{D}_{ij}$ can be obtained by Vignes equation $\left(\tilde{D}_{ij}=\left(\tilde{D}_{iM}\right)^{\frac{C_{H,i}}{C_{H,i}+C_{H,j}}}\left(\tilde{D}_{jM}\right)^{\frac{C_{H,i}}{C_{H,i}+C_{H,j}}}\right)$. Moreover, $\tilde{D}_{iM}$ and $\tilde{D}_{jM}$ are dependent on the amount adsorbed $\left(\tilde{D}_{iM}=\tilde{D}_{iM}\left(0\right)\left(1-C_{H,i}-C_{H,j}\right),\ \tilde{D}_{jM}=\tilde{D}_{jM}\left(0\right)\left(1-C_{H,i}-C_{H,j}\right)\right)$.

According to the results, Maxwell-Stefan theory was consistent with experimental pervaporation data for the first case scenario when no interactions took place between the components, and the diffusion coefficients of the components through the membrane were independent from the amount adsorbed. In addition, prediction performed with the second scenario's prediction for the calculation of the flux of components demonstrated to be closer to the experimental data compared to the first scenario. However, the last two case scenarios did not have a good fit with experimental data.

In another work, the mass transfer through a PDMS commercial membrane for pervaporation separation of the butanol from aqueous solution has been studied by Ebneyamini et al. [170]. A semi-empirical approach on the Maxwell-Stefan model was extended to consider the effect of membrane swelling and the operating temperature on the diffusion coefficient and sorption properties. In order to estimate the effect of the operating temperature on the diffusion coefficients and the sorption of each species, Arrhenius-type equations were incorporated into the Maxwell-Stefan model. Moreover, similar to the free volume theory, an exponential relationship was used to express the diffusion coefficient of each component as a function of the degree of swelling of the membrane at a constant temperature (Eq. 40).

$$D_{M,i}=D_i^0 e^{A_i\psi\left(C_{f,i}T\right)} \tag{40a}$$

$$\psi_{\left(C_{f,i}T\right)}=\frac{C_{f,i}k_{D,i}^{*}e^{\frac{-\Delta H_i}{RT}}+C_{f,j}k_{D,j}^{*}e^{\frac{-\Delta H_j}{RT}}}{\rho_M} \tag{40b}$$

The result of the extended Maxwell-Stefan model showed a better agreement with the experimental data in comparison to the Maxwell-Stefan model. Moreover, the model was able to

predict the membrane properties such as solubility and diffusivity at different operating temperatures and feed concentrations.

Pore-flow model

The other proposed model for the overall mass transfer in a pervaporation separation process is the pore-flow model. The difference between this model and the solution-diffusion model is that, the solution-diffusion model considers no phase change in the membrane while in the pore flow model, there is a phase change inside the membrane at a certain distance from the membrane surface. Considering the phase change inside the membrane, there should be a phase boundary between the liquid and the vapor for the mass transfer equations. In 1991, Okada and Matsuura [34] considered a pore flow model for describing the mass transfer through a cellulose membrane in pervaporation separation of ethyl alcohol/heptane mixtures. In this model, it is assumed that the selective layer of the membrane is formed by a pack of straight cylindrical pores distributed within the membrane surface and isothermal conditions are assumed. Furthermore, the length of the pores is equal to the thickness of the active layer.

Three steps have been proposed for this model: (1) liquid transport from the pore inlet to the liquid-vapor phase boundary; (2) evaporation at the phase boundary; (3) vapor transport from the phase boundary to the pore outlet [35,36]. Moreover, it was assumed that at the liquid-vapor phase boundary, the components reach to their saturated pressure in equilibrium with the feed solution.

According to the above-mentioned assumptions, at steady state for single component permeation, the flux in the liquid and vapor segments can be calculated according to Eq. (41).

$$J_L = \frac{A^{Pore}}{l_L}\left(p_L - p^{sat}\right) \tag{41a}$$

$$J_V = \frac{B^{Pore}}{l_V}\left(\left(p^{sat}\right)^2 - p_V\right) \tag{41b}$$

$$J = J_V = J_L \tag{41c}$$

where subscripts *L* and *V* represent the liquid and vapor phases, while *l* is the thickness of each phase inside the pore. *A* and *B* constants are obtained using the Darcy's equation and Henry's law (Eq. (42)).

$$A^{pore} = \frac{\pi r_{pore}^4 \rho_i N_t}{8\eta_i M_i} \tag{42a}$$

$$B^{pore} = \frac{\pi\left(2r_{pore}l_{ad} - l_{ad}^2\right)^2 l_{ad} N_t}{8r_{pore}} \frac{RT}{\mu_i^*}\left(k_{D,i}^{'}\right)^2 \tag{42b}$$

where l_{ad} is the thickness of the adsorption monolayer.

Since the constants A and B are determined empirically, the pore-flow model would be limited to assist only in process and module design and it is not applicable for membrane development.

Moreover, there are additional models such as pseudo phase-change solution-diffusion, which combines the specifications of both the solution-diffusion and the pore-flow models in one single framework. The pseudo phase-change solution-diffusion takes the coupling effect from the solution-diffusion model and the pseudo phase-change inside the membrane from the pore-flow model into consideration [171,172]. The pore-flow model has not been used yet for the separation of butanol by pervaporation.

Conclusion

Pervaporation is an appropriate process for the separation of butanol from different aqueous solutions especially ABE fermentation broths. However, to be employed at an industrial level using lab-scale experimental data, mathematical models will be essential to have an accurate prediction of the pervaporation process performances. Such models could help in the design phase of membrane modules for the purpose of optimization, flow patterns prediction, and vessel design. In addition, the membrane development using modeling could provide valuable information before membrane fabrication.

Mass transfer modelling in a pervaporation separation of butanol from ABE fermentation broth, ABE model solutions and aqueous solutions was reviewed in this study.

Considering the previous works for the pervaporation of butanol, although the number of the diffusion models is very limited, the overall mass transfer was mainly used by researchers to estimate the mass transfer coefficient of the components using sorption models. As shown in Table 5-3, solution-diffusion model has been the most frequently used model for the description of the mass transfer in pervaporation separation of butanol. However, the application of the Maxwell-Stefan theory for this purpose has been very limited and, to our knowledge, the pore-flow model has not been reported in the literature for the pervaporation of butanol.

Most of the models used for the pervaporation separation of butanol are semi-empirical models which fall in between theoretical and empirical models in terms of complexity. Although, in the semi-empirical models, the driving force is well established, the permeability would be experimentally estimated. The complexity of the model increases with the number of components involved in the mass transfer and it further increases by considering the coupling effects. In this case, the Maxwell-Stefan theory seems to be an appropriate option for considering the coupling phenomenon. In addition, it is an accurate model for membrane separation in pervaporation due to its ability to predict the flux and selectivity of the multi-component systems based on the results of single components, which significantly decreases the number of pervaporation experiments to be performed. In addition, it has the potential to be used for module and process design together with membrane development.

Furthermore, while the information obtained via the overall mass transfer models would be used for fundamental understanding of the process and module design, other information such as concentration polarization, pressure drop, flow pattern, and heat transfer also need to be considered for the purpose of process design. Moreover, molecular simulation could become in the future a very valuable tool for membrane development in the pervaporation of butanol.

This study can be helpful in combining different sorption and diffusion models to achieve more rigorous models for the prediction of butanol separation by pervaporation.

Table 5-3 Mathematical models which have been used for the pervaporation separation of butanol.

Membrane	Feed	Modelling method	Ref
Supported gelled ionic liquid	ABE mixtures	Solution diffusion model	[33]
Composite PVA membrane on PAN support	butanol/water	Solution diffusion model	[143]
Composite PDMS	ABE fermentation	Solution-diffusion model	[19]
Tri-layer PDMS	butanol/water	Solution-diffusion model	[147]
PVA/PAN	water/butanol	Solution-diffusion model	[148]
PERVAP 2510	water/butanol	Solution-diffusion model	[150]
PE	butanol/water	Solution-diffusion model	[151]
PDMS	ABE water binary	Non-equilibrium solution-diffusion model	[146]
PDMS	butanol/water	Maxwell–Stefan model	[170]
Methylated microporous silica	butanol/water, butanol/methanol	Maxwell–Stefan model	[34]

Abbreviation

ABE	Acetone, Butanol, Ethanol
CIRC	Circulation equilibrium still
COSMO-RS	Conductor like screening model for real solvents
DDST	Differential distillation
EBUL	Ebuliometry
EPDM	Ethylene propylene diene rubber
GEM-RS	Generalized regular solution model

GLC	Gas-liquid chromatography
HSA	Headspace analysis
IGS	Inverse gas chromatography
LLE	Liquid-liquid extraction
LSG	Local surface guggenheim equation
MBEA	Molecular beams
MMM	Mixed matrix membrane
MOSCED	Modified separation of cohesive energy density model
NRTL	Non-random two-liquid model
NSGLC	Non-steady state gas-liquid chromatography
PAI	Polyamide-imide
PAN	Polyacrylonitrile
PAV	Polyarylene vinylene
PDMS	Polydimethylsiloxane
PE	Polyethylene
PET	Polyethylene terephthalate
PEBA	Polyether block-amide
PRV	Phase ratio variation method
PV	Pervaporation
PVA	Poly(vinyl acetate)
PI	Polyimide
POMS	Poly(octhylmethyl siloxane)
PMS	Poly (methoxy siloxane)
PP	Polypropylene
PRV	Phase ratio variation

PTFE	Polytetrafluoroethylene
PTMSP	Poly (1-(trimethylsilyl)-1-propyne)
RDIST	Rayleigh distillation
RO	Reverses osmosis
TENS	Tensimetry
UNIQUAC	Universal quasichemical
VPC	Vapour phase calibration
WWC	Wetted wall column

Nomenclature

a	activity [-]
A_{di}	free volume parameter of component *i* for the glassy region in polymer [-]
A_i	dimensionless constant in Eq. (40)
A_M	membrane area [m^2]
A^{pore}	constant defined for a pure component system in the pore flow model [-]
b	adsorption or hole affinity constant [bar^{-1}]
B	coupling coefficients in semi-empirical model after Meyer-Blumenroth [$kmol.m^{-1}.s^{-1}.bar^2$]
B^*	Constant parameter in Eq. (35) [-]
B^{pore}	constant for a pure component system in the pore flow model [-]
B_{di}	free volume parameter of component *i* for the glassy region in polymer [-]
B^{FV}	generalised free volume parameter [-]
C	concentration [$kmol.m^{-3}$, $kg.m^{-3}$]
C_D	concentration of diffusing in membrane [$kmol.m^{-3}$, $kg.m^{-3}$]
C_H	concentration in microvoids [$kmol.m^{-3}$, $kg.m^{-3}$]
$C_H^{'}$	Langmuir maximum sorption capacity in the polymeric membrane [$kmol.m^{-3}$, $kg.m^{-3}$]
D	diffusion coefficient [$m^2.s^{-1}$]

D^0	diffusion coefficient in infinite dilution [$m^2.s^{-1}$]
D_D	diffusion coefficient in the Henry's Law mode [$m^2.s^{-1}$]
D_H	diffusion coefficient in the Langmuir mode [$m^2.s^{-1}$]
D^T	thermodynamic diffusion coefficient [$m^2.s^{-1}$]
$\bar{D}^T$	modified thermodynamic diffusion coefficient [$m^2.s^{-1}$]
$\tilde{D}$	effective concentration-dependent diffusion coefficient [$m^2.s^{-1}$]
$\hat{D}$	Maxwell-Stefan interaction parameter [$m^2.s^{-1}$]
$\dot{D}$	permeance [$kg.m^{-2}.s^{-1}$]
$\Delta E_{di,}$	energy required to overcome dispersion polar interactions [$J.mol^{-1}$]
ΔE_{hb}	energy required to overcome hydrogen [$J.mol^{-1}$]
ΔE_{vap}	energy of vaporisation [$J.mol^{-1}$]
f	fugacity [bar]
f^{FV}	free volume [-]
F	as defined in Eq. (24) [-]
ΔH	heat of adsorption [$J.mol^{-1}$]
J	flux [$kmol.m^{-2}.s^{-1}$]
k_d	desorption constant [$m.s^{-1}$]
$k_{D,i}$	Henry's law constant referring to component *i* [bar^{-1}]
$k^*_{D,i}$	dimensionless Henry's law constant [$g.m^{-3}/g.m^{-3}$]
k	boundary layer mass transfer coefficient [-]
k_s	sorption constant [$m.s^{-1}$]
$k'_{D,i}$	(unit weight of polymer per volume of adsorbed gas molecule *i*) × $k_{D,i}$ [$mol.m^{-3}.bar^{-1}$]
K_i	as defined in Eq. (24) [-]
K_{ov}	overall mass transfer coefficient across the membrane [-]
l_{ad}	thickness of the adsorption monolayer [m]
l_M	thickness of membrane *M* [m]
l_L	length of the liquid-filled proportion of the pore in the pore flow model [m]
l_V	length of the vapour-filled proportion of the pore in the pore flow model [m]
M	molar weight [$kg.kmol^{-1}$]

N_t	total number of pores per effective membrane area [-]
p	partial pressure [bar, Pa]
p^*	Pressure in boundary layer in Eq. (27) [bar]
P	permeability with reference to an activity driving force [kmol.m^{-1}.s^{-1}.bar^{-1}]
r_{pore}	pore radius [m]
R	gas constant [J.mol^{-1}.K^{-1}]
Re	Reynolds number [-]
S	Solubility coefficient [kmol.m^{-3}]
Sc	Schmidt number [-]
Sh	Sherwood number [-]
t	time [s]
T	temperature [K]
v	velocity [m^2.s]
V	molar volume [m^3.mol^{-1}]
V_0^T	the volume in feeding tank [m^3]
W_1, W_2, W_3	weight factors for three dimensional solubility parameters [-]
x	mole fraction [-]
$x_{i,b}$	the bulk mole fraction [-]
x^*	the interface mole fraction [-]
z	z-co-ordinate [m]
β	proportional constant in free volume theory [-]
γ_i	activity coefficient [-]
$\gamma_{M,i}$	average activity coefficient of component i in membrane [-]
δ_i	solubility parameter [J$^{1/2}$.m$^{-3/2}$]
$\delta_{hb,i}$	solubility parameter due to hydrogen bonds with reference to component i [J$^{1/2}$.m$^{-3/2}$]
$\delta_{df,i}$	solubility parameter due to dispersion forces with reference to component i [J$^{1/2}$.m$^{-3/2}$]
$\delta_{di,i}$	solubility parameter due to dispersion polar interactions with reference to component i [J$^{1/2}$.m$^{-3/2}$]

ε	empirical constant or 'softener' [-]
η	liquid viscosity [Pa.s]
μ	chemical potential [J.mol^{-1}]
μ^*	Surface viscosity of adsorptive layer of vapour [Pa.s]
ρ	density [kg.m^{-3}]
ϕ_c	crystallinity of polymer *P* [-]
ϕ	volume fraction [-]
θ	as defined in Equation (32) [-]
ψ	as defined in Equation (40), (degree of swelling) [g.g^{-1}]
χ	Flory-Huggins binary interaction parameter [-]
$\Delta_{p,i}$	distance between polymer *P* and component *i* in _-space [J$^{1/2}$.m$^{-3/2}$]

Subscripts

b	butanol concentration
b0	initial butanol concentration
f	feed
i,j	component *i* and *j*
L	liquid phase
m	module
M	membrane
p	polymer
P	permeate
sat	saturated
tot	total
V	vapour phase

Superscripts

0	reference
FV	free volume
L	liquid phase
mix	mixture

References

[1] N. Abdehagh, J. Thibault, F.H. Tezel, Separation techniques in butanol production: Challenges and developments, Biomass Bioenergy. 60 (2014) 222–246. doi:10.1016/j.biombioe.2013.10.003.

[2] F. Pedram, Production of Biofuels from Cellulose of Woody Biomass, in: licensee InTech., 2013.

[3] Y. Zhu, F. Xin, Y. Chang, Y. Zhao, W. Weichong, Feasibility of reed for biobutanol production hydrolyzed by crude cellulase, Biomass Bioenergy. 76 (2015) 24–30. doi:10.1016/j.biombioe.2015.02.013.

[4] V. Ujor, A.K. Bharathidasan, K. Cornish, T.C. Ezeji, Feasibility of producing butanol from industrial starchy food wastes, Appl. Energy. 136 (2014) 590–598. doi:10.1016/j.apenergy.2014.09.040.

[5] V. Erick, A. Tom, D. Sofie, Industrial biomass: Source of chemicals, materials, and energy!., BACAS. (2011) 0455–02.

[6] M.G. Buonomenna, J. Bae, Membrane processes and renewable energies, Renew. Sustain. Energy Rev. 43 (2015) 1343–1398. doi:10.1016/j.rser.2014.11.091.

[7] I.L. Borisov, G.S. Golubev, V.P. Vasilevsky, A.V. Volkov, V.V. Volkov, Novel hybrid process for bio-butanol recovery: Thermopervaporation with porous condenser assisted by phase separation, J. Membr. Sci. 523 (2017) 291–300. doi:10.1016/j.memsci.2016.10.009.

[8] J. Du, A. McGraw, J.A. Hestekin, Modeling of Clostridium tyrobutyricum for Butyric Acid Selectivity in Continuous Fermentation, Energies. 7 (2014) 2421–2435. doi:10.3390/en7042421.

[9] C. Park, C. Geng, Mathematical, modeling of fed-batch butanol fermentation with simultaneous pervaporation, Korean J. Chem. Eng. 13 (1996) 612–619. doi:10.1007/BF02706028.

[10] Z. Li, Z. Shi, X. Li, Models construction for acetone-butanol-ethanol fermentations with acetate/butyrate consecutively feeding by graph theory, Bioresour. Technol. 159 (2014) 320–326. doi:10.1016/j.biortech.2014.02.095.

[11] S.B. Bankar, S.A. Survase, H. Ojamo, T. Granstrom, Biobutanol: the outlook of an academic and industrialist, Rsc Adv. 3 (2013) 24734–24757. doi:10.1039/c3ra43011a.

[12] H. Dong, W. Tao, Z. Dai, L. Yang, F. Gong, Y. Zhang, Y. Li, Biobutanol, Adv. Biochem. Eng.-Biotechnol. 128 (2012) 85–100. doi:10.1007/10_2011_128.

[13] G. Festel, BUTALCO "Competence for Second Generation Biofuels Based on Lignocellulose," BUTALCO GmbH company, 2014.

[14] C.L. Gabriel, Butanol fermentation process, Ind. Eng. Chem. 20 (1928) 1063–1067. doi:10.1021/ie50226a020.

[15] V. Garcia, J. Pakkila, H. Ojamo, E. Muurinen, R.L. Keiski, Challenges in biobutanol production: How to improve the efficiency?, Renew. Sustain. Energy Rev. 15 (2011) 964–980. doi:10.1016/j.rser.2010.11.008.

[16] D. Ramey, Butanol: The Other Alternative Fuel, Agric. Biofuels Technol. Sustain. Profitab. (2007) 137–147.

[17] T. Ezeji, N. Qureshi, H. Blaschek, Butanol fermentation research: Upstream and downstream manipulations, Chem. Rec. 4 (2004) 305–314. doi:10.1002/tcr.20023.

[18] B. Bharathiraja, J. Jayamuthunagai, T. Sudharsanaa, A. Bharghavi, R. Praveenkumar, M. Chakravarthy, D. Yuvaraj, Biobutanol - An impending biofuel for future: A review on upstream and downstream processing tecniques, Renew. Sustain. Energy Rev. 68 (2017) 788–807. doi:10.1016/j.rser.2016.10.017.

[19] S.-Y. Li, R. Srivastava, R.S. Parnas, Study of in situ 1-Butanol Pervaporation from A-B-E Fermentation Using a PDMS Composite Membrane: Validity of Solution-Diffusion Model for Pervaporative A-B-E Fermentation, Biotechnol. Prog. 27 (2011) 111–120. doi:10.1002/btpr.535.

[20] G. Liu, D. Hou, W. Wei, F. Xiangli, W. Jin, Pervaporation Separation of Butanol-Water Mixtures Using Polydimethylsiloxane/Ceramic Composite Membrane, Chin. J. Chem. Eng. 19 (2011) 40–44. doi:10.1016/S1004-9541(09)60174-9.

[21] N. Qureshi, M.M. Meagher, J. Huang, R.W. Hutkins, Acetone butanol ethanol (ABE) recovery by pervaporation using silicalite-silicone composite membrane from fed-batch reactor of Clostridium acetobutylicum, J. Membr. Sci. 187 (2001) 93–102. doi:10.1016/S0376-7388(00)00667-0.

[22] N. Qureshi, M.M. Meagher, R.W. Hutkins, Recovery of butanol from model solutions and fermentation broth using a silicalite silicone membrane, J. Membr. Sci. 158 (1999) 115–125. doi:10.1016/S0376-7388(99)00010-1.

[23] N. Abdehagh, F.H. Tezel, J. Thibault, Adsorbent screening for biobutanol separation by adsorption: kinetics, isotherms and competitive effect of other compounds, Adsorption. 19 (2013) 1263–1272. doi:10.1007/s10450-013-9566-8.

[24] Q. Wang, Y. ding, L. Liu, J. Shi, J. Sun, Y. Xue, Engineering Escherichia coli for autoinducible production of n-butanol, Electron. J. Biotechnol. 18 (2015) 138–142. doi:10.1016/j.ejbt.2015.01.003.

[25] A.P. Mariano, N. Qureshi, R. Maciel Filho, T.C. Ezeji, Assessment of in situ butanol recovery by vacuum during acetone butanol ethanol (ABE) fermentation, J. Chem. Technol. Biotechnol. 87 (2012) 334–340. doi:10.1002/jctb.2717.

[26] A. Oudshoorn, L.A.M. van der Wielen, A.J.J. Straathof, Adsorption equilibria of bio-based butanol solutions using zeolite, Biochem. Eng. J. 48 (2009) 99–103. doi:10.1016/j.bej.2009.08.014.

[27] N. Qureshi, H.P. Blaschek, Recovery of butanol from fermentation broth by gas stripping, Renew. Energy. 22 (2001) 557–564. doi:10.1016/S0960-1481(00)00108-7.

[28] W.J. Groot, H.S. Soedjak, P.B. Donck, R.G.J.M. van der Lans, K.C.A.M. Luyben, J.M.K. Timmer, Butanol recovery from fermentations by liquid-liquid extraction and membrane solvent extraction, Bioprocess Eng. 5 (n.d.) 203–216. doi:10.1007/BF00376227.

[29] N. Qureshi, I.S. Maddox, Reduction in Butanol Inhibition by Perstraction, Food Bioprod. Process. 83 (2005) 43–52. doi:10.1205/fbp.04163.

[30] A. Garcia, E.L. Iannotti, J.L. Fischer, Butanol fermentation liquor production and separation by reverse osmosis, Biotechnol. Bioeng. 28 (1986) 785–791. doi:10.1002/bit.260280603.

[31] N. Qureshi, H.P. Blaschek, Butanol recovery from model solution/fermentation broth by pervaporation: evaluation of membrane performance, Biomass Bioenergy. 17 (1999) 175–184. doi:10.1016/S0961-9534(99)00030-6.

[32] C. Shin, X. Chelsea Chen, J.M. Prausnitz, N.P. Balsara, Effect of block copolymer morphology controlled by casting-solvent quality on pervaporation of butanol/water mixtures, J. Membr. Sci. 523 (2017) 588–595. doi:10.1016/j.memsci.2016.09.054.

[33] A. Plaza, G. Merlet, A. Hasanoglu, M. Isaacs, J. Sanchez, J. Romero, Separation of butanol from ABE mixtures by sweep gas pervaporation using a supported gelled ionic liquid

membrane: Analysis of transport phenomena and selectivity, J. Membr. Sci. 444 (2013) 201–212. doi:10.1016/j.memsci.2013.04.034.

[34] B. Bettens, A. Verhoef, H.M. van Veen, C. Vandecasteele, J. Degrève, B. Van der Bruggen, Pervaporation of binary water–alcohol and methanol–alcohol mixtures through microporous methylated silica membranes: Maxwell–Stefan modeling, Comput. Chem. Eng. 34 (2010) 1775–1788. doi:10.1016/j.compchemeng.2010.03.014.

[35] T. Okada, T. Matsuura, A New Transport Model for Pervaporation, J. Membr. Sci. 59 (1991) 133–150. doi:10.1016/S0376-7388(00)81179-5.

[36] T. Okada, M. Yoshikawa, T. Matsuura, A Study on the Pervaporation of Ethanol Water Mixtures on the Basis of Pore Flow Model, J. Membr. Sci. 59 (1991) 151–168. doi:10.1016/S0376-7388(00)81180-1.

[37] Hoang Vinh-Thang, S. Kaliaguine, Predictive Models for Mixed-Matrix Membrane Performance: A Review, Chem. Rev. 113 (2013) 4980–5028. doi:10.1021/cr3003888.

[38] S. Semenova, H. Ohya, K. Soontarapa, Hydrophilic membranes for pervaporation: An analytical review, Desalination. 110 (1997) 251–286. doi:10.1016/S0011-9164(97)00103-3.

[39] P. Shao, R.Y.M. Huang, Polymeric membrane pervaporation, J. Membr. Sci. 287 (2007) 162–179. doi:10.1016/j.memsci.2006.10.043.

[40] B. Smitha, D. Suhanya, S. Sridhar, M. Ramakrishna, Separation of organic-organic mixtures by pervaporation - a review, J. Membr. Sci. 241 (2004) 1–21. doi:10.1016/j.memsci.2004.03.042.

[41] L.M. Vane, A review of pervaporation for product recovery from biomass fermentation processes, J. Chem. Technol. Biotechnol. 80 (2005) 603–629. doi:10.1002/jctb.1265.

[42] J. Villaluenga, A. Tabe-Mohammadi, A review on the separation of benzene/cyclohexane mixtures by pervaporation processes, J. Membr. Sci. 169 (2000) 159–174.

[43] J.G. Wijmans, R.W. Baker, The solution-diffusion model: a review, J. Membr. Sci. 107 (1995) 1–21. doi:10.1016/0376-7388(95)00102-I.

[44] H. Karlsson, G. Tragardh, Pervaporation of Dilute Organic-Waters Mixtures - a Literature-Review on Modeling Studies and Applications to Aroma Compound Recovery, J. Membr. Sci. 76 (1993) 121–146. doi:10.1016/0376-7388(93)85211-E.

[45] F. Lipnizki, G. Tragardh, Modelling of pervaporation: Models to analyze and predict the mass transport in pervaporation, Sep. Purif. Methods. 30 (2001) 49–125. doi:10.1081/SPM-100102985.

[46] X.S. Feng, R.Y.M. Huang, Liquid separation by membrane pervaporation: A review, Ind. Eng. Chem. Res. 36 (1997) 1048–1066. doi:10.1021/ie960189g.

[47] P.A. Kober, Pervaporation, Perstillation and Percrystallization (Reprinted from the Journal of the American-Chemical-Society, Vol 39, Pg 944, 1917), J. Membr. Sci. 100 (1995) 61–64. doi:10.1016/0376-7388(94)00234-P.

[48] A. Jonquières, C. Arnal-Herault, J. Babin, E.M.V. Hoek, V.V. Tarabara, Pervaporation, in: Encycl. Membr. Sci. Technol., John Wiley & Sons, Inc., 2013. http://onlinelibrary.wiley.com/doi/10.1002/9781118522318.emst092/abstract (accessed September 8, 2016).

[49] J. Néel, P. Aptel, R. Clément, Basic aspects of pervaporation, Desalination. 53 (1985) 297–326. doi:10.1016/0011-9164(85)85069-4.

[50] F. Lipnizki, R.W. Field, Integration of vacuum and sweep gas pervaporation to recover organic compounds from wastewater, Sep. Purif. Technol. 22–23 (2001) 347–360. doi:10.1016/S1383-5866(00)00118-0.

[51] S.M. Zhang, E. Drioli, Pervaporation Membranes, Sep. Sci. Technol. 30 (1995) 1–31. doi:10.1080/01496399508012211.

[52] E.J. Jeon, A.S. Kim, Y.T. Lee, Pervaporation of butanol/water mixtures using siloxane polymer/ceramic composite membranes, Desalination Water Treat. 48 (2012) 17–26. doi:10.1080/19443994.2012.698723.

[53] F. Lipnizki, S. Hausmanns, G. Laufenberg, R. Field, B. Kunz, Use of pervaporation/bioreactor hybrid processes in biotechnology, Chem. Ing. Tech. 70 (1998) 1587–1595. doi:10.1002/cite.330701221.

[54] J. Kujawa, S. Cerneaux, W. Kujawski, Removal of hazardous volatile organic compounds from water by vacuum pervaporation with Hydrophobic ceramic membranes, J. Membr. Sci. (n.d.). doi:10.1016/j.memsci.2014.08.054.

[55] H. Zhou, D. Korelskiy, T. Leppäjärvi, M. Grahn, J. Tanskanen, J. Hedlund, Ultrathin zeolite X membranes for pervaporation dehydration of ethanol, J. Membr. Sci. 399–400 (2012) 106–111. doi:10.1016/j.memsci.2012.01.036.

[56] Q. Liu, R.D. Noble, J.L. Falconer, H.H. Funke, Organics/water separation by pervaporation with a zeolite membrane, J. Membr. Sci. 117 (1996) 163–174. doi:10.1016/0376-7388(96)00058-0.

[57] T.C. Bowen, R.D. Noble, J.L. Falconer, Fundamentals and applications of pervaporation through zeolite membranes, J. Membr. Sci. 245 (2004) 1–33. doi:10.1016/j.memsci.2004.06.059.

[58] S.-L. Wee, C.-T. Tye, S. Bhatia, Membrane separation process—Pervaporation through zeolite membrane, Sep. Purif. Technol. 63 (2008) 500–516. doi:10.1016/j.seppur.2008.07.010.

[59] H. Essawy, M. Tawfik, S. El-Sabbagh, A. El-Gendi, E. El-Zanati, H. Abdallah, Novel amphiphilic conetworks based on compatibilized NBR/SBR–montmorillonite nanovulcanizates as membranes for dehydrative pervaporation of water–butanol mixtures, Polym. Eng. Sci. 54 (2014) 1560–1570. doi:10.1002/pen.23699.

[60] K.D. Jitesh, V.G. Pangarkar, K. Niranjan, Pervaporative stripping of acetone, butanol and ethanol to improve ABE fermentation, Bioseparation. 9 (2000) 145–154. doi:10.1023/A:1008129713552.

[61] D.L. Vrana, M.M. Meagher, R.W. Hutkins, B. Duffield, Pervaporation of Model Acetone-Butanol-Ethanol Fermentation Product Solutions using Polytetrafluoroethylene Membranes, Sep. Sci. Technol. 28 (1993) 2167–2178. doi:10.1080/01496399308016741.

[62] M. Müller, M.-N. Pons, Coupling of gas membrane smooth pervaporation and alcoholic fermentation, J. Chem. Technol. Biotechnol. 52 (1991) 343–358. doi:10.1002/jctb.280520307.

[63] M. Hu, L. Gao, W. Fu, X. Liu, F. Huang, Y. Luo, C. Huang, High-performance interpenetrating polymer network polyurethane pervaporation membranes for butanol recovery, J. Chem. Technol. Biotechnol. 90 (2015) 2195–2207. doi:10.1002/jctb.4533.

[64] F. Liu, L. Liu, X. Feng, Separation of acetone–butanol–ethanol (ABE) from dilute aqueous solutions by pervaporation, Sep. Purif. Technol. 42 (2005) 273–282. doi:10.1016/j.seppur.2004.08.005.

[65] T.A. Jalal, N.M.S. Bettahalli, N.L. Le, S.P. Nunes, Hydrophobic Hyflon AD/Poly(vinylidene fluoride) Membranes for Butanol Dehydration via Pervaporation, Ind. Eng. Chem. Res. 54 (2015) 11180–11187. doi:10.1021/acs.iecr.5b02754.

[66] P.J. Hickey, F.P. Juricic, C.S. Slater, The Effect of Process Parameters on the Pervaporation of Alcohols through Organophilic Membranes, Sep. Sci. Technol. 27 (1992) 843–861. doi:10.1080/01496399208019729.

[67] I.L. Borisov, A.O. Malakhov, V.S. Khotimsky, E.G. Litvinova, E.S. Finkelshtein, N.V. Ushakov, V.V. Volkov, Novel PTMSP-based membranes containing elastomeric fillers: Enhanced 1-butanol/water pervaporation selectivity and permeability, J. Membr. Sci. 466 (2014) 322–330. doi:10.1016/j.memsci.2014.04.037.

[68] Y. Wang, T.S. Chung, H. Wang, Polyamide–imide membranes with surface immobilized cyclodextrin for butanol isomer separation via pervaporation, AIChE J. 57 (2011) 1470–1484. doi:10.1002/aic.12360.

[69] G. Liu, W. Wei, W. Jin, Pervaporation Membranes for Biobutanol Production, Acs Sustain. Chem. Eng. 2 (2014) 546–560. doi:10.1021/sc400372d.

[70] X. Wang, J. Chen, M. Fang, T. Wang, L. Yu, J. Li, ZIF-7/PDMS mixed matrix membranes for pervaporation recovery of butanol from aqueous solution, Sep. Purif. Technol. 163 (2016) 39–47. doi:10.1016/j.seppur.2016.02.040.

[71] H. Azimi, H.F. Tezel, J. Thibault, Effect of embedded activated carbon nanoparticles on the performance of Polydimethylsiloxane (PDMS) membrane for pervaporation separation of butanol, J. Chem. Technol. Biotechnol. (2017) n/a-n/a. doi:10.1002/jctb.5306.

[72] A. Jonquières, A. Fane, Filled and unfilled composite GFT PDMS membranes for the recovery of butanols from dilute aqueous solutions: influence of alcohol polarity, J. Membr. Sci. 125 (1997) 245–255. doi:10.1016/S0376-7388(96)00191-3.

[73] P. Peng, B. Shi, Y. Lan, Preparation of PDMSSilica Nanocomposite Membranes with Silane Coupling for Recovering Ethanol by Pervaporation, Sep. Sci. Technol. 46 (2011) 420–427. doi:10.1080/01496395.2010.527896.

[74] E. Drioli, S. Zhang, A. Basile, On the coupling effect in pervaporation, J. Membr. Sci. 81 (1993) 43–55. doi:10.1016/0376-7388(93)85030-Z.

[75] S. Tan, L. Li, Z. Xiao, Y. Wu, Z. Zhang, Pervaporation of alcoholic beverages - the coupling effects between ethanol and aroma compounds, J. Membr. Sci. 264 (2005) 129–136. doi:10.1016/j.memsci.2005.04.028.

[76] O. Kedem, The Role of Coupling in Pervaporation, J. Membr. Sci. 47 (1989) 277–284. doi:10.1016/S0376-7388(00)83080-X.

[77] M. She, S. Hwang, Effects of concentration, temperature, and coupling on pervaporation of dilute flavor organics, J. Membr. Sci. 271 (2006) 16–28. doi:10.1016/j.memsci.2005.07.005.

[78] M. Franke, Auslegung und Optimierung von Pervaporationsanlagen zur Entwässerung von Lösungsmitteln und Lösungsmittelgemischen, PhD Thesis, University of Aachen, 1990.

[79] X. Feng, R.Y.M. Huang, Concentration polarization in pervaporation separation processes, J. Membr. Sci. 92 (1994) 201–208. doi:10.1016/0376-7388(94)00056-5.

[80] C.-C. Hu, T.-C. Liu, K.-R. Lee, R.-C. Ruaan, J.-Y. Lai, Zeolite-filled PMMA composite membranes: influence of coupling agent addition on gas separation properties, Desalination. 193 (2006) 14–24. doi:10.1016/j.desal.2005.04.137.

[81] G.M. Monsalve-Bravo, S.K. Bhatia, Extending effective medium theory to finite size systems: Theory and simulation for permeation in mixed-matrix membranes, J. Membr. Sci. 531 (2017) 148–159. doi:10.1016/j.memsci.2017.02.029.

[82] D. Hofmann, C. Schepers, Molecular simulation study on sorption and diffusion processes in polymeric pervaporation membrane materials, Mol. Simul. 32 (2006) 73–84. doi:10.1080/08927020500474292.

[83] H. Okuno, K. Renzo, T. Uragami, Sorption and permeation of water and ethanol vapors in poly(vinylchloride) membrane, J. Membr. Sci. 103 (1995) 31–38. doi:10.1016/0376-7388(94)00303-G.

[84] W.J. Koros, Model for sorption of mixed gases in glassy polymers, J. Polym. Sci. Polym. Phys. Ed. 18 (1980) 981–992. doi:10.1002/pol.1980.180180506.

[85] M. Buckley-Smith, The Use of Solubility Parameters to Select Membrane Materials for Pervaporation of Organic Mixtures, Thesis, The University of Waikato, 2006. http://researchcommons.waikato.ac.nz/handle/10289/2625 (accessed May 10, 2017).

[86] A.F.M. Barton, CRC Handbook of Solubility Parameters and Other Cohesion Parameters, Second Edition, CRC Press, 1991.

[87] C.M. Hansen, The three dimensional solubility parameter and solvent diffusion coefficient: Their importance in surface coating formulation, Danish Technical Press, 1967.

[88] H. Zhou, Y. Su, X. Chen, Y. Wan, Separation of acetone, butanol and ethanol (ABE) from dilute aqueous solutions by silicalite-1/PDMS hybrid pervaporation membranes, Sep. Purif. Technol. 79 (2011) 375–384. doi:10.1016/j.seppur.2011.03.026.

[89] A. Hasanoglu, Y. Salt, S. Keleser, S. Ozkan, S. Dincer, Pervaporation separation of organics from multicomponent aqueous mixtures, Chem. Eng. Process. 46 (2007) 300–306. doi:10.1016/j.cep.2006.06.010.

[90] J. Niemisto, W. Kujawski, R.L. Keiski, Pervaporation performance of composite poly(dimethyl siloxane) membrane for butanol recovery from model solutions, J. Membr. Sci. 434 (2013) 55–64. doi:10.1016/j.memsci.2013.01.047.

[91] E.T. Zellers, Three-dimensional solubility parameters and chemical protective clothing permeation. I. Modeling the solubility of organic solvents in Viton® golves, J. Appl. Polym. Sci. 50 (1993) 513–530. doi:10.1002/app.1993.070500315.

[92] Wiley: Kirk-Othmer Encyclopedia of Chemical Technology, Index to Volumes 1 - 26, 5th Edition - Kirk-Othmer, (n.d.). http://www.wiley.com/WileyCDA/WileyTitle/productCd-0471484962.html (accessed February 24, 2017).

[93] P.E. Froehling, D.M. Koenhen, A. Bantjes, C.A. Smolders, Swelling of linear polymers in mixed swelling agents; predictability by means of solubility parameters, Polymer. 17 (1976) 835–836.

[94] A.W. Islam, A. Javvadi, V.N. Kabadi, Universal Liquid Mixture Models for Vapor−Liquid and Liquid−Liquid Equilibria in the Hexane−Butanol−Water System, Ind. Eng. Chem. Res. 50 (2011) 1034–1045. doi:10.1021/ie902028y.

[95] Online Services - DDBST GmbH, (n.d.). http://www.ddbst.com/online.html (accessed March 23, 2017).

[96] J.R. Snider, G.A. Dawson, Tropospheric light alcohols, carbonyls, and acetonitrile: Concentrations in the southwestern United States and Henry's Law data, J. Geophys. Res. Atmospheres. 90 (1985) 3797–3805. doi:10.1029/JD090iD02p03797.

[97] A. Klamt, F. Eckert, COSMO-RS: a novel and efficient method for the a priori prediction of thermophysical data of liquids, Fluid Phase Equilibria. 172 (2000) 43–72. doi:10.1016/S0378-3812(00)00357-5.

[98] P. Vrbka, D. Fenclová, V. Laštovka, V. Dohnal, Measurement of infinite dilution activity coefficients of 1-alkanols (C1–C5) in water as a function of temperature (273–373 K), Fluid Phase Equilibria. 237 (2005) 123–129. doi:10.1016/j.fluid.2005.08.018.

[99] B.V. Ioffe, A.G. Vitenberg, Application of the headspace analysis to systems with unknown partition coefficients, Chromatographia. 11 (1978) 282–286. doi:10.1007/BF02282954.

[100] A.K. Gupta, A.S. Teja, X.S. Chai, J.Y. Zhu, Henry's constants of n-alkanols (methanol through n-hexanol) in water at temperatures between 40°C and 90°C, Fluid Phase Equilibria. 170 (2000) 183–192. doi:10.1016/S0378-3812(00)00350-2.

[101] Š. Hovorka, V. Dohnal, A.H. Roux, G. Roux-Desgranges, Determination of temperature dependence of limiting activity coefficients for a group of moderately hydrophobic organic solutes in water, Fluid Phase Equilibria. 201 (2002) 135–164. doi:10.1016/S0378-3812(02)00087-0.

[102] N.H. Sagert, D.W.P. Lau, Limiting activity coefficients for butyl alcohols in water, n-octane, and carbon tetrachloride, J. Chem. Eng. Data. 31 (1986) 475–478. doi:10.1021/je00046a026.

[103] A. Lebert, D. Richon, Infinite dilution activity coefficients of n-alcohols as a function of dextrin concentration in water-dextrin systems, J. Agric. Food Chem. 32 (1984) 1156–1161. doi:10.1021/jf00125a056.

[104] J. a. V. Butler, C.N. Ramchandani, D.W. Thomson, 58. The solubility of non-electrolytes. Part I. The free energy of hydration of some aliphatic alcohols, J. Chem. Soc. (1935) 280–285. doi:10.1039/JR9350000280.

[105] K. Tochigi, M. Uchiyama, K. Kojima, Measurement of infinite-dilution activity coefficients of alcohols in water using relative gas-liquid chromatographic method, Korean J. Chem. Eng. 17 (2000) 502–505. doi:10.1007/BF02707156.

[106] G.J. Pierotti, C.H. Deal, E.L. Derr, Activity Coefficients and Molecular Structure, Ind. Eng. Chem. 51 (1959) 95–102. doi:10.1021/ie50589a048.

[107] K. Fischer, J. Gmehling, P-x and $\gamma\infty$ data for the different binary butanol-water systems at 50 °C, J. Chem. Eng. Data. 39 (1994) 309–315.

[108] M.G. Burnett, Determination of Partition Coefficients at Infinite Dilution by the Gas Chromatographic Analysis of the Vapor above Dilute Solutions., Anal. Chem. 35 (1963) 1567–1570. doi:10.1021/ac60204a007.

[109] V. Dohnal, D. Ondo, Refined non-steady-state gas–liquid chromatography for accurate determination of limiting activity coefficients of volatile organic compounds in water: Application to C1–C5 alkanols, J. Chromatogr. A. 1097 (2005) 157–164. doi:10.1016/j.chroma.2005.08.015.

[110] R.G. Buttery, L. Ling, D.G. Guadagni, Food volatiles. Volatilities of aldehydes, ketones, and esters in dilute water solution, J. Agric. Food Chem. 17 (1969) 385–389. doi:10.1021/jf60162a025.

[111] J. Howard Rytting, L.P. Huston, T. Higuchi, Thermodynamic Group Contributions for Hydroxyl, Amino, and Methylene Groups, J. Pharm. Sci. 67 (1978) 615–618. doi:10.1002/jps.2600670510.

[112] M.. Hofstee, A. Kwantes, G.W.A. Rijnders, Determination of activity coefficients at infinite dilution by gas–liquid chromatography, Proc. Int. Symp. Distill. Brighton Engl. (1960) 105–109.

[113] I. Landau, A.J. Belfer, D.C. Locke, Measurement of limiting activity coefficients using non-steady-state gas chromatography, Ind. Eng. Chem. Res. 30 (1991) 1900–1906. doi:10.1021/ie00056a034.

[114] B. Kolb, C. Welter, C. Bichler, Determination of partition coefficients by automatic equilibrium headspace gas chromatography by vapor phase calibration, Chromatographia. 34 (1992) 235–240. doi:10.1007/BF02268351.

[115] J. Li, P.W. Carr, Measurement of water-hexadecane partition coefficients by headspace gas chromatography and calculation of limiting activity coefficients in water, Anal. Chem. 65 (1993) 1443–1450.

[116] S. Merk, M. Riederer, Sorption of volatile C1 to C6 alkanols in plant cuticles, J. Exp. Bot. 48 (1997) 1095–1104. doi:10.1093/jxb/48.5.1095.

[117] P.G. Whitehead, S.I. Sandler, Headspace gas chromatography for measurement of infinite dilution activity coefficients of C4 alcohols in water, Fluid Phase Equilibria. 157 (1999) 111–120. doi:10.1016/S0378-3812(99)00014-X.

[118] J. Altschuh, R. Brüggemann, H. Santl, G. Eichinger, O.G. Piringer, Henry's law constants for a diverse set of organic chemicals: Experimental determination and comparison of estimation methods, Chemosphere. 39 (1999) 1871–1887. doi:10.1016/S0045-6535(99)00082-X.

[119] B.R. Kim, E.M. Kalis, T. Dewulf, K.M. Andrews, Henry's Law Constants for Paint Solvents and Their Implications on Volatile Organic Compound Emissions from Automotive Painting, Water Environ. Res. 72 (2000) 65–74. doi:10.2175/106143000X137121.

[120] K. Tochigi, K. Kojima, The Determination of Group Wilson Param Eters to Activity Coefficients by Ebulliometer, J. Chem. Eng. Jpn. 9 (1976) 267–273. doi:10.1252/jcej.9.267.

[121] G.M. Lobien, J.M. Prausnitz, Infinite-dilution activity coefficients from differential ebulliometry, Ind. Eng. Chem. Fundam. 21 (1982) 109–113. doi:10.1021/i100006a002.

[122] L.T. Iraci, B.M. Baker, G.S. Tyndall, J.J. Orlando, Measurements of the Henry's Law Coefficients of 2-Methyl-3-buten-2-ol, Methacrolein, and Methylvinyl Ketone, J. Atmospheric Chem. 33 (1999) 321–330. doi:10.1023/A:1006169029230.

[123] S.L. Friant, I.H. Suffet, Interactive effects of temperature, salt concentration, and pH on head space analysis for isolating volatile trace organics in aqueous environmental samples, Anal. Chem. 51 (1979) 2167–2172. doi:10.1021/ac50049a027.

[124] K. Ochi, K. Kojima, A Measurement of Vapor-Liquid Equilibria at Extreme Dilution, J. Chem. Eng. Jpn. 20 (1987) 6–10. doi:10.1252/jcej.20.6.

[125] M. Yoshikawa, H. Yokoi, K. Sanui, N. Ogata, Pervaporation of water-ethanol mixture through poly(maleimide-co-acrylonitrile) membrane, J. Polym. Sci. Polym. Lett. Ed. 22 (1984) 125–127. doi:10.1002/pol.1984.130220211.

[126] M. Yoshikawa, T. Yukoshi, K. Sanui, N. Ogata, Separation of water and ethanol by pervaporation through poly(acrylic acid-co-acrylonitrile) membrane, J. Polym. Sci. Polym. Lett. Ed. 22 (1984) 473–475. doi:10.1002/pol.1984.130220902.

[127] M. Yoshikawa, H. Yokoi, K. Sanui, N. Ogata, Selective separation of water–alcohol binary mixture through poly(maleimide-co-acrylonitrile) membrane, J. Polym. Sci. Polym. Chem. Ed. 22 (1984) 2159–2168. doi:10.1002/pol.1984.170220917.

[128] K.. Boddeker, Pervaporation durch Membranen und ihre Anwendung zur Trennung von Flüssiggemischen, Fortsch Ber VDI Reihle 3 Nr VDI-Verl. 129 (1986).

[129] M.H.V. Mulder, C.A. Smolders, On the mechanism of separation of ethanol/water mixtures by pervaporation I. Calculations of concentration profiles, J. Membr. Sci. 17 (1984) 289–307.

[130] R.B. Long, Liquid Permeation through Plastic Films, Ind. Eng. Chem. Fundam. 4 (1965) 445–451. doi:10.1021/i160016a015.

[131] F.W. Greenlaw, W.D. Prince, R.A. Shelden, E.V. Thompson, Dependence of Diffusive Permeation Rates on Upstream and Downstream Pressures .1. Single Component Permeant, J. Membr. Sci. 2 (1977) 141–151. doi:10.1016/S0376-7388(00)83240-8.

[132] R.A. Shelden, E.V. Thompson, Dependence of diffusive permeation rates on upstream and downstream pressures, J. Membr. Sci. 4 (1978) 115–127. doi:10.1016/S0376-7388(00)83288-3.

[133] A. K. Doolittle, Studies in Newtonian Flow. II. The Dependence of the Viscosity of Liquids on Free-Space, J. Appl. Phys. 22 (1951) 1471–1475. doi:10.1063/1.1699894.

[134] A. K. Doolittle, Studies in Newtonian Flow. III. The Dependence of the Viscosity of Liquids on Molecular Weight and Free Space (in Homologous Series), J. Appl. Phys. 23 (1952) 236–239. doi:10.1063/1.1702182.

[135] A. Kreituss, H.L. Frisch, Free-volume estimates in heterogeneous polymer systems. I. Diffusion in crystalline ethylene–propylene copolymers, J. Polym. Sci. Polym. Phys. Ed. 19 (1981) 889–905. doi:10.1002/pol.1981.180190515.

[136] H. Fujita, Diffusion in polymer-diluent systems, in: Fortschritte Hochpolym.-Forsch., Springer, Berlin, Heidelberg, 1961: pp. 1–47. doi:10.1007/BFb0050514.

[137] C.K. Yeom, R.Y.M. Huang, Modelling of the pervaporation separation of ethanol-water mixtures through crosslinked poly(vinyl alcohol) membrane, J. Membr. Sci. 67 (1992) 39–55. doi:10.1016/0376-7388(92)87038-Y.

[138] İ. Şentarlı, S. Dinçer, Ö.T. Savaşçı, Pervaporation Separation of Methanol-Carbontetrachloride Binary Mixtures Using Low Density Polyethylene Membranes, Chem. Eng. Technol. 21 (1998) 359–364. doi:10.1002/(SICI)1521-4125(199804)21:4<359::AID-CEAT359>3.0.CO;2-5.

[139] W.J. Koros, R.T. Chern, V. Stannett, H.B. Hopfenberg, A model for permeation of mixed gases and vapors in glassy polymers, J. Polym. Sci. Polym. Phys. Ed. 19 (1981) 1513–1530. doi:10.1002/pol.1981.180191004.

[140] H. Okuno, K. Renzo, T. Uragami, Sorption and permeation of water and ethanol vapors in poly(vinylchloride) membrane, J. Membr. Sci. 103 (1995). doi:10.1016/0376-7388(94)00303-g.

[141] Y. Tamai, H. Tanaka, K. Nakanishi, Molecular Simulation of Permeation of Small Penetrants through Membranes. 1. Diffusion Coefficients, Macromolecules. 27 (1994) 4498–4508. doi:10.1021/ma00094a011.

[142] L. Fritz, D. Hofmann, Molecular dynamics simulations of the transport of water-ethanol mixtures through polydimethylsiloxane membranes, Polymer. 38 (1997) 1035–1045. doi:10.1016/S0032-3861(96)00600-3.

[143] E. El-Zanati, E. Abdel-Hakim, O. El-Ardi, M. Fahmy, Modeling and simulation of butanol separation from aqueous solutions using pervaporation, J. Membr. Sci. 280 (2006) 278–283. doi:10.1016/j.memsci.2006.01.029.

[144] H.R. Cascon, S.K. Choudhari, 1-Butanol pervaporation performance and intrinsic stability of phosphonium and ammonium ionic liquid-based supported liquid membranes, J. Membr. Sci. 429 (2013) 214–224. doi:10.1016/j.memsci.2012.11.028.

[145] O. Vopička, V. Hynek, K. Friess, P. Izák, Blended silicone–ionic liquid membranes: Transport properties of butan-1-ol vapor, Eur. Polym. J. 46 (2010) 123–128. doi:10.1016/j.eurpolymj.2009.10.011.

[146] X. Yang, Z. Wu, F. Manquan, L. Jiding, Nonequilibrium Dissolution-diffusion Model for PDMS Membrane Pervaporation of ABE Water Binary System, J Membra Sci Technol. 6 (2016) 1.

[147] S.-Y. Li, R. Srivastava, R.S. Parnas, Separation of 1-butanol by pervaporation using a novel tri-layer PDMS composite membrane, J. Membr. Sci. 363 (2010) 287–294. doi:10.1016/j.memsci.2010.07.042.

[148] N. Valentínyi, E. Cséfalvay, P. Mizsey, Modelling of pervaporation: Parameter estimation and model development, Chem. Eng. Res. Des. 91 (2013) 174–183. doi:10.1016/j.cherd.2012.07.001.

[149] R.W. Baker, Membrane Transport Theory, in: Membr. Technol. Appl., John Wiley & Sons, Ltd, 2004: pp. 15–87. doi:10.1002/0470020393.ch2.

[150] M.T. Ashraf, J.E. Schmidt, J. Kujawa, W. Kujawski, H.A. Arafat, One-dimensional modeling of pervaporation systems using a semi-empirical flux model, Sep. Purif. Technol. 174 (2017) 502–512. doi:10.1016/j.seppur.2016.10.043.

[151] R. Petrychkovych, K. Setnickova, P. Uchytil, The influence of water on butanol isomers pervaporation transport through polyethylene membrane, Sep. Purif. Technol. 107 (2013) 85–90. doi:10.1016/j.seppur.2013.01.014.

[152] G. Cocchi, M.G. De Angelis, F. Doghieri, Solubility and diffusivity of liquids for food and pharmaceutical applications in crosslinked polydimethylsiloxane (PDMS) films: I.

Experimental data on pure organic components and vegetable oil, J. Membr. Sci. 492 (2015) 600–611. doi:10.1016/j.memsci.2015.04.063.

[153] P. Radovanovic, S.W. Thiel, S.-T. Hwang, Transport of ethanol-water dimers in pervaporation through a silicone rubber membrane, J. Membr. Sci. 48 (1990) 55–65. doi:10.1016/S0376-7388(00)80795-4.

[154] E. Favre, P. Schaetzel, Q.T. Nguygen, R. Clément, J. Néel, Sorption, diffusion and vapor permeation of various penetrants through dense poly(dimethylsiloxane) membranes: a transport analysis, J. Membr. Sci. 92 (1994) 169–184. doi:10.1016/0376-7388(94)00060-3.

[155] J.M. Watson, M.G. Baron, The behaviour of water in poly(dimethylsiloxane), J. Membr. Sci. 110 (1996) 47–57. doi:10.1016/0376-7388(95)00229-4.

[156] J.M. Watson, P.A. Payne, A study of organic compound pervaporation through silicone rubber, J. Membr. Sci. 49 (1990) 171–205. doi:10.1016/S0376-7388(00)80786-3.

[157] J.M. Watson, G.S. Zhang, P.A. Payne, The diffusion mechanism in silicone rubber, J. Membr. Sci. 73 (1992) 55–71. doi:10.1016/0376-7388(92)80186-N.

[158] C. Zeng, J. Li, D. Wang, T. Chen, C. Zhao, C. Chen, Infinite Dilute Activity and Diffusion Coefficients in Polymers by Inverse Gas Chromatography, J. Chem. Eng. Data. 51 (2006) 93–98. doi:10.1021/je050241s.

[159] Fermentation coupled with pervaporation: a kinetic study, (n.d.). http://www.academia.edu/27356851/Fermentation_coupled_with_pervaporation_a_kinetic_study (accessed September 9, 2016).

[160] V.S. Nayak, J.B. Moffat, Sorption and diffusion of alcohols in heteropoly oxometalates and ZSM-5 zeolite, J. Phys. Chem. 92 (1988) 7097–7102. doi:10.1021/j100336a014.

[161] T.C. Bowen, R.D. Noble, J.L. Falconer, Fundamentals and applications of pervaporation through zeolite membranes, J. Membr. Sci. 245 (2004) 1–33. doi:10.1016/j.memsci.2004.06.059.

[162] A. Plaza, G. Merlet, A. Hasanoglu, M. Isaacs, J. Sanchez, J. Romero, Separation of butanol from ABE mixtures by sweep gas pervaporation using a supported gelled ionic liquid membrane: Analysis of transport phenomena and selectivity, J. Membr. Sci. 444 (2013) 201–212. doi:10.1016/j.memsci.2013.04.034.

[163] W.A.J. Krishna.R, The maxwell stefane approach to mass transfer, Chem. Eng. Sci. 52 (1997) 861–911.

[164] Bitter.J.G.A, Transport Mechanisms in Membrane Separation Processes, Plenum Press. (1991) 219.

[165] F. Kapteijn, J.A. Moulijn, R. Krishna, The generalized Maxwell–Stefan model for diffusion in zeolites:: sorbate molecules with different saturation loadings, Chem. Eng. Sci. 55 (2000) 2923–2930. doi:10.1016/S0009-2509(99)00564-3.

[166] R. Krishna, L.J.P. van den Broeke, The Maxwell-Stefan description of mass transport across zeolite membranes, Chem. Eng. J. Biochem. Eng. J. 57 (1995) 155–162. doi:10.1016/0923-0467(94)02951-2.

[167] A. Heintz, W. Stephan, A generalized solution—diffusion model of the pervaporation process through composite membranes Part II. Concentration polarization, coupled diffusion and the influence of the porous support layer, J. Membr. Sci. 89 (1994) 153–169. doi:10.1016/0376-7388(93)E0223-7.

[168] P. Izák, L. Bartovská, K. Friess, M. Šípek, P. Uchytil, Description of binary liquid mixtures transport through non-porous membrane by modified Maxwell–Stefan equations, J. Membr. Sci. 214 (2003) 293–309. doi:10.1016/S0376-7388(02)00580-X.

[169] R. Krishna, J.A. Wesselingh, The Maxwell-Stefan approach to mass transfer, Chem. Eng. Sci. 52 (1997) 861–911. doi:10.1016/S0009-2509(96)00458-7.

[170] A. Ebneyamini, H. Azimi, J. Thibault, F.H. Tezel, Description of Butanol Aqueous Solution Transport through Commercial PDMS Membrane via Pervaporation Using Extended Maxwell–Stefan Model, J. Sep. Sci. Technol. (2017) Submitted.

[171] J.-J. Shieh, R.Y.M. Huang, A Pseudophase-Change Solution-Diffusion Model for Pervaporation. I. Single Component Permeation, Sep. Sci. Technol. 33 (1998) 767–785. doi:10.1080/01496399808544875.

[172] J.-J. Shieh, R.Y.M. Huang, A Pseudophase-Change Solution-Diffusion Model for Pervaporation. II. Binary Mixture Permeation, Sep. Sci. Technol. 33 (1998) 933–957. doi:10.1080/01496399808545000.

6. Chapter 6

On the Effective Permeability of Mixed Matrix Membranes

Hoda Azimi, F. Handan Tezel and Jules Thibault*

Abstract

Mixed matrix membranes (MMMs) are attracting significant interest for applications such as pervaporation and gas separation. To better comprehend the impact of filler particles within polymer matrices, the species permeation mass transport was theoretically studied by numerical simulation using finite differences method. The Fick's second law of diffusion equations was solved for a three-dimensional MMM to obtain the concentration profile within the membrane and consequently the steady-state permeation flux of the species. The effective permeability of MMMs was then calculated using the steady-state permeation flux of the permeants. The effects of various structural parameters such as the filler volume fraction, particle size, shape and orientation, the ratio of permeability coefficients in the dispersed and continuous phases (P_d/P_c), membrane thickness and particle sorption isotherms have been investigated. Results revealed that the effective permeability of MMMs strongly depends on the permeability ratio of the dispersed phase to the continuous phase and the volume fraction of the filler material. Moreover, the shape and the size of the particle material had no influence on the effective permeability of the MMMs for filler volume fractions less than 0.4. For numerical simulations performed with different sorption isotherms, results showed that the effective permeability of the membrane depends on the type and parameters of the isotherm as well as the feed concentration.

Keywords: Mixed matrix membrane; Finite difference numerical solution; Pervaporation model; Effective permeability

Introduction

Pervaporation process is a membrane-based separation technique which is widely used for the separation of alcohols from dilute aqueous solutions due to its advantages such as good separation performance and low energy consumption [1–5]. Membrane materials are commonly divided into two categories: polymeric membranes and inorganic membranes. Polymeric

membranes are well-known due to their wide range of properties, ease of fabrication, high mechanical stability and low cost [6]. However, separation processes using polymeric membranes are restricted by the trade-off between membrane permeability (or permeate flux) and selectivity [7]. On the other hand, organic membranes have higher selectivity and permeability than the polymeric membranes, but they are expensive and fragile. In order to overcome these barriers, it has been suggested to embed porous inorganic filler materials such as zeolites [8], metal organics frameworks (MOF_s) [9], silicalites [10], activated carbons (AC) [11] and carbon nanotubes (CNT_s) [12] into the host polymer matrix to manufacture mixed matrix membranes (MMMs) or hybrid composite membranes. It has been reported that the presence of filler materials embedded within the polymer matrix could enhance the effective permeability of the membranes [8,10,13,14]. In addition, the presence of fillers might also improve the mechanical and thermal stability of membranes [11,15]. However, there are still important challenges (e.g. selecting the most appropriate pair of polymer-filler materials) which have to be overcome before applying these types of membranes at an industrial scale.

Modelling of mass transport is paramount to obtaining a better understanding about the influence of permeable and barrier fillers within the membrane, on the permeation of species through mixed matrix membranes. Different analytical and numerical solutions have been introduced to estimate the effective permeability of ideal mixed matrix membranes as a function of different parameters such as membrane thickness, filler size, volumetric filler loading and permeability of the components in the continuous and dispersed phases [7,16,17]. Recently, Ebneyamini et al. [18] proposed a semi-empirical resistance-based model to estimate the effective permeability of ideal MMMs. This model was developed by introducing a correction factor to a simple one-directional resistance-based analytical solution. The model was referred to as RB model and it was then extended to include a correction factor to account for the three-directional diffusional pathway. The correction factor was based on the ratio of the estimated effective permeability determined by a finite difference (FD) numerical solution and the simple RB model. The model was obtained under the assumptions of homogenous dispersion cubical filler materials throughout the polymeric matrix and an ideal morphology at the polymer-filler interface. In addition, it was assumed that the solubility of the permeants in both the continuous and dispersed phases followed a linear sorption isotherm (Henry's law) which implied a fixed permeability of the penetrants in the two individual phases within the membrane [18].

In this study, a three-directional (3D) numerical solution of the Fickian diffusion equations is used to investigate the influence of the different parameters such as the filler content, the permeability ratio between the dispersed and the continuous phase (P_d/P_c), the filler shape (cubical, spherical, cylindrical), size and orientation of the filler, linear and non-linear sorption isotherms of species in the filler material and the membrane thickness on the effective permeability of the ideal mixed matrix membrane with a homogenous and random dispersion of filler materials. To the best of our knowledge, this work is one of the first few investigation to simulate comprehensively the effect of filler properties effects on the relative permeability of the mixed matrix membranes.

Development of Finite-Difference Numerical Solution

Finite difference numerical solution has been used to study the mass transfer of species through mixed matrix membranes. It was assumed that polymer-particle interface morphology was ideal. Moreover, it was assumed that the particle geometrical and intrinsic specifications of filler particles are identical throughout the membrane matrix. The overall membrane can be represented by a number of repeatable unit elements where each element contains a distribution of random or uniformly dispersed particles that is statistically identical to the distribution of particles of any other element of the membrane. For illustration purposes, a uniform distribution of cubical particles within the membrane is considered. Each element consists of a centrally-located cubical particle surrounded by the polymer matrix (Figure 6-1). All membrane elements and their permeability are identical. The permeability of each unit is also identical to the entire membrane. Figure 6-1(a) represents a specific case of cubical elements (Figure 6-1(b)) of dimension 2 ×2 ×2 μm^3 homogenously distributed within a 10 ×10×10 μm^3 ideal mixed matrix membrane. The filler size and the solid volume fraction in Figure 6-1 are 1 μm^3 and 0.125, respectively.

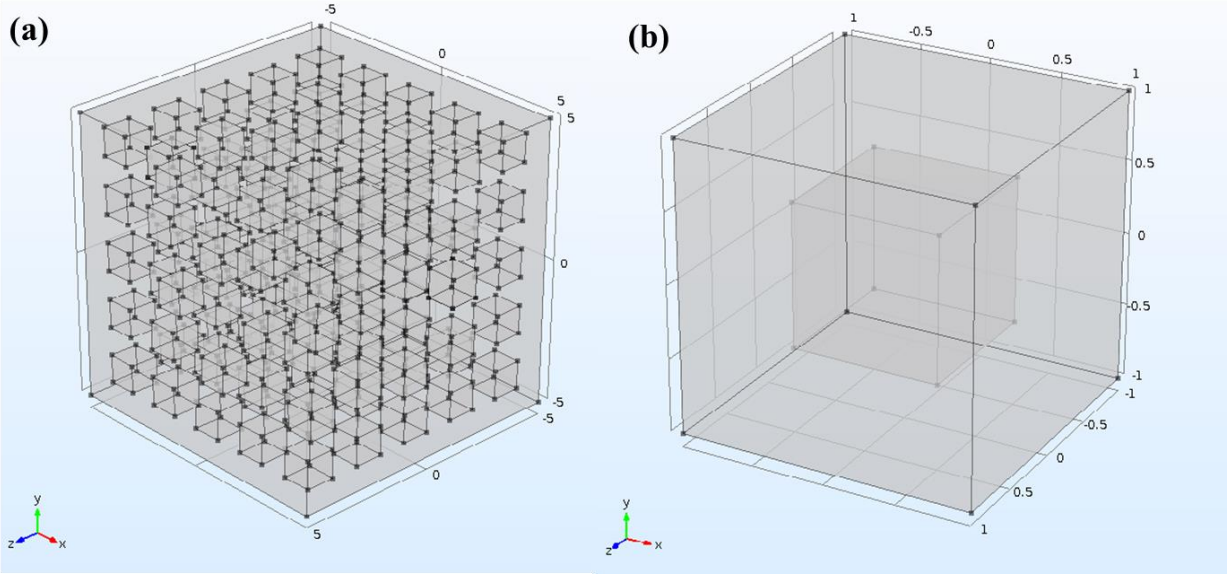

Figure 6-1 Schematic diagram of (a) 10×10×10 μm3 mixed matrix membrane containing 1 μm cubical particle and (b) its repeatable element with a filler volume fraction of 0.125.

To determine the steady and unsteady state concentration profiles of the penetrants through the mixed matrix membrane, the three-dimensional Fick's second law of diffusion (Eq. (1)) was solved by finite differences in Cartesian coordinates.

$$\frac{\partial C}{\partial t} = \frac{\partial}{\partial x}\left(D_{x,y,z}\frac{\partial C}{\partial x}\right) + \frac{\partial}{\partial y}\left(D_{x,y,z}\frac{\partial C}{\partial y}\right) + \frac{\partial}{\partial z}\left(D_{x,y,z}\frac{\partial C}{\partial z}\right) \qquad (1)$$

In this investigation, it was assumed that the concentration of the feed solution in contact with the retentate side of the membrane remains constant and perfect vacuum prevails on the permeate side. The unsteady state equation was solved to determine the time required to achieve steady state. However, for the majority of the results presented in this investigation such as to determine the effective permeability of mixed matrix membranes, the steady-state solution was required. It would therefore be possible to solve Eq. (1) with the time derivative term equal to zero. The finite differences code developed for this investigation had both the steady and unsteady state options. However, it turned out that solving the very large sparse matrix for the steady state case took significantly more computation time than solving the unsteady state equation while assuming a linear profile as the initial conditions. It is important to note that the final steady-state concentration profile and permeate flux are independent of initial conditions. For this reason, the

unsteady state equation was used throughout this investigation. In addition, in the case where the solubility of permeants in the continuous and dispersed phases is nonlinear, it is required solving for the unsteady state equation. The initial and boundary conditions considered in this investigation are given in Eq. (2).

$$IC: \quad C(x,y,z)\big|_{t=0} = \begin{cases} 0 \\ \text{or} \\ C(x,0,z) - \left[C(x,0,z) - C(x,L,z)\right]\dfrac{y}{L} \end{cases} \tag{2a}$$

$$BC1: \quad C(x,0,z) = S_{x,0,z} C_f \tag{2b}$$

$$BC2: \quad C(x,L,z) = 0 \tag{2c}$$

$$\text{BC3 \& BC4:} \quad \left.\frac{\partial C}{\partial x}\right|_{x=0} = \left.\frac{\partial C}{\partial x}\right|_{x=L} = 0 \tag{2d}$$

$$\text{BC5 \& BC6:} \quad \left.\frac{\partial C}{\partial z}\right|_{z=0} = \left.\frac{\partial C}{\partial z}\right|_{z=L} = 0 \tag{2e}$$

For BC1, at the feed solution membrane interface, the surface concentration within the membrane is in equilibrium with the feed solution which was assumed constant over the entire membrane surface. For BC2, the concentration is equal to zero as perfect vacuum is assumed. For BC3-BC6, symmetry conditions (or periodic conditions) are assumed where the portion of the membrane that is solved using Eq. (1) is representative of all the other equal-size volumes forming the membrane. It will be shown in the results that the permeability of a representative element has the same permeability of the entire membrane.

Eq. (1) was discretized using a sufficiently large number of mesh points and solved by finite differences. Eq. (3) determines the concentration of a permeant m at a mesh point (i,j,k) at time t + Δt as a function of the current concentration at mesh point (i,j,k) and the concentration at the six neighbouring mesh points at time t. Eq. (1) prevails for all interior mesh points. This equation was solved iteratively to obtain the steady-state concentration profile and permeate flux of components.

$$C_{i,j,k}^{m,t+\Delta t} = C_{i,j,k}^{m,t} + \Delta t \left[\begin{array}{l} -D_{i,j,k}^{L_x} \dfrac{\left(C_{i,j,k}^{m,t} - \dfrac{S_{i,j,k}}{S_{i-1,j,k}} C_{i-1,j,k}^{m,t} \right)}{\Delta x^2} + D_{i,j,k}^{R_x} \dfrac{\left(\dfrac{S_{i,j,k}}{S_{i+1,j,k}} C_{i+1,j,k}^{m,t} - C_{i,j,k}^{m,t} \right)}{\Delta x^2} \\ -D_{i,j,k}^{L_y} \dfrac{\left(C_{i,j,k}^{m,t} - \dfrac{S_{i,j,k}}{S_{i,j-1,k}} C_{i,j-1,k}^{m,t} \right)}{\Delta y^2} + D_{i,j,k}^{R_y} \dfrac{\left(\dfrac{S_{i,j,k}}{S_{i,j+1,k}} C_{i,j+1,k}^{m,t} - C_{i,j,k}^{m,t} \right)}{\Delta y^2} \\ -D_{i,j,k}^{L_z} \dfrac{\left(C_{i,j,k}^{m,t} - \dfrac{S_{i,j,k}}{S_{i,j,k-1}} C_{i,j,k-1}^{m,t} \right)}{\Delta z^2} + D_{i,j,k}^{R_z} \dfrac{\left(\dfrac{S_{i,j,k}}{S_{i,j,k+1}} C_{i,j,k+1}^{m,t} - C_{i,j,k}^{m,t} \right)}{\Delta z^2} \end{array} \right] \quad (3)$$

The concentrations of all six neighboring mesh points in Eq. (3) are converted to their equilibrium concentrations relative to the phase of the central mesh point (*i*,*j*,*k*) using the ratio of the solubility coefficients in the two respective phases. For boundary mesh points, Eq. (3) was adapted to take into account boundary conditions of Eq. 2(b)-2(e).

An effective diffusion coefficient between neighbouring mesh points was considered due to the different properties of the surrounding mesh points such as the diffusivity and solubility coefficients. A mass balance has been performed to calculate the effective diffusivity coefficient of each mesh point within the matrix of the membrane. Eq. (4) was used to estimate the effective diffusivities in the *x*-direction between mesh point *(i, j, k)* and its left neighbour (*i-1*, *j*, *k*), and between mesh point (*i*, *j*, *k*) and its right neighbour (*i+1*, *j*, *k*), respectively. Similar equations have been used for the effective diffusion coefficients in *y* and *z*-directions.

$$\frac{1}{D_{i,j,k}^{L_x}} = \frac{S_{i,j,k}}{S_{i-1,j,k}} \frac{1}{2D_{i-1,j,k}} + \frac{1}{2D_{i,j,k}} \quad (4a)$$

$$\frac{1}{D_{i,j,k}^{R_x}} = \frac{S_{i,j,k}}{S_{i+1,j,k}} \frac{1}{2D_{i+1,j,k}} + \frac{1}{2D_{i,j,k}} \quad (4b)$$

The Fick's first law of diffusion (Eq. (5)) was used to estimate the average steady-state permeation flux of a permeant at the permeate side of the membrane based on all surface mesh points of the *x*-*z* plane. A similar equation was used for estimating the permeation flux at the feed side of the membrane.

$$J_{(i,N_y,k)} = -D_{x,y,z}\left.\frac{\partial C}{\partial y}\right|_{y=L} \tag{5a}$$

$$J_{y=L} = \sum_{i=1}^{N_x}\sum_{k=1}^{N_z}\frac{J_{(i,N_y,k)}}{(N_x-1)(N_y-1)} \tag{5b}$$

where J is the permeation flux calculated for a x-z plane. N_x, N_y and N_z are the number of mesh points used to discretize Eq. (1) in the x, y and z directions, respectively. Given the estimation of the permeation flux, the concentration driving force and the thickness, the effective steady-state permeability of a permeant in MMMs can be calculated (Eq. (6)).

$$P_{eff} = \frac{JL}{\Delta C} \tag{6}$$

Table 6-1 Values of solubility and diffusion coefficients used for various case studies for linear sorption isotherms.

	Material	D (m^2/s)	S (g/L)/(g/L)	P (m^2/h)	P_d / P_c
Case 1	Continuous phase	5.00×10^{-10}	0.01	5.00×10^{-12}	500
	Dispersed phase	1.00×10^{-10}	25.00	2.50×10^{-09}	
Case 2	Continuous phase	5.00×10^{-10}	0.01	5.00×10^{-12}	10.00
	Dispersed phase	2.00×10^{-12}	25.00	5.00×10^{-11}	
Case 3	Continuous phase	5.00×10^{-10}	0.01	5.00×10^{-12}	1.00
	Dispersed phase	5.00×10^{-10}	0.01	5.00×10^{-12}	
Case 4	Continuous phase	5.00×10^{-10}	0.01	5.00×10^{-12}	0.1
	Dispersed phase	2.00×10^{-14}	25.00	5.00×10^{-13}	

To investigate the effect of embedded filler material on the effective permeability of the mixed matrix membrane, the finite difference algorithm was coded in FORTRAN and solved for different case studies. Moreover, in the case when the filler is an adsorbent for a given permeant, the impact of different adsorption isotherms of the filler material on the effective permeability of the MMMs was also studied. Both linear (Henry's law) and nonlinear (Langmuir) equilibrium adsorption models were investigated. Table 6-1 presents the value of the solubility and diffusion coefficients which have been used in this study for the continuous and dispersed phase for various numerical simulations when sorption follows a linear isotherm (Henry's law).

Results and discussion

Comparison between analytical and numerical solutions for neat polymeric membranes

Since numerical solutions are used extensively in this investigation, it is important to validate the precision of the finite difference scheme with a benchmark analytical solution. An analytical solution does not exist for mixed matrix membranes such that the validation of the numerical solution will be done with the analytical solution for a pure polymeric membrane. The analytical solution was used to calculate the time-dependent concentration profile within the membrane and the time-dependent permeation fluxes at the two interfaces of the membrane. The analytical solution for both the concentration profile and the permeation flux can be found in Wu et al. [19].

Both the analytical and numerical solutions were obtained as a function of time for a neat membrane having a diffusion and solubility coefficients ($D = 5\times10^{-10}$ m^2/s and $S = 25$ $(g/L)/(g/L)$), respectively. For the numerical solution, Eq. (3), subjected to boundary conditions of Eq. (2b-2e), was used to calculate the concentration profile of the permeants and the permeation flux at the two interfaces as a function of time. For this validation, the initial condition of the concentration within the membrane was set to zero. The number of mesh points, (N_x, N_y, N_z), for this numerical solutions as well as for the majority of the numerical solutions was (41, 41, 41).

Results of the validation for the time-dependent concentration profile and the permeation fluxes at the two interfaces are presented in Figures 6-2 and 6-3. Figure 6-2 compares the numerical solution with the analytical solution for the concentration profile across the membrane at three different permeation times. Results clearly show that the numerical solution is very precise with an average error of 0.01% based on the three concentration profiles.

Figure 6-3 shows the time-dependent upstream and downstream permeation fluxes of a penetrant in a neat polymeric membrane which were calculated using both the analytical model and the numerical solution. Results clearly show that the calculated permeation flux with the numerical method is a very good estimation of the analytical permeation flux with an average error of

0.5%. A much higher precision for the estimation of the steady-state permeation flux was obtained such that the numerical scheme developed in this investigation can be used with confidence for calculating the concentration profiles and the steady-state permeation flux of permeants mixed matrix membranes.

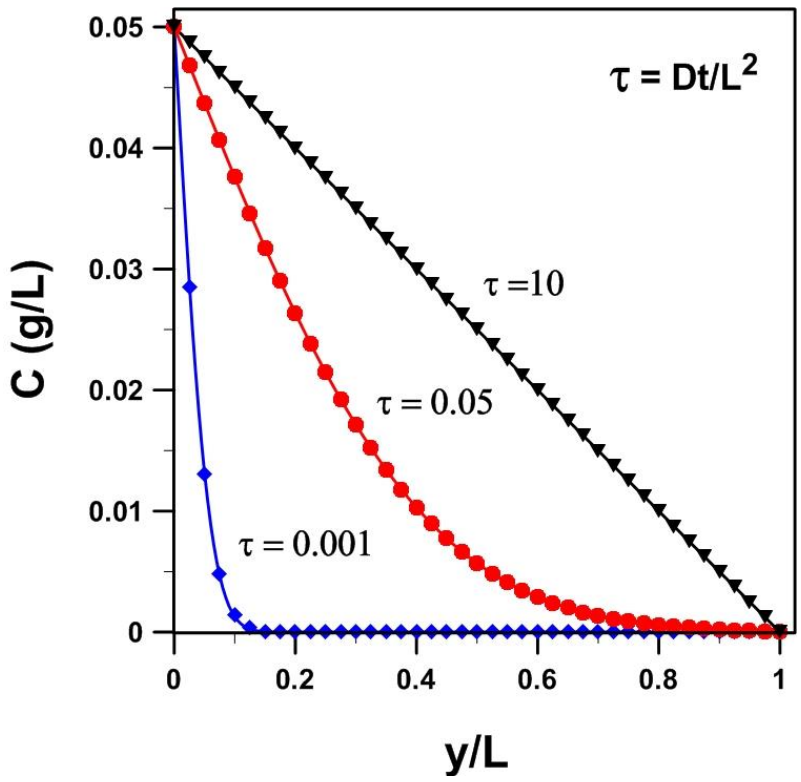

Figure 6-2 Concentration profile of the penetrant within a neat polymeric membrane as a function of the normalized length of the membrane at three different dimensionless times of the permeation process (Symbols: FD numerical solution; Lines: Analytical solution).

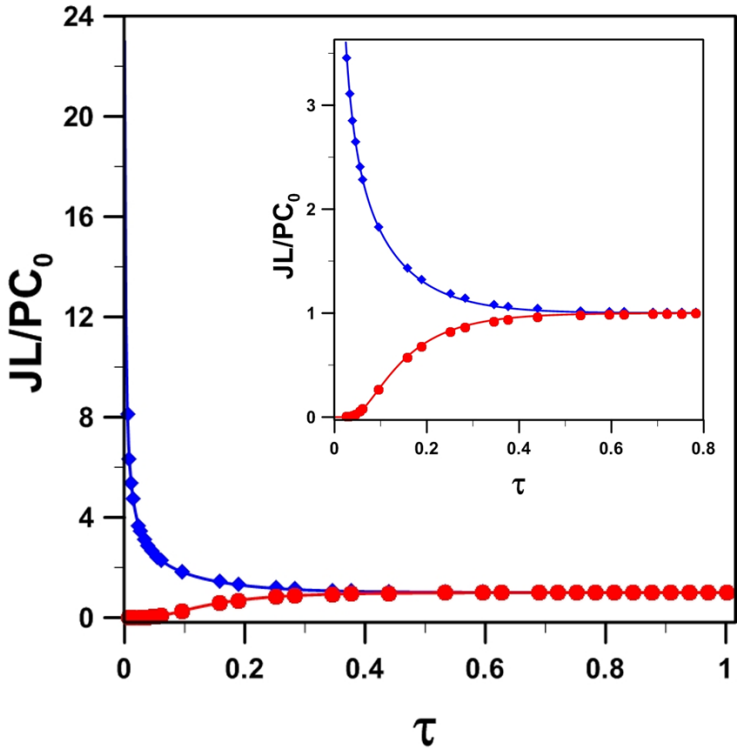

Figure 6-3 Upstream and downstream dimensionless permeation fluxes as a function of the dimensionless time for a neat polymeric membrane (Symbols: FD numerical solution; Lines: Analytical solution).

Concentration profile

In order to investigate the impact of the pesence of particles on the concentration profile of the penetrants through a mixed matrix membrane, different permeability ratios of the dispersed to the continuous phase were considered for a single spherical filler located at the centre of a cubical repeatable element and with a filler volume fraction of 0.065. Figure 6-4 presents the concentration profile, normalized by their solubility, through the centre of the cubical unit element as indicated in the insert in Figure 6-4. When the permeability of the dispersed and continuous phases are identical, the concentration profile is obviously linear throughout the membrane. When the permeability of the disperesed phase is larger than the permeability of the continuous phase, the solid particle acts as an attractor where the concentration streamlines will deviate slightly toward the solid particle since it offers an easier diffusion path. As a result, the overall permeation flux across the membrane will increase such that the slope of the

concentration within the polymeric phase will increase to support this higher flux as observed for the concentration profile for (P_d/P_c) of 10. However, away from the path of the particle, the concentration profile will not be as steep as the one shown in the centre line of the cubical element. Since the permeability of the particle is higher, the concentration gradient within the particle is smaller and the total concentration profile under steady state will adjust such that the average permeation flux at all *x-z* planes will be identical across the membrane (*y*-direction).

On the other hand, when the dispersed to the continuous permeability ratio is less than one, the particle acts as a barrier to the permeation of the penetrant and the concentration streamlines deviate away from the particle and the average permeation flux across the membrane becomes smaller. This is evidenced by the lower concentration gradient in the continuous phase above and below the particle in Figure 6-4. It is obvious that for mixed matrix membranes used for pervaporation and gas separation, a larger dispersed to continuous permeability ratio is required.

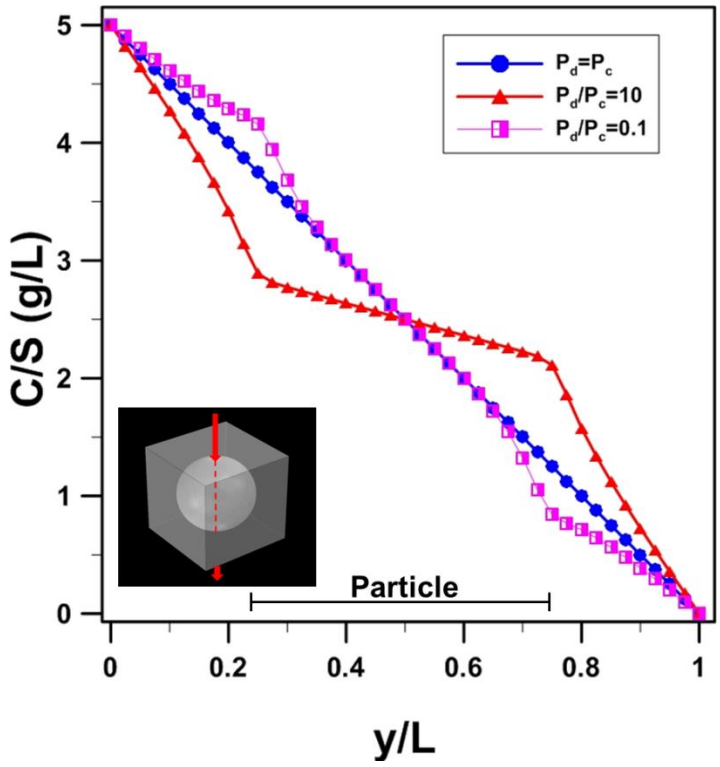

Figure 6-4 Effect of presence of fillers on the concentration profile of the penetrants through a mixed matrix membrane. Concentration profile is along the line passing through the poles of the spherical particle.

Effect of the filler volume fraction (ϕ) and permeability ratio (P_d/P_c)

A series of numerical experiments were performed to determine the effect of the volumetric filler content of the dispersed phase in the polymer matrix of MMMs on the effective membrane permeability. Since the effective permeability of a homogenously dispersed mixed matrix membrane is identical to the permeability of its repeatable unit element [18], to reduce the computing time, the numerical solution was performed on the repeatable element instead of the whole MMM. In addition to the filler volume fraction, another very important parameter impacting on the relative permeability of mixed matrix membranes is the ratio of the permeability coefficient of the dispersed to the continuous phase (P_d/P_c).

Figure 6-5 shows the variation of the relative effective permeability (P_{eff}/P_c) as a function of the ratio of the permeability coefficient of the dispersed to the continuous phase for three different filler volumetric fractions for a spherical particle located at the centre of the repeatable cubical unit element. The variation of the relative effective permeability follows a sigmoid-shape variation with the ratio (P_d/P_c) with amplitude that increases rapidly with the filler volume fraction. When the permeability of the dispersed phase is smaller than the one of the continuous phase, filler particles act as a barrier material and the permeant diffusion streamlines will partly move away from the particles to preferentially diffuse through the polymeric continuous phase. For lower values of the (P_d/P_c), the particles inhibits the permeation of penetrants across the membrane.

Results of Figure 6-5 show that there is a steep increase in the relative effective permeability for a dispersed to continuous permeability ratio between 1 and 10 and then increase more slowly to attain a maximum increase in the relative effective permeability of the membrane at a dispersed to continuous permeability ratio of approximately 100. For lower values (P_d/P_c) lower than one, the particles inhibit the permeation of penetrants across the membrane.

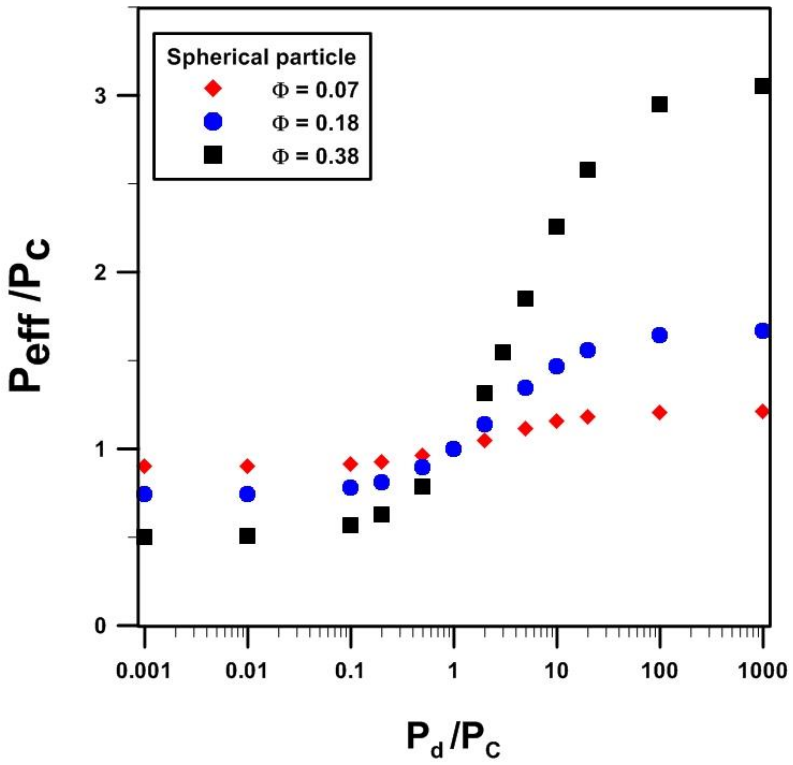

Figure 6-5 Effect of the dispersed to the continuous permeability ratio (Pd/Pc) on the relative permeability (Peff/Pc) of the membrane for one spherical particle centrally located at the centre of a repeatable cubical element.

Figure 6-6 compares the calculated relative effective permeability of ideal MMMs containing spherical and cubical fillers for two different ratios of P_d/P_c as a function of the volumetric filler content. Results of Figure 6-6 clearly show that relative permeability increases exponentially with the filler volume fraction. In addition, for the same relative ratio of the dispersed to the continuous phase, the relative effective permeability of the cubical and spherical particles is identical up to a particle volume fraction of 0.4.

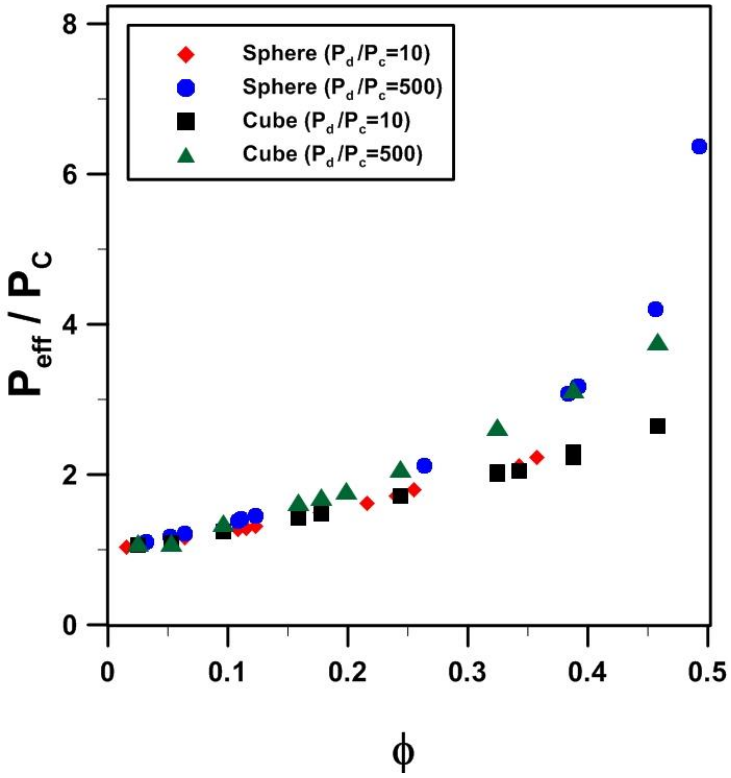

Figure 6-6 Effect of the dispersed to continuous permeability ratio on the relative permeability of the homogenously-dispersed mixed matrix membrane for cubical and spherical particles.

Effect of the filler size

The effect of the size of the filler particles on the effective permeability of ideal MMMs was investigated using a single cubical element and a homogenous dispersion of spherical particles within the polymeric matrix. Results for different sizes of a single spherical particle and of numerous dispersed smaller spherical particles are presented in Figure 6-7. Results clearly show that it is not the size of the spherical particles that matters but rather the total dispersed phase volume fraction. However, by increasing the size of the particles, the probability of particle-particle interaction (e.g. agglomeration) increases in the case of homogeneous or random dispersion which resulted in an important increase on the effective permeability of the membrane especially at higher dispersed to continuous phase permeability ratios (P_d/P_c). This observed increase is due to the creation of highly permeable (low resistance) pathways inside the membrane along the network of agglomerated particles. Results presented in Figure 6-7 are for

non-interacting particles. The effective permeability of a mixed matrix membrane with a homogenously dispersed particle is independent of the particle size and is identical to the permeability of its repeatable element. However, potential non-ideality such as interface void, rigidification and pore blockage may in practice affect the effective permeability of mixed matrix membranes. It would be possible to investigate the effect of non-idealities provided they can be quantified. Nevertheless, in this study the effect of non-ideality was not considered as it can be neglected in many cases [11,20,21].

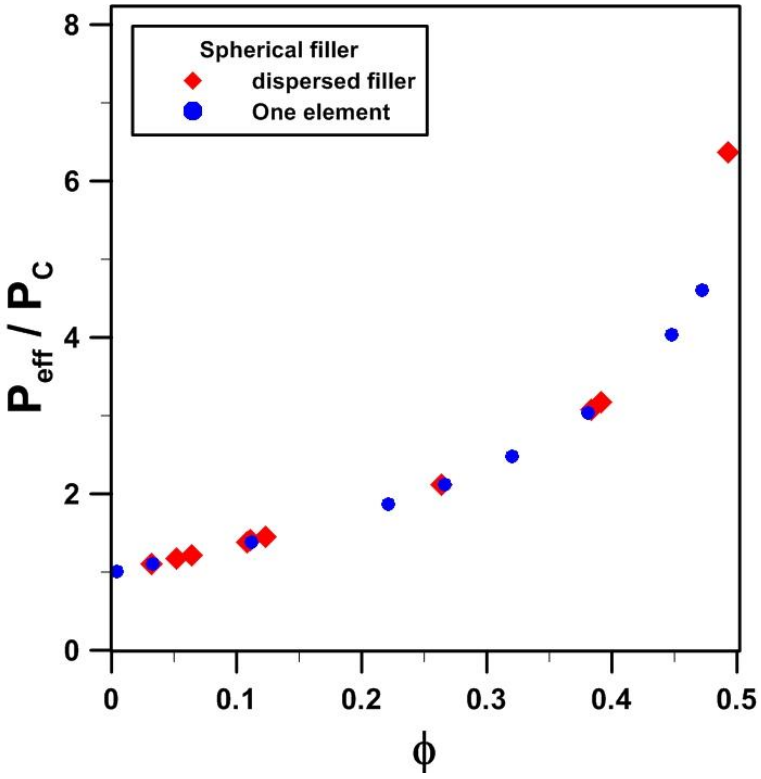

Figure 6-7 Effect of the filler size on the relative permeability of mixed matrix membranes

Effect of the filler shape

The shape of the filler particle is another parameter which could affect the permeation properties of MMMs. For each geometrical shape and orientation, there exists a maximum filler volume fraction. To investigate the influence of the particle shape on the effective permeability of an ideal mixed matrix membrane with homogenous dispersion of particles, different geometric shapes such as cubical, spherical and cylindrical filler particles were used. Moreover, two

different orientations of the cylindrical fillers (horizontal and vertical) were studied while it was assumed that the diffusion and solubility coefficients were identical in all directions. In the numerical solution by finite differences, the repeatable element consisted of a particle of the desired geometry that was centrally located in a cubical polymeric matrix surrounding the particle.

A series of simulations were performed for each particle shape over a wide range of filler volume fraction with a constant dispersed to continuous phase permeability ratio of 500 (case 1 in Table 6-1). The calculated effective permeability obtained numerically for the different geometrical shapes and filler volume fractions is presented in Figure 6-8. Simulation results show that the effect of particle shape and orientation is not significant until a volumetric filler content reaches approximately 0.4. Beyond this volumetric filler content, the difference in the effective permeability for various particle shapes becomes more important. It appears that the cubical and horizontal cylindrical particles have very similar effective permeability over a wide range of volumetric filler content. Spherical particles are limited to smaller maximum dispersed phase volume fraction and have slightly higher effective permeability values than the cubical and horizontal cylindrical particles. Moreover, the relative effective permeability for the vertical cylinder is significantly greater than the relative effective permeability of the horizontal cylindrer. A large-size vertical cylinder provides a large surface areas, the two edges of the cylinder, that are close to the surfaces of the membrane and a small diffusional pathway within the polymeric membrane exists before the permeant can access the highly permeable dispersed phase. As a result, a large permeation flux occurs through the vertical cylinder and the overall permeation flux over the area of the membrane is significantly greater. For this reason, some researchers have used carbon nanotubes as filler in mixed matrix membranes and have attempted to align vertically embedded carbon nanotubes.

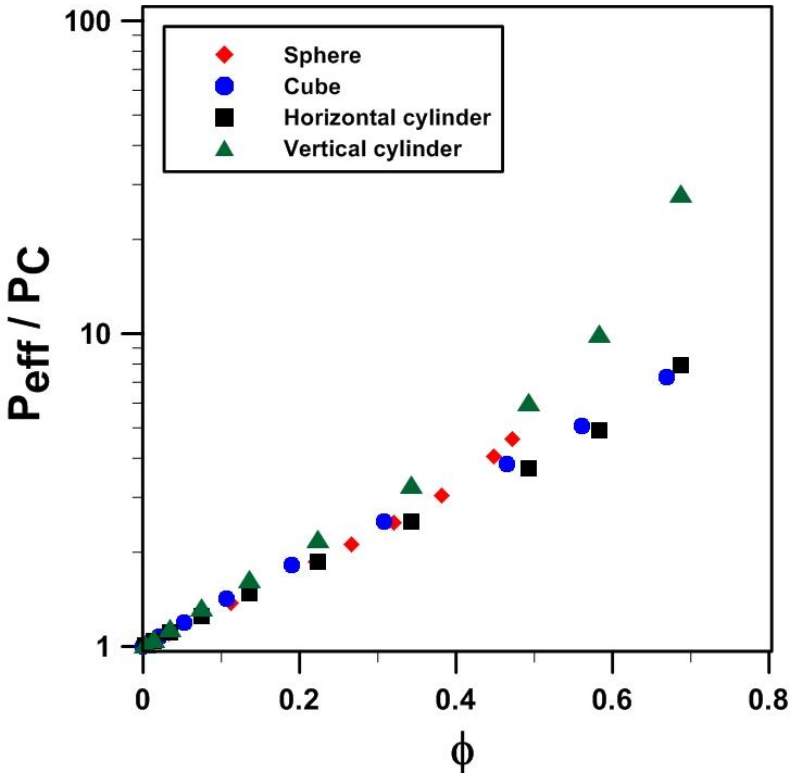

Figure 6-8 Effect of the particle shape on the relative effective permeability of mixed matrix membranes with a constant dispersed to continuous phase permeability ratio (Pd/Pc) of 500 (case 1 in Table 6-1).

Effect of the membrane thickness and mesh independency

A series of numerical simulations were performed to validate the hypothesis that the permeability of a repeatable unit element has an identical permeability of the entire membrane. Mixed matrix membranes of different thicknesses were simulated for a constant filler volume fraction of $\phi = 0.17$ and with a cubical filler particle located at the centre of a cubical repeatable unit element. In all simulation, a constant dispersed to continuous phase permeability ratio (P_d/P_c) of 500 (case 1 in Table 6-1). Results obtained confirmed that, as predicted by Eq. (6), the effective permeability remained constant regardless of the thickness of the membrane. A thicker membrane for an identical concentration driving force leads to an equal decrease in the permeation flux such that the product *JL* in Eq. (6) remains unchanged. An additional series of experiments were performed where a number of repeatable unit elements were stacked one on top of the other to form a thick membrane. As expected, the effective permeability of the stack of

repeatable unit elements had an identical effective permeability than a single repeatable unit element. These results imply that it is possible and desirable solving the Fick's second law of diffusion for a section of the mixed matrix membrane provided that it is representative of all the other sections of the membrane.

Most simulations by finite differences performed in this investigation were performed with 41 mesh points to discretize each the three dimensions of a repeatable cubical unit element. To confirm that this number of mesh points was sufficient to accurately calculate the effective permeability of mixed matrix membranes, the same problem was solved with three different numbers of mesh points. Figure 6-9 presents the variation of the relative effective permeability of the mixed matrix membrane as a function of the volumetric filler content for three different number of mesh points. It is obvious that the discretization scheme used in this investigation is sufficient and can predict accurately the effective membrane permeability.

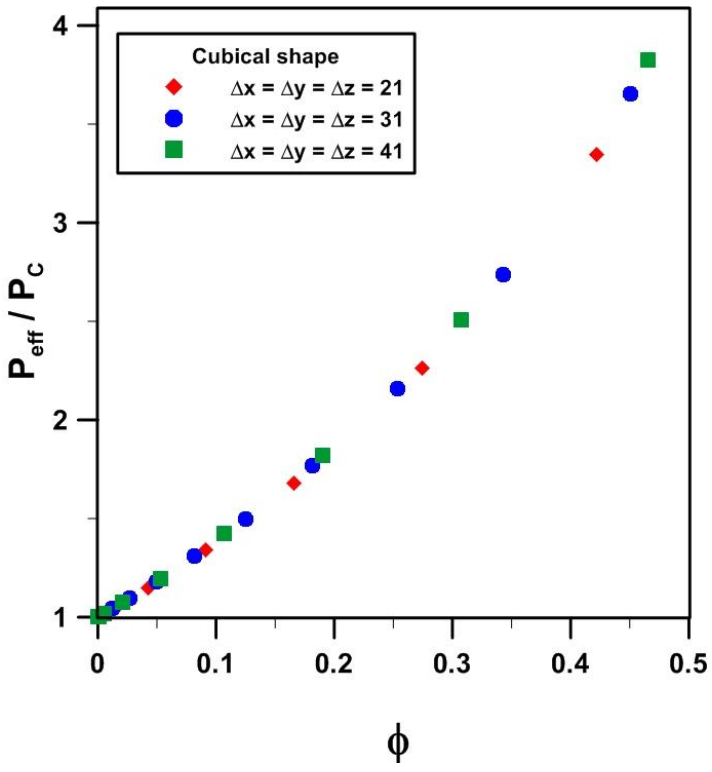

Figure 6-9 Effect of the discretization size or number of mesh points on the relative effective permeability of mixed matrix membranes.

Effect of the sorption isotherm

The solubility coefficient (or partition coefficient) is a representative parameter to relate the equilibrium concentration of a permeant at the surface of a polymer or a particle to its equivalent concentration in the bulk solution in contact with the membrane. So far, the proposed models for the prediction of effective permeability of MMMs has been developed based on the assumption of a linear sorption isotherm (Henry's law) of the permeant in both polymer and particle materials. This assumption is often valid for dense polymeric membranes as reported in various investigations [22]. However, the large majority of filler materials are adsorbent particles and they do not follow a Henry's law isotherm except for very low concentrations. Over a wider range of concentration, the adsorbent particles will follow a nonlinear isotherm where the equilibrium bulk concentration is no longer a linear function of the liquid bulk concentration or partial pressure in the case of a gas. As a result, for a nonlinear isotherm, the solubility coefficient of each mesh point in the solution domain will have a different value.

To investigate the effect of nonlinearity for species sorption in the filler material, Langmuir isotherm (Eq. (7)) was used in the numerical solution as the sorption mechanism of species in the filler material. Consequently, an apparent solubility coefficient $S_{i,j,k}$ associated to each mesh point corresponding to a particle was calculated using Eq. (8). The concentration profile was then calculated iteratively while the solubility coefficient of each node within a filler particle was also changing with the changing concentration until reaching the steady-state.

$$q = \frac{q_m b C}{1 + bC} \tag{7}$$

$$S = \frac{q}{C} = \frac{q_m b}{1 + bC} \tag{8}$$

In Eqs. (7) and (8), b is the microvoid affinity constant and represents the ratio of sorption and desorption rate constants of the penetrant through the free space and q_m is the Langmuir maximum sorption capacity of component in the dispersed filler. Parameter b is a constant related to the energy of adsorption and indicates the adsorption nature to be either unfavourable (low b values) or favourable (high b values).

With the presence of filler particles characterized with a nonlinear isotherm, the solubility coefficient becomes a function of the concentration. A series of simulations as a function of the feed solution concentration were performed to calculate the relative effective permeability of a mixed matrix membrane with a homogenously dispersed spherical particles for three different values of the Langmuir constant b for a fixed value of q_m of 10. Results for a filler volume fraction of 0.12 and a diffusion coefficient of 1×10^{-10} (m^2/s) for the dispersed phase, are presented in Figure 6-10. The relative effective permeability of the mixed matrix membrane decreases when the isotherm changes from a favorable to a less favorable Langmuir isotherm. Figure 6-10 also shows the decrease in the relative effective permeability with an increase in the permeant feed concentration. As the feed concentration increases, the adsorbed concentration becomes progressively saturated such that the average solubility as expressed by Eq. (8), will decrease and, as a result, a decrease in the permeability of the filler material is observed. A decrease in the permeability of the filler material leads to a decrease in the effective permeability of the membrane.

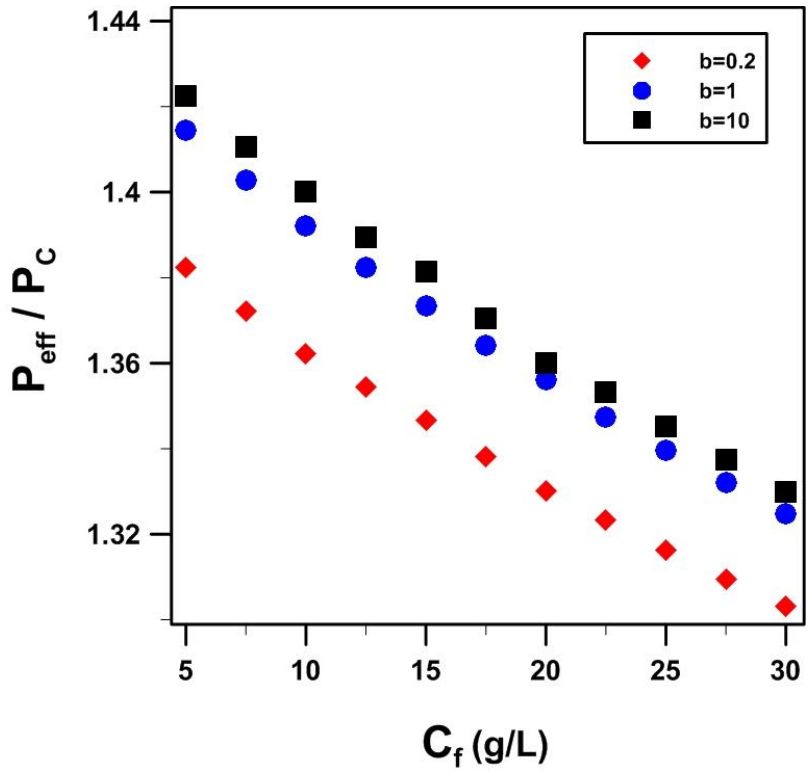

Figure 6-10 Effect of the sorption isotherm on the relative effective permeability of mixed matrix membranes as a function of the permeant feed concentration and for three different values of the Langmuir constant b with q_m=10.

The average solubility of MMMs was calculated numerically based on the actual isotherm of the filler particle. In another work, Hashemifard et al. introduced an analytical solution based on the Langmuir sorption isotherm, the Darken equation and the Fick's second law of diffusion to estimate the avarage solubilty coefficent of the penetrants in particles within the MMMs (Eq. (9)) [23].

$$S = \frac{q_m}{C} + \ln(1 + bC) \tag{9}$$

The model proposed by Hashemifard et al. represents an average solubility coefficent of species in the particles within the MMMs. The average solubility determined numerically for the entire membrane was compared with the prediction of Hashemifard et al. Results of this comparison is presented in Figure 6-11. The predictions of Hashemifard et al. model tend to overestimate the

average solubility across the membrane. The difference between the average solubility coefficent calculated with two methods increases with the value of Langmuir constant *b*.

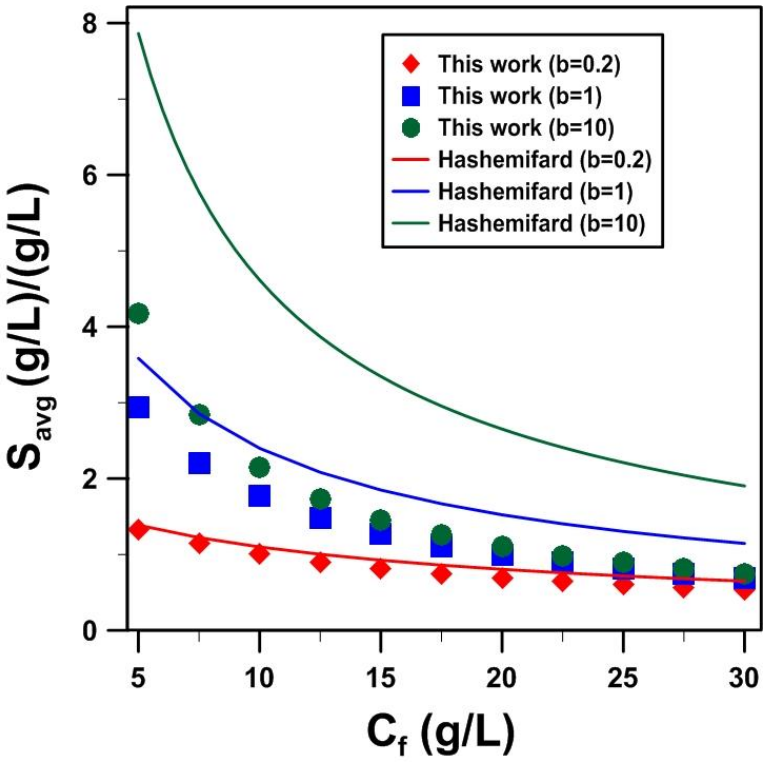

Figure 6-11 Comparison of the average solubility of the filler particle as a function of the permeant feed concentration for three values of the Langmuir constant b with qm = 10.

Figure 6-12 presents the effect of the average solubility on the relative effective permeability of MMMs for three different values of the Langmuir constant *b*. Results were obtained for a maximum sorption capacity (q_m=10), a filler volume fraction of 0.12 and for a spherical particle located at the centre of a cubical unit element. Results show that the highest relative effective permeability is obtained, as expected, for the highest average solubility which is obtained with very favorable isotherm (high values of *b*). Since the relative effective permeability falls on the same curve for all three values of *b*, it is really the effect of the average solubility that dictates the effective permeability for a constant diffusion coefficient.

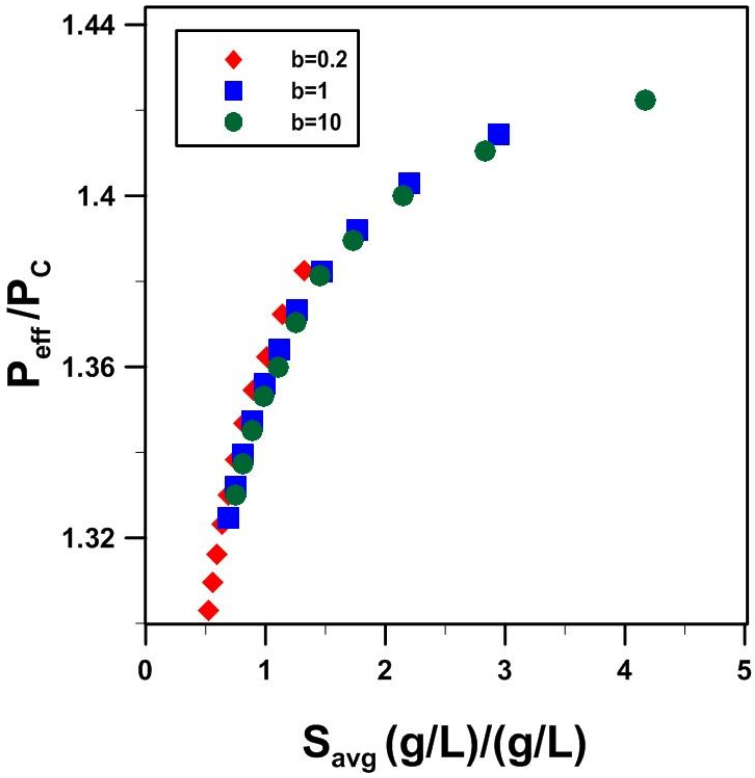

Figure 6-12 Effect of the average solubility and Langmuir constant b on the relative effective permeability of mixed matrix membranes for a filler particle having a Langmuir isotherm (q_m = 10).

Another parameter in the Langmuir isotherm is the maximimum adsorption capacity q_m. To investigate the influence of the particle sorption capacity on the effective permeability of the membrane, two different values of the maximum sorption capacity (q_m) for a Langmuir constant b=0.2 was considered under the identical particle volume fraction of the spherical filler (ϕ = 0.12). Results of Figure 6-13 indicate that the relative effective permeability of mixed matrix membranes increases with an increase in the maximum sorption capacity of the filler for a given penetrant. This increase was expected since the average solubility coefficient of the mixed matrix membrane is higher. Results clearly show that increasing the value of b results in an increase in the effective permeability of the membrane for less favorable isotherm. On the other hand, for very favorable isotherms (larger values of b), the effective permeability becomes independent of b and the difference in the effective permeability for the two drastically different values of maximum adsorption capacity q_m is very small. This difference would be higher for a higher

filler volume fraction. It therefore desirable to have a filler particle having an isotherm that is favorable with an acceptable adsorption capacity.

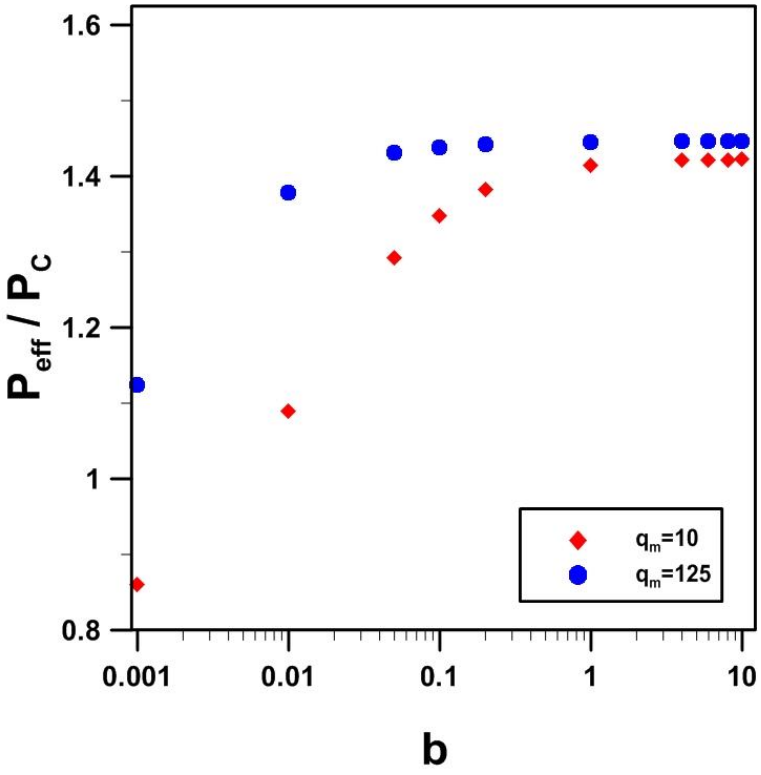

Figure 6-13 Relative effective permeability as a function of the Langmuir constant b and the maximum sorption capacity qm of mixed matrix membranes.

Conclusion

In this study, a 3D finite differences method was used to model the mass transport of a permeant through ideal mixed matrix membranes comprised of a dispersion of filler particles embedded in the matrix of a continuous phase. The numerical solution was used to investigate the influence of the filler properties (filler volume fraction, size, shape and orientation, sorption isotherm), the permeability ratio of the dispersed to the continuous phase, and membrane thickness. Results showed that the effective permeability of mixed matrix membranes is a strong function of the particle volume fraction and the ratio of the dispersed phase permeability to the continuous phase permeability. In addition, results revealed that the filler size has no effect on the relative permeability of a homogenous dispersion of particles in the matrix of the membrane. It was shown that the effective permeability of a repeatable cubical unit element could be used to

estimate the effective permeability of a mixed matrix membrane with homogenous dispersion of the filler material. The shape of the filler particles such as cubical, spherical and cylindrical particle had a negligible effect on the relative effective permeability of the membrane when the particle volume fraction in the matrix of the membrane was less than 0.4. Results also showed that the relative effective permeability of MMMs was higher for cylindrical particles with a vertical orientation compared to horizontal cylinders under identical conditions. Finally, numerical simulations revealed that the effective permeability of the mixed matrix membranes is favoured with filler particles having a favorable isotherm (high *b* values) whereas the maximum adsorption capacity q_m leads to a large increase in the effective permeability for small values of b but a relatively small increase for higher values of *b*.

Nomenclature

b	Microvoid affinity constant *(L/g)*
C	Concentration *(g/L)*
D	Diffusion coefficient *(m^2/s)*
J	Permeate flux *(g/m^2h)*
L	Thickness of the membrane or repeatable unit element *(m)*
N	Number of nodes in one Cartesian coordinate
P	Permeability *(m^2/h))*
q	Amount adsorbed (*g/L*)
q_m	Langmuir maximum sorption capacity *(g/L)*
R	Particle radius (*m*)
S	Solubility coefficient *((g/L)/(g/L))*
t	Time *(s)*

Δt	Time step *(s)*
ϕ	Volume fraction of the filler
τ	Dimensionless time

Subscripts

avg	Average
c	Continuous
d	Dispersed
eff	Effective
f	Feed solution in contact with membrane
x, y, z	Direction of Cartesian coordinates
i, j, k	Position of a discretization node

Superscripts

m	Type of component

Abbreviations

AC	Activated carbon
CNTs	Carbon nanotubes
FD	Finite differences
MMM	Mixed matrix membrane
MOFs	Metal organics frameworks

References

[1] A. Hasanoglu, Y. Salt, S. Keleser, S. Ozkan, S. Dincer, Pervaporation separation of organics from multicomponent aqueous mixtures, Chem. Eng. Process. 46 (2007) 300–306. doi:10.1016/j.cep.2006.06.010.

[2] E.J. Jeon, A.S. Kim, Y.T. Lee, Pervaporation of butanol/water mixtures using siloxane polymer/ceramic composite membranes, Desalination Water Treat. 48 (2012) 17–26. doi:10.1080/19443994.2012.698723.

[3] F.F. Liu, L. Liu, X.S. Feng, Separation of acetone-butanol-ethanol (ABE) from dilute aqueous solutions by pervaporation, Sep. Purif. Technol. 42 (2005) 273–282. doi:10.1016/j.seppur.2004.08.005.

[4] N. Qureshi, H.P. Blaschek, Butanol recovery from model solution/fermentation broth by pervaporation: evaluation of membrane performance, Biomass Bioenergy. 17 (1999) 175–184. doi:10.1016/S0961-9534(99)00030-6.

[5] H. Tan, Y. Wu, T. Li, Pervaporation of n-butanol aqueous solution through ZSM-5-PEBA composite membranes, J. Appl. Polym. Sci. 129 (2013) 105–112. doi:10.1002/app.38704.

[6] P. Shao, R.Y.M. Huang, Polymeric membrane pervaporation, J. Membr. Sci. 287 (2007) 162–179. doi:10.1016/j.memsci.2006.10.043.

[7] G.M. Monsalve-Bravo, S.K. Bhatia, Extending effective medium theory to finite size systems: Theory and simulation for permeation in mixed-matrix membranes, J. Membr. Sci. 531 (2017) 148–159. doi:10.1016/j.memsci.2017.02.029.

[8] M. Fang, C. Wu, Z. Yang, T. Wang, Y. Xia, J. Li, ZIF-8/PDMS mixed matrix membranes for propane/nitrogen mixture separation: Experimental result and permeation model validation, J. Membr. Sci. 474 (n.d.) 103–113. doi:10.1016/j.memsci.2014.09.040.

[9] T. Rodenas, I. Luz, G. Prieto, B. Seoane, H. Miro, A. Corma, F. Kapteijn, F.X. Llabrés i Xamena, J. Gascon, Metal–organic framework nanosheets in polymer composite materials for gas separation, Nat. Mater. 14 (2015) 48–55. doi:10.1038/nmat4113.

[10] P. Peng, B. Shi, Y. Lan, Preparation of PDMSSilica Nanocomposite Membranes with Silane Coupling for Recovering Ethanol by Pervaporation, Sep. Sci. Technol. 46 (2011) 420–427. doi:10.1080/01496395.2010.527896.

[11] H. Azimi, F.H. Tezel, J. Thibault, Effect of embedded activated carbon nanoparticles on the performance of polydimethylsiloxane (PDMS) membrane for pervaporation separation of butanol, J. Chem. Technol. Biotechnol. (2017). doi:10.1002/jctb.5306.

[12] C. Xue, G.-Q. Du, L.-J. Chen, J.-G. Ren, J.-X. Sun, F.-W. Bai, S.-T. Yang, A carbon nanotube filled polydimethylsiloxane hybrid membrane for enhanced butanol recovery, Sci. Rep. 4 (2014) 5925–5925. doi:10.1038/srep05925.

[13] X. Wang, J. Chen, M. Fang, T. Wang, L. Yu, J. Li, ZIF-7/PDMS mixed matrix membranes for pervaporation recovery of butanol from aqueous solution, Sep. Purif. Technol. 163 (2016) 39–47. doi:10.1016/j.seppur.2016.02.040.

[14] A. Jonquières, A. Fane, Filled and unfilled composite GFT PDMS membranes for the recovery of butanols from dilute aqueous solutions: influence of alcohol polarity, J. Membr. Sci. 125 (1997) 245–255. doi:10.1016/S0376-7388(96)00191-3.

[15] O. Bakhtiari, S. Mosleh, T. Khosravi, T. Mohammadi, Preparation, Characterization and Gas Permeation of Polyimide Mixed Matrix Membranes, J. Membr. Sci. Technol. 30 (2011) 589–597. doi:10.4172/2155-9589.1000101.

[16] T. Singh, D.-Y. Kang, S. Nair, Rigorous calculations of permeation in mixed-matrix membranes: Evaluation of interfacial equilibrium effects and permeability-based models, J. Membr. Sci. 448 (2013) 160–169. doi:10.1016/j.memsci.2013.08.010.

[17] A.-C. Yang, C.-H. Liu, D.-Y. Kang, Estimations of effective diffusivity of hollow fiber mixed matrix membranes, J. Membr. Sci. 495 (2015) 269–275. doi:10.1016/j.memsci.2015.08.030.

[18] A. Ebneyamini, H. Azimi, F.H. Tezel, J. Thibault, Mixed Matrix Membranes for Pervaporation and Gas separation Applications: Part I - Development of a Resistance-Based Model, J. Membr. Sci. Submitted (2017).

[19] H. Wu, N. Al-Qasas, B. Kruczek, J. Thibault, Simulation of Time-Lag Permeation Experiments Using Finite Differences, J. Fluid Flow Heat Mass Transf. (2015). doi:10.11159/jffhmt.2015.003.

[20] G. Liu, W.-S. Hung, J. Shen, Q. Li, Y.-H. Huang, W. Jin, K.-R. Lee, J.-Y. Lai, Mixed matrix membranes with molecular-interaction-driven tunable free volumes for efficient bio-fuel recovery, J. Mater. Chem. A. 3 (2015) 4510–4521. doi:10.1039/C4TA05881J.

[21] E. Okumus, T. Gurkan, L. Yilmaz, Development of a Mixed-Matrix Membrane for Pervaporation, Sep. Sci. Technol. 29 (1994) 2451–2473. doi:10.1080/01496399408002203.

[22] D.M. Aguilar-Valencia, M.Á. Gómez-García, J. Fontalvo, Effect of pH, CO2, and High Glucose Concentrations on Polydimethylsiloxane Pervaporation Membranes for Ethanol Removal, Ind. Eng. Chem. Res. 51 (2012) 9328–9334. doi:10.1021/ie3002765.

[23] S.A. Hashemifard, A.F. Ismail, T. Matsuura, Prediction of gas permeability in mixed matrix membranes using theoretical models, J. Membr. Sci. 347 (2010) 53–61. doi:10.1016/j.memsci.2009.10.005.

7. Chapter 7

Optimisation of the in-situ recovery of butanol from ABE fermentation broth via pervaporation

Hoda Azimi, Handan Tezel and Jules Thibault*

Abstract

Butanol produced via the ABE fermentation is plagued with low final concentrations and low yield. The selective removal of butanol from the fermentation broth by integrating a separation process to the fermenter for the in situ recovery of butanol has been proposed by many researchers. In this investigation, the integration of a membrane pervaporation separation process with the continuous ABE fermentation system has been simulated and optimized using a genetic algorithm. The ABE fermentation model proposed by Mulchandani and Volesky was used and a multi-objective optimisation problem was defined to simultaneously maximize the butanol productivity, the overall butanol concentration and the sugar conversion. The three objective functions, if non-dominated, define the Pareto domain of the optimisation problem along with the four decision variables, namely the dilution rate, the feed sugar concentration, the cell retention factor and the membrane surface area. The optimal solutions of the integrated process for two different pervaporation membrane models were compared to the stand-alone continuous fermentation. By adding an in situ separation system to the continuous ABE fermentation, the optimal butanol productivity and overall butanol concentration increased by approximately 300% compared to those of the non-integrated fermenter. Furthermore, the sugar conversion increased.

Keywords: ABE fermentation; butanol; optimisation; Pervaporation; plate-and-frame membrane module

Introduction

The biological production of butanol from renewable resources via the acetone-butanol-ethanol (ABE) fermentation process has attracted significant interest in the last decades because this alcohol is considered to have numerous advantages favouring its use as a biofuel [1–6]. Butanol is seen as an ideal candidate for the partial replacement of gasoline because it can be used in cars without engine modifications and can use existing distribution infrastructure. However, to make

the biological production of butanol an economically-viable biofuel, some important challenges need to be resolved: low final butanol concentration, low yield, and low productivity. One way to overcome these challenges is to find a more efficient bioconversion of cellulose and hemicellulose to butanol. On the biological side, some researchers are examining potential genetic modifications of microorganisms, especially *Clostridia* species, to increase the yield of butanol, increase their tolerance to fermentation products and, most importantly butanol, to reduce or eliminate the formation of the other co-products such as acetone and ethanol. On the process engineering aspects, many researchers have suggested to partly remove butanol from the fermenter during the fermentation process to reduce its toxic effect, which will allow a greater utilization of fermentable sugars and will increase the final butanol concentration and productivity [7]. Some of the separation methods that could be integrated to the fermenter for the in situ recovery of butanol are: vacuum fermentation [8,9], adsorption [10], gas-stripping [11], liquid-liquid extraction (LLE) [12], perstraction [13], reverse osmosis (RO) [14] and pervaporation (PV) [15]. Among these separation processes, pervaporation, a membrane based process, has been suggested as a very enviable process for the in-situ removal of butanol from ABE fermentation broths [16] due to its numerous advantages. However, to introduce pervaporation as a successful separation process at an industrial scale, it is paramount to develop membranes with high selectivity and permeability for butanol in addition to have excellent physical robustness. At the same time, it is important to operate the overall process at the optimal operating conditions.

A wide variety of polymers have been studied with the objective to improve the butanol pervaporation separation from ABE fermentation: styrene butadiene rubber (SBR) [17], ethylene propylene diene rubber (EPDM) [18], polytetrafluoroethylene (PTFE) [19], polypropylene (PP) [20], polyurethane (polyether based) (PUR) [21], polyether block-amide (PEBA) [22], poly (vinylidinedifluoride) (PVDF) [23], poly (methoxy siloxane) (PMS) [24], poly (dimethylsiloxane) (PDMS) [25,26], poly (1-(trimethylsilyl)-1-propyne) (PTMSP) [27] and polyamide-imide (PAI) containing cyclodextrin (CD) [28]. Among all these membranes, PDMS membranes stand out for their higher performance for butanol pervaporation separation, for their higher permeation flux and selectivity [29–32].

While numerous studies have attempted to improve the performances of membranes and to determine the effects of the main operating conditions on the pervaporation separation of butanol [15,30,32–34], investigations aiming at optimizing the butanol fermentation process at an industrial scale with and without the integration of an in situ butanol recovery process are very scarce. The main focus of the present investigation is to perform the multi-objective optimisation of the continuous ABE fermentation integrated with a membrane pervaporation separation process and to compare the performance enhancement with the optimal stand-alone continuous fermentation. For the integrated pervaporation process, literature data for the polydimethylsiloxane (PDMS) membranes were used to establish the pervaporation process simulator [15,35,36]. The kinetic ABE fermentation model for ABE fermentation using *Clostridium acetobutylicum* used in this investigation was the one proposed by Mulchandani and Volesky [37].

This paper is divided as follows. The main equations that were used for the simulation of the overall integrated process are first presented with an emphasis on the pervaporation models. Two scenarios are presented: 1) a simple membrane pervaporation scenario and 2) a more comprehensive membrane pervaporation scenario. The definition of the optimisation problem for the fermentation system with and without the integration of an in situ butanol recovery unit is presented next. Results of the optimisation studies for the fermentation without a pervaporation membrane separation unit and of the fermentation integrated with a pervaporation membrane separation unit, using two different approaches, are compared and discussed. Then, a general discussion on the fermentation model is presented before providing the main conclusions.

Development of the simulation model

The hybrid fermentation-pervaporation process that was simulated and optimized in this investigation is presented schematically on Figure 7-1. This process is comprised of a continuous fermenter, a microfiltration unit and a membrane pervaporation system. Given a set of input operating conditions for the overall process, the system of equations describing the different parts of the process is solved as a function of time until steady state conditions are achieved. The main input conditions to the process, referred here as decisions variables in the optimisation problem, are the fermenter dilution rate, the sugar concentration of the input stream, the cell

retention factor and the membrane area of the pervaporation unit. A set of stream and component mass balances were performed based on the block flow diagram of Figure 7-1. The species considered in this investigation were acetone, acetic acid, butanol, butyric acid, ethanol, microorganism and glucose and water. The complete set of mass balances is presented in Appendix I of this paper.

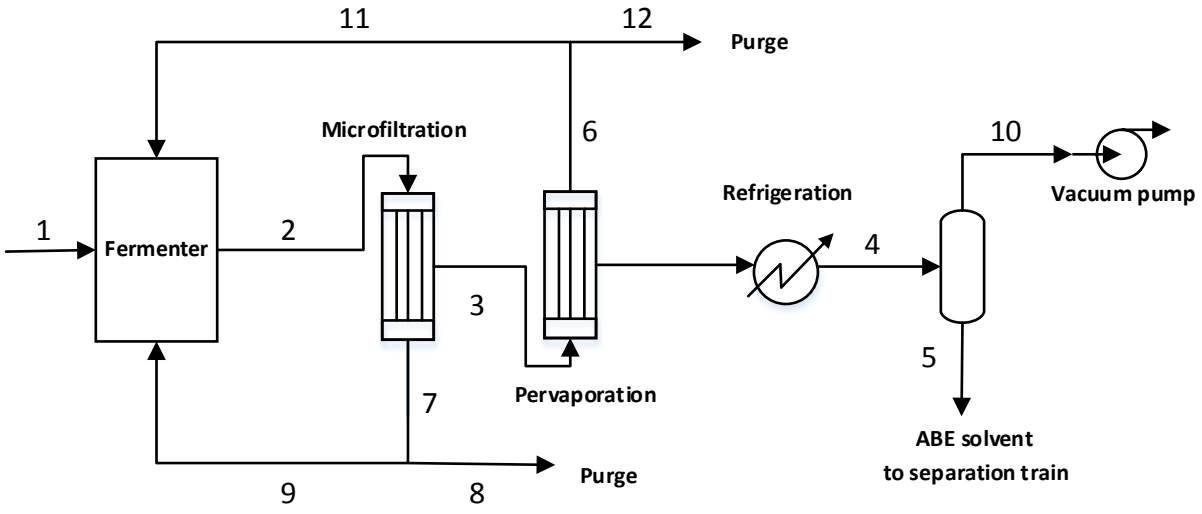

Figure 7-1 A simplified schematic diagram of a fermentation system integrated with microfiltration unit and membrane pervaporation separation process.

In this process, the feed continuously enters the fermenter at a constant flow rate and with a constant sugar concentration. The volume of the fermenter was set constant at 400 m^3. A set of initial concentrations were given for all species inside the fermenter but, most importantly, an initial concentration of the microorganism. The kinetic microbial reactions taking place inside the fermenter were the ones proposed by Mulchandani and Volesky [33]. Their model, widely used in the literature, considered the carbon substrate limitation as well as butanol and butyric acid inhibition while assuming that acetone was not toxic to the microorganisms. This model calculates the solvent production (acetone, butanol, and ethanol), the production of butyric acid and acetic acid, the formation of biomass, and the consumption of sugars while keeping the bacterial microorganism as *Clostridium acetobutylicum* in the fermenter. To achieve steady state, it is necessary to resolve the overall mass balance by removing the same quantity of material through Streams 5, 8, 10 and 12 as the one entering into the process in Stream 1.

In a continuous operation, Stream 2 is removed from the fermenter at 15 times of the input flow rate to the fermenter (Stream 1) and is sent to the microfiltration membrane unit where half of the cell-free flow rate passes through the membrane to form Stream 3. It would also be possible to calculate, using a membrane microfiltration membrane model, the permeate flux of the microfiltration separation process given process operating parameters or to calculate the design and operating parameters for a given permeate flow rate [38–40]. The retentate stream (Stream 7) has the same cell-free concentration of all components as Streams 2 and 3 but contains all the microorganism cells of Stream 2. A large portion of Stream 7 is returned to the fermenter through Stream 9 and the remaining portion is purged and sent to the separation train (Stream 8). The objective of the microfiltration is to maintain an optimal microorganism concentration inside the fermenter and to have a cell-free stream sent to the pervaporation separation unit (Stream 3). The purge stream has the advantage of keeping an optimal amount of biomass cells in the fermenter to prevent the washout phenomenon, while removing enough cells to maintain the steady state conditions within the fermenter. Moreover, the purge stream contributes to maintain metabolites, not removed through the product recovery system, at a level below an inhibitory level [41]. Stream 3 is then sent to the membrane pervaporation unit. Depending on the area of the membrane, the stream temperature, the concentration of each component and the membrane permeability for each component, a portion of the Stream 3 permeates through the pervaporation membrane to form Stream 4 at the permeate side of the membrane, where it was kept under a very low pressure (assumed near zero). Stream 4 is condensed to mainly give Stream 5, which normally contains much higher concentration of ABE solvents than Stream 3. A very small quantity of Stream 4 may escape through the vacuum pump (Stream 10) depending on the temperature of the cold trap and the residence time within the cold trap. In this investigation, it was assumed that 1% of Stream 4 ended up in Stream 10. Stream 5 is then sent to the separation train. The majority of the retentate of the membrane pervaporation unit (Stream 6) is returned to the fermenter. The other fraction, Stream 12, is purged and served to maintain, along with Stream 5, a constant mass balance of the overall process.

Pervaporation stage

Plate-and-frame membrane modules have been chosen for the visualized pervaporation separation system since the permeation data of flat sheets of polydimethylsiloxane (PDMS)

membranes has been used to optimize the integrated fermentation process. Plate-and-frame membrane modules are a common type of modules which have been used in industry for their ability to scale up. In the pervaporation separation method, the membrane performance is defined by key membrane parameters such as the separation factor for each component and the permeation flux or the permeability of each component through the membrane [42–44]. As a result, obtaining the values of these parameters experimentally for the separation via pervaporation of the ABE components using a flat PDMS membrane is essential for the proper design of the pervaporation separation unit.

Two different case studies for the pervaporation membrane system were considered for the ABE fermentation coupled with a pervaporation separation unit. The first case study uses a simple permeation model where literature values of experimental separation factors for acetone, butanol, ethanol, and water as well as the average total permeation flux of each component were used in the pervaporation process simulations [36]. From this data, it was not possible to calculate the permeability of each component because the thickness of the membrane was not reported. The flux and separation factors are given in Table 7-1 and they were assumed to be constant. For this scenario, the separation of butyric acid and acetic acid were considered to be negligible. In addition, fouling effects were not considered. With these parameters and the area of the PDMS pervaporation membrane, it was possible to calculate the composition of each component in the permeate stream (Stream 4) given the composition of Stream 3.

Table 7-1 Pervaporation PDMS membrane performance parameters used for the first case study.

Total Flux ($kg/m^2.h$)	**Separation factor**				**Ref**
	Acetone	**Butanol**	**Ethanol**	**Water**	
0.993	27.78	16.56	7.15	0.044	[36]

The first case study strictly used the limited information from the literature from Wu et al. [36] such that the effect of the initial temperature, the change in temperature and the composition along the length of the membrane was not taken into account.

In the second case study, the mass and heat transfer are considered in the pervaporation separation process and optimized along with all the other operating conditions of the integrated

fermentation process. Appendix II of this paper provides the set of equations and permeability values that were used to simulate the more comprehensive pervaporation unit. In this more realistic scenario, the overall process remains the same except that the membrane pervaporation module is modified as indicated in Figure 7-2. The permeate output stream of the microfiltration membrane module is heated to the desired temperature prior to entering the first series of pervaporation modules in order to enhance the permeability of each component. As the stream flows through the membrane module, components migrate to the permeate side depending on the overall mass transfer and their respective permeability. Since the components vaporize due to the very low pressure on the permeate side, the heat of vaporization needs to be provided by the retentate stream such that its temperature decreases progressively as it flows through the pervaporation module. At one point, the stream needs to be reheated to increase the pervaporation rate and then sent to another pervaporation module for additional solvent removal. In Figure 7-2, three such modules in series with inter-module heaters and heat integration are shown. The optimisation of this process requires deciding on the number of parallel pervaporation modules, here referred as stacked pervaporation modules, and the number of stacked modules in series with their associated heat exchangers.

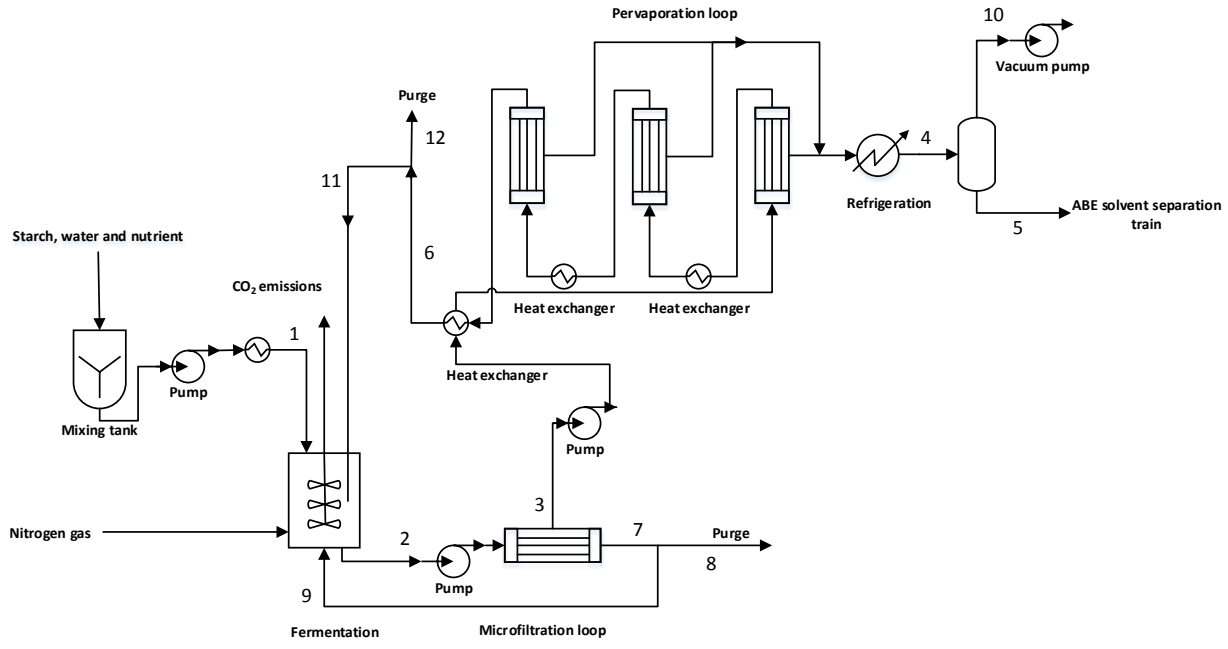

Figure 7-2 Schematic of a continuous fermenter coupled with a series of stacked pervaporation membrane modules used for the in situ recovery of ABE solvents.

Multi-objective Optimization

The optimisation of a continuous fermentation process coupled with a membrane pervaporation separation unit was performed for the two case studies described in the previous section. The optimisation results of these two case studies will be compared to the optimal results obtained for of a continuous fermenter without the integrated pervaporation separation unit.

To optimize a process, the optimisation problem first needs to be formulated. In particular, it is necessary to define the objective functions to be optimized. In this investigation, it was desired to maximize three objective functions simultaneously: (1) the butanol productivity, (2) the average butanol output concentration, and (3) the sugar conversion. These three variables, as defined in Table 7-2, are the outputs of the optimisation problem. It is now required to select process variables that can be modified to lead to the best compromise between the three objective functions. These variables are called decision variables and, in this investigation, the following process variables were chosen: (1) the feed dilution rate or the input flow rate (Stream 1), (2) the sugar concentration of the input stream, (3) the cell retention factor to control the microorganism inside the fermenter, and (4) the total membrane area. These three objective functions and four decision variables were used for the optimisation for Scenario 1. Table 7-2 lists the three objective functions with their calculations and the four decision variables with their feasible selection range. For the fermentation without the incorporation of a membrane pervaporation unit, the same three objective functions were used along with the first three decision variables, which are identical to Scenario 1 except that the pervaporation membrane area was set to zero. For Scenario 2 of the integrated system, the same objective functions were used while the fourth decision variable, i.e. the membrane area, was replaced by two decision variables: (1) the number of membrane units stacked in parallel and (2) the number of stacked modules in series. With the information of these last two decision variables, it was possible to calculate the total membrane area. At the exit of each stacked module, except for the final module, the exit stream temperature was raised to the desired module inlet temperature prior to entering the next stacked module, using an inter-module heat exchanger.

To solve the optimisation problem, a genetic algorithm was used. In this investigation, the Dual Population Evolutionary Algorithm (DPEA) was used [45]. For the first generation, a set of

random values of the decision variables are selected within their feasible ranges and used to perform the simulation of the whole system until steady state is achieved. Upon achieving steady state, the three objective functions are calculated. This procedure is performed as many times as required to obtain the desired number of individuals in the population. In this study, a population of 3000 individuals was used. When the first generation of the population is complete, the objective functions of each individual in the population are compared to the objectives of all the other individuals to determine the number of times a solution is dominated. A point or solution is said to be dominated if another solution within the population is better for all three objective functions. All non-dominated points and a fraction of the least dominated points are kept as parents for the next generation. For all subsequent generations, two parents from the previous generations are used to give rise to a new individual using crossover and mutation operators. This procedure is performed to reach once more the total population size, and this procedure is repeated for many generations until the desired number of points in the population represents non-dominated points. With this procedure, a good approximation of the Pareto domain is obtained, which only contains non-dominated points.

The Pareto domain was obtained without any bias or preferences from the decision maker. The next step is to rank all points in the Pareto domain based on the preferences of an expert or decision maker. In this investigation, the Net Flow method was used [46]. This method uses four parameters to rank the whole Pareto domain, namely the relative weights of the three objective functions and three threshold values for each objective function: the indifference threshold, the preference threshold and the veto threshold.

Table 7-2 Definition of objective functions and decision variables with their lower and upper bounds

	Parameter	Definition
Objective functions	Butanol productivity, ($kg/m^3.h$)	$\frac{1}{V} MW_B \left(C_{B5}F_5 + C_{B8}F_8 + C_{B12}F_{12}\right)$
	Butanol concentration, (kg/m^3)	$MW_B \left(C_{B5}F_5 + C_{B8}F_8 + C_{B12}F_{12}\right)/F_1$
	Sugar conversion	$1-\left(\left(C_{S5}F_5 + C_{S8}F_8 + C_{S12}F_{12}\right)/F_1\right)$
Decision variables	Dilution rate (h^{-1})	$\frac{F_1}{V}$ $0.01 \le \mathrm{D}_F \le 2.0$
	Sugar feed concentration (kg/m^3)	S_0 $5 \le S_0 \le 150$
	Biomass retention factor, $\alpha_{8\text{-}12}$ ($m^3.h/m^3.h$)	$\frac{F_8}{F_8 + F_{12}}$ $0.1 \le \alpha_{8-12} \le 1$
	Membrane area (m^2)	A $10 \le A \le 80000$

Result and discussion

The Pareto domain for the fermentation with and without the pervaporation separation process containing 3000 Pareto-optimal solutions was ranked with the Net Flow method. The Net Flow method relative weights and the three thresholds values for each objective function are given in Table 7-3. Figure 7-3 presents the plots of the objective functions and the decision variables for the fermentation system without the integration of a pervaporation separation module. The Pareto domain is plotted for four different regions: (1) the best solution (light green point); (2) the first best 5% (red points); (3) the next best 45% (blue points), and (4) the remaining 50% (black points).

Table 7-3 Net Flow Method parameters used to rank Pareto-optimal solutions.

Criteria	Relative weight	Thresholds		
		Indifference	Preference	Veto
Productivity	0.4	1.0	2.0	4.0
Concentration	0.3	1.0	2.0	4.0
Sugar conversion	0.3	0.02	0.04	0.08

Figure 7-3a presents the plot of the sugar conversion versus the butanol productivity whereas Figure 7-3b shows the plot of the average output butanol concentration versus the butanol productivity. The best ranked solution is located at a butanol productivity of 4.63 ($kg.\ m^{-3}.h^{-1}$), an average butanol concentration of 9.67 ($kg.m^{-3}$) and a sugar conversion of 83%. Figure 7-3b

clearly shows the compromise that exists between the average butanol concentration and the butanol productivity as an increase of one objective leads to the decrease of the other. A similar compromise exists between sugar conversion and butanol productivity as shown in Figure 7-3a where to increase the butanol productivity, it is necessary to accept a decrease in the conversion of sugar. As the three objective functions need to be maximized, a trade-off between them needs to prevail and this is how the optimal solution was obtained via the Net Flow ranking algorithm. Two of the associated decision variables, the dilution rate and the feed sugar concentration, are plotted in Figure 7-3c. The best ranked solution shows that the optimal trade-off was obtained for a feed sugar concentration of 61 ($kg.m^{-3}$) and a dilution rate of 0.48 (h^{-1}). The third decision variable, the cell retention factor, was constant at its lower limit of 0.1. This optimisation algorithm attempts to keep the cell retention factor as low as possible to have a higher steady-state amount of microorganisms inside the fermenter to produce more butanol. The lower limit was imposed to make sure the microorganism renewal occurs and some other metabolites that could be toxic to the microorganism are purged. The latter could also be achieved through the purge of Stream 12.

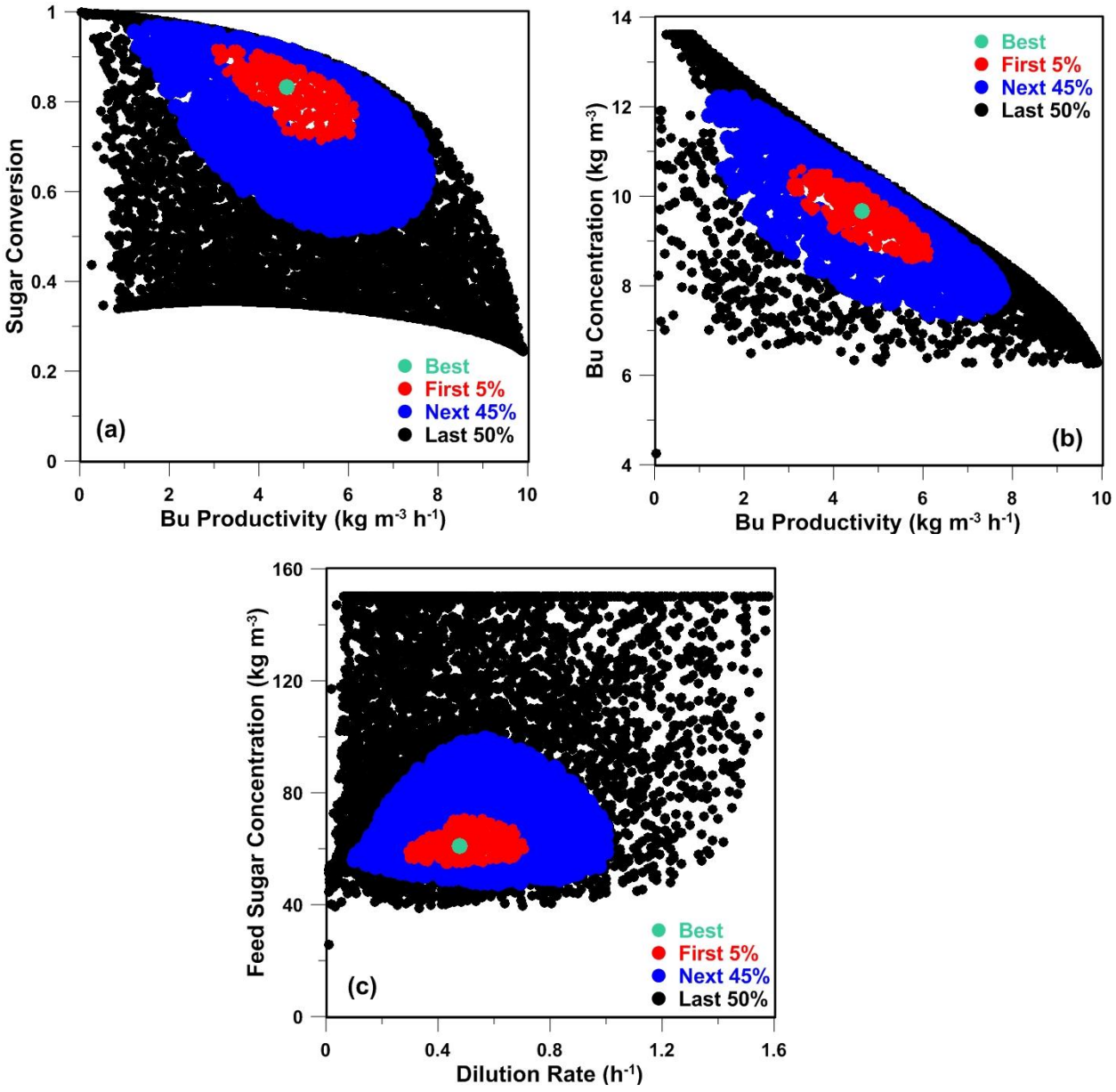

Figure 7-3 Plot of the objectives and decision variables for continuous fermentation without the in-situ membrane pervaporation recovery unit: (a) Sugar conversion versus butanol productivity, (b) Average butanol concentration versus butanol productivity, and (c) Feed sugar concentration versus dilution rate.

Results of the optimisation for the continuous fermentation integrated with a pervaporation membrane module (Scenario 1) are presented in Figure 7-4. The plot of the sugar conversion versus the butanol productivity is shown in Figure 7-4a, whereas Figure 7-4b shows the plot of

the average output butanol concentration versus the butanol productivity. When compared to the fermentation without a pervaporation membrane module, the sugar conversion increased from 83% to 96%, the butanol productivity increased from 4.63 to 13.39 ($kg\ m^{-3}h^{-1}$) and the average output butanol concentration increased from 9.67 to 29.83 ($kg\ m^{-3}$). It is clear that the addition of a pervaporation membrane module increased the performance of the butanol production process drastically. This enhanced performance was obviously obtained at the expense of a large total membrane area (39520 m^2) as can be observed in Figure 7-4d, where the membrane area is plotted as a function of the dilution rate. Again, the trade-off occurring in the three objective functions is clearly shown in Figure 7-4a and 7-4b. For example, the highest butanol productivity is achieved when the average butanol concentration and the sugar concentration are at their lowest values. On the other hand, to obtain the highest average butanol concentration and sugar conversion, the butanol productivity would be at its lowest value.

Three of the decision variables for the integrated fermentation process (Scenario 1) are plotted in Figure 7-4c and 7-4d. The dilution rate decreased slightly from 0.48 to 0.45 (h^{-1}) as compared to the fermentation without integrating a pervaporation membrane separation unit. The cell retention factor was equal to its lower limiting value of 0.10 as it was the case for the fermentation process without the pervaporation membrane module.

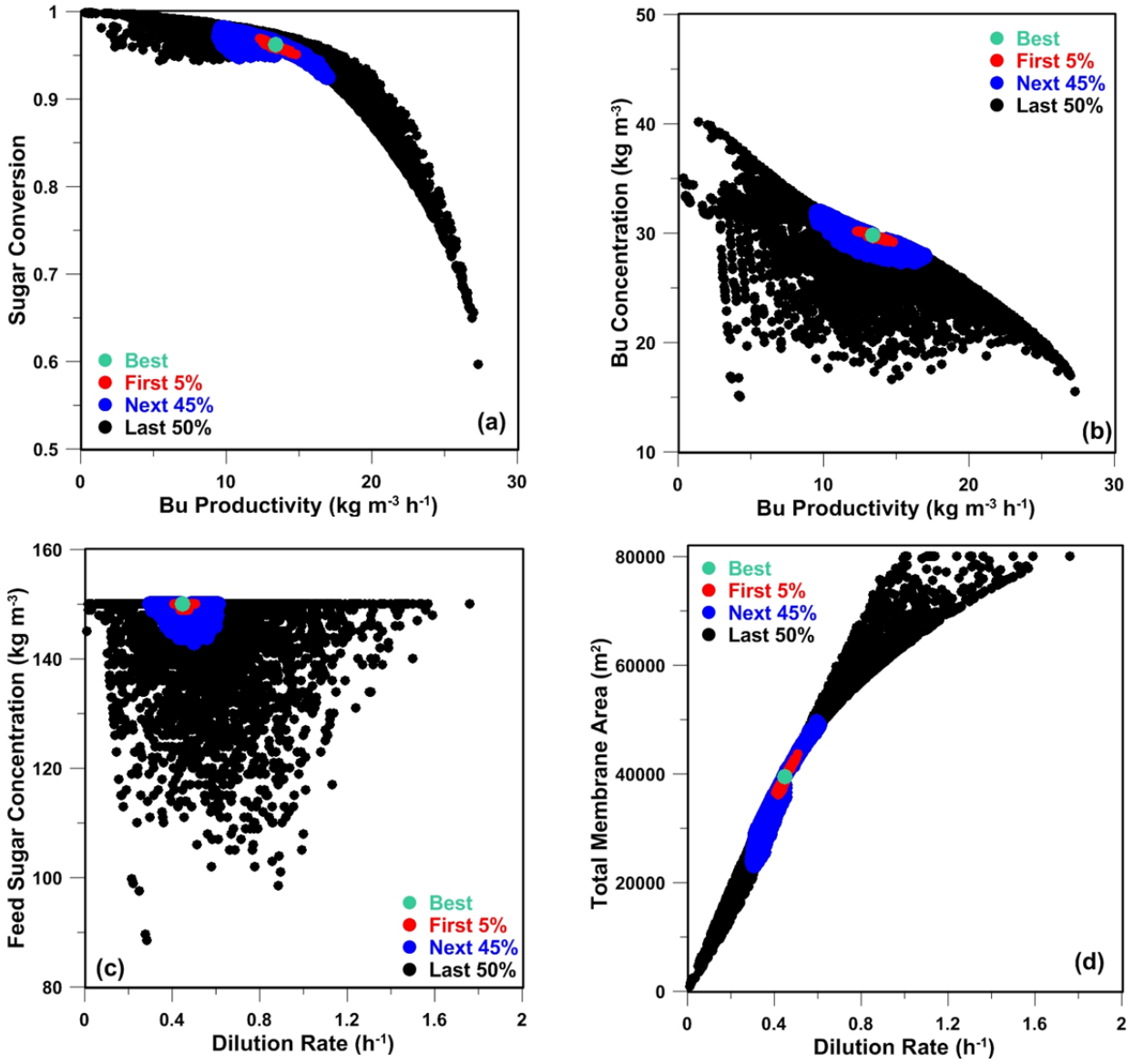

Figure 7-4 Plots of the objective and decision variables for the continuous fermentation with the in-situ recovery using membrane pervaporation for Scenario 1: (a) Sugar conversion versus butanol productivity, (b) Average butanol concentration versus butanol productivity, (c) Feed sugar concentration versus dilution rate. (d) Total membrane area versus dilution rate.

In Scenario 1, the permeation of ABE solvents and water through the membrane was calculated using a constant total permeation flux per unit membrane surface area and a constant selectivity for each component. In reality, the permeation flux is a function of the permeation of each component, which is in turn function of their individual permeability and temperature. The

stream temperature on the retentate side of the membrane will progressively decrease since it must supply the latent heat of vaporisation for the permeated species. A decrease in the stream temperature leads to a decrease in the permeation flux of each species. In the optimisation procedure for Scenario 2, it was assumed that a membrane unit consists of the superposition of 40 flat plate PDMS membranes of 0.5 m by 0.5 m surface area for a total of 10 m^2 per membrane unit. The fourth and fifth decision variables were defined as the number of the total membrane pervaporation units in parallel and in series, respectively. A schematic diagram of the pervaporation system used in Scenario 2 is illustrated in Figure 7-5.

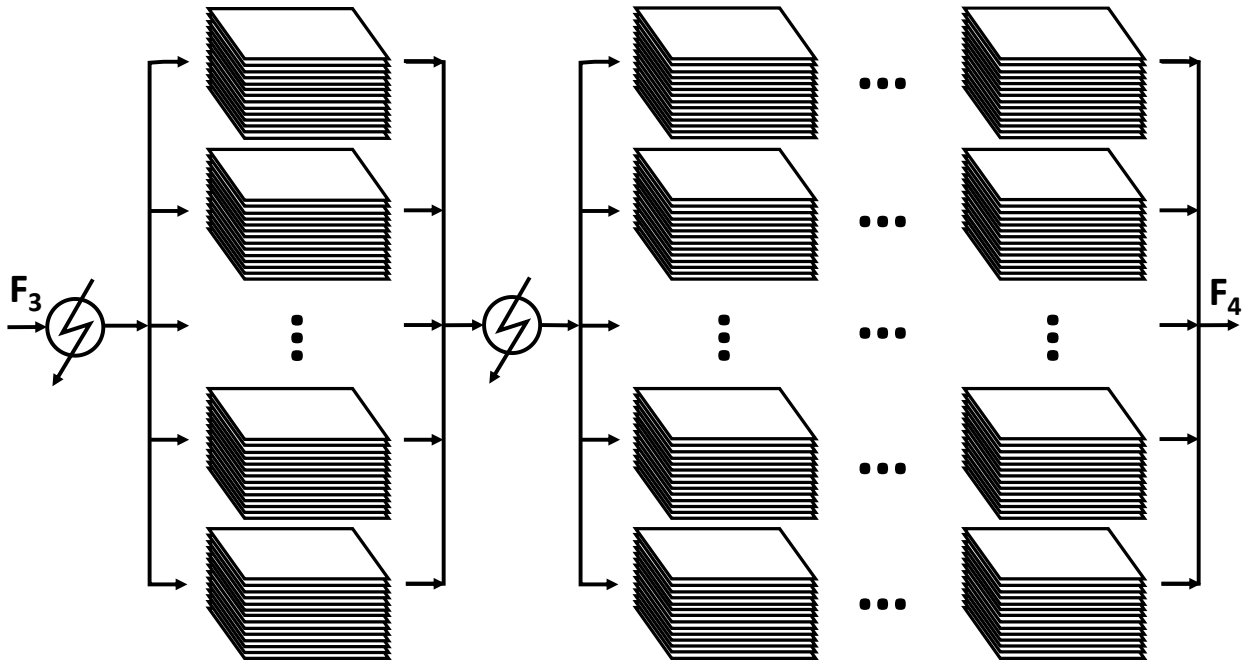

Figure 7-5 Schematic diagram of the membrane pervaporation separation system. Each unit consists of 40 flat membranes (0.5 m x 0.5 m). A number of units in parallel and in series, as decision variables, are shown with an inter-module heat exchanger between units in series. Only the stream on the retentate side is shown.

Results of the optimisation of Scenario 2 for the continuous fermentation integrated with multiple pervaporation membrane units in parallel and in series are shown in in Figure 7-6. Figure 7-6a shows the plot of the sugar conversion as a function of the butanol productivity where the best ranked solution has a productivity of 12.7 ($kg.\ m^{-3}h^{-1}$) associated with a sugar conversion of 93%. This butanol productivity is 4.85% less than the value achieved in Scenario

1. In addition, the sugar conversion decreased from 96% to 93% in comparison with the simple pervaporation model. Figure 7-6b presents the plot of the average output butanol concentration as a function of the butanol productivity. Compared to Scenario 1, the average output butanol concentration of Scenario 2 is essentially the same with a small decrease from 29.8 to 28.6 ($kg\ m^{-3}$). As for the other cases, an increase in the butanol productivity is associated with a decrease in the average butanol concentration and the sugar conversion.

Figure 7-6c and 7-6d present the plots of the feed sugar concentration and the total membrane area as a function of the dilution rate. The total membrane area for the best ranked solutions 8200 m^2 which is significantly less than the area obtained in Scenario 1 with a value of nearly 40000 m^2. The significant decrease in the membrane area is due to the higher permeability of the species at higher temperature and, as a result, a much higher permeation flow rate was achieved. To obtain this total area for the best ranked solution, a total of 10 modules in series composed of 82 stacked parallel units were required along with their associated heat exchangers. In the end, the three objective functions are essentially the same for both membrane pervaporation scenarios. Scenario 2 is more realistic as it takes the effect of the stream hydrodynamics, individual permeability and temperature into consideration.

The dilution rates for both scenarios were essentially the same. The minimum cell retention factor was increased to 0.2 for Scenario 2 compared to 0.1 for Scenario 1. The higher minimum value was necessary to maintain the cell concentration to a reasonable value. Since the permeation flowrate (F_4) was significantly higher than for Scenario 1, flowrates of Streams 8 and 12 were lower and a higher cell retention factor was required to limit the cell concentration inside the fermenter.

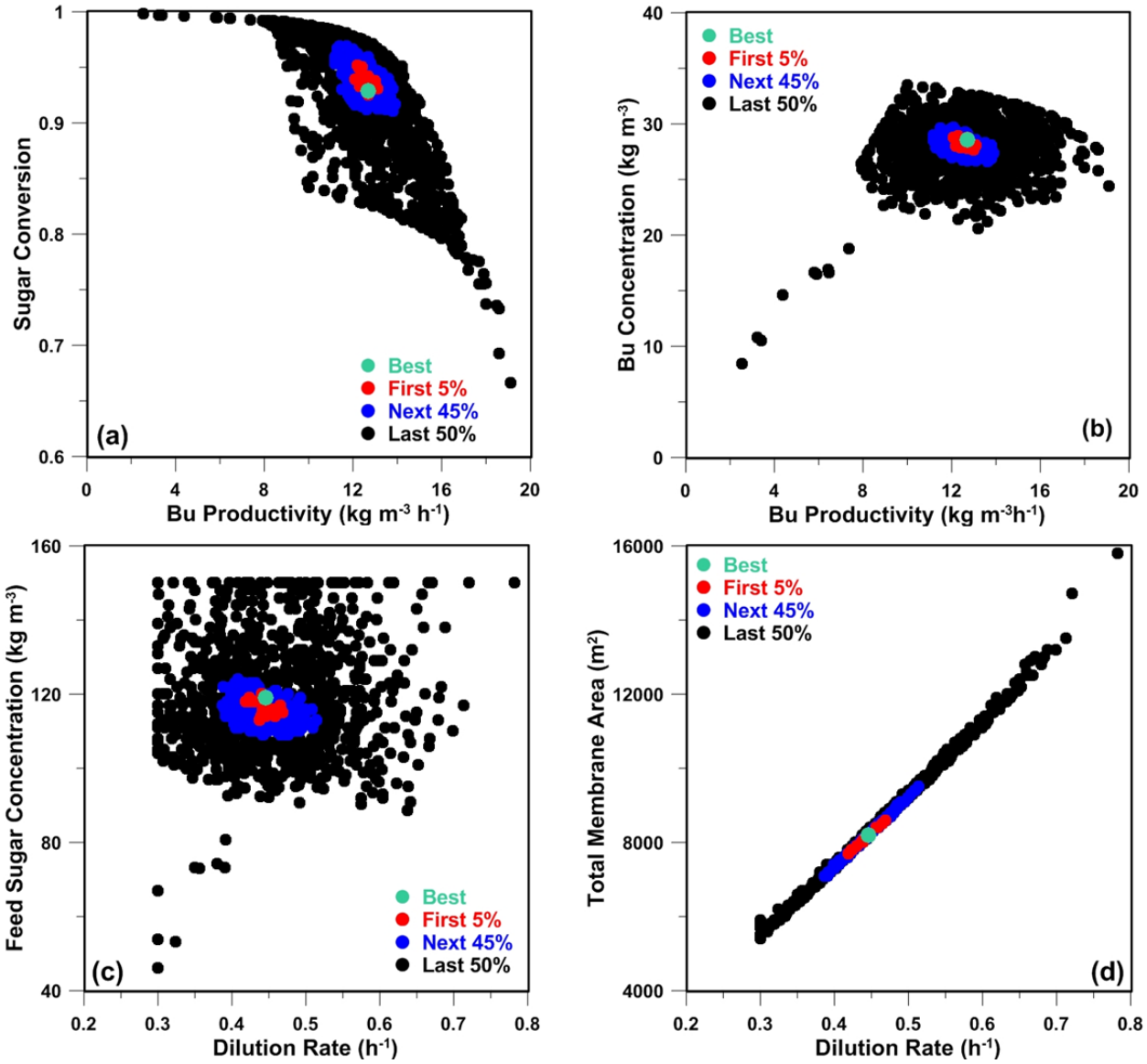

Figure 7-6 Plot of the objective and decision variables for the continuous fermentation with the in-situ recovery using membrane pervaporation for Scenario 2. (a) Sugar conversion versus butanol productivity, (b) Butanol concentration versus butanol productivity, (c) Feed sugar concentration versus dilution rate, (d) Total membrane area versus dilution rate.

Table 7-4 presents the summary of the results for three case studies at steady state for the best ranked solution: the final concentration of the components in the fermenter, the values of the decision variables and the values of the objectives. These results indicate that the concentration of the cellular biomass increased in the fermenter when fermentation is integrated with a membrane pervaporation process. The use of a pervaporation membrane allows to remove a

fraction of the butanol that is produced and to reduce product inhibition. The reduction in production inhibition allows to have a higher feed sugar concentration and to convert a greater amount of sugar, resulting in a higher butanol productivity and higher average butanol concentration. Moreover, the concentration of the intermediate products such as acetic acid and butyric acid reached a relatively small value in the fermenter for Scenario 2 when compared to the other case studies.

Table 7-4 Summary of the steady state concentrations inside the fermenter, values of the decision variables and the objective functions under optimal conditions for the three case studies.

Components	Non-integrated fermentation	Scenario 1	Scenario 2
	Concentration in fermenter (kg/m^3)		
Acetone	5.64	2.45	2.72
Acetic acid	2.10	5.88	0.70
Butanol	9.68	6.54	11.94
Butyric acid	2.00	5.61	1.64
Ethanol	7.25	0.76	0.20
Sugar	10.29	7.30	52.38
Biomass	14.74	52.62	94.55
Decision variables			
Dilution rate (h^{-1})	0.48	0.45	0.45
Sugar feed concentration (kg/m^3)	60.96	150	118.60
Cell retention factor, $\alpha_{8\text{-}12}$ ($m^3.h/m^3.h$)	0.1	0.1	0.2
Membrane area (m^2)	-	39520	8200
Number of stacks	-	-	82
Number of modules	-	-	10
Objective functions			
Butanol productivity, ($kg/m^3.h$)	4.63	13.39	12.74
Butanol concentration, (kg/m^3)	9.67	29.83	28.60
Sugar conversion	83%	96%	93%

The model of Mulchandani and Volesky [37] takes into consideration the inhibition effect of the combined concentration of butanol and butyric acid such that the fermentation will cease when the combined concentration reaches 13.9 kg/m^3. However, the fermentation model does not consider a limitation to the concentration of cellular biomass such that it is possible to reach unfeasible concentrations. The cellular biomass concentration can be controlled by manipulating

the cellular retention factor ($\alpha_{8\text{-}12}$). In the optimisation for all case studies, the cell retention factor converged to its minimum set values, which were 0.1 for the fermentation without a membrane pervaporation process and the fermentation with the integration of a pervaporation unit (Scenario 1) whereas a limiting lower value of 0.2 was used for Scenario 2. To examine the impact of the cell retention factor on the three objectives and the steady state biomass concentration in the fermenter for the best ranked solutions for the three case studies, a series of optimisation studies were performed for different values of the minimum cell retention factor. Results are presented in Figure 7-7. It is shown that the butanol productivity (Figure 7-7a) and the cellular biomass concentration (Figure 7-7d) decreases exponentially as the cell retention factor is increased. For Scenario 2 of the fermentation system with the integration of a membrane pervaporation process, the biomass concentration reaches physically unrealistic values at lower values of the cell retention factor and it is the reason why the lower limiting value for Scenario 2 was set at 0.2. The average butanol concentration (Figure 7-7b) remains essentially constant for the whole range of the cell retention factor. The sugar conversion (Figure 7-7c) remain essentially constant as a function of the cell retention factor for the two cases studies for the fermentation with the integration of a membrane pervaporation process whereas the sugar conversion increases with the cell retention factor for the fermentation without a membrane pervaporation process. These results point to the necessity to adapt the fermentation model to realistically determine the impact of the cell concentration on the rate of production and consumption of all species in the fermenter. This can only be done with a well-planned series of fermentation with cell recycling with and without a membrane pervaporation process.

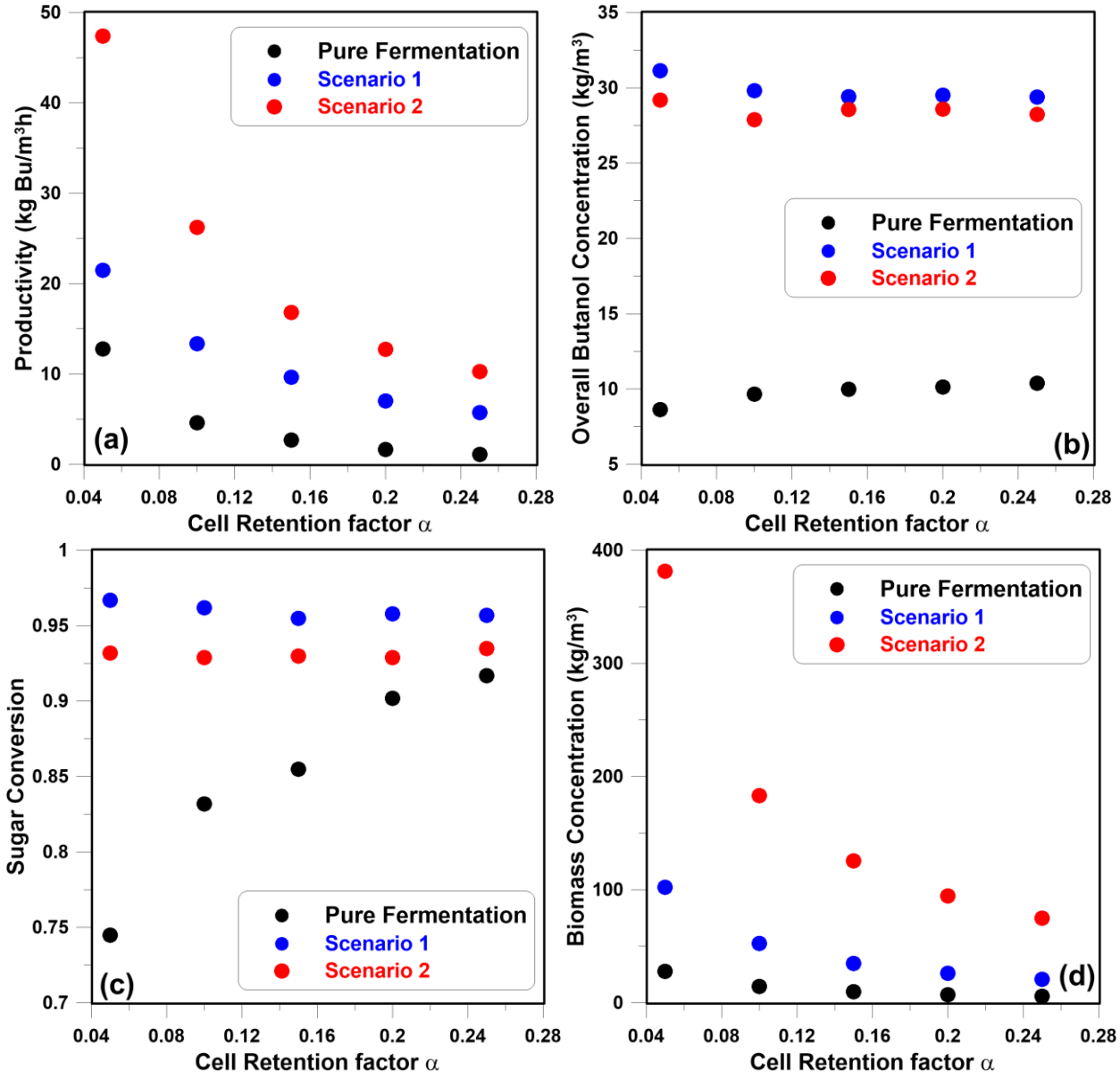

Figure 7-7 Plots showing the impact of the cell retention factor on the (a) productivity, (b) overall butanol concentration, (c) sugar conversion and (d) biomass concentration in the fermenter for the best ranked solution for the non-integrated fermentation, Scenarios 1 and 2.

Conclusion

The simulation and the multi-objective optimisation of the ABE continuous fermentation process integrated with and without a membrane pervaporation in-situ recovery process was performed to determine optimal steady state solution. The investigation was performed for three different

case studies, including the non-integrated fermentation process and two scenarios of an integrated fermentation process with a membrane pervaporation unit with a different level of complexity. The optimal solution of the integrated process was compared with the stand-alone continuous fermentation. By adding an in situ separation system to the continuous ABE fermentation, the productivity, the overall concentration and the sugar conversion have significantly increased. Moreover, the results of the integrated fermentation systems showed that the average total area of the membrane decreased when the pervaporation system changed from a unit membrane module to a multiple membrane modules system. Results also revealed that the cell retention factor has an important effect in the optimisation process and it should be controlled. This is due to the tendency of the optimisation algorithm to keep this value as low as possible to have a higher population of microorganisms inside the fermenter to produce more butanol. It would be important to perform a comprehensive fermentation study with cell recycle, with and without the integration of a membrane pervaporation process, to gather reliable data that would allow adapting the fermentation model.

Nomenclature

a	Activity
A	Membrane area (m^2)
A_f	Flow area (m^2)
$C_{1...8}$	Concentration of the ABE fermentation components (mol/m^3)
C_p	Specific molar heat capacity $(J/mol.K)$
d_h	Hydraulic diameter (m)
D	Mass diffusivity (m^2/s)
D_F	Dilution rate for feed stream (h^{-1})
D_{ij}	Inter-diffusion coefficient in an infinitely-dilute solution (m^2/s)
E	Activation energy of permeation (kJ/mol)
$F_1...F_{12}$	Flow rate of stream 1 to 12 $(kmol/h)$
J	Permeation flux $(kmol/m^2.h)$
k_b	Mass transfer coefficient (m/s)
l_M	Membrane thickness (m)

l_{module}	Length of the membrane module *(m)*
M_w	Molecular weight *(kg/mol)*
p	Pressure *(kPa)*
P	Permeability *(mol/m.s)*
Q	Flow *(mol/h)*
R	Universal gas constant *(J/mol K)*
R_{tot}, R_{boun}, R_{sel}	Mass transfer resistance
Re	Reynolds number
S_0	Sugar feed concentration (kg/m^3)
Sc	Schmidt number
Sh	Sherwood number
T	Temperature *(K)*
V	Volume *(m^3)*
V_A	Molar volume of solute *(m^3/mol)*

Greek symbols

$\alpha_{2\text{-}3}$	Fraction of Stream 2 passing through the microfiltration
$\alpha_{4\text{-}10}$	Fraction of Stream 4 exiting in Stream 10
$\alpha_{8\text{-}12}$	Cell retention factor
γ	Activity coefficient
η_w	Water viscosity *(N s/m^2)*
μ	Dynamic viscosity *(Pa.s)*
v	Velocity *(m/s)*
ρ	Density *(kg/m^3)*
ρ_m	Molar density *(kmol/m^3)*

Subscripts

b	Bulk
B	Butanol
$bond$	Boundary
F	Feed
i	Index of components

M	Membrane
n	Element number
P	Permeate
S	Sugar
sel	Selective
tot	Total

Superscripts

ref	Reference
sat	Saturation
0	Saturated

Abbreviations

ABE	Acetone-Butanol-Ethanol
EPDM	Ethylene propylene diene rubber
LLE	Liquid-liquid extraction
PAI	Polyamide-imide
PAN	Polyacrylonitrile
PDMS	Polydimethylsiloxane
PE	Polyethylene
PEBA	Polyether block-amide
PMS	Poly (methoxy siloxane)
PP	Polypropylene
PTFE	Polytetrafluoroethylene

References

[1] N. Abdehagh, J. Thibault, F.H. Tezel, Separation techniques in butanol production: Challenges and developments, Biomass Bioenergy. 60 (2014) 222–246. doi:10.1016/j.biombioe.2013.10.003.

[2] S.B. Bankar, S.A. Survase, H. Ojamo, T. Granstrom, Biobutanol: the outlook of an academic and industrialist, Rsc Adv. 3 (2013) 24734–24757. doi:10.1039/c3ra43011a.

[3] H. Dong, W. Tao, Z. Dai, L. Yang, F. Gong, Y. Zhang, Y. Li, Biobutanol, Adv. Biochem. Eng.-Biotechnol. 128 (2012) 85–100. doi:10.1007/10_2011_128.

[4] M.G. Buonomenna, J. Bae, Membrane processes and renewable energies, Renew. Sustain. Energy Rev. 43 (2015) 1343–1398. doi:10.1016/j.rser.2014.11.091.

[5] A. Garcia, E.L. Iannotti, J.L. Fischer, Butanol fermentation liquor production and separation by reverse osmosis, Biotechnol. Bioeng. 28 (1986) 785–791. doi:10.1002/bit.260280603.

[6] G. Merlet, F. Uribe, C. Aravena, M. Rodríguez, R. Cabezas, E. Quijada-Maldonado, J. Romero, Separation of fermentation products from ABE mixtures by perstraction using hydrophobic ionic liquids as extractants, J. Membr. Sci. 537 (2017) 337–343. doi:10.1016/j.memsci.2017.05.045.

[7] V. Garcia, J. Pakkila, H. Ojamo, E. Muurinen, R.L. Keiski, Challenges in biobutanol production: How to improve the efficiency?, Renew. Sustain. Energy Rev. 15 (2011) 964–980. doi:10.1016/j.rser.2010.11.008.

[8] A.P. Mariano, M.J. Keshtkar, D.I.P. Atala, F. Maugeri Filho, M.R. Wolf Maciel, R. Maciel Filho, P. Stuart, Energy Requirements for Butanol Recovery Using the Flash Fermentation Technology, Energy Fuels. 25 (2011) 2347–2355. doi:10.1021/ef200279v.

[9] A. Sharif Rohani, P. Mehrani, J. Thibault, Comparison of in-situ recovery methods of gas stripping, pervaporation, and vacuum separation by multi-objective optimization for producing biobutanol via fermentation process, Can. J. Chem. Eng. 93 (2015) 986–997. doi:10.1002/cjce.22186.

[10] N. Abdehagh, F.H. Tezel, J. Thibault, Adsorbent screening for biobutanol separation by adsorption: kinetics, isotherms and competitive effect of other compounds, Adsorption. 19 (2013) 1263–1272. doi:10.1007/s10450-013-9566-8.

[11] N. Qureshi, H.P. Blaschek, Recovery of butanol from fermentation broth by gas stripping, Renew. Energy. 22 (2001) 557–564. doi:10.1016/S0960-1481(00)00108-7.

[12] W.J. Groot, H.S. Soedjak, P.B. Donck, R.G.J.M. van der Lans, K.C.A.M. Luyben, J.M.K. Timmer, Butanol recovery from fermentations by liquid-liquid extraction and membrane solvent extraction, Bioprocess Eng. 5 (1990) 203–216. doi:10.1007/BF00376227.

[13] N. Qureshi, I.S. Maddox, Reduction in Butanol Inhibition by Perstraction, Food Bioprod. Process. 83 (2005) 43–52. doi:10.1205/fbp.04163.

[14] K.O. Agenson, T. Urase, Change in membrane performance due to organic fouling in nanofiltration (NF)/reverse osmosis (RO) applications, Sep. Purif. Technol. 55 (2007) 147–156. doi:10.1016/j.seppur.2006.11.010.

[15] H. Azimi, F.H. Tezel, J. Thibault, Effect of embedded activated carbon nanoparticles on the performance of polydimethylsiloxane (PDMS) membrane for pervaporation separation of butanol, J. Chem. Technol. Biotechnol. (2017). doi:10.1002/jctb.5306.

[16] G. Liu, W. Wei, W. Jin, Pervaporation Membranes for Biobutanol Production, Acs Sustain. Chem. Eng. 2 (2014) 546–560. doi:10.1021/sc400372d.

[17] H. Essawy, M. Tawfik, S. El-Sabbagh, A. El-Gendi, E. El-Zanati, H. Abdallah, Novel amphiphilic conetworks based on compatibilized NBR/SBR–montmorillonite nanovulcanizates as membranes for dehydrative pervaporation of water–butanol mixtures, Polym. Eng. Sci. 54 (2014) 1560–1570. doi:10.1002/pen.23699.

[18] K.D. Jitesh, V.G. Pangarkar, K. Niranjan, Pervaporative stripping of acetone, butanol and ethanol to improve ABE fermentation, Bioseparation. 9 (2000) 145–154. doi:10.1023/A:1008129713552.

[19] D.L. Vrana, M.M. Meagher, R.W. Hutkins, B. Duffield, Pervaporation of Model Acetone-Butanol-Ethanol Fermentation Product Solutions using Polytetrafluoroethylene Membranes, Sep. Sci. Technol. 28 (1993) 2167–2178. doi:10.1080/01496399308016741.

[20] M. Müller, M.-N. Pons, Coupling of gas membrane smooth pervaporation and alcoholic fermentation, J. Chem. Technol. Biotechnol. 52 (1991) 343–358. doi:10.1002/jctb.280520307.

[21] M. Hu, L. Gao, W. Fu, X. Liu, F. Huang, Y. Luo, C. Huang, High-performance interpenetrating polymer network polyurethane pervaporation membranes for butanol recovery, J. Chem. Technol. Biotechnol. 90 (2015) 2195–2207. doi:10.1002/jctb.4533.

[22] F. Liu, L. Liu, X. Feng, Separation of acetone–butanol–ethanol (ABE) from dilute aqueous solutions by pervaporation, Sep. Purif. Technol. 42 (2005) 273–282. doi:10.1016/j.seppur.2004.08.005.

[23] T.A. Jalal, N.M.S. Bettahalli, N.L. Le, S.P. Nunes, Hydrophobic Hyflon AD/Poly(vinylidene fluoride) Membranes for Butanol Dehydration via Pervaporation, Ind. Eng. Chem. Res. 54 (2015) 11180–11187. doi:10.1021/acs.iecr.5b02754.

[24] P.J. Hickey, F.P. Juricic, C.S. Slater, The Effect of Process Parameters on the Pervaporation of Alcohols through Organophilic Membranes, Sep. Sci. Technol. 27 (1992) 843–861. doi:10.1080/01496399208019729.

[25] G. Liu, D. Hou, W. Wei, F. Xiangli, W. Jin, Pervaporation Separation of Butanol-Water Mixtures Using Polydimethylsiloxane/Ceramic Composite Membrane, Chin. J. Chem. Eng. 19 (2011) 40–44. doi:10.1016/S1004-9541(09)60174-9.

[26] S.-Y. Li, R. Srivastava, R.S. Parnas, Study of in situ 1-Butanol Pervaporation from A-B-E Fermentation Using a PDMS Composite Membrane: Validity of Solution-Diffusion Model for Pervaporative A-B-E Fermentation, Biotechnol. Prog. 27 (2011) 111–120. doi:10.1002/btpr.535.

[27] I.L. Borisov, A.O. Malakhov, V.S. Khotimsky, E.G. Litvinova, E.S. Finkelshtein, N.V. Ushakov, V.V. Volkov, Novel PTMSP-based membranes containing elastomeric fillers: Enhanced 1-butanol/water pervaporation selectivity and permeability, J. Membr. Sci. 466 (2014) 322–330. doi:10.1016/j.memsci.2014.04.037.

[28] Y. Wang, T.S. Chung, H. Wang, Polyamide–imide membranes with surface immobilized cyclodextrin for butanol isomer separation via pervaporation, AIChE J. 57 (2011) 1470–1484. doi:10.1002/aic.12360.

[29] H. Zhou, Y. Su, X. Chen, Y. Wan, Separation of acetone, butanol and ethanol (ABE) from dilute aqueous solutions by silicalite-1/PDMS hybrid pervaporation membranes, Sep. Purif. Technol. 79 (2011) 375–384. doi:10.1016/j.seppur.2011.03.026.

[30] S. Li, F. Qin, P. Qin, M.N. Karim, T. Tan, Preparation of PDMS membrane using water as solvent for pervaporation separation of butanol-water mixture, Green Chem. 15 (2013) 2180–2190. doi:10.1039/c3gc40291f.

[31] S.-Y. Li, R. Srivastava, R.S. Parnas, Separation of 1-butanol by pervaporation using a novel tri-layer PDMS composite membrane, J. Membr. Sci. 363 (2010) 287–294. doi:10.1016/j.memsci.2010.07.042.

[32] N.L. Mai, S.H. Kim, S.H. Ha, H.S. Shin, Y.-M. Koo, Selective recovery of acetone-butanol-ethanol from aqueous mixture by pervaporation using immobilized ionic liquid polydimethylsiloxane membrane, Korean J. Chem. Eng. 30 (2013) 1804–1809. doi:10.1007/s11814-013-0116-6.

[33] M. Fang, C. Wu, Z. Yang, T. Wang, Y. Xia, J. Li, ZIF-8/PDMS mixed matrix membranes for propane/nitrogen mixture separation: Experimental result and permeation model validation, J. Membr. Sci. 474 (n.d.) 103–113. doi:10.1016/j.memsci.2014.09.040.

[34] S.-Y. Li, R. Srivastava, R.S. Parnas, Study of in situ 1-Butanol Pervaporation from A-B-E Fermentation Using a PDMS Composite Membrane: Validity of Solution-Diffusion Model for Pervaporative A-B-E Fermentation, Biotechnol. Prog. 27 (2011) 111–120. doi:10.1002/btpr.535.

[35] N. Qureshi, M.M. Meagher, R.W. Hutkins, Recovery of butanol from model solutions and fermentation broth using a silicalite/silicone membrane1This paper is published as paper no. 12061, Journal Series, Nebraska Agricultural Experiment Station, Lincoln, NE 68583-0704.1, J. Membr. Sci. 158 (1999) 115–125. doi:10.1016/S0376-7388(99)00010-1.

[36] H. Wu, X.-P. Chen, G.-P. Liu, M. Jiang, T. Guo, W.-Q. Jin, P. Wei, D.-W. Zhu, Acetone-butanol-ethanol (ABE) fermentation using Clostridium acetobutylicum XY16 and in situ recovery by PDMS/ceramic composite membrane, Bioprocess Biosyst. Eng. 35 (2012) 1057–1065. doi:10.1007/s00449-012-0721-5.

[37] A. Mulchandani, B. Volesky, Modelling of the acetone-butanol fermentation with cell retention, Can. J. Chem. Eng. 64 (1986) 625–631. doi:10.1002/cjce.5450640413.

[38] T.C. Ezeji, N. Qureshi, H.P. Blaschek, Microbial production of a biofuel (acetone-butanol-ethanol) in a continuous bioreactor: impact of bleed and simultaneous product removal, Bioprocess Biosyst. Eng. 36 (2013) 109–116. doi:10.1007/s00449-012-0766-5.

[39] L. Giorno, E. Piacentini, F. Bazzarelli, The Principle of Microfiltration, in: E. Drioli, L. Giorno (Eds.), Encycl. Membr., Springer Berlin Heidelberg, 2015: pp. 1–4. doi:10.1007/978-3-642-40872-4_2233-1.

[40] W.J. Groot, M.R. Kraayenbrink, R.G.J.M. van der Lans, K.C.A.M. Luyben, Ethanol production in an integrated fermentation/membrane system. Process simulations and economics, Bioprocess Eng. 8 (1993) 189–201. doi:10.1007/BF00369829.

[41] L.F.F. Faria, M. Di Luccio, R. Nobrega, C.P. Borges, Development and characterization of microfiltration hollow-fiber modules for sterilization of fermentation media, Braz. J. Chem. Eng. 19 (2002) 141–150. doi:10.1590/S0104-66322002000200009.

[42] W.J. Groot, C.E. Vandenoever, N.W.F. Kossen, Pervaporation for Simultaneous Product Recovery in the Butanol Isopropanol Batch Fermentation, Biotechnol. Lett. 6 (1984) 709–714. doi:10.1007/BF00133061.

[43] N. Qureshi, H.P. Blaschek, Butanol recovery from model solution/fermentation broth by pervaporation: evaluation of membrane performance, Biomass Bioenergy. 17 (1999) 175–184. doi:10.1016/S0961-9534(99)00030-6.

[44] N. Qureshi, H. Blaschek, Production of acetone butanol ethanol (ABE) by a hyper-producing mutant strain of Clostridium beijierinckii BA101 and recovery by pervaporation, Biotechnol. Prog. 15 (1999) 594–602. doi:10.1021/bp990080e.

[45] H. Halsall-Whitney, J. Thibault, Multi-objective optimization for chemical processes and controller design: Approximating and classifying the Pareto domain, Comput. Chem. Eng. 30 (2006) 1155–1168. doi:10.1016/j.compchemeng.2006.02.010.

[46] G.P. Rangaiah, Multi-Objective Optimization: Techniques and Applications in Chemical Engineering, World Scientific, 2016.

Appendix I

Stream and component mass balances for the fermentation process integrated with a membrane pervaporation system

This appendix describes the procedure used to perform stream and component mass balances for the integrated fermentation process (Table I-1). Eight components are considered in these mass balance models. Each component is designated with an index *i* as follows: 1=Acetone, 2=Acetic acid, 3=Butanol, 4=Butyric acid, 5=Ethanol, 6=Sugar, 7=Biomass, 8=Water). The fraction of stream F_2 flowing through the microfiltration membrane is defined by $\alpha_{2\text{-}3}$ *and* is equal to 0.5. Finally, the cell retention factor $\alpha_{8\text{–}12} = F_8/(F_8 + F_{12})$ is a decision variable that will be determined via the optimisation algorithm.

Table I-1 Description of the stream and component mass balances.

Stream	Calculation	Concentration
F_1	DV	$C_{6,0}$ and $C_{8,0}$ are given; $C_{i,0} = 0$ for i = 1-5,7
Fermenter	-	$C_{i,1}$ calculated by kinetic reaction model
F_2	$15F_1$	$C_{i,2} = C_{i,1} \quad \forall i \in [1,8]$
F_3	$\alpha_{23}F_2$	$C_{i,3} = C_{i,2} \quad \forall i \in [1-6,8]$ and $C_{7,3} = 0$
F_4	Calculated from pervaporation model	
F_5	$(1-\alpha_{4-10})F_4$	$C_{i,5} = \frac{C_{i,4}F_4 - C_{i,10}F_{10}}{F_5}$
F_6	$F_3 - F_4$	$C_{i,6} = \frac{C_{i,3}F_3 - C_{i,4}F_4}{F_6}$
F_7	$F_2 - F_3$	$C_{i,7} = C_{i,2} \quad \forall i \in [1-6,8]$ and $C_{7,7} = \frac{F_2 \times C_{7,2}}{F_7}$
F_8	$F_8 = \alpha_{8-12} \times (F_1 - F_5 - F_{10})$	$C_{i,8} = C_{i,7} \quad \forall i \in [1,8]$
F_9	$F_7 - F_8$	$C_{i,9} = C_{i,7} \quad \forall i \in [1,8]$
F_{10}	$\alpha_{4-10}F_4$	$C_{i,10} = 0$ for i=2,4,6,7 $C_{1,10} = 0.45C_{1,4}$ $C_{3,10} = 0.2C_{3,4}$ $C_{5,10} = 0.35C_{5.4}$ $C_{8,10} = \frac{\rho_{tot} - (C_{1,10}MW_1 + C_{3,10}MW_3 + C_{5,10}MW_5)}{MW_8}$
F_{11}	$F_6 - F_{12}$	$C_{i,11} = C_{i,6} \quad \forall i \in [1,8]$
F_{12}	$(1-\alpha_{8-12}) \times (F_1 - F_5 - F_{10})$	$C_{i,12} = C_{i,11} \quad \forall i \in [1,8]$

Appendix II

Set of equations for the pervaporation model of Scenario 2

In this appendix the set of equations which have been used for the pervaporation model of Scenario 2 is presented. Figure II-1 shows the basic diagram of a plate-and-frame pervaporation module. In this study, the length of the membrane in the direction of the flow was divided into a number of discrete elements. It was assumed that the mass transfer driving force through these discrete elements is proportional to the difference between activities of permeate and feed side and the component properties remain constant.

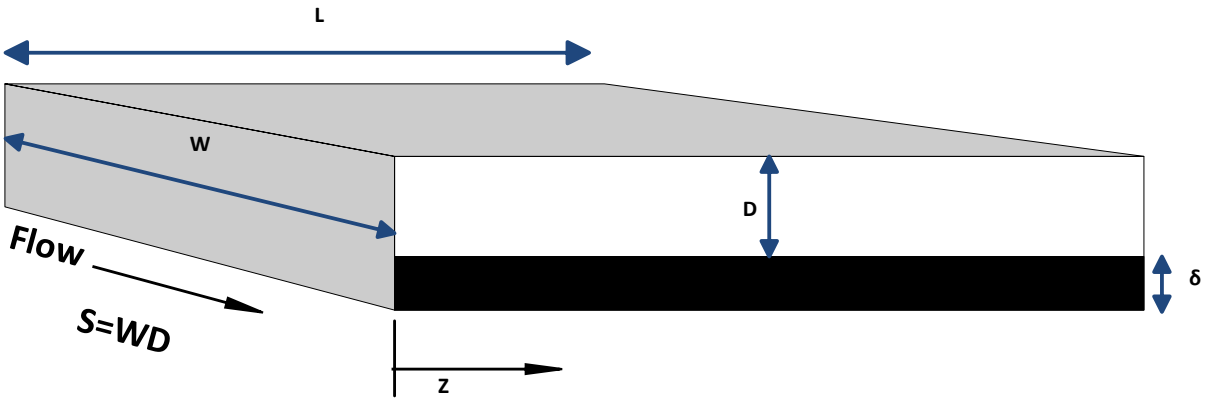

Figure II-1 Basic diagram of the flat pervaporation membrane module used in this study.

Permeate and retentate streams exiting the pervaporation module were calculated based on the permeability of each component through the PDMS membranes. The values of the permeability of the four compound of interest, obtained from the literature, are presented in Table [35].

Table II-1 Pervaporation PDMS membrane performance parameters used for the first case of study.

Permeability *(mol/m.s)*				**Ref**
Acetone	**Butanol**	**Ethanol**	**Water**	[35]
5.18×10^{-8}	2.26×10^{-7}	2.00×10^{-7}	1.68×10^{-8}	

In this investigation, the number of pervaporation units stacked in parallel and the number of stacked modules in series were two deviation variables that are determined using the optimisation algorithm. These two numbers allow determining the total membrane area. In this scenario, to compensate the decrease in temperature as the stream on the retentate side flows along the membrane and provide the latent heat of vaporisation to the permeating stream. Inter-module heat exchangers are used to return the temperature of the retentate stream between two modules to a higher value to enhance permeation.

Factors such as the permeation flux of each component through the membrane, the feed side hydrodynamics and the feed side component concentration were considered to establish the mass transfer equations on the feed side. In Eq. (II-1), the permeation flux of the component *i* can be estimated based on the activity of this component in the liquid bulk ($a_{i,F}$) and its activity at the membrane surface ($a_{i,FM}$).

$$J_i = \frac{k_{b,i}\bar{\rho}_m}{\gamma_{i,F}}\left(a_{i,F} - a_{i,FM}\right) \qquad \text{(II-1)}$$

In order to determine the mass transfer coefficient ($k_{b,i}$), the Sherwood correlation was used (Eq. (II-2)).

$$Sh = a\,\mathrm{Re}_F^b\,Sc^c\left(\frac{d_{h,F}}{l_{\mathrm{module}}}\right)^d \qquad \text{(II-2a)}$$

$$Sh = \frac{k_{b,i}d_{h,F}}{D_{ij}} \qquad \text{(II-2b)}$$

$$d_h = \frac{4\times \text{volume between plates}}{\text{wetted surface between plates}} \qquad \text{(II-2c)}$$

$$\mathrm{Re} = \frac{\rho v d_{h,F}}{\mu} \qquad \text{(II-2d)}$$

$$Sc = \frac{\mu}{\rho D} \qquad \text{(II-2e)}$$

$$D_{ij} = 7.4\times10^{-8}\left[\left(2.6\times M_w\times\rho\right)^{\frac{1}{2}}\frac{T}{\eta_w V_A^{0.6}}\right] \qquad \text{(II-2f)}$$

where, the inter-diffusion coefficient in an infinitely-dilute solution has been estimated based on the Wilke and Chang equation. In this equation, D_{ij} is the inter-diffusion coefficient in an infinitely-dilute solution (cm^2/s), ϕ is the parameter of association of solvent (recommended value for water is 2.6), M_w is the molecular mass of water, V_A is the molar volume of solute (A)

at a boiling point under normal conditions (cm^3/mol), η_w is the water viscosity ($N\ s/m^2$), and T is the temperature (K). In addition, the diffusion coefficient D_{ij} is calculated as binary coefficient relative to water since the solution is dilute with concentrations much less than 10 mol%. Table shows the constant of a, b, c and d for Eq. (II-2).

Table II-2 Variables used in the Sherwood correlation.

Flow region	a	b	c	d
Laminar (Re < 2300)	1.615	0.33	0.33	0.33
Turbulent (Re > 2300)	0.026	0.8	0.3	-

In addition, the solution-diffusion model was used to determine the mass transfer through the membrane. Based on this model, the flux of the penetrant can be calculated based on the driving force corresponding to the difference between the membrane surface activity on the feed side ($a_{i,FM}$) and the activity on the permeate side ($a_{i,P}$) (Eq. (II-3)).

$$J_i = \frac{P_i}{l_M}\left(a_{i,FM} - a_{i,P}\right) \tag{II-3}$$

Based on the resistance-in-series model, there are two main resistances for the mass transport for membrane pervaporation. As a result, expressing this equation in terms of the overall resistance and the driving force, Eq. (II-4) gives the resistance-in-series permeation flux for component i.

$$J_i = \frac{1}{R_{i,tot}}\left(a_{i,F} - a_{i,P}\right) \tag{II-4a}$$

$$J_i = \frac{1}{R_{i,bond} + R_{i,sel}}\left(a_{i,F} - a_{i,P}\right) \tag{II-4b}$$

$$R_{i,bond} = \frac{\left(a_{i,F} - a_{i,FM}\right)}{J_i} = \frac{\gamma_{i,F}}{k_{b,i}\bar{\rho}_m} \tag{II-4c}$$

$$R_{i,sel} = \frac{\left(a_{i,F} - a_{i,P}\right)}{J_i} = \frac{l_M}{P_i} \tag{II-4d}$$

Based on Eq. (II-4) and assuming steady state, Eq. (II-5) can be obtained.

$$J_i = \frac{1}{\frac{\gamma_{i,F}}{k_{b,i}\bar{\rho}_m} + \frac{l_M}{P_i}}\left(a_{i,F} - a_{i,P}\right) \tag{II-5}$$

where $a_{i,P}$ is considered to be zero.

To calculate the variation of the permeability with temperature, Eq. (II-6) was used.

$$P_i\left(T_F\right) = P_i^{ref} \exp\left(\frac{E_i}{R}\left(\frac{1}{T^{ref}} - \frac{1}{T_F}\right)\right) \quad \text{(II-6)}$$

Moreover, to simulate the change in temperature along the membrane module, a heat balance was performed (Eq. (II-7)).

$$Q_{n+1,tot} C_{P_{avg,n+1}} T_{n+1} = Q_{n,tot} C_{P_{avg,n}} T_n - \Delta H_{avg,n} J_n dA_f \quad \text{(II-7a)}$$

$$T_{n+1} = \frac{Q_{n,tot} C_{P_{avg,n}} T_n - \Delta H_{avg,n} J_n dA_f}{Q_{n+1,tot} C_{P_{avg,n+1}}} \quad \text{(II-7b)}$$

where Q is the molar flowrate, $C_{p,avg}$ is the molar average heat capacity of the solution, ΔH_{avg} is the average latent heat of vaporization, J is the average permeate molar flux, dA_f is the flow area of the discrete element and n shows the element number.

Some of the values that are required for the equations in this appendix are provided in Appendix III.

Appendix III

Required information for the pervaporation model of Appendix II

Saturated partial pressure of components

Antoine equation has been used to calculate the saturated partial pressure of each component in the retentate stream at each discrete element (Eq. III-1).

$$p_i^{sat} = 10^{A-\frac{B}{T+C}} \quad \text{(III-1)}$$

where A, B and C are the constants of the Antoine equation. The Antoine constants for each component are presented in Table III-1. In Eq. III-1, T is in $°C$ and p_i is in $mmHg$.

Table III-1 Antoine equation constants for each permeating component.

Component	A	B	C
Butanol	7.3666	1305.198	173.427
Water	7.96681	1668.21	228
Acetone	7.11714	1210.595	229.664
Ethanol	8.1122	1592.364	226.184

Activity coefficient of the components

The activity coefficients of the four components of interest at different temperatures were estimated using Eqs. (III-2a-III-2d). These equations have been obtained by fitting experimental data of the activity coefficients from the literature at different temperatures.

$$\gamma_{butanol} = -0.0069T^2 + 4.71T - 738.07 \quad \text{(III-2a)}$$

$$\gamma_{water} = 1 \quad \text{(III-2b)}$$

$$\gamma_{acetone} = -0.00162T^2 + 1.053T - 162.24 \quad \text{(III-2c)}$$

$$\gamma_{Ethanol} = 0.053T - 11.847 \quad \text{(III-2d)}$$

Activation energy of permeation

Table III-2 presents the activation energy of permeation of the components for PDMS membrane based on the reported data in the literature.

Table III-2 Activation energy of the permeation of the components for PDMS membrane.

Component	Butanol	Water	Acetone	Ethanol
E_i *(kJ/mol)*	46.4	36.56	29.11	48.05

Properties of components of interest

Table shows the required properties which have been used for the optimisation process in this investigation.

Table III-3 Physical properties of the components.

Component	Butanol	Water	Acetone	Ethanol
Mw (kg/mol)	0.07412	0.01801	0.05808	0.4607
ρ *(kg/m^3)*	810	1000	791	789
η *(Pa.s)*	0.002593	0.00089	0.000304	0.001078
V_A *(cm^3/mol)*	85.9	18.7	66.8	53.7
C_p *(J/mol.K)*	177.06	75.29	126.6	112.25
ΔH *(J/kmol)*	43.29	40.66	29.1	38.56
Additional information				
R(J/K.mol)	8.31451			
p_P *(kPa)*	0			
T^{ref} *(K)*	298			

Module properties

The membrane and module geometry used in the optimisation process for the pervaporation process are given in Table .

Table III-4 Membrane and module geometry used in this study.

Membrane	**Thickness (*m*)**	**Module Type**	**Module length (*m*)**	**Module width (*m*)**	**Feed channel height (*m*)**	**Permeate channel height (*m*)**
PDMS	$5x10^{-06}$	Plate-and-frame	0.5	0.5	0.004	0.004

8. Chapter 8

Conclusions and recommendations

Biobutanol produced from ABE fermentation could be used as an alternative for fossil fuels. However, the low final concentration of this alcohol is limiting its economic viability and its widespread adoption. In this thesis, the pervaporation separation of butanol from binary aqueous solutions and ABE model solutions have been investigated in an attempt to improve the in situ and ex situ recovery of the butanol from ABE fermentation broths. This chapter includes the accomplishments of this work and the recommendations and suggestions for future works.

Conclusions

In this study, activated carbon nanoparticles have been embedded into the matrix of PDMS membranes to enhance their separation performance for pervaporation separation of butanol. Results of the experimental program showed that activated carbon nanoparticles could enhance the performance of PDMS membranes up to a certain particle loading. It was found that a particle concentration of 6 wt% within the matrix of the PDMS gave the best performance for the pervaporation separation of butanol from binary aqueous solutions where the total permeation flux and butanol separation factor increased by 42.6% and 51.9%, respectively, compared to neat PDMS membranes. With respect to ABE model solutions, an 8 wt% nanoparticle loading led to the best performance for the separation of butanol. Both the separation factor for butanol and the total permeation flux more than doubled in comparison to neat PDMS membranes prepared in this work. Furthermore, a commercial PDMS membrane was used in order to compare PDMS membranes available on the market with the PDMS/AC mixed matrix membranes developed in our laboratory. They were compared in terms of performance for pervaporation separation of butanol from binary and ABE model solutions. Results of butanol separation from ABE model solutions showed that mixed matrix membranes with 8 wt% nanoparticle loading had a better performance than the commercial once. Indeed, results revealed that the presence of activated carbon nanoparticles embedded in the matrix of PDMS would be beneficial for the pervaporation separation of butanol from ABE fermentation broths.

Experiments were performed to assess the effect of pH of the feed solution on the separation of butyric acid from dilute aqueous solutions using three separation methods: distillation, pervaporation and adsorption. Results confirmed that the pH of the solution, which dictates the

level of butyric acid dissociation, controls the degree of separation of butyric acid from dilute aqueous solutions. Furthermore, results showed that the separation performance is strongly correlated with the pH of the feed solution and, as anticipated, an increase of pH reduces the level of separation for these three processes.

A review has been done on the mathematical models which have been used for pervaporation separation of butanol. Based on the literature, Maxwell-Stefan model was an accurate model for membrane separation in pervaporation due to its ability to predict the flux and selectivity of the multi-component systems based on the results of single components, which decreases the number of pervaporation experiments to be performed. Moreover, this model has the potential to be used for module and process design together with membrane development.

To better understand the underlying mechanism and the reasons for the enhancement in performance following the addition of activated carbon nanoparticles in the polymeric membranes, a series of numerical simulations were performed. The Fick's second law of diffusion was solved by finite differences to determine the concentration profile and the fluxes of permeants in mixed matrix membranes by pervaporation for a wide range of permeability ratios of the dispersed to the continuous phase, the nanoparticle loading, the particle shape, particle size and for different filler adsorption isotherms. Results revealed that the effective permeability of MMMs strongly depends on the permeability ratio of the dispersed phase to the continuous phase and the volume fraction of the filler material. Moreover, the shape and the size of the particle material had no influence on the effective permeability of the MMMs for filler volume fractions less than 0.4. For numerical estimations performed with different sorption isotherms, results showed that the effective permeability of the membrane depends on the type and parameters of the isotherm.

Finally, the optimization of butanol pervaporation separation process from ABE fermentation broth at an industrial scale was studied. For the continuous ABE fermentation coupled with pervaporation, results revealed that increasing butanol productivity in pervaporation requires higher membrane area which will increase the overall process costs.

Recommendations for future works

In this work, pervaporation separation of the butanol from binary aqueous solutions and ABE model solutions have been investigated via using PDMS/AC mixed matrix membranes. It was required to first validate the performance of mixed matrix membranes for ideal solutions, which was the purpose of this thesis. The next step is to evaluate the performance of mixed matrix membranes for butanol separation from a real ABE fermentation broth. In addition, the in-situ recovery of the product from an ABE fermentation broth in view of increasing the final concentration of the butanol using PDMS/AC mixed matrix membranes should be undertaken.

This study demonstrated that the presence of activated carbon nanoparticles embedded in the matrix in a PDMS membrane is beneficial for the pervaporation separation of butanol. However, the particle concentrations were limited to relatively low values. It is therefore suggested to examine surface modification of the nanoparticles in order to enhance the surface interaction between particles and the matrix of the host polymer since a higher particle loading could further increase the performance of these membranes.

Since PDMS membranes are subjected to the trade-off between the permeability and selectivity, the modification of PDMS membranes by having the block copolymer of the PDMS and an appropriate polymer such as PTMSP is recommended with the objective of improving the weaknesses of PDMS polymeric membranes.

The mass transfer of the components through mixed matrix membranes has been studied in this work using finite differences. It would be interesting to examine the impact of non-ideal interface morphology by considering a third phase in the numerical simulation. The impact would be evaluated in terms of the effective permeability and flux.